UNIVERSITY OF SOUTHAMPTON

FACULTY OF ENGINNERING AND THE ENVIRONMENT

Energy and Climate Change

Volume 1 of 1

Coastal Evolution of Soft Cliff Coasts:
Headland Formation and Evolution on the Southwest Isle of Wight

by

Caroline Stuiver

Thesis for the degree of Doctor of Philosophy

October 2013

UNIVERSITY OF SOUTHAMPTON

ABSTRACT

FACULTY OF ENGINEERING AND THE ENVIRONMENT

Coastal Geomorphology

Thesis for the degree of Doctor of Philosophy

COASTAL EVOLUTION OF SOFT CLIFF COASTS: HEADLAND FORMATION AND EVOLUTION ON THE SOUTHWEST ISLE OF WIGHT

Caroline Shirley Stuiver

The standard model of headland formation assumes a coastline with discordant geology, where the less resistant rock is eroded at a higher rate than the more resistant geology. The indentation of the coastline will continue to increase until variations in wave energy due to refraction balance with the variation in rock strength and beach volume. On soft cliff coasts, where no systematic variations in cliff lithology or strength exist subtle headlands are still seen. Several examples of this can be seen on the southwest coast of the Isle of Wight, a coastline of complex interbedded soft rock lithology. Its relatively straight planform is punctuated by three established and one potentially emerging headland. All of these headlands are fronted by locally elevated intertidal shore platforms. It was hypothesised that these platform potentially act in three ways. Firstly by reducing the amount of wave energy reaching the cliff base, thus reducing local cliff recession rates. The second may counteract the first by increasing the wave energy directed at the cliff base due to refraction, the balance between these two effects will determine if a headland will grow, be maintained or decline. Thirdly by blocking longshore transport of beach sediment, building a protective beach up-drift, while starving the downdrift coast of sediment, potentially accelerating erosion in that area. To test these three possible mechanisms, investigation into the geological and geotechnical properties of the cliff and platform, beach volumes and sediment budget, wave refraction, and historical recession rates was undertaken. The elevation of the shore platform is controlled by their resistance to erosion, which is related to aspects of their lithology and structural geology. These include clay

content, mass properties, dip and strike in relation to the orientation of the coastline and the strength of the surrounding beds. Although two of the established headlands, Hanover and Atherfield Points act as a partial barrier to sediment transport the sediment volumes along the coastline were insufficient to significantly influence recession rates. The results of the sediment budget indicate that the low sediment volumes observed are likely to have been consistent over time due to the low inputs of beach grade sediment. Wave refraction modelling revealed that concentration of wave energy occurs towards the established headlands of Hanover and Atherfield Points this is reflected in the higher than average recession rates seen at these headlands. It is concluded that the major control of the formation and evolution of headlands on the southwest coast is the geological and geotechnical properties of the intertidal platforms. Once established these headlands exist in a state of dynamic equilibrium controlled by the persistence of the platform forming beds and the balance between refraction and attenuation of wave energy across the platform surface. These results may have widespread implications on soft cliffed sediment-starved coasts where similar processes are dominant.

Contents

List of Tables

List of Figures

List of accompanying materials

Stuiver, C., Nicholls, R.J., Barton, M. and Richards, D. 2013. Formation and Evolution of Headlands on Soft Cliff Coasts: Lessons from the Isle of Wight. Proceedings of Coasts, Marine Structures & Breakwaters 2013, Edinburgh. ICE.

DECLARATION OF AUTHORSHIP

I, Caroline Stuiver

declare that the thesis entitled

Coastal Evolution on Soft Cliff Coasts: Headland Formation and Evolution on the Southwest Isle of Wight

and the work presented in the thesis are both my own, and have been generated by me as the result of my own original research. I confirm that:

- this work was done wholly or mainly while in candidature for a research degree at this University;

- where any part of this thesis has previously been submitted for a degree or any other qualification at this University or any other institution, this has been clearly stated;

- where I have consulted the published work of others, this is always clearly attributed;

- where I have quoted from the work of others, the source is always given. With the exception of such quotations, this thesis is entirely my own work;

- I have acknowledged all main sources of help;

- where the thesis is based on work done by myself jointly with others, I have made clear exactly what was done by others and what I have contributed myself;

- Parts of this work have been published as:

  Stuiver, C., Nicholls, R.J., Barton, M. and Richards, D. 2013. Formation and Evolution of Headlands on Soft Cliff Coasts: Lessons from the Isle of Wight. Proceedings of Coasts, Marine Structures & Breakwaters 2013, Edinburgh. ICE.

  Carpenter, N. E., Stuiver, C., Nicholls, R. J., Powrie, W. A., and Walkden, M. 2012. Investigating the recession process of complex soft cliff coasts: An Isle of

Wight case study. In Proceedings of the 33rd Conference on Coastal Engineering. Ed. by P. Lynett, and J. Mckee Smith. ICCE, Santander, Spain.

Redshaw, P. G., Barton, M. E. & Stuiver, C. In Review. Landslides on a Cretaceous Fluvial Sediment. World Landslide Forum 3, 2-6 June 2014. In Review Beijing.

Signed: …………………………………………………………………..

Date:………………………………………………………….

Acknowledgements

Definitions and Abbreviations

A – Lithology Contribution Factor

AARR – Average Annual Recession Rate

AONB – Area of Outstanding Natural Beauty

AP – Atherfield Point

BGS – British Geological Survey

BS – Backshore

BWA – Beach Wedge Area: represents the volume of sand above MHWS (Lee, 2008)

C1 to C4 – Coherence Levels

CBU – Cliff Behavioural Unit

CCO – Channel Coastal Observatory (www.channelcoast.org/)

dGPS – differential Global Positioning System

DSAS – Digital Shoreline Analysis System

EA – Environment Agency

FS - Foreshore

GIS – Geographical Information System

GPS - Global Positioning System

HP – Hanover Point

Hs – Significant Wave Height

IOW – Isle of Wight

K – Composition Factor

LCD – Littoral Cut-off Diameter

LD – Laser Diffraction

MHWS – Mean High Water Spring tidal level

MLWS – Mean Low Water Spring tidal level

NERC – National Environmental Research Council

NRA – National River Authority

OS – Ordnance Survey

PSD – Particle Size DIstribution

RCPWAVE - **R**egional **C**oastal **P**rocesses Monochromatic **WAVE** Model

SAC – Special Area of Conservation

SBAS – Sediment Budget Analysis System

SCAPE – Soft Cliff And Platform Erosion model

SL – Ship Ledge

SMP – Shoreline Management Plan

SP – Sudmoor Point

Tp – Peak Wave Period

XRD – X Ray Diffraction

1. Introduction

1.1   Background

Soft cliff erosion poses a threat to property and infrastructure in many areas of the UK, Europe, and globally. Recently it has been recognised that the cost of coastal defences has often been large when compared to the associated benefits (HR Wallingford, 2002). This fact, combined with the conservation and amenity value of natural coastlines means that managed retreat is likely to become increasingly common in the future. Understanding the processes and controls on recession rates is fundamental to predicting future rates and patterns of recession, which will aid in the design of appropriate coastal defence / management strategies.

The standard model of headland formation assumes a coastline with discordant geology where the less resistant rock is eroded at a higher rate than the more resistant geology. Erosion of these cliffs will produce beach sediment. Variations in wave energy alongshore will move that sediment into the resulting bay, protecting the less resistant cliffs. The indentation of the coastline will continue to increase until variations in wave energy due to refraction balance with the variation in rock strength and beach volume. At this point the recession rate for the headlands and bays are equal and the indentation is maintained as recession continues (Schwartz, 2005). Another common feature of headland bound bays is their crenulate planform as outlined by Silvester (1985) and seen widely, such as in Christchurch and Poole Bays (Figure 1.1). A crenulate bay can be separated into two components: 1) the shadow zone, an area protected by the updrift headland displaying a log-spiral curve, and 2) the tangential end, the straight stable section of coastline leading to the downdrift headland (Finkelstein, 1982). The planform of a headland bound bay is a response to the prevailing swell wave conditions. The log-spiral curve of the shadow zone is caused by refraction of the waves near the headland, while the tangential stretch is developed parallel to the dominant wave approach away from the influence of the headland (Wright, 1981).

On coastlines with limited sediment supply and complex underlying geology with variable material strength the crenulate planform is disrupted. Examples of this can be seen along the south coast of England around Kimmeridge Bay and Ringstead in Dorset, and at several locations around the Isle of Wight. The

southwest coast of the Isle of Wight will be used as a case study site in this project. The platform/headlands have the potential to control the coastal evolution; therefore prediction of future coastal evolution, with or without direct human intervention, requires a better understanding of the processes controlling these headlands.

1.2   Study Area

The southwest coast of the Isle of Wight is a 16 km length of coast unaffected by coastal engineering, making it a good natural laboratory. It is a section of coastline that can be considered to be the tangential length of a larger headland bound bay system incorporating Christchurch and Poole Bays, with Hengistbury Head, the Solent and the western tip of the Island breaking the smooth curve (Figure 1.1a). The orientation of the southwest coast (128°) reflects that of Chesil Beach (129°) running parallel to the dominant wave crest approach. As such it would be expected that this coastline should have a smooth straight plan form. However localised variations in foreshore elevation caused by differences in geological resistance have led to the formation of localised intertidal shore platforms. These platforms appear to protect the cliff base from erosion, reducing recession rates and creating subtle headlands behind them. There are three well-established headlands (Hanover, Sudmoor and Atherfield Points) dividing the coast into four bays (Compton, Brook, Brighstone and Chale Bays). There is also one potentially emerging headland at Ship Ledge, which provides a unique opportunity to study the formation of these as yet unexplored geomorphological features. The evolution of the coastline appears to be controlled by the presence of these intertidal platforms. Since the focus of this research is the headlands the study area is confined to the area between Compton Chine and Whale Chine (Figure 1.1b).

If an understanding of how these shore platforms effectively reduce recession rates is established, the theory could potentially be used to develop less intrusive coastal defence options with low visual impact where artificial platforms could be used to manipulate recession rates. It will also help to more accurately predict the future evolution of soft cliffed coastlines where individual, relatively resistant beds are the dominant control. These improved predictions will be a valuable tool for planning authorities at local and regional scales, in particular in areas where fixed

hard defences are not appropriate due to economic and/or environmental considerations.
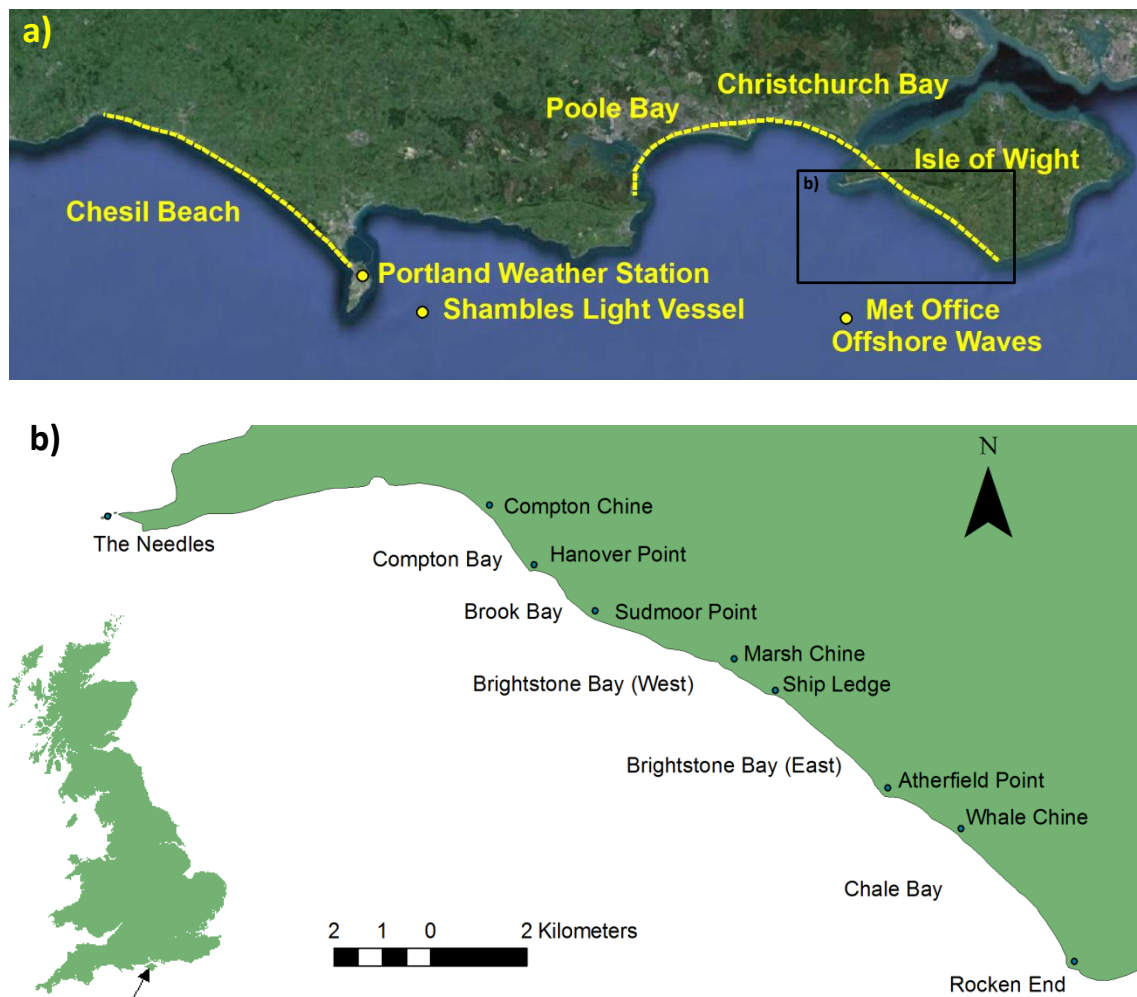
Figure 1.1: a) Outline of the headland bound bay that incorporates Christchurch and Poole Bays and the southwest coast of the Isle of Wight. Note its similar orientation to Chesil Beach. Also shows the location of the sources of wave data used in the study. b) Map showing the location of various landmarks along the southwest coast of the Isle of Wight, including the headlands, bays and chines.

1.3   Research Aims and Objectives

Little research has been carried out on the formation and evolution of soft rock headlands as described above and no work has been done on these specific, shore platform related headlands on the Isle of Wight. On sediment starved coastline with complex underlying geology, subtle longshore variation in strength can have a significant influence on planform evolution. Therefore it is important to understand these influences for the provision of effective coastal defence and/or management strategies.

1.3.1   Aims

The aim of this research is to evaluate the controls on headland formation and evolution on soft rock, cliffed coasts. These controls potentially include 1) the geological/geotechnical properties of the cliff and platform, 2) longshore wave energy distribution and 3) sediment volume and supply. This will be carried out using the southwest coast of the Isle of Wight as a case study. The Isle of Wight was chosen to study these headlands as it is a unique sediment starved area of complex geology eroding at a rate of 0.5 m a^{-1} making it possible to study changes in its planform over a period of 150 years for which quality maps are available. The historic interest in the coastline by early geologist and fossil hunters has produced literature on the geology of the coastline dating back to the late 18th Century. The coastline has good access for field surveys and is unaffected by hard engineering works, making it an ideal natural laboratory.

1.3.2   Objectives

To achieve this aim the following objectives have been set:

1) Determine the importance of longshore variations in shore platform and cliff lithology, in particular the influence of their geotechnical properties on local recession rates.

2) Examine the longshore variations in sea bed geology and associated near shore bathymetry to consider how those variations influence the distribution of wave energy and hence recession rates along the shoreline.

3) To study the interaction between beach volumes, sediment budget and cliff recession rates, in the presence of intertidal shore platforms and the influence these features have on local recession rates.

4) Investigate how the above factors influence headland formation and evolution through the refinement and testing of a number of conceptual process-based models.

5) Consider the generic applications of this information for the management of the southwest coast and other coastlines.

These issues are explored in more detail in Chapter 2.

1.4   Thesis Outline

The thesis begins with a literature review of the factors that control cliff recession rates in soft cliff coasts. In particular the factors that influence the exposure of the cliff toe, i.e. beach and shore platform characteristics, looking at both the cross-shore, and longshore interactions of those factors with recession rates. This review of the literature leads to the development of the hypotheses concerning the formation and evolution of the soft headlands, which considers the effects of shore platform elevation, beach morphodynamics and wave energy concentration (Chapter 2). All the methods used in the study are described in Chapter 3. The methods are divided into five categories, 3.1) Historical Shoreline Analysis; 3.2) Geological and Geotechnical Investigation 3.4) Wave Refraction Analysis; 3.5) Beach and Platform Morphology and Sediment Analysis and 3.5.4) Sediment Budget Calculations.

The methods are followed by the four main results Chapters, which are designed to address the first four objectives outlined in Chapter 1.2. The results of the geological and geotechnical assessment of the cliffs and platforms are presented in Chapter 4. The longshore distribution of wave energy is presented in Chapter 5 along with consideration of the influence of near shore bathymetry on wave refraction. The sediment distribution and longshore variations in beach and platform dimensions are presented in Chapter 6, as are the results of the sediment budget. The final results Chapter (Chapter 7) explores the coastal planform evolution of the southwest coast describing the recession rates around the headlands and considering the factors which appear to influence them. Chapter 8, the Discussion, aims to summarise and interpret the results of Chapters 4 to 7. Objective four, the refinement of the conceptual process based model described in Chapter 2, will also be addressed in the discussion. The generic lessons that can be taken from the work along with the opportunities for further work complete the Discussion. Finally the Conclusions of the project will be presented in Chapter 9.

2. Controls on Soft Rock Cliff Recession

Soft rock cliffs cover approximately 12% of the European coastline (Eurosion, 2004). Within the UK soft cliffs are wide spread and their erosion presents a significant threat to land use and development, especially on the south and east coasts of England (Lee and Clark, 2002). To understand how headlands form and evolve on a soft cliffed coast it is important to understand the coastal features and processes that influence cliff recession rates on an exposed coastline (for which the southwest Isle of Wight is an example). Coastal erosion of soft cliffs is a complex process, both episodic and stochastic, controlled by the balance between the resistive strength of the cliffs and destructive forces acting on them (Hall et al., 2002). A cliff's resistance to erosion is a function of its lithology, structure, morphology and the presence of a protective beach or shore platform (del Rio and Gracia, 2009). The erosive forces acting on a cliff can be defined as marine (waves, tides and sea level), and sub-aerial (rain, frost, ground & surface water, and gravity). In a marine-dominated environment, the cliffs will tend to be steeper than areas where sub-aerial processes dominate (Schwartz, 2005). On the open coast it has been found that geological material and exposure of the cliff toe are the critical factors in determining recession rates (Davidson-Arnott and Ollerhead, 1995, Jones and Williams, 1991, Trenhaile, 2009). Valvo et al. (2006), Limber and Murray (2011) and Dickson et al. (2007) also argue that changes in beach volume alongshore influence recession rates. The rate at which a cliff erodes is a reflection of the site specific conditions, which can vary spatially in both a cross-shore and longshore direction within a single study area (Lee, 2002).

The literature review presented below begins with a discussion of the cross-shore interactions between cliff recession rates and beach sediment and shore platforms, with the conclusions presented in the form of a conceptual model. The longshore interactions are then explored, looking at longshore variations in wave energy, sediment transport and lithology. The information gathered through the review of the cross-shore and longshore interactions leads to the refinement of the hypotheses of headland formation and evolution that are explored in this thesis.

2.1   Cross-shore Interactions

Research into cliff erosion has concentrated on the cross-shore interactions between the factors that control exposure of the cliff toe to the erosive power of waves, in particular how the presence and character of the shore platform and beach material interact and influence recession rates. The following Section (2.1.1) summarises the links between each of these features in turn, bringing them together into a conceptual model.

2.1.1   Shore Platform vs. Cliff Recession

Shore platforms fall under one of two morphological categories (Figure 2.1); Type A platforms that gently slope out to sea, and Type B platforms that are nearly horizontal, ending in a cliff or steep ramp at their seaward edge (Inkpen et al., 2004).
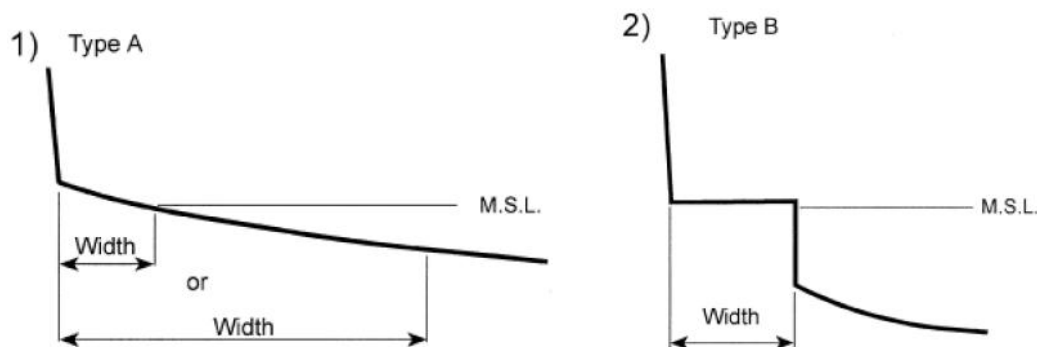
Figure 2.1: The two shore platform types; 1) Type A, gently sloping out to sea, and 2) Type B, near horizontal with a steep ramp or cliff at their seaward edge. Figure reproduced from Stephenson and Kirk (2000).

Shore platforms act to protect the cliff toe by attenuating wave energy. The efficiency with which a platform attenuates wave energy has been seen to vary with type (Ogawa et al., 2012). For example, wave energy was found to be reduced by up to five orders of magnitude when passing over the gently sloping (Type A) shore platforms of the Kaikoura Peninsula, New Zealand (Stephenson and Kirk, 2000). However, when studying wave attenuation over a Type B platform in Victoria, Australia Thornton and Stephenson (2006) reported a 10% to 40% reduction in wave energy. They suggested that in common with sandy beaches, shore platforms can attenuate wave energy in different ways, with Type A being more dissipative and Type B more reflective. Dissipation of wave energy is a

function of a number of key parameters, including shoreface gradient and abrupt changes in slope. In reality there is a continuum between Type A and Type B platforms.

The width and elevation of the shore platform are both important. Walkden and Hall (2005) found that the profile of soft rock cliffs and their associated shore platforms are in dynamic equilibrium where negative feedbacks regulate the erosional processes. For example, high recession rates create wider shore platforms reducing wave energy reaching the cliff toe thus slowing erosion rates (Dornbusch et al., 2008). Alternatively a period of excessive platform erosion or lowering will allow greater occurrence of wave attack at the toe, accelerating recession rates (Walkden and Hall, 2005). This relationship between wave attenuation and platform elevation and gradients means that cliff recession rates are controlled by the erosion of the intertidal and sub-tidal shore platform (Trenhaile, 2009). It is generally accepted that rates of cliff recession are directly linked to the rate of shore platform lowering (Walkden and Dickson, 2008). In fact Davidson-Arnott and Ollerhead (1995) stated that toe erosion exists in dynamic equilibrium with foreshore lowering. Platform lowering occurs due to its consistent exposure to the erosional power of the waves and weathering by sub-aerial processes (Trenhaile, 2009). These processes can be enhanced or moderated by the presence of sediment across the shore platform surface.

2.1.2   Shore Platform vs. Beach and Surficial Sediment

The size and existence of a beach on a shore platform is controlled by both the amount of available sediment, from cliff erosion and longshore sediment transport, and the relative beachface and platform gradients. The lithology controls the supply of beach grade sediment and the elevation of the shore platform. Since platform and beachface gradients tend to be rather similar, shore platforms are often unable to store much sediment (Trenhaile, 2004). That said, the erosion rate of tills and other cohesive substrates is strongly related to the presence/absence of mobile sediment (Skafel and Bishop, 1994, Thompson and Amos, 2004, Twidale et al., 2005). Surficial sediment can protect the shore platform from wave action, or work with it to abrade the platform surface (Davidson-Arnott and Ollerhead, 1995). Laboratory based experiments by Skafel and Bishop (1994) looked at till erosion under various sand conditions. It was concluded that thick or stationary layers of

sand protected the underlying platform while thin layers of mobile sediment produced the greatest erosion rates. In the absence of mobile sand, recession rates offshore of the surf zone are very small, but this is an unlikely situation in nature (Skafel and Bishop, 1994).

The thickness of the surficial sediment in relation to the sediment mixing depth, i.e. the depth on a beach where sand movement occurs, is a critical factor in the erosion of the underlying shore platform (Ciavola et al., 1997). The sediment mixing depth is related to the significant wave height, grain size and beach slope (Sunamura and Kraus, 1984), with the significant wave height and beach slope being the most important as they determine the type of breaker present (Anfuso, 2005). The mixing depth was found to be greater on steep beaches, being 20-40% of the significant wave height compared to 1-4% on gently sloping beaches (Anfuso, 2005). This is a result of the tendency of steep (reflective) beaches to produce a higher proportion of plunging breakers, where the wave's energy is dissipated over a narrow area compared to the slower energy loss across the gentle slope of a dissipative beach. Studies where platform erosion rates and sediment cover have been measured have failed to demonstrate a significant relationship between the two; this is thought to be due to the change in sediment thickness and mobility between low wave conditions, when measurements of thickness were made, and high wave conditions, when erosion occurs (Davidson-Arnott and Ollerhead, 1995).

2.1.3   Beach Size vs. Cliff Recession

A large beach will protect a cliff from erosion by preventing the waves reaching the cliff base or at least by dissipating wave energy and regulating the frequency of exposure (Lee, 2008). Various beach characteristics have been correlated with both temporal and spatial variations in recession rates including beach width, volume and elevation (Hapke et al., 2009, Jones and Williams, 1991, Lee, 2008, Moore and Griggs, 2002, Quinn et al., 2010). Having found that a 37m wide beach in East Sussex had failed to prevent erosion at the cliff toe, Dornbusch et al. (2008) suggested that the elevation of the beach compared to the high tide level was a more appropriate measure of the protection a beach provides. This suggestion supports work by Ruggiero et al. (2001) who developed a simple beach-cliff erosion model where cliff toe erosion can only occur when the combined tidal elevation and wave run-up is greater than the elevation of the cliff-beach junction (Figure 2.2).
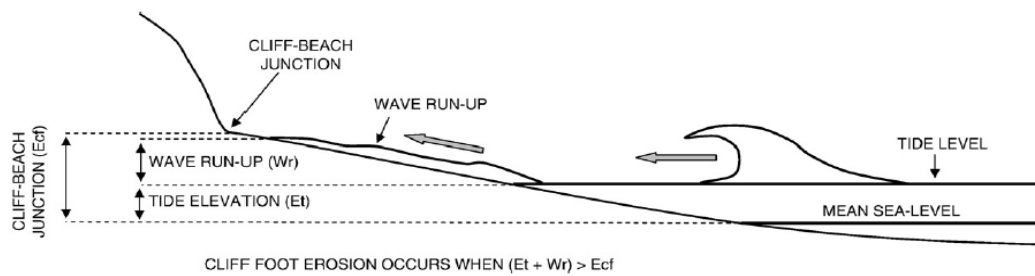
Figure 2.2: A simple beach cliff erosion model, as described by (Ruggiero et al., 2001)

Hence, it is the volume of beach material above mean high water that is most significant in protecting the cliff toe from erosion; Lee (2008) defined this as the Beach Wedge Area (BWA), an area described by a right angle triangle defined as the width and the maximum elevation of the beach above MHWS, assumed to be the elevation of the cliff/platform junction (Figure 2.3). A study by Wright (1970) found that for the majority of shore platforms around southern England, the platform cliff junction was between Mean High Water Neap and Mean High Water Spring levels, including those along the southwest Isle of Wight coast.
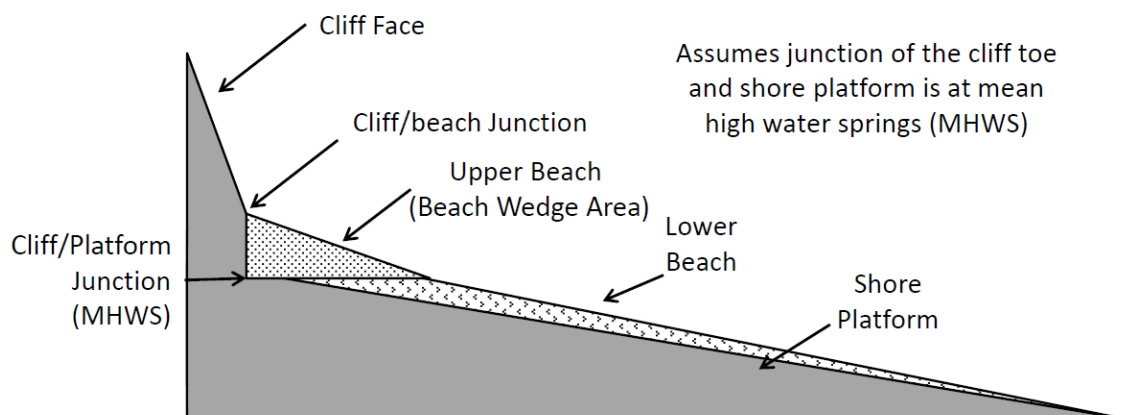
Figure 2.3: Definition of Beach Wedge Area (BWA) adapted from Lee (2008)

In a study of the Norfolk and Suffolk coasts, Lee (2008) found a non-linear relationship between recession rates and BWA, the former increasing as the latter decreased over a decadal timescale. The highest recession rates found in areas of low BWA (<20 $m^3\,m^{-1}$) also showed the greatest variability, while cliffs protected by a large BWA (>40 $m^3\,m^{-1}$) showed almost no recession with limited variability. This indicates that below a critical level, beach volume has little influence on the

recession rate and it is other factors such as wave climate, tidal levels and geotechnical considerations that control the recession rate. Interestingly the value of 20 $m^3\,m^{-1}$ for BWA, cited by Lee (2008) as the threshold at which erosion rates significantly increase was also suggested by Walkden and Dickson (2006) as the threshold value of beach volume, according to results gained using the SCAPE (Soft Cliff And Platform Erosion) model. The value of 20 $m^3\,m^{-1}$ was calculated for the Naze coast, Essex, but was later revised to 30 $m^3\,m^{-1}$ (Walkden and Dickson, 2008). In both cases the value represented the total beach volume not just that above MHWS so the values cannot be directly compared to the BWA results of Lee (2008) and Quinn et al. (2010). Although highly site specific, it seems that a threshold value of beach volume exists, below which recession rates are no longer significantly influenced by the beach.

2.1.4   Conceptual Model of Cross-Shore Interactions

Using the current understanding of how variations in shore platforms and beach levels can influence recession rates, described above, a conceptual model has been developed to show the cross-shore interactions of these three elements (Figure 2.4). There are a series of feedbacks operating simultaneously that regulate recession rates. An increase in recession rates will lead to an increase in the width of the shore platform, sediment supplied to the beach and hence beach levels. These consequences of an increased recession rate will protect the cliff toe from the force of the waves reducing the recession rate. This will reduce the supply of sediment, depleting the beach and surficial sediments leading to platform lowering and increased cliff toe exposure, accelerating the recession once more. The time scale over which this cycle proceeds is related to the magnitude of failure events (in terms of the talus produced that will protect the cliff base), the percentage of beach grade sediment in the cliff and the rate of longshore and on/offshore transport, which will be influenced by tidal levels, variations in the wave climate and the wave transformations over the offshore and near shore bathymetry.
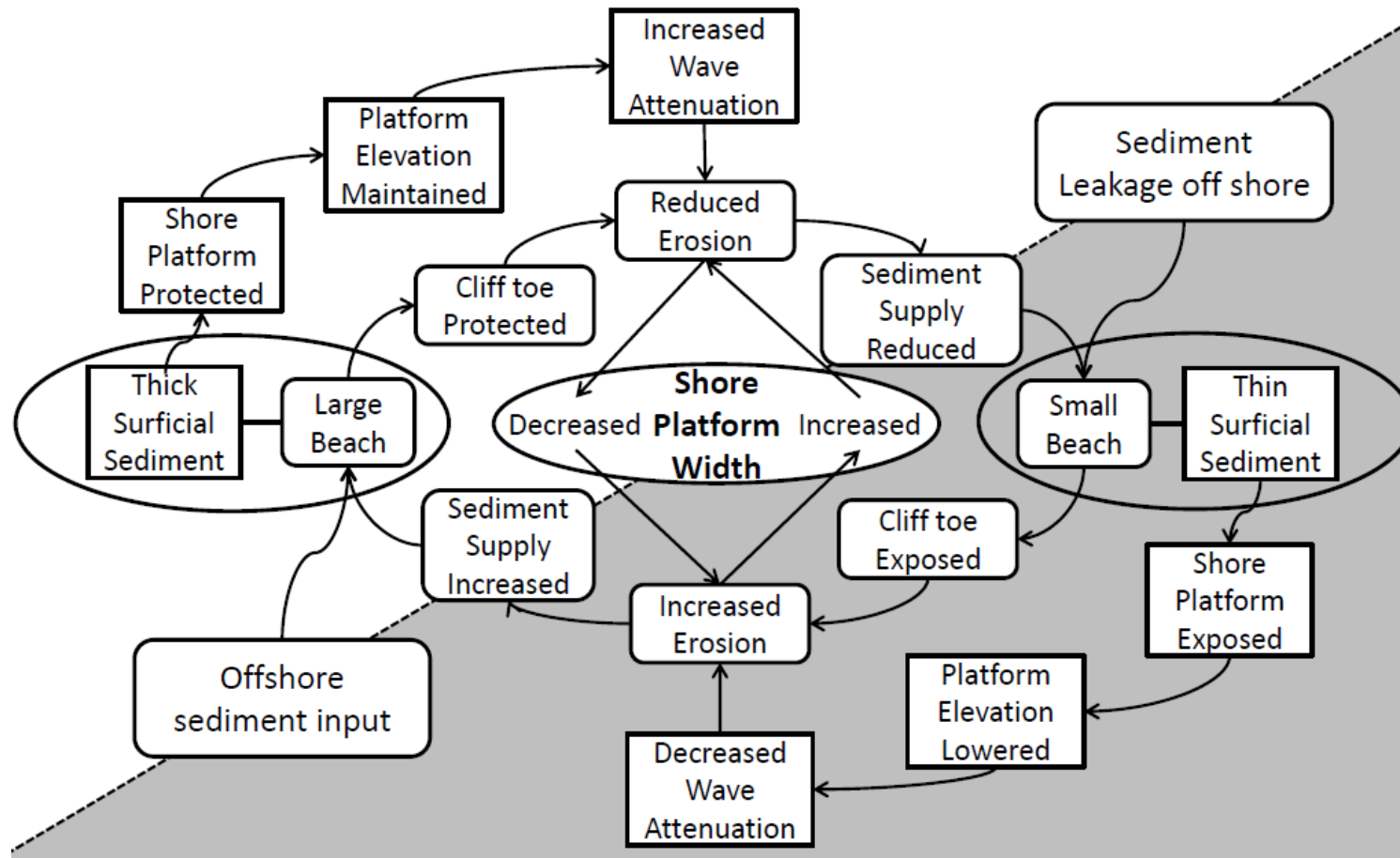
Figure 2.4: Conceptual model of cross-shore interactions between platform, beach and cliff recession on a soft cliff system. The rate at which this cycle proceeds is related to longshore and on/offshore sediment transport rates, the resistive strength of the cliff toe to erosion and the proportion of cliff material that will contribute to the beach.

2.2   Longshore Interactions

The literature has concentrated on the cross-shore interactions between incoming waves and shore platform and beach characteristics on coastlines of fairly uniform geology (Davidson-Arnott and Ollerhead, 1995, Dornbusch et al., 2008, Trenhaile, 2009, Walkden and Hall, 2005). The non-uniform nature of the geology of the southwest coast of the Isle of Wight and other similar coastlines makes investigation of longshore interactions and variations vital. A study of the Norfolk coast by Dickson et al. (2007) found that variations in sediment supply and longshore transport had a significant influence on longshore variations in downdrift recession rates, with erosion from one area allowing the build-up of protective beaches downdrift. This phenomenon was also described by Valvo et al. (2006). Changes in the angle of wave approach, and the related longshore sediment transport rates, were found to be more important than an increase in offshore significant wave height (Dickson et al., 2007). Since an increase in offshore wave height will generally lead to wave energy dissipation occurring further offshore, the effect is not seen at the shoreline, where as a change in wave angle can lead to an increase or decrease in longshore sediment transport rates. Understanding the impact of longshore variations in platform elevation on wave refraction and sediment transport was an integral part of this research.

2.2.1   Wave Transformations and Sediment Transport

As waves approach a shoreline through shallow water and pass over a non-uniform surface, transformations will occur changing the direction and intensity of those waves, a process known as refraction. Waves slowdown in shallow water causing the wave orthogonals to bend towards/away from shallow/deep areas respectively (Sunamura, 1992). In practice this will lead to wave energy being focused towards headlands where shore platform elevation tends to be greatest, and dispersed along bays helping to smooth the coastal planform over time. This theoretical distribution of wave energy was the basis for two papers investigating headland erosion. The first by May and Tanner (1973) was based on the littoral transport potential driven by variations in the wave energy distribution, i.e. sediment will be transported from the area of highest wave energy (i.e. the headland) to the area of lowest wave energy (i.e. the bay head) (Figure 2.5).The change in the rate of

longshore transport is greatest on the flanks of the headland (b), this relates to the greatest erosion potential (May and Tanner, 1973). Therefore the maximum erosion occurs on the flanks and the minimum erosion will take place at the headland itself leading to the formation of a needle like promontory (Figure 2.5a). This model assumes the headland acts as a transport divide, the patterns shown in Figure 2.5 are mirrored on both sides of the headland.
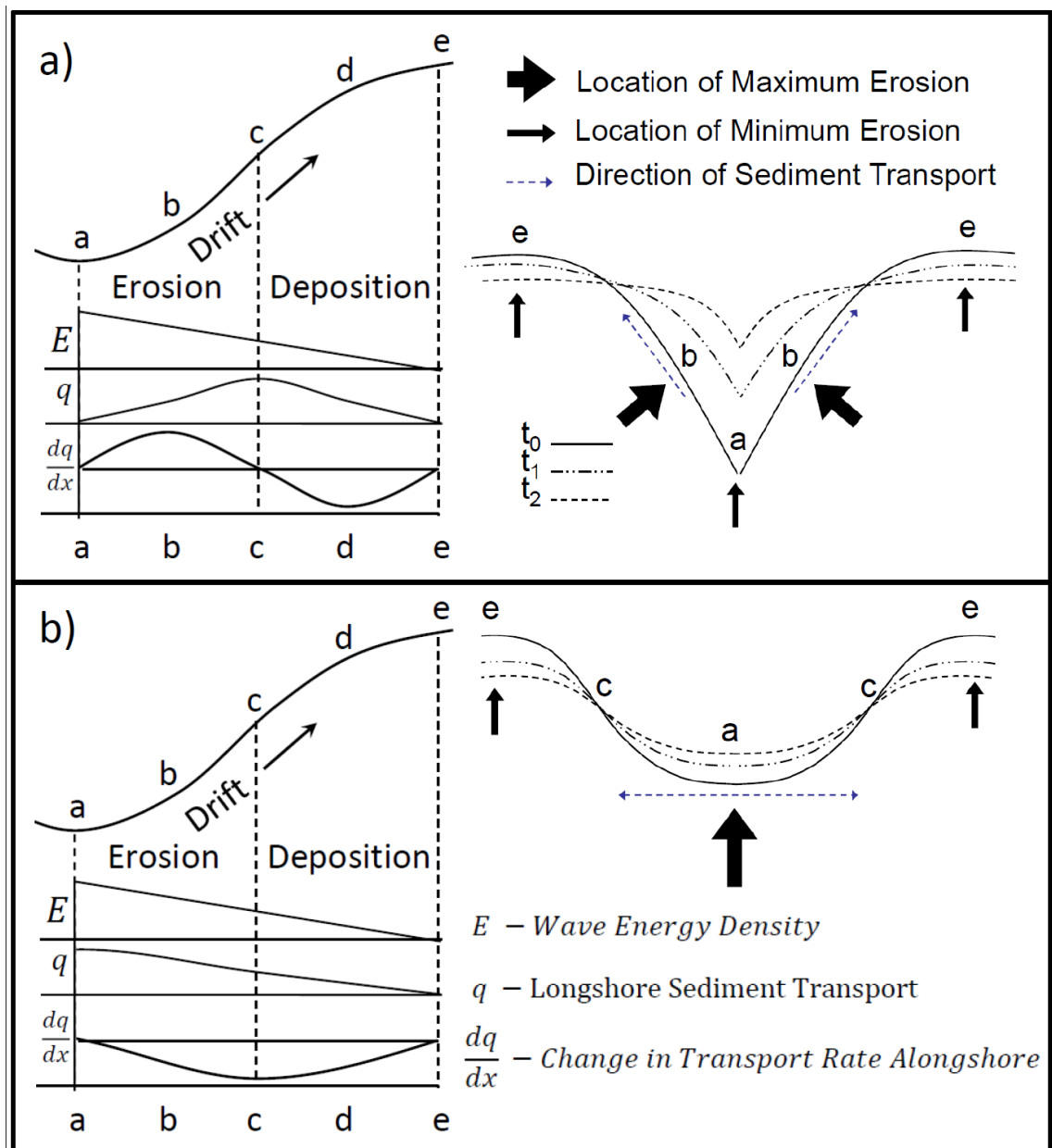
Figure 2.5: a) The May and Tanner (1973) and b) the Komar (1985) models of headland erosion. Graphs show theoretical changes in wave energy density (E), longshore transport rates (q) and the change in transport rates alongshore (dq/dx) between the headland (a) and the bay head (e). The arrows show the location of maximum and minimum erosion and the direction of longshore transport.

The second model by Komar (1985) suggested that maximum erosion would be at the headland as it was subject to maximum wave energy due to refraction, leading to the formation of a subdued headland, but did not necessarily view the headland as a transport divide so eroded material would be carried away from the headland (Figure 2.5b). Both models assumed that the material eroded from the headlands would be deposited in the bays where wave energy and transport potential is lowest, leading to a reduction in the indentation of a bay as the beach builds up to protect the bay head and the headland remains exposed. Carter et al. (1990) compared the two models and found that there was room for both theories. Within the study area on the Isle of Wight both the rounded headland (e.g. Sudmoor Point) and the pointed headland (e.g. Hanover Point) can be seen (Figure 2.6). Although not thought to be a major transport divide, a localised reversal in sediment transport direction has been predicted by Rix (2000) at Hanover Point but not at Sudmoor Point. This may have some influence on the shape of the headlands, though the extent and character of the shore platform is also important.

Figure 2.6: Aerial photograph showing the rounded headland at Sudmoor Point and the pointed headland at Hanover Point

2.2.2   Beach Levels, Littoral Drift Barriers

It has been noted that longshore variations in beach levels can have a significant effect on cliff recession rates (Jones and Williams, 1991, Quinn et al., 2010, Lee, 2008). So called, "hot spots" of erosion along the Californian coast were seen to coincide with locally reduced beach levels (Hapke et al., 2009, Moore and Griggs, 2002). In general local beach levels are controlled by the supply of sediment from cliffs, fluvial inputs, off shore sources and by longshore transport rates removing that sediment (Kana, 1995, Limber et al., 2008). The use of retaining structures to maintain beach levels has been common place since the mid-19th Century, and has

brought with it the problem of down drift erosion also known as the terminal groyne syndrome (Brown, 2008). It is possible that naturally occurring intertidal shore platforms and subtle headlands could act as a natural barrier to longshore transport starving the down drift coast of sediment while building up a protective beach updrift. The consequences of this reduction in sediment supply down drift is a diminished beach that offers little protection to the cliff toe from the action of waves and thus increased recession rates (Brown and Barton, 2007). The possibility of shore platforms acting as a transport barrier will be explored as part of this research.

2.2.3   Lithology

The lithology of a cliff will influence recession rates in two ways. The primary control is the geotechnical properties and strength of the lithology, i.e. its resistance to erosion. The second is a more indirect influence related to its role as a source of beach grade sediment. Cliffs with a high proportion of beach grade material may lead to the build-up of a protective beach which regulates recession rates. In soft rock clay cliffs the magnitude of erosion is controlled by the shear strength of the cliffs and the resistance to erosion. The shear strength controls the formation of landslides and slumps while resistance to erosion is a function of grain size (finer sediment, i.e. clays, being held together by electrostatic forces), unit weight and water content (Gelinas and Quigley, 1973). Davidson-Arnott and Langham (2000) found that the resistive strength of clay rapidly increased with depth, corresponding to a decrease in water content. Softening of the cohesive material by the addition of water allowed direct erosion by wave-induced shear stress (Davidson-Arnott and Ollerhead, 1995).

Although geological factors are thought to be as important as climatic and wave conditions in determining the shape of the cliff profile, it has proved difficult to identify significant spatial variations in long term recession rates that correlate with variations in geology (Jones and Williams, 1991). One consideration that could explain the difficulty of identifying trends caused by factors such as geology is the spatial sampling interval. If the spacing of survey lines is too great then variations in recession rate may be missed. For example the erosion post system in place along the Holderness coast cannot record spatial variations in recession rate at scales less than 500m compared with the 10-20m length of individual failures (Lee,

2002). This issue is being addressed with the emergence of Terrestrial Laser Scanner (TLS) techniques in recent years (Quinn et al., 2010, Poulton et al., 2006) however these measurements only represent short term erosion rates at this time. Moore and Griggs (2002) found that despite the considerable variation of lithology along the Monterey Bay coastline the long-term recession rates for much of the coast fell between 7 and 15 cm a^{-1}. The areas where recession was higher coincided with structural weaknesses or jointing in the cliff, along with narrow beaches. It appears that variations in lithology over the long-term had little influence on the recession rate.

The uniform nature of recession rate in the longshore could be a result of the variations in wave loading along a coastline caused by the emergence of headlands and bays. The more resistant headlands will experience higher wave loading due to the refraction of wave orthogonals towards them, while the less resistant bays experience lower loadings as the wave energy is spread out across the bay. In this situation the difference in rock strength is balanced by the difference in wave loadings, the planform is maintained and recession rate is uniform along the coast (Schwartz, 2005). Valvo et al. (2006) considered the effects of variations in lithology alongshore on recession rates and found that longshore transport of sediment filled in indentations resulting from weaker or fine grained lithologies, protecting the cliffs and reducing recession rates, leading to a uniform alongshore retreat rate in the long-term. This self-regulation of long-term recession rates by coastal planform and beach evolution may explain why lithology is difficult to correlate with changes in recession rate measured from historic maps and photos, particularly on sediment rich coastlines. Therefore the influence of lithology on recession rates will be most significant on sediment starved coastlines where beach volumes are small.

Areas where 'hotspots' emerge may be the result of a lateral change in the lithology exposed as the cliff retreats, upsetting the balance of energy, or are perhaps areas where inherently weak strata outcrop causing landslide activity. Studies by Benumof and Griggs (1999); Dornbusch et al. (2008) and Rust and Gardener (2002) did conclude that spatial variations in recession rates could be explained by variations in the lithology of the cliffs. Structural weaknesses such as faults and joints are often exploited by waves and suffer accelerated erosion rates (Moore and Griggs, 2002). These localised changes in recession rate can be both ephemeral and

persistent features over time. The nature and scale of the change are important considerations, along with feedbacks of sediment distribution and wave refraction changes. If ephemeral, feedbacks will act to regulate variations in recession rates. If persistent these variations will be expressed in a change in the coastal planform.

2.3   Headland Formation

Typically headlands form along a coastline where discordant geology is exposed, rocks of different strengths erode at different rates, leading to the formation of headlands and bays in areas of relatively high and low rock strength, respectively. The indentation of the coastline will increase until longshore variations in beach volume and the refraction of wave energy towards the headlands effectively cancels out their greater resistance to erosion (Valvo et al., 2006). At this point the erosion rate is expected to become uniform across both headlands and bays maintaining that level of indentation (Schwartz, 2005). The apparently uniform cliff strength of the soft rock cliffs such as those found on the southwest Isle of Wight mean that the subtle headlands formed on these coastlines must differ from the model described above in both their mode of formation and their evolution, with the shore platforms playing a more significant role. The hypothesis outlined below, is based on the current understanding of the cross-shore and longshore interactions between shore platforms, beaches and recession rates outlined in Sections 2.1 and 2.2.

Shore platform elevation has been shown, in a study at Lake Ontario, Canada, to be one of the major controlling factors in cliff recession rates (Davidson-Arnott and Ollerhead, 1995), it is hypothesised that the local shore platform elevation and lithology, not that of the cliff material, is responsible for the reduced erosion rates in these situations. As recession proceeds on a coastline, laterally discontinuous beds can emerge and disappear, creating and withdrawing the intertidal platform. Figure 2.7 describes the influence that a newly created shore platform may have on localised recession rates. Where established, the platforms will potentially act in three ways:

- Firstly by reducing the amount of wave energy reaching the cliff base, thus reducing local cliff recession rates (Stephenson and Kirk, 2000) (Figure 2.7.a).

19

Legend

- Sea
- Beach
- Cliff Top
- Cliff Face
- Resistant Platform Forming Bed
- ⎯·⎯·⎯ Initial Cliff Position
- → Direction of Longshore Transport
- ⟹ Wave Energy Reaching the Cliff Base

Changes over time
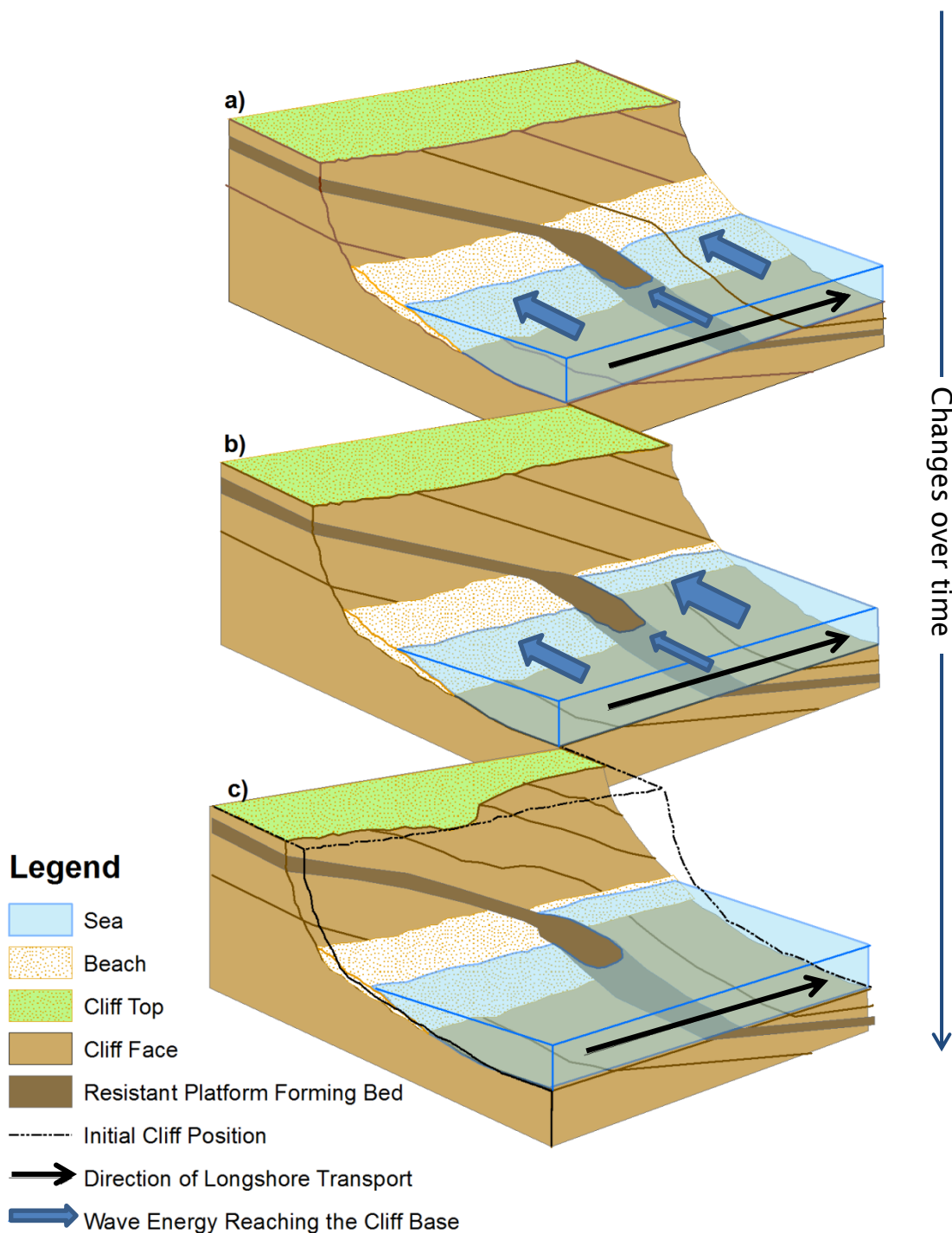
Figure 2.7: Schematic showing the hypothetical influence of an intertidal platform on headland formation over time. Panel a) indicates the reduction in wave energy reaching the cliff base due to the presence of the resistant platform. Panel b) demonstrates the potential of an intertidal platform to block longshore transport and the influence that may have on wave energy reaching the cliff base. Panel c) shows the result of the variation in wave energy reaching the cliff base may have on the coastal planform evolution, leading to the formation of a subtle headland.

- The second may counteract the first by increasing the wave energy directed at the cliff base due to refraction, the balance between these two effects will determine if a headland will grow, be maintained or decline (Figure 2.8).

- Thirdly by blocking longshore transport of beach sediment, building a protective beach up-drift, while starving the downdrift coast of sediment, potentially accelerating erosion in the manner of terminal groyne syndrome (Brown, 2008, Brown and Barton, 2007) (Figure 2.7.b).

If this hypothesis is correct then the highest rates of recession should be found downdrift of the shore platform/headland while the lowest rates would be expected at the platform/headland itself (Figure 2.7c). This pattern of recession would then lead to the formation of a subtle headland, as outlined in Figure 2.7.

2.4   Headland Evolution

Once a headland is formed, the increase in wave energy directed towards the platform/headland due to refraction may lead to increased erosion at the headland. This will limit the formation of prominent headland and bay features and maintain the subtle nature of the headlands through a dynamic equilibrium. The balance of forces involved in the formation, maintenance and erosion of these subtle headlands is described in Figure 2.8.

Refraction Dominated   *Balanced*   *Attenuation Dominated*

$\Delta E_R > \nabla E_A$ $\Delta E_R = \nabla E_A$ $\Delta E_R < \nabla E_A$

Headland Declines   *Headland Maintained*   *Headland Grows*
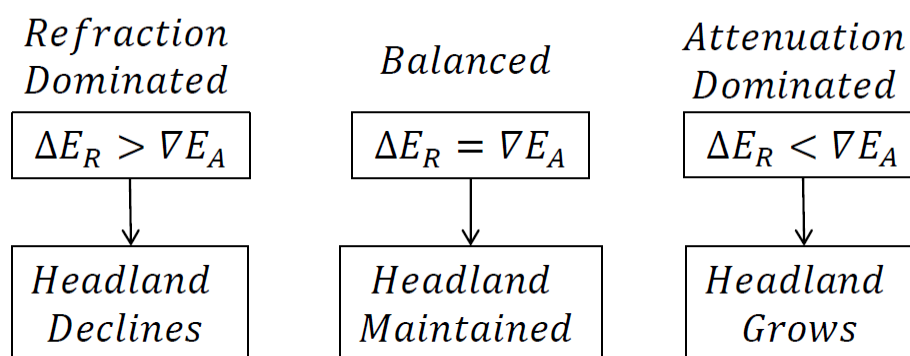
$\Delta E_R = Change\ (increase)\ in\ wave\ energy\ due\ to\ refraction$
$\nabla E_A = Change\ (decrease)\ in\ wave\ energy\ due\ to\ attenuation$

Figure 2.8: Conceptual diagram showing how the relationship between refraction and attenuation of waves over the shore platform can control the stability of a headland.

Essentially, if the increase in wave energy reaching the cliff base due to refraction is greater than the reduction in wave energy reaching the cliff base due to attenuation then the headland will decline. If the situation is reversed and the effects of attenuation outweigh those of refraction then the headland will grow. Since it appears to be the elevation of the shore platform relative to sea level that controls the refraction and attenuation of wave energy, it is important to be able to predict how that may change as the coastline erodes. The lateral continuity of the platform producing bed is crucial to the maintenance of the platform. If the bed thins or disappears in the intertidal zone as the cliff erodes, its influence is reduced and eventually removed allowing recession to continue at a higher rate.

Another consideration in terms of headland evolution is the strike of the beds in relation to the coastline. If the strike of the platform forming bed is not perpendicular to the overall coastal orientation as it recedes the platform, and therefore the headland, may migrate with time. Figure 2.9 shows two hypothetical headlands fronted by shore platforms striking at an angle of 50° and 130° from the general shoreline orientation, respectively. In both cases lateral continuity of the beds is assumed. In the first instance the migration of the headland is down drift (assuming left to right sediment transport), while in the second the migration is updrift. A similar effect could be seen with a rise in sea level altering the "intertidal level" and the location where the platform forming bed interacts with marine processes.
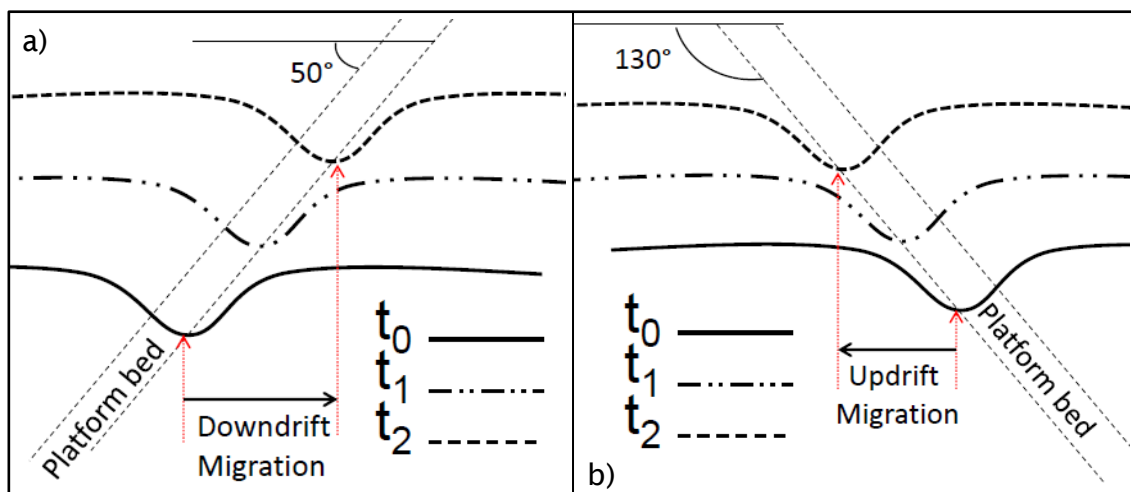
Figure 2.9: Diagram showing the potential migration of two theoretical headlands between t_0 and t_1, assuming the thickness and strike of the platform forming beds remain uniform as the cliff erodes.

If the platform forming beds are not laterally continuous this could result in the loss of a headland over time as the platform forming bed is eroded, similarly if a platform forming bed emerges through cliff recession a new headland may form over time.

2.5   Summary

In simple terms, the driving force of cliff recession is the exposure of the cliff toe to the erosive power of waves versus the strength of the cliff. It is the interaction of a number of factors that control the exposure of the cliff toe including beach and shore platform parameters, i.e. their width, elevation and volume. The geological and geotechnical characteristics of the cliffs and shore platform control the resistance of the cliff toe to erosion. It is the cross-shore and longshore interaction between the beach, shore platform and cliff that control the localised rates of cliff recession and consequently the formation and evolution of headlands. Over long time scales the variations in recession rate due to slope processes/cliff morphology become decreasingly significant. The impact these effects have on local recession rates and the formation of the subtle headlands will be an original contribution to this field of research.

The formation and evolution of subtle headlands such as those seen on the southwest coast of the Isle of Wight appears to be controlled by the presence and character of localised intertidal shore platforms. Headlands will form behind an intertidal platform whose elevation and extent is great enough to significantly reduce cliff recession rates through wave attenuation and in some cases by building a protective beach updrift by blocking longshore transport. Once formed, the fate or evolution of the platform related headland is controlled by the balance between wave refraction and wave attenuation, and the lateral continuity and strike of the platform forming beds compared to the orientation of the coastline. Understanding the processes involved in the formation of intertidal platforms and related headlands, and predicting the future of these headlands, using the southwest coast of Isle of Wight as a case study, will form the basis of this research. Further investigation of the different controlling factors such as structural geology, geotechnical strength, wave refraction and attenuation, sediment budgets and beach morphodynamics are required to develop an understanding of the role of these individual factors and how they might interact.

The aim of this research is to evaluate the controls on headland formation and evolution on soft rock, cliffed coasts. Headland formation and evolution is controlled by variations in recession rates. From the literature review outlined in this chapter it was found that cliff recession and the factors controlling it represent a coupled system. So it is necessary to consider a number of factors and how they interact to fully understand the system as a whole. The areas requiring study defined in the aims and objectives include: 1) the geological and geotechnical properties of the cliff and platform; 2) longshore variations in wave energy distribution; 3) beach sediment volumes and supply; and 4) historical recession rates. A number of methods are required to investigate these controls and their influence on recession rates; these are described in detail in Chapter 3. They include the analysis of long term recession rates to determine the influence of the controls and as part of the calculation of sediment supply. Mapping the cliff face and platform geology is necessary for both the geological investigation and as an input to the sediment supply calculations. Similarly sampling and analysis of the beach sediment is required for the sediment supply calculations and will provide an insight into the beach morphology. Wave refraction analysis provided information on the longshore distribution of wave energy in relation to the headlands along the study frontage. The methods used in this study take a broad look at each factor to determine their importance, with no single factor studied in great detail. This will highlight the areas requiring further research.

3. Methods

Given that Chapter 2 demonstrated the need for an integrated approach to the study of this coupled cliff system, a broad range of methods must be utilised to study the different system components. The research methods required for this study are both varied and interconnected. Completion of one aspect is not always possible without the results of another. This Chapter begins with a detailed research design (3.1) followed by an overview of all the data used in the study (3.2). Only then are the methods used described in detail.

3.1 Research Design and Data Overview

The methodologies used in this study are directly related to the first three objectives outlined in Section 1.3.2. The first is concerned with the geological and geotechnical properties of the cliffs and platforms, the second considers the longshore distribution of wave energy, and the third is concerned with beach volumes and the sediment budget. In addition each of these objectives also refers to the influence these factors have on cliff recession rates. On this basis the methods can be divided into six categories:

1) Historical Shoreline Analysis. Can be divided into two categories, pre 1866 when maps are only able to provide an insight into previous coastline configurations, and post 1866 where recession rates can be measured directly from maps and surveys for comparison with the factors outlined in the objectives and to study headland formation and evolution (Section3.2). The results are also used in the sediment budget to calculate the sediment input form the cliffs (Section 3.6).
2) Geological and Geotechnical Investigation. Involves mapping of the cliff face and platform in terms of lithology, morphology and coherence. Consideration of the mass properties, clay mineralogy and particle size distribution of the cliff material was also made (Section 3.3). The results of the lithological mapping and particle size distribution are also used in the sediment budget to calculate the beach grade sediment input from the cliff (Section 3.6).
3) Wave Refraction Analysis. Calculates the distribution of wave energy along the shoreline (Section 3.4). Results are also used in the sediment budget to calculate potential longshore sediment transport.

4) Beach and Platform Morphology and sedimentology. Involves sampling of beach sediment and considers the beach sediment particle size distribution, beach width and volume, and platform width and elevation (Section 3.5). The results of the beach sediment PSD are also used in the sediment budget to calculate the beach grade input of cliff sediment (Section 3.6)

5) Sediment Budget Calculation. Utilises the results from the previous methodologies as outlined above to produce a sediment budget (Section 3.6)

6) Multivariate Statistical Analysis. A Principal Component Analysis carried out on all results to determine the dominant controls on recession rates and therefore coastal planform evolution.

A number of pre-existing datasets are used within the study. Their sources, errors, and application within the study methodology are summarised in Table 3.1. Each data set is described in more detail in Sections 3.1.1 to 3.1.6

Table 3.1: Summary of the pre-existing data sets used in this study including the source, errors and use/limitation to use. N.b. CCO – Channel Coastal Observatory.

Data	Source	Errors	Use in Thesis
OS Map 1866, 1909, 1946, 1975	Digimap	± 5m	Recession rates, beach width, platform width, morphology
OS Map 1981	Digimap	± 5m	Platform area
Aerial Photo 2001,2005,2008	CCO	± 5m	Aid in BWA calculations. Beach Width
LiDAR 2004-5 and 2007-9	CCO	Vertical ±0.15m Horizontal ± 0.4m	All years - BWA calculations. 2007 - Wave model bathymetry and cliff top elevation for cliff sections. Does not extend below MSL and cannot distinguish between sediment and platform so unsuitable for platform elevation measurements
Swath Bathymetry 2010	CCO	Unknown	Wave model bathymetry
Bathymetry contours 2000	Admiralty Chart SC5600.2	Unknown	Wave model bathymetry
NRA/EA Profiles	IOW Council	n/a	Platform elevation. Does not extend to the cliff beach junction and has no information on distance of start point for cliff beach junction so cannot be used for BWA calculations

3.1.1 Historic Maps

Historic Ordnance Survey (OS) maps are used in the historic shoreline analysis to calculate recession rates. They are also used to measure past beach and platform widths and to study cliff morphology, headland formation and evolution. The historic maps dating back to 1866 were created by the Ordnance Survey and made available by the online resource "Digimap". This study uses a series of 1:2500 OS Maps from 1866, 1909, 1946 and 1975. Pervious work into mapping errors has provided estimates ranging from ± 2-3 m (Dornbusch et al., 2008) to ± 10 m (Brown, 2008, Esteves et al., 2009). Table 3.2 contains a summary of the error estimates used in various studies. A number of the studies in Table 3.2, including Crowell et al. (1991); Esteves et al. (2009) and Taylor et al. (2004) have given the error of mean high water (MHW). According to Moore (2000), using MHW as a proxy for shoreline position leads to errors due to natural migration within seasons and tidal cycles. The errors quoted by Brown (2008) were based on the approach of Crowell et al. (1991) who calculated the "worst case" errors.

Table 3.2: Summary of errors quoted for historical maps used in the literature

Author and date of publication	Shoreline position Indicator	Errors (m)
Brown (2008)	Cliff top	± 10
Crowell et al. (1991)	MHW	± 8.4 (pre-1940) ± 6.1 (post-1940)
Dornbusch et al. (2008)	Cliff top	± 2 – 3
Esteves et al. (2009)	MHW	± 10
Nicholls et al. (2000)	Cliff top	± 10
Stuiver (2010)	Cliff top	± 5 (calculated from fixed points on maps of the southwest IOW)
Sutherland (2012)	Cliff top	±2.6 – 3.47
	MHW	± 6 – 10
	MLW	±14 – 37
Taylor et al. (2004)	MHW	± 5 (pre-1945) ± 3.5 (post-1945)
Valentin (1954)	Cliff top	± 3

The scale has a large impact on the precision of measurements, e.g. 1 mm on a map can represent 20 m, 10 m or 2.5 m on 1:20,000, 1:10,000 or 1:2500 scale maps, respectively (Lee and Clark, 2002). All the papers in Table3.2 except Brown (2008) and Stuiver (2010) use small scale maps (i.e. 1:10,000 to 1:20,000). This study, like Stuiver (2010) uses large scale maps (1:2500) to minimise errors.

The three main sources of error associated with the use of historical maps and aerial photographs are outlined below (Lee and Clark, 2002):

1) Plotting Errors: The positional accuracy of defined objects on an OS maps can be as little as ± 0.8 m, although inaccessible features may not be plotted so accurately.

2) Interpretative Errors: These result from misinterpretation of a feature in the original survey and subsequent use, for example the position of the cliff top could be obscured by vegetation (Figure 3.1)

3) Distortion Errors: Caused by damage to maps in storage, e.g. shrinkage or distortion, or distortion during georectifying to national grid in a geographical information system (GIS)
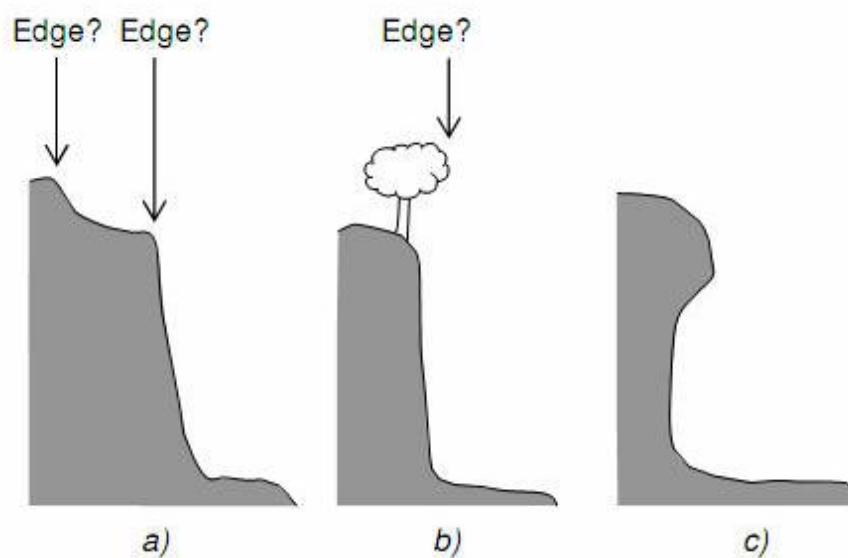
Figure 3.1: Potential errors when defining cliff top line. A) Geometric profile makes an uncertain edge; b) Vegetation obscures cliff top line; c) Undercutting of cliff (Gulyaev and Buckeridge, 2004, Anders and Byrnes, 1991).

Plotting and interpretative errors will occur at the time of production, interpretative errors can also occur when digitising the map in a GIS. The distortion errors are a result of post-production issues. The potential errors associated with both production and post-production are listed in Table 3.3 and Table 3.4 respectively.

Table 3.3: Potential sources of errors during map production. List compiled by Brown, 2008 from Anders and Byrnes (1991), Carr (1962) and Oliver (1996)

1. Imprecise copying from one map to another.
2. Map interpretation.
3. Survey methods employed.
4. Misleading cartographic evidence.
5. Accidental errors.
6. Partial revision and mistakes not corrected from one survey to the next.
7. Geographical features not present when map published or vice versa.
8. Misleading dates of survey or publication dates, or a large range of dates.
9. Lack of understanding of changes on maps.
10. Compromise between time spent on mapping and the importance of the area.
11. Difficulty in mapping low tide.
12. Exaggeration of features, displacing true position of coast to emphasise minor promontories.
13. Map irregularity on different scales and transference of maps to different scales.
14. Hachuring (attempting to give a 3D illustration in a 2D medium).
15. Maps symbolically rather than architecturally correct.
16. Changes in horizontal datum.
17. Pen thickness and annotation errors.
18. Survey and digitiser error.

Table 3.4: Potential sources of error in maps post production. List compiled by Brown, 2008 from Anders and Byrnes (1991); Crowell et al. (1991); Moore (2000)

1. Scale changes.
2. Stretching and shrinking in different directions.
3. Change in survey standards.
4. Change in publication standards.
5. Change in photographic methods.
6. Map projection.
7. Tears.
8. Folds.
9. Creases.

The error on the maps use in this study was calculated by comparing the position of fixed points, such as churches, on the maps used. The RMS error on the movement of these fixed points was calculated at 4.6m and was rounded up to 5m for use in this study.

3.1.2   Aerial Photographs

Aerial Photographs were provided by the Channel Coastal Observatory (CCO) from 2001, 2005 and 2008. Within this study they are used to aid the calculation of Beach Wedge Area, a measure of beach volume (Section 3.5.4), by identify the cliff beach junction. The 2008 photographs were also used to measure beach width. Error estimates for aerial photographs quoted in the literature range from ±0.2-0.3m by Dornbusch et al. (2008) to ±15m by Esteves et al. (2009) (Table 3.5).

Table 3.5: Summary of errors quoted for aerial photographs from the literature

Author and date of publication	Errors (m)
(Brown, 2008)	±10
(Crowell et al., 1991)	±7.7
(Dornbusch et al., 2008)	±0.2-0.3
(Esteves et al., 2009)	±15

Aerial photographs do not have plotting errors associated with them, but are equally open to interpretation errors as described in Figure 3.1. Plotting errors are replaced by the errors caused by variations in the tilt of the camera and variations in scale between photographs due to changes in altitude (Crowell et al., 1991). Table 3.6 summarises the distortions associated with aerial photography, Figure 3.2 visualises how camera tilt and changes in relief can create errors in aerial photographs. The errors on aerial photographs used in this study was calculated in the same way as the mapping errors, i.e. my measuring the displacement of fixed points such as churches between successive images. This produced and estimate of errors for aerial photographs of ±2.5 m.

Table 3.6: Distortions associated with aerial photographs. List compiled by Brown (2008) from Anders and Byrnes (1991); Crowell et al. (1991); Moore (2000); Lee and Clark (2002)

Image space distortion - lens distortion
1. Radial distortion due to imperfections in the lens element. Distorts image on long radial lines from the principle point.
2. Tangential distortion caused by faulty centring of the camera lens. Distorts image rectangles to radial lines from the principle point.
Image space distortion - film deformation
3. Buckling of film in camera with changes of humidity, temperature or film spool tension.
4. Buckling, shrinking or stretching of film during processing.
5. Instability of photographic media once image has been printed.
Object space displacements - displaced objects from the true position
6. Ground relief - objects above ground level are displayed outwards from the centre.
7. Aerial camera tilt - Near vertical images have a different scale.
8. Atmospheric refraction - depends on flight altitude, camera focus length and direction of optical axes relative to the ground.
9. Scale difference - results in change of altitude, from one photograph adjacent to the next.
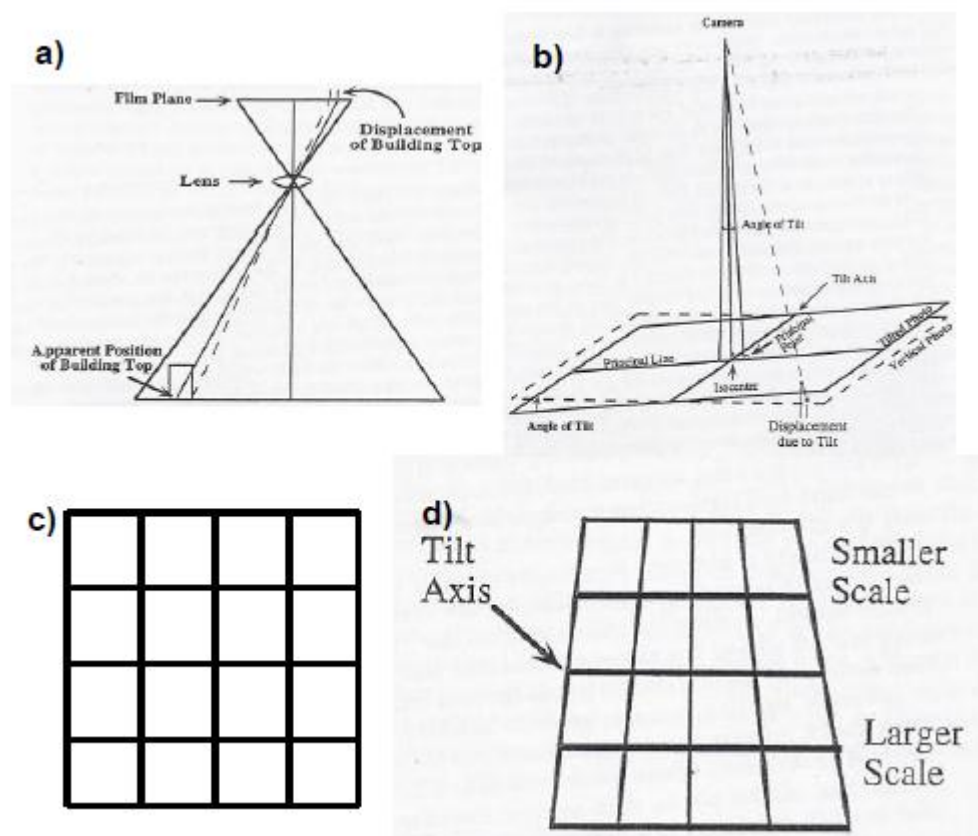
Figure 3.2: Errors in aerial photography occurring due to distance from the centre of the photograph and any slight tilt in the camera. a) Relief displacement, causing objects above the ground to be displaced toward the edge of the photograph; b) Any slight tilt of the camera from vertical will displace objects from their true position; c) on an untilted photograph the scale is uniform, d) tilted photograph, the scale is reduced on the down tilt side and increased on the up tilt side. Taken from Moore (2000)

3.1.3   LiDAR

LiDAR data covering the study site were made available from the Channel Coastal Observatory (CCO) for 2004, 2005, 2007, 2008 and 2009. All data was used to calculate the BWA. The 2007 data set was used in the wave model bathymetry for elevations above 0m and for cliff top elevations in the geological cliff sections. It was hoped to use the LiDAR data to determine platform elevation, however the difficulty of identifying sediment from platform in the data and the timings of the data collection (i.e. mid to high tide) this was not possible. The errors associated with the LiDAR are ±0.15m in the vertical and ±0.4m in the horizontal. Data is relative to Ordnance Datum Newlyn.

3.1.4   Swath Bathymetry

Swath bathymetry for the study area to approximately 1km off shore was surveyed in 2010 by CCO. The data was used to build the bathymetry in the wave model. Data is relative to Ordnance Datum Newlyn.

3.1.5   Admiralty Charts

The remainder of the bathymetry for the wave model extent not covered by the LiDAR or swath bathymetry was filled in with the contours digitised from the Admiralty Chart SC5600.2 The bathymetry contours are at Chart Datum and were converted to Ordnance Datum Newlyn for use in the model.

3.1.6   Beach Profiles

A series of beach profiles recorded by the National River Authority (NRA) and Environment Agency (EA) between 1991 and 1998 were made available by the Isle of Wight Council. Figure 3.3 shows the profile locations. Initially it was planned to uses these successive profiles in conjunction with LiDAR data from CCO to measure changes in beach volume over time for the sediment budget. However the data did not extend to the cliff beach junction and did not include information on the distance of initial measurements from the cliff beach junction. Therefore the data was not suitable for BWA calculations. However the profile locations were used across the study for consistency between results. Uses included; sampling

locations for beach sediments, dividing lines in the geological cross sections; and to extract LiDAR data for BWA calculations.
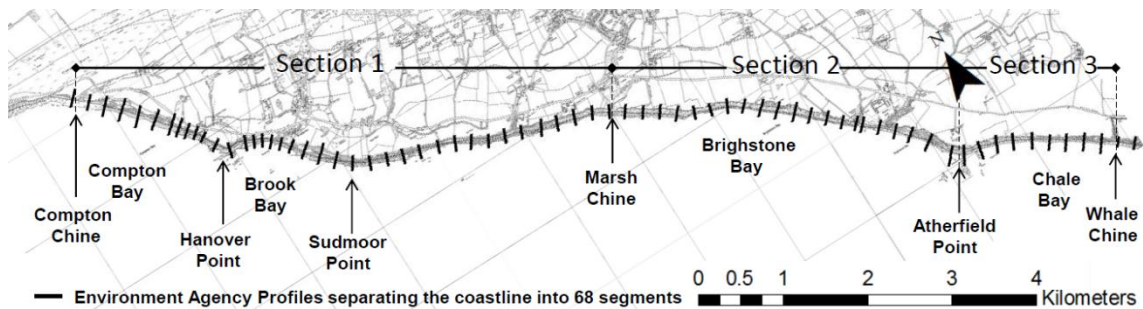
Figure 3.3: Location of the Environment Agency beach profiles used as beach sampling locations

3.2 Historical Shoreline Analysis

3.2.1 Shoreline Analysis pre-1866

The first reliable maps were produced by the Ordnance Survey (OS) as part of the County Series, which later became the National Grid Series. Prior to this maps were produced on an ad hoc basis. These maps are not accurate enough to be used to calculate recession rates but can provide an insight into changes in the coastline configuration. In particular the persistence of the subtle headlands which are the focus of this study. A large number of maps are available but four were chosen. One for each century, the details of these maps are displayed in Table 3.7.

Table 3.7: Maps available prior to 1866. Information includes the year or period of production and the cartographers involved in their production. The source website of each map is shown, see reference list for full URLs.

Production Year	Cartographer	Source
1570	J. Rudd for the Burghley Atlas	www.islandeye.co.uk
1611	J. Speed	www.islandeye.co.uk
1760	T. Kitchin	www.ancestry.com
1815	T. Webster	www.ancestry.com

Each of these maps was examined to identify the location and persistence of the three established headlands, Hanover, Sudmoor and Atherfield Points.

3.2.2 Shoreline Analysis post 1866

The historical shoreline analysis was carried out to calculate the past cliff top and base recession rates from a series of historical maps dating back to 1866, and two recent dGPS (differential Global Positioning System) surveys, carried out in 2011 and 2012 for the cliff base and top, respectively. The cliff base line was measured by Hackney et al. (2013), using a dGPS that did not require base stations; the cliff top line was surveyed for this project using cliff top base stations. ArcGIS 9.3 and the Digital Shoreline Analysis System 4.0 (DSAS) extension version 4.0, developed by Thieler et al. (2009), were used. The measure of shoreline change calculated was end point retreat rate, meaning the amount of retreat was measured from the oldest line to the most recent. Two shoreline position indicators are used in this study, the cliff top and cliff base line. The cliff top line is easier to identify than the cliff base and is more consistent, i.e. it is not influenced by talus creation and removal; however cliff top rates are affected by the spatial and temporal scale of landside events. Therefore both will be used to study the formation and evolution of the headlands. The cliff base line is also used in conjunction with the cliff top line to calculate the volume of cliff material lost though erosion.

Initially the cliff top and base position were digitised from a series of maps from 1866, 1909, 1946 and 1975 using ArcGIS 9.3. An arbitrary baseline is then drawn with DSAS 4.0 running roughly parallel to the coastline. There are two aspects of this project that require recession data, at different scales.

1) Long-term recession rates of both cliff top and base for the whole coastline are needed to calculate the average annual input of sediment to the beach, for this transects were spaced at 10m intervals and only the oldest and most recent data sets were used.

2) To investigate the formation and evolution of the headlands over the past 150 years. This required the transect spacing to be reduced to 5m intervals within 600m of a headland and its associated intertidal platform. An interval of 5m was chosen as it represents the minimum usable spatial interval due to the errors inherent in the historic maps.

For both tasks, transects affected by the presence of the chines (coastal gullies) were disregarded (Figure 3.4). Recession rates were determined by dividing the

distance between the intercepts of the cliff top or base lines with transects by the number of years between those two survey lines.
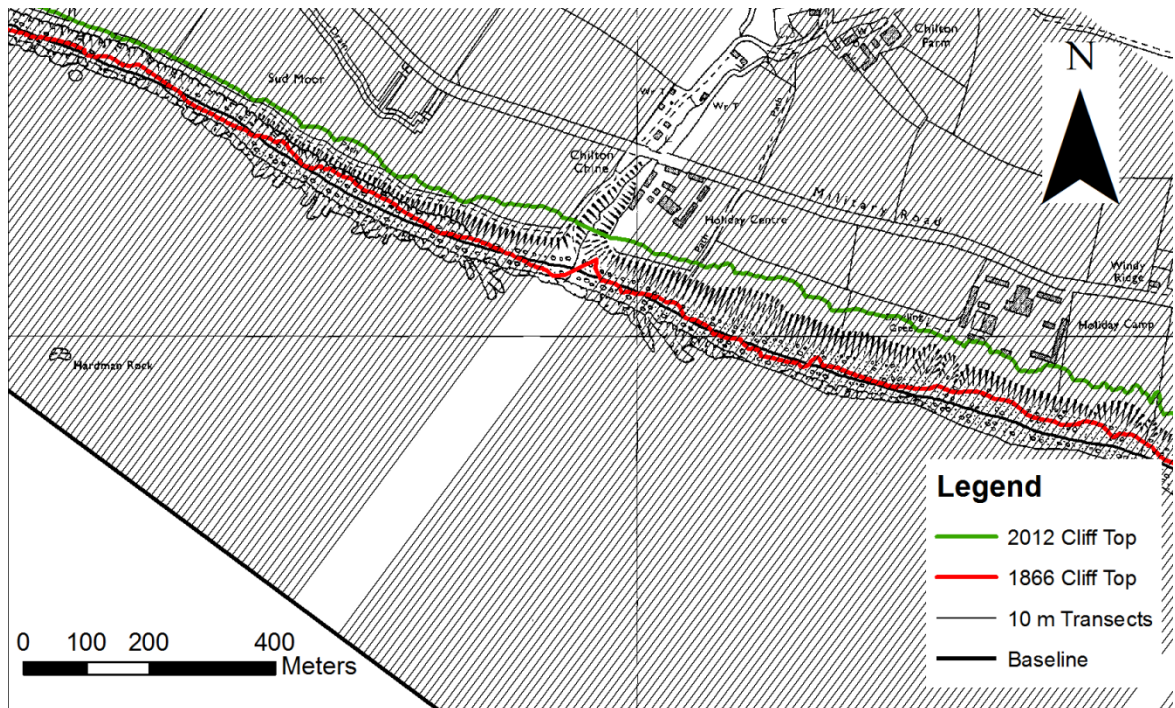
Figure 3.4: Method used to calculate recession rate. Transects cast from a base line every 10 m. Transects that cross a chine are removed, to prevent their influence skewing the results (e.g. at Chilton Chine). N.b the baseline does follow the overall orientation of the coastline, leading to some deviations from baseline locally as seen here.

As described in Section 3.1.1 the estimated errors of the maps used in this study will be ± 5m. This is based on measuring the movement of fixed points, such as churches, between different map editions and aerial photographs. The dGPS itself has an error in the range of tens of centimetres, however due to health and safety consideration during surveying the cliff top the error will be approximately ± 1m. For the rates calculated between successive maps to be valid the change in cliff top location must be greater than the combined errors. Equation 3.1 can be used to determine the minimum reliable retreat rate between two successive surveys (Lee, 2002):

$$E = \frac{eT1 + eT2}{T} \tag{3.1}$$

Where E is the error estimate related to the map period (m a^{-1}), eT$_1$ is the error associated with the first map, eT$_2$ is that of the second map and T is the time period between the two maps. If E is equal to or greater than the average annual recession rate the data shows no evidence of change and must be disregarded (Lee,

2002). Table 3.8 shows the estimated errors and average annual recession rates (AARR) of the successive maps and surveys to be used in this study. In all cases E is less than AARR making the time steps viable.

Table 3.8: Estimates of combined error compared with average annual recession rates calculated for successive maps or surveys

Date (T$_1$)	Date (T$_2$)	Time (a)	Error Estimate (m a^{-1})	Average Annual Cliff top Recession Rate (ma^{-1})
1866	1909	43	± 0.23	0.34
1909	1946	37	± 0.27	0.46
1946	1975	29	± 0.34	0.59
1975	2012	37	± 0.16	0.69
1866	2012	146	± 0.08	0.50

3.2.3   Analysis of Significance

When considering the patterns of erosion around the headlands in an attempt to understand their formation and evolution it is important to know if the variations seen are statistically significant. To achieve this, a series of one-tailed z-tests and t-tests were carried out in excel to compare the average recession rates between two areas: for example, the area behind the shore platform at Atherfield Point compared to the area just up or down drift. Z-tests were used if the sample size exceeded 30, while t-test were used if the sample size was less than 30. The null hypothesis stated that there was no difference between the means, if the calculated z or t exceeds the critical values of z or t the hypothesis is rejected. The difference in the means can be considered statistically significant to the 95% confidence interval.

3.3   Geological and Geotechnical Investigation

For the purposes of this project the geological and geotechnical properties of the cliff face and shore platform are investigated. The geological investigation involved creating a geological section of all the cliffs in the study area. This project concentrates on the marine forcing impacts on cliff recession rates; the geotechnical properties and behaviour of the cliff as a whole are beyond its remit (however the coastline was divided into a number of Cliff Behavioural Units though field observations of cliff geomorphology). Therefore the geotechnical investigation focused on the strength or coherence of the platform and cliff toe.

3.3.1   Geological Cliff Sections

There are a number of geological cliff sections for this coastline, but many are outdated due to coastal recession (Norman, 1887, White, 1921), or have no meaningful scale (Stewart et al., 1991). The geological sections in this study are intended to act as a tool in the calculation of a sediment budget. Therefore the following method was devised to provide a realistic, up-to-date representation of the cliff face geology. To create the cliff sections the coastline was divided into five units using the chines (or coastal gullies) as boundaries. These units were subdivided into segments using the Environment Agency Profiles (Figure 3.5). Information on the changes in cliff face lithology was collected in the field, and cliff sections were constructed in Excel.
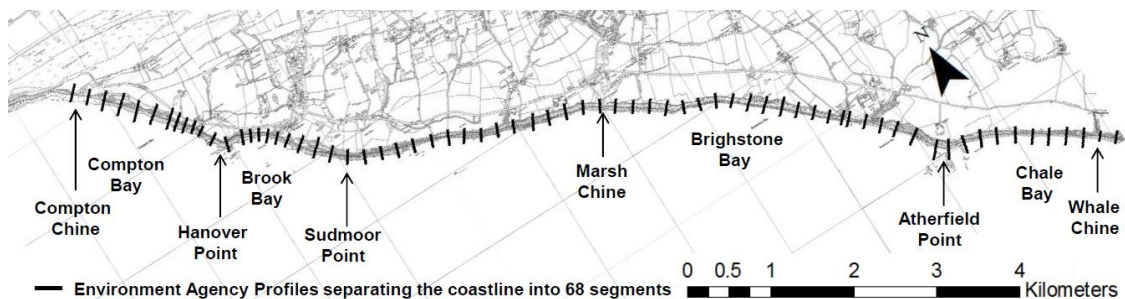
Figure 3.5: Environment Agency Profiles used to divide the coastline in to 68 cliff segments for the geological cliff sections and sediment budget analysis (Section 3.5). Also used in the beach sediment and volume analysis (Section 3.4)

The techniques used to collect data on the cliff face lithology varied along the coast due to cliff height, slope and exposure. Where the cliff was low and steep, i.e. around Compton and Brook Bays, and where the cliff was topped with River Terrace Deposits a weighted tape measure was lowered over the cliff edge and the distance between the cliff top and any bedding planes or unconformities was recorded. The longshore spacing of the measurements also varied in response to the number of beds present and the lateral scale of their variations, i.e. more regular measurements were taken where several sandstone beds were running up the cliff compared to an area of cliff that was consistently mudstone.

Where the cliff was too high for the weighted tape measure to be safely used, i.e. 73% of the coastline, the location where each bedding plane reached the cliff top and cliff base was recorded and lines were interpolated between the two points. This technique was also used where the exposure of the cliff was poor, such as between Marsh and Whale Chine.
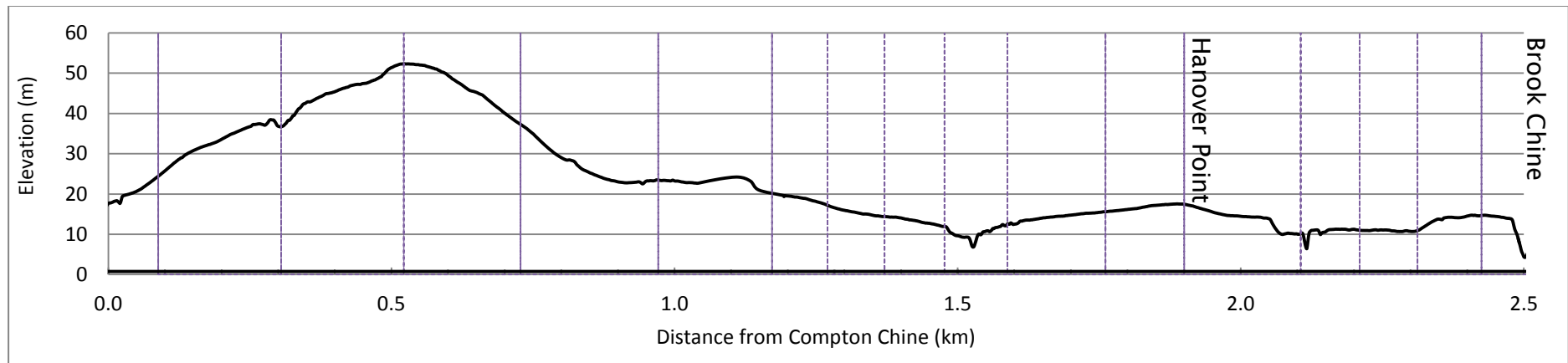
Figure 3.6: Cliff top elevation between Compton Chine and Brook Chine from the 2007 CCO LiDAR data, forming the basis of the cliff section
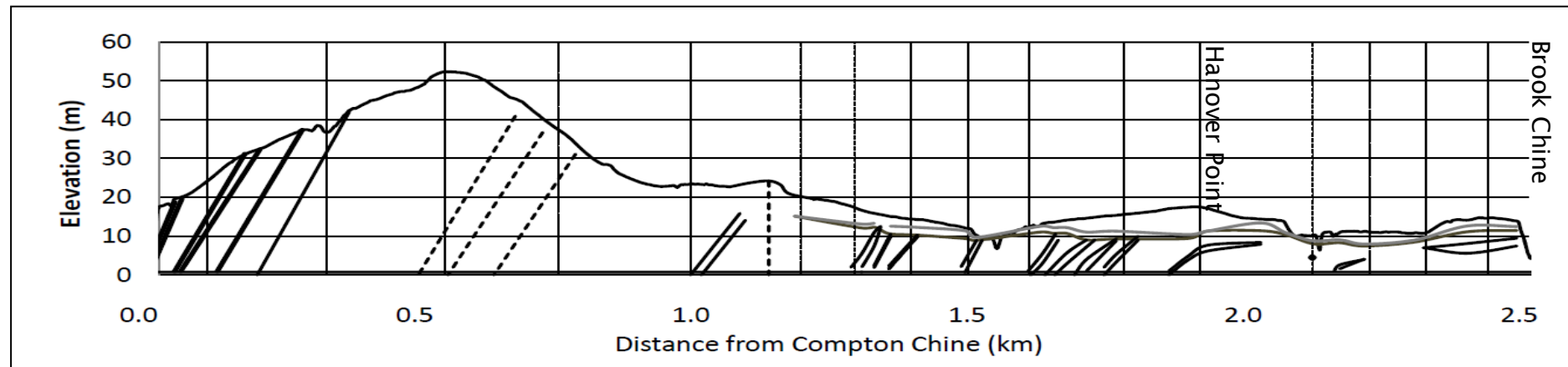
Figure 3.7: Cliff section between Compton Chine and Brook Chine with all beds and formation boundaries marked on

Finally a 5 m levelling rod was used along Sudmoor Point where the Sudmoor Point Sandstone runs horizontally along the cliff for some distance. The rod was used to measure the height of the boundary between the mudstone and sandstone above beach level. Cliff top elevation was taken from the 2007 LiDAR data provided by CCO. In all cases, a handheld GPS with an accuracy of approximately 3m, was used to mark significant locations as waypoints. These waypoints were entered into ArcGIS 9.3 where they were converted into a longshore distance from the start point (or chine). The conversion to longshore distance within ArcGIS 9.3 will introduce an additional error which has been estimated to be ± 2m , giving a maximum horizontal positional error of ± 5m for the location of bedding planes. Digitisation of the cliff sections was carried out in several stages. First the cliff section outline was created in Excel using cliff top and base elevations extracted from 2007 LiDAR and Mean High Water Spring tidal surfaces respectively (Figure 3.6). The 2007 LiDAR data was provided by the Channel Coastal Observatory (CCO; www.channelcoast.org/). The MHWS tidal surface was extrapolated from tidal levels, at Ventnor and Freshwater, taken from the Isle of Wight Shoreline Management Plan, in ArcGIS 9.3.
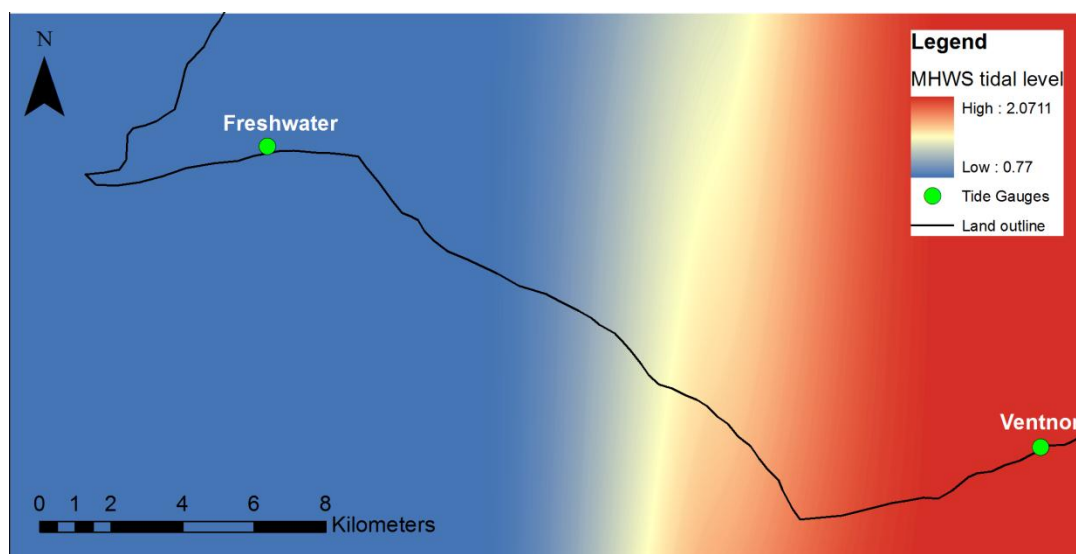
Figure 3.8: Mean High Water Spring (MHWS) tidal surface used to extract cliff base levels for the geological cliff sections. Created in ArcGIS 9.3 by interpolating between the Freshwater and Ventnor tidal values

The cliff top lines were extracted along a line several meters back from the 2008 cliff top line, to be closer to the current cliff top position, as defined by the dGPS Survey results, and avoid uneven land at the cliff edge. The waypoints converted

into long shore distance from the start chine (in this case Compton Chine) were added with elevation data to the excel graph as line features to create the bedding planes and formation boundaries shown in Figure 3.4.

3.3.2 Cliff Behavioural Units

The cliffs along the study frontage were divided into a number of Cliff Behaviours Units (CBU), a concept taken from (Lee and Clark, 2002). The classification used within this study was devised from the literature (Barton and Coles, 1984, Moore et al., 2002) to best represent the cliff morphology of the Southwest coast. Seven categories were defined as follows:

- Steep cliff with talus at base
- Compound Landslides
- Steep cliff with high level slides
- Undercliff formed through seepage erosion
- Mudslides
- Large complex landslides with unknown structure

The CBUs were mapped through field observations, with the boundaries between units recorded using a handheld GPS, and the study of aerial photographs.

3.3.3 Geotechnical Assessment

The purpose of the geotechnical assessment is simply to evaluate the role of cliff and platform strength. Of course the presence of an intertidal shore platform is related to the strength of the geology it is formed from, but along much of this coastline the low angle of dip means that the platform bed is not necessarily the same lithology or strength as the beds in the cliff above it.

The restrictive costs and labour intensive nature of many geotechnical tests meant that a visual appraisal method was chosen to determine cliff and platform strength. During preliminary field data collection, the British Standard classification of soils and rocks were used. This involves a separate classification system for the sandstones and the clays, mudstones and shales, each with seven or more categories. The results using this system were complicated and comparison of the soils and rock was difficult. Hence it was recognised that a simplified classification system was required. A further consideration was that the cliffs and platforms of the southwest coast are composed of soft rock or hard soil, i.e.

materials which are intermediate between soils and rocks, in terms of porosity, strength and compressibility (Clayton and Serratice, 1993). Therefore it was not appropriate to use the classifications devised for either soils or rocks to divide them. The coherence of soft rocks has been applied by Soares (1993) using examples in Brazil. This classification system uses only four categories and through a series of laboratory tests carried out by Soares (1993) these categories can be correlated with compressive strength through the visual classification of coherence. The classifications are shown in Table 3.9

Table 3.9: The descriptive categories used to assess the coherence of soft rocks with an estimate of the related compressive strength. Taken from Soares (1993)

	Code	Characteristics	Compressive strength (MPa)
Coherent	C1	- Hard to break by hammer impact, producing few fragments with sharp edges - Surface scratch by steel blade with difficulty.	> 20.0
Intermediately Coherent	C2	- Relatively easy to break with hammer impact, producing fragments with edges breakable by finger pressure - Can be scratched by steel blade, leaving shallow furrows	Between 20.0 and 10.0
Less Coherent	C3	- Crumbles on hammer impact, producing fragments that can be broken by hand - Surface easily scratched by steel blade, leaving deep furrows	Between 10.0 and 5.0
Non Coherent	C4	- Breaks easily under finger pressure, disintegrating - Can be cut by steel blade	< 5.0

The coherence of a rock will influence its vulnerability to erosion, as such it is proposed as a reasonable measure of the relative strength/resistance to erosion of the cliff base along the coastline. This allows a rudimentary measure of geotechnical strength, and resistance to erosion, to be determined quickly in the field with the use of a pen knife and geological hammer. In the context of this study, quantifying the coherence of the cliffs along with observations of their mass properties should be sufficient to characterise the geotechnical qualities of the geology. Since it has been stated (in Chapter 2) that the exposure of the cliff toe to wave energy on the open coast is the most important influence on cliff recession rates it follows that the strength at the cliff base is also critical. Assessment was made at least every 50 m along the coast at the base of the cliff (Figure 3.9),

spacing of measurements were reduced in areas where the lithology changes were at a scale less than 50 m.
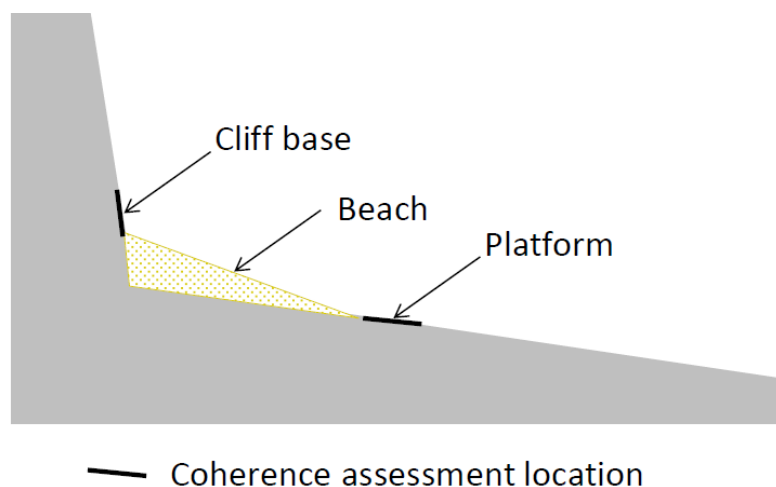
Figure 3.9: Schematic indicating the locations where assessments were made of cliff and platform coherence.

The outer layer of weathered material was removed using a geological hammer; material was removed until an intact unweathered surface was exposed for assessment of the bed's unweathered strength. The depth of weathered material varied from approximately 1 to 10cm across all lithologies. Measurement of shore platform strength was carried out close to the beach platform boundary where platforms were present (Figure 3.9). The measurement interval for the platform was higher than the cliff at approximately every 100m, since the platform lithology is more consistent than that of the cliff base. Where variations in platform lithology occurred more measurements were made. There was less need to remove weathered material from the platform as the action of waves removes any weathered material on a regular basis.

Observations of the mass properties of each of the geological formations were also made, along with a series of grain size analyses. The percentage of clay and the type of mineral within a soft rock will influence its behaviour. Analysis of the particle size distribution of the >63µm fraction was carried out as part of the sediment budget calculations (Section 3.6.1). To determine the percentage clay present in the various geological formations, and the mineralogy of those clays, analysis was carried out on 8 samples collected from the Vectis and Atherfield Clay Formations. The details of these samples are presented in Table 3.10.

Table 3.10: Samples collected for clay fraction analysis (LD – Laser Diffraction, XRD – X Ray Diffraction)

Formation	Member	Location	Tests
Vectis	Shepherd's Chine	GR 44783, 79704 GR 45060, 79214	LD / XRD LD / XRD
	Cowleaze Chine	GR 44306, 80145	LD / XRD
Atherfield Clay	Chale Clay	GR 45277, 79031 GR 45646, 78950	LD / XRD LD / XRD
	Lower Lobster Bed	GR 46171, 78656	LD / XRD
	Perna Bed (cliff) Perna Bed (platform)	GR 45232, 79028 GR 45247, 78979	LD / XRD LD

Results for the Wessex Formation were taken from the work of Redshaw (2013), the methods used are consistent for both sources. The particle size distribution analysis of the <63 µm fraction was carried out through laser diffraction using a L5130 Coulter Counter. X-Ray Diffraction (XRD) on the same samples was completed using a Phillips X'Pert pro XRD machine with a CU X-Ray tube, However XRD analysis was not possible on the Perna Bed platform sample as no clay was recovered (for a more detailed methodology see Appendix 1. All analysis was carried out at the National Oceanography Centre, Southampton.

3.4   Wave Refraction Analysis

A number of open access wave refraction models are available. For the purposes of this project a simple single input wave model was sufficient. The wave propagation model RCPWAVE (**R**egional **C**oastal **P**rocesses Monochromatic **WAVE** Model) was chosen. RCPWAVE is a 2D, steady state, monochromatic short wave model for simulating wave propagation over arbitrary bathymetry, developed by Ebersole et al. (1986) for the US Army Corps of Engineers. It is available as part of the Coastal Engineering and Design Analysis System (CEDAS) package. The model uses linear wave theory and is based on the mild-slope equation (Vincent et al., 2002). The model was run for a range of wave heights and periods typical of a number of representative wave conditions. The model input and outputs are described below.

3.4.1   Model Inputs

The inputs required for RCPWAVE include bathymetric data, offshore wave data and water levels. Two sets of bathymetry data were used in the model. The first was derived from a number of sources interpolated within RCP grid generator to create a 20 m bathymetric grid within the RCPWAVE model which represented the actual bathymetry of the coastline (Figure 3.12).

The sources included:

1) 2007 LiDAR data provided by CCO. This covered elevations between 0 and 10m Ordnance Datum. To reduce the size of the dataset the LiDAR was converted in to a series of contours (0, 2, 5 and 10m).

2) 2010 Swath bathymetry data, also provided by CCO. This covered the area from the -4m contour out to around 1km offshore. Again the size of the dataset was reduced by converting to contours in ArcGIS 9.3

3) Admiralty chart data taken from chart SC5600.2 (2000 edition). The contours where digitised in ArcGIS 9.3 and converted to Ordnance Datum from Chart Datum by subtracting 1.83m from each contour to bring the data in line with the LiDAR and swath bathymetry. This data covered the rest of the offshore area out to -40m.

All the contours were converted into point data for input into RCPWAVE grid generator. The point data is shown in Figure 3.10 divided by source and in Figure 3.11 divided by depth. The second set of bathymetry data was synthetic, designed to provide a simplified representation of the coastline to determine the influence of the complex bathymetry found in the field Figure 3.13.

This simplified bathymetry was created assuming an equilibrium beach profile in the cross-shore direction calculated using Equation 3.2 from Dean (1991):

$$d = ax^{2/3} \qquad\qquad (3.2)$$

Where d is depth, x is the cross-shore distance from still water level and a is the profile coefficient (in this case 0.13 which represents the average profile of the coastline). This synthetic bathymetry takes into account the influence of the

headlands only. Comparison of the results gained with each bathymetry data set will highlight the influence of the complex bathymetry of the study site.
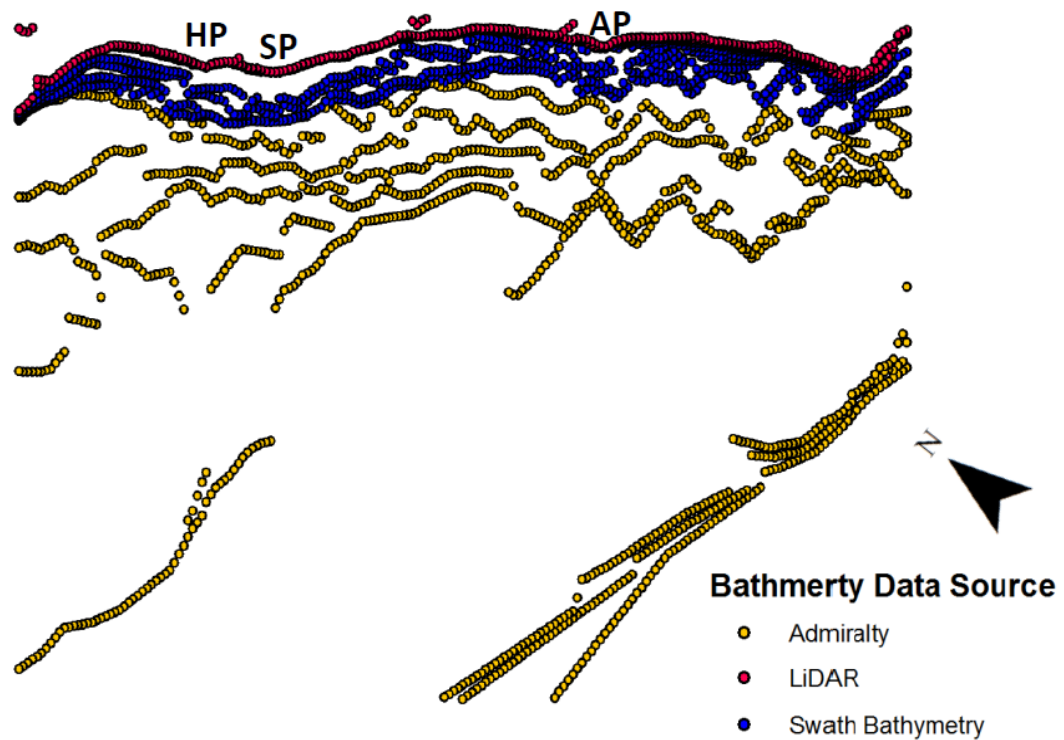
Figure 3.10: Bathymetry point data input for RCPWAVE divided by their source. HP-Hanover Point, SP-Sudmoor Point and AP –Atherfield Point
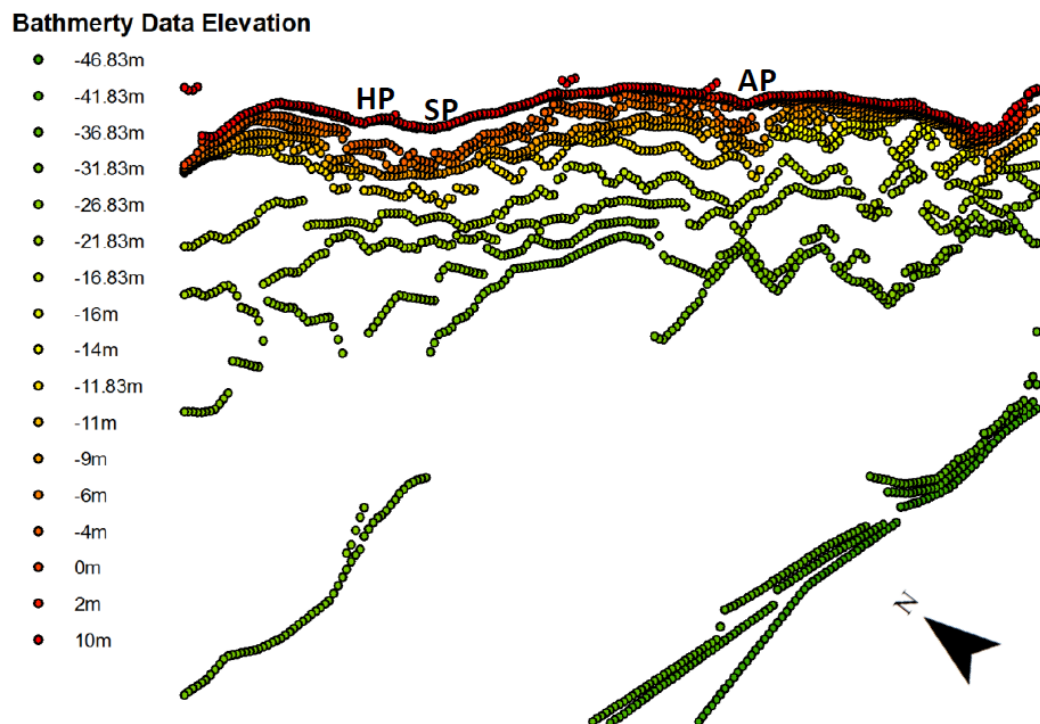
Figure 3.11: Bathymetry point data input for RCPWAVE divided by depth. HP-Hanover Point, SP-Sudmoor Point and AP –Atherfield Point
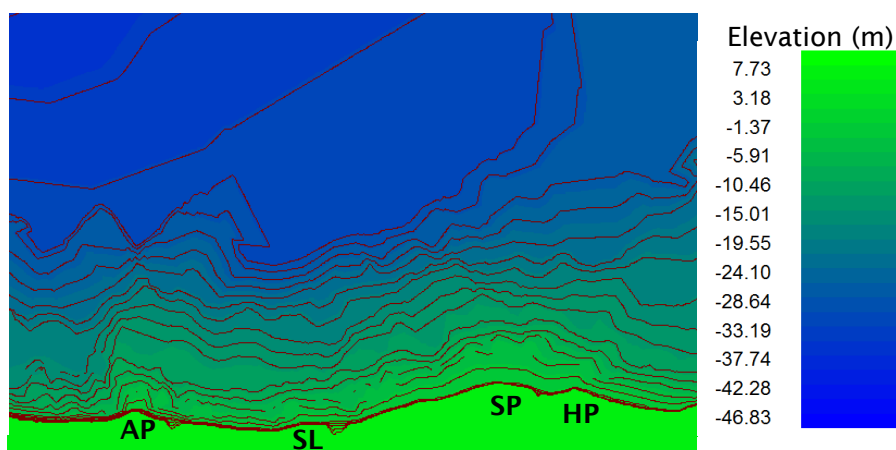
Figure 3.12: Bathymetry representing real world conditions, compiled from a number of sources (see text). N.b. AP - Atherfield Point, SL - Ship Ledge, SP - Sudmoor Point and HP - Hanover Point
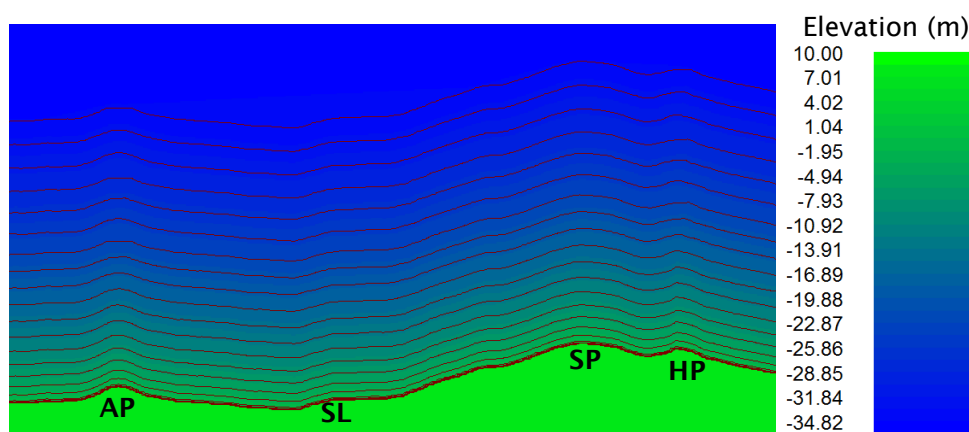
Figure 3.13: Simplified bathymetry of the coastline, constructed using an equilibrium beach profile and the current (2011) cliff base line. N.b. AP - Atherfield Point, SL - Ship Ledge, SP - Sudmoor Point and HP - Hanover Point

The offshore wave parameters were taken from two sources and are summarised in Table 3.9. Common wave, significant wave height (Hs) and peak wave period (Tp) values came from a scatter diagram of Hs and Tp of the 1968 data form the Shambles Light Vessel near Portland Bill (Figure 3.14). Common waves are defined as waves that occur 35 times in 1 year (35:1 year) that is the equivalent of once every 10.4 days. The scatter diagram did not provide directional data for the waves. Analysis of Met Office data from the 12km grid wave model showed the majority of waves approach from the west-south-west (240°), representing 74% of all waves (Figure 5.1a). The value of 74% was calculated from waves that have the potential to reach the coastline, i.e. waves approaching from between 285° and 135° were removed from the data set because the orientation of the coastline means waves from those directions would not reach the shoreline. As no directional data

for the common waves was available the prevailing wave direction was used; models were run with common waves from 225°, 240° and 255° so variations caused by the changes of angle could be studied.

Figure 3.14: Location of wave data used in this study

Table 3.11: RCPWAVE model input parameters

Wave Type	Wave Direction (°)	Wave Height (m)	Wave Period (sec)	Water Level (m O.D.)
Common waves 35:1 year	225°,240°, 255°	1	5.5	+1.11
5:1 year storm wave	240°	3.5	6.5	+1.46
1:50 year storm wave	240°	6.02	8.1	+2.30

The storm waves were taken from a study by Andrews (1990), who calculated 5:1 and 1:50 year storm events (i.e. a storm that will occur five times in a single year and once in 50 years respectively) using HINDWAVE from Portland wind data. The water level chosen for the common waves was 1.1m, to represent average high tide (high tide varies along the coastline). The storm waves were modelled with extreme water levels due to the low pressure zones commonly connected to high wind speeds, particularly from the southwest. The water level values used were also taken from Rix (2000) and represent typical high water levels under the storm wave conditions incorporating the potential increase due to storm surges.

3.4.2   Model outputs

Wave height and direction can be recorded by RCPWAVE, and later extracted, at a number of predetermined points, known as stations. These stations were placed at approximately the same depth relative to mean sea level (-1 m to -1.5 m) along the

coastline, the elevation of which are shown in Figure 3.15. Due to the 20m grid size the range of station elevation increases into Chale Bay where the shoreface steepens.
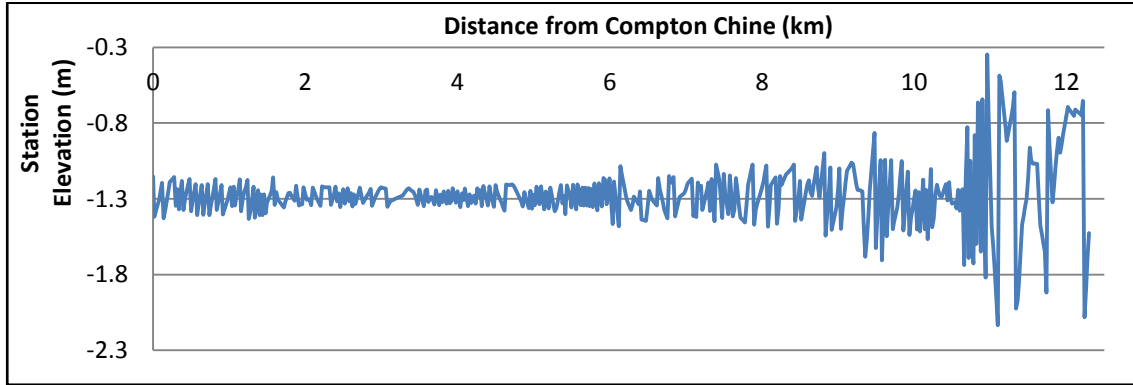
Figure 3.15: The elevation of the station points within RCPWAVE at which wave height and direction data are extracted from the model.

To determine the influence of the headlands on wave energy concentration the wave heights extracted at these stations were converted into wave energy density using the following equation:

$$E = \frac{1}{8}\rho g H^2 \tag{3.3}$$

Where E = Wave energy density (KJ m^{-1}), ρ = Density of sea water (1025kg m^{-3}), g = Acceleration due to gravity (9.81m s^{-1}) and H = Wave height (m).

3.5   Beach and Platform Morphology and Sedimentology

To maintain consistency across all results the EA beach profiles were used to determine the location at which sediment samples would be collected and where measurements of beach volume (BWA) and platform elevation would be made. An attempt was made to calculate BWA from the EA beach profiles between 1991 and 1998, however the information regarding the location of the cliff base relative to the start point of the profiles was unavailable.

3.5.1   Sediment Sampling

Beach sediment samples were collected along the 68 Environment Agency (EA) profiles (Figure 3.3), one from the backshore, close to the cliff, and one from the foreshore, in the intertidal zone. The EA profiles were chosen to ensure results

were consistent with existing data and with all results across this project; the profiles were also used to split the cliff into smaller segments for sediment input calculations. To ensure the foreshore samples were taken from a consistent location the mid-tide level was chosen. Samples locations were predetermined and loaded into a hand held GPS unit. Figure 3.16 shows a number of representative beach profiles from four locations along the study frontage. The sampling locations of foreshore and backshore samples are marked. Samples were collected in pre-labelled heavy duty plastic bags. In locations were the foreshore was occupied by the shore platform no samples were taken. All samples were collected over a four day period (26th to the 29th of September 2011) of low wave energy to obtain a snapshot of the cross-shore and longshore surface sediment distribution without disturbance by storm waves over the sampling period.
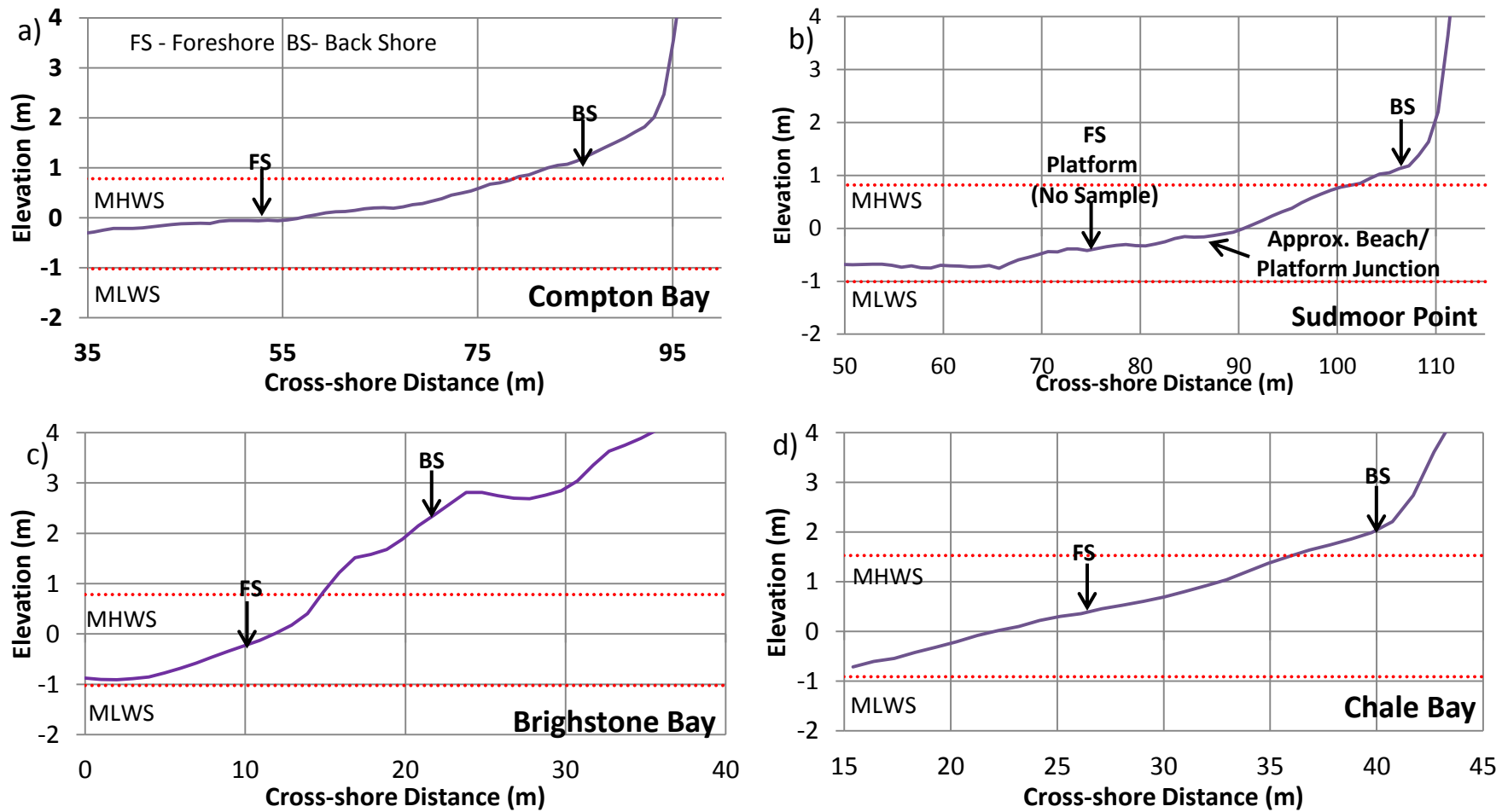
Figure 3.16: Cross-shore sampling locations at four representative profiles: a) Compton Bay, b) Sudmoor Point, c) Brighstone Bay and d) Chale Bay. FS – Foreshore, BS- Back Shore, MHWS – Mean High Water Spring tides, MLWS – Mean Low Water Spring tides.

3.5.2   Laboratory Grain Size Analysis

Grain size analysis of the 128 beach sediment samples collected was carried out by dry sieving of the sand and gravel fractions. The method used was consistent with the British Standard (BS 1377-2:1990). The first step was to wash the salt water from the samples. The samples were then dried at 105°C for at least 24 hours. Once dry the samples were weighed to within 1% of their total mass. The samples were put through a series of sieves in three stages, where appropriate (Table 3.10). The larger fractions are progressively removed (i.e. 75mm to 20mm; then 20mm to 6.3mm) before the sand fraction is riffled, i.e. randomly reduced to around 100g if necessary. The post riffling results are corrected using the correction factor (Equation 3.4):

$$\frac{m_2}{m_3} \times \frac{m_4}{m_5} \qquad\qquad (3.4)$$

Where m_2 is the weight of sample passing the 20mm sieve, m_3 is the riffled weight going into the second round of sieving (13.2mm sieve), m_4 is the weight of the sample passing through the 6.3mm sieve and m_5 is the riffled weight of the sample entering the final stage of sieving (3.35mm sieve). An example of this is shown in Table 3.10.

The first two stages of sieving with the larger grain sizes were carried out manually with some particles hand placed, but not forced, to see if they would fall through the sieves. The final stage of sieving was done with a mechanical shaker; the minimum period of shaking was ten minutes. After sieving, the contents of each sieve was carefully emptied out, weighed and recorded on a sample sheet or lab book. To ensure the accuracy of the results the samples were sieved again when the total post sieving weight was more than 2% out from the pre-sieving weight.

Table 3.12: Example of sample sheet for particle size distribution (Based on Form 2.M from BS 1377-2:1990)

Location: Chale Bay (GR: 446710, 78342)				
Test method	BS 1377-2:1990:9.3			
Initial Dry mass m_1	1075.42	g	Sample: H434 Backshore	
BS Test sieve	Mass retained (g)		Percentage retained $(m/m_1)100$	Cumulative percentage passing
	actual	corrected m		
75mm (-6.23φ)		0	0	100
63mm (-6.23φ)		0	0	100
50mm (-5.98φ)		0	0	100
37.5mm (-5.64φ)		0	0	100
28mm (-5.23φ)		0	0	100
20mm (-4.32φ)		0	0	100
Passing 20mm m_2	1075.4			
Total (check with m_1)	1075.4			
Riffled m_3	1075.4			
Correction factor m_2/m_3	1			
13.2mm (-3.72φ)		0	0	100
10mm (-3.32φ)	4	4	0.4	99.6
6.3mm (-2.66φ)	2.51	2.51	0.2	99.4
Passing 6.3mm m_4	1068.9			
Total (check with m_3)	1075.4			
Riffled m_5	304.7			
Correction factor $(m_2/m_3)*(m_4/m_5)$	3.51			
3.35mm (-1.74φ)	1.52	5.3	0.5	98.9
2mm (-1.00φ)	36.39	127.7	11.9	87.0
1.18mm (-0.24φ)	120.54	422.9	39.3	47.7
600μm (0.74φ)	100.81	353.6	32.9	14.8
300μm (1.74φ)	33.24	116.6	10.8	4.0
150μm (2.74φ)	9.25	32.4	3.0	1.0
63μm (3.99φ)	0.91	3.2	0.3	0.7
Passing 63μm mF or mE	2.04	7.2	0.7	0.0
total (check with m_5)	304.7		99.8	

3.5.3   Statistical Analysis of Particle Size Distribution

To gain useful insights into the sediment distribution of the beach sediment statistics are required. The parameters measured include the median, mean, sorting and skewness, all of which require the grain size to be expressed in the phi scale (Φ) not mm (Table 3.11). To convert mm to Φ Equation 3.5 is used:

$$\varphi = -\log 2(\frac{d}{d_0})$$ (3.5)

Where d is the diameter of the particle in millimetres and d_0 is the standard grain diameter, i.e. 1mm (Krumbein, 1934). Because sediments are log normal converting them to a logarithmic scale, such as the phi scale allows more detailed analysis of sediment distribution. It also allows statistical analysis of the sorting and skewness to be made (Krumbein, 1934).

Table 3.13: Grain size classification, including the phi scale

Wentworth Scale		Phi Units (φ)	Grain Diameter
Boulder		< -8	> 256 mm
Cobble		-6 to -8	64 – 256 mm
Pebble		-2 to -6	4 – 64 mm
Granule		-1 to -2	2 – 4 mm
Sand	Very Coarse	0 to -1	1 – 2 mm
	Coarse	1 to 0	0.5 – 1 mm
	Medium	2 to 1	250 - 500 μm
	Fine	3 to 2	125 – 250 μm
	Very Fine	4 to 3	62.5 – 125 μm
Silt		8 to 4	3.91 – 62.5 μm
Clay		> 8	< 3.91 μm

The median and mean both describe the average size of sediment, the median (φ_{50}) of a sample is the "middle" grain size, for which 50% of the sample is larger and 50% is smaller. The mean grain size (M) is calculated by averaging the φ_{16}, φ_{50} and φ_{84} i.e. the 16th, 50th and 84th percentiles respectively (Equation 3.6). They both give an indication of the magnitude of force applied to the sediment by waves and currents (Pethick, 1984).

$$M = \frac{\varphi16 + \varphi50 + \varphi84}{3}$$ (3.6)

The sorting (ο) is basically the standard deviation of grain size (Equation 3.7); it is a measure of scatter or dispersion and provides information on the range of energies the sediment was subjected to (Lacey, 1985, Pethick, 1984).

$$\sigma\varphi = \frac{\varphi84- \varphi16}{4} + \frac{\varphi95- \varphi5}{6.6}$$
(3.7)

Well sorted sediment is likely to have been subjected to a steady level of energy over a prolonged period, while poorly sorted sediment is a common feature of flood or glacial deposits which have been deposited rapidly. Table 3.12 shows the sorting classifications used in this study.

Table 3.14: Sorting and skewedness categories

Sorting	Phi (φ)	Skewedness	Phi (φ)
Very Well Sorted	< 0.35	Strongly Fine Skewed	> 0.3
Well Sorted	0.35 to 0.50	Fine Skewed	0.3 to 0.1
Moderately Well Sorted	0.50 to 0.71	Near Symmetrical	0.1to -0.1
Moderately Sorted	0.71 to 1.0	Coarse Skewed	-0.1 to -0.3
Poorly Sorted	1.0 to 2.0	Strongly Coarse Skewed	<-0.3
Very Poorly Sorted	2.0 to 4.0		
Extremely Poorly Sorted	> 4.0		

Skewness (Sk; Equation 3.8) is a measure of the asymmetry of the sediment distribution, a normal distribution has a Sk value of zero, while a sample with a fine or coarse tail will have a positive or negative skew respectively. Generally beach sediment display a negative skew, i.e. the mean grain size is larger than the median (Bird, 2008). Table 3.12 shows the skewness classifications.

$$Sk = \frac{\varphi16+ \varphi84-2\varphi50}{2(\varphi84- \varphi16)} + \frac{\varphi5+ \varphi95-2 \varphi50}{2(\varphi95- \varphi5)}$$
(3.8)

Kurtosis was also calculated but the results did not reveal any further insight into the beach sediment distribution. The φ values used to calculate the above parameters were extracted from sediment distribution curves, plotted using the results of the sieve analysis, an example of which is shown in Figure 3.17.

The errors from estimating values from the graph are an interpretive error in the order of 0.1 φ. These errors will be propagated through all the calculations. Statistics for gravel and sand fractions were calculated as a single sample.
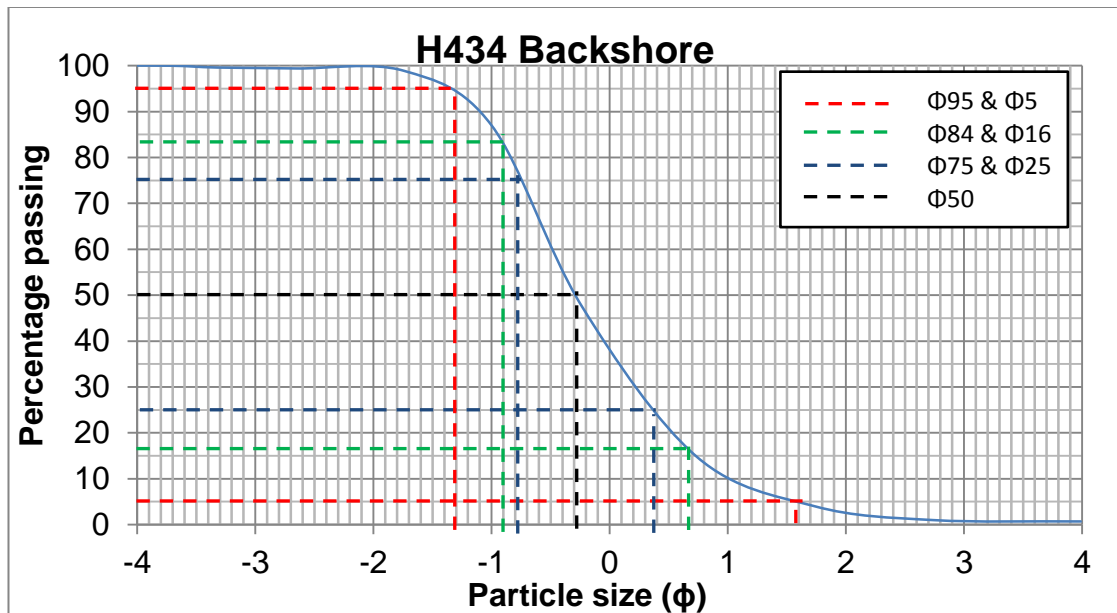
Figure 3.17: Example of a sediment distribution curve, used to obtain values of various percentiles for the calculation of particle size distribution statistics

3.5.4 Beach Width, Beach Wedge Area and Beach Slope

Beach width was calculated from the 1866, 1909 and 1975 OS maps (from Digimap) and the 2008 aerial photographs (from CCO). The cliff base line and the low tide line or beach/ platform junction were used as the upper and lower limits of the beach, respectively. These lines were digitised in ArcGIS 9.3 and the Digital Shoreline Analysis System (DSAS 4.0) was used to measure the distance between the two to give an approximation of beach width at 10 m intervals.

The Beach Wedge Area (BWA) was defined by Lee (2008) as the area described by a triangle defined as the width and the maximum elevation of the beach above MHWS tidal level (Figure 2.3). It is a useful measure of a beaches ability to protect the cliff base from erosion. Estimates of the BWA were made using ArcGIS, LiDAR data (2005, 2007, 2008 and 2009), aerial photographs (2005, 2008), all provided by the Channel Coastal Observatory, as follows. Calculations were made at each of the 68 Environment Agency (EA) profiles (Figure 3.3). The same profiles were used for consistency across all methods and results. The first step was to extract topographic data for each year and each of the EA profiles, which was then plotted in Excel along with the interpolated Mean High Water Spring (MHWS) tidal level. The beach/cliff junction intersection was identified in these plots with the aid of the aerial photographs, while the beach/ MHWS intersection was simply read off the

plots. These intersections were used to define a right angle triangle representing the BWA as shown in Figure 3.18.
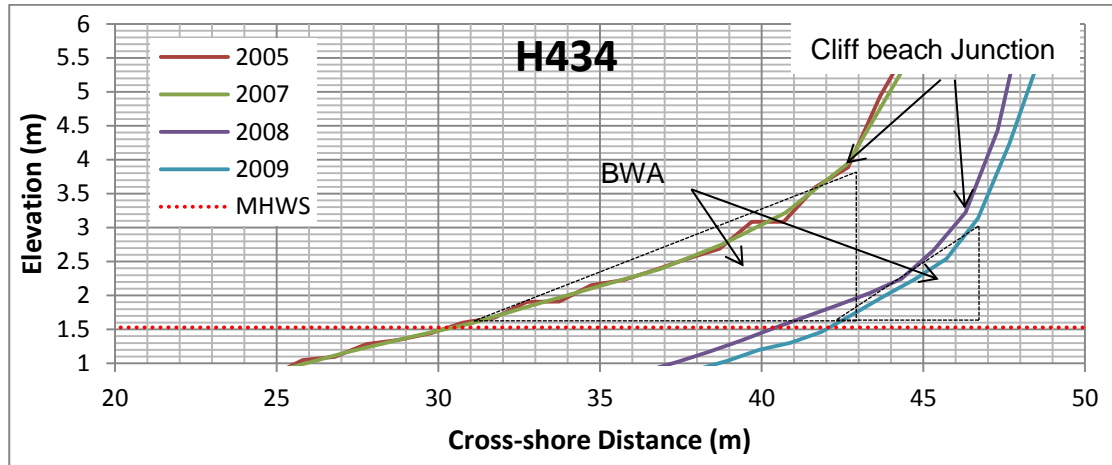
Figure 3.18: Example of Beach Wedge Area (BWA) calculations for a sample profile

Beach slope was calculated at each of the EA profiles using equation 3.9:

$$tan^{-1}(\frac{W}{E}) \hspace{4cm} (3.9)$$

where W is the width of the beach between the cliff-beach junction and 0m ODN and E is the elevation of the cliff-beach junction. The values of W and E were taken from the extracted LiDAR data profiles for 2004-5 and 2007-9. The level of 0m ODN was chosen as LiDAR was not flown at low tide and the calculations could not be extended to that level.

3.5.5   Shore Platform Width and Elevation

Since beach morphology is controlled in part by the presence and characteristics of shore platforms it is also necessary to measure the width and elevation of shore platforms where present. The width of the intertidal shore platform was calculated through the method used to calculate beach width, i.e. digitising the seaward and landward limits of their exposure on maps from 1909 and 1975 in ArcGIS 9.3, and then using DSAS (Digital Shoreline Analysis System) to obtain platform widths at 10 m intervals.

It was not possible to extract platform elevations from the LiDAR data available due to the measurements not being taken at low tide and the issue of discerning platform from beach sediment. An attempt was made to measure platform elevation along the beach platform junction using the dGPS but due to the cliff top

location of the base stations creating a shadow zone on the beach reducing the accuracy of measurements to ~ ± 0.5m the results were meaningless. Therefore an estimate of the platform elevation along the beach platform junction was taken from the NRA/EA (National River Authority/Environment Agency) beach profiles between 1991 and 1998. The profiles provide information on the beach material at each elevation recorded, i.e. sand, gravel or exposed bed rock. The landward limit of the exposed rock is taken as an estimate of the platform elevation along the coast. An example is shown in Figure 3.19; the black diamonds indicate the landward limit of the exposed platform and hence the location platform elevation was measured. The profiles themselves were measured by levelling. The values will vary with the sand cover but give a reasonable indication of the platform elevation and its changes. The elevation of the platform along this boundary will provide an insight into the platform beach interactions along the coast line.
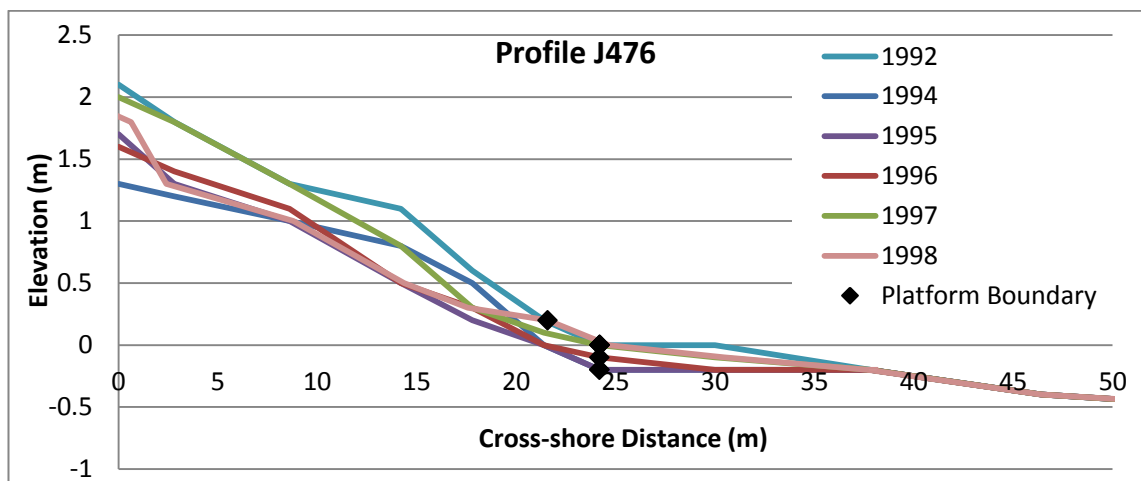
Figure 3.19: Example of platform elevation data extracted from NRA/EA profiles.

3.6 Sediment Budget Calculations

A sediment budget is a balance of the input (sources) and outputs (sinks) of sediment into the beach (store) based on the continuity of mass (Chapman, 1981). On the southwest coast of the island the major source of sediment is from the cliffs, and potentially some onshore transport from the sea bed. The main pathways are longshore and on and offshore transport by waves and currents. The major sediment sink is offshore. These sources, sinks and pathways are summarised for the beach cell in the sediment budget in Figure 3.20. To ensure an accurate estimate of the volume of beach grade material entering the beach in each cell, the

Littoral Cut off Diameter (LCD), and corresponding volume of beach grade material entering from the cliff is calculated for each cell. The LCD is the minimum grain size stable on the beach under prevailing wave conditions (Limber et al., 2008); Hicks (1985) defines the LCD as the grain size for which 95% of sediment is greater and 5% is smaller, this is the definition used in this study. All material from the cliff that is finer than the LCD is assumed to be lost offshore; this includes sediment transported by longshore transport to a cell with a higher LCD.
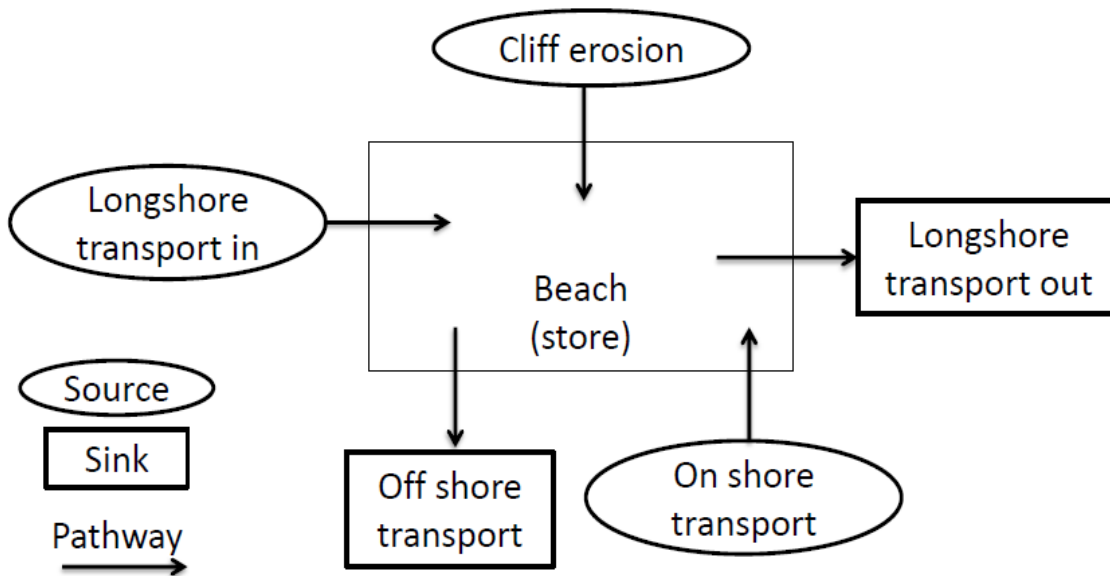
Figure 3.20: Sources, sinks and pathways for all beach cells in the sediment budget

3.6.1 Cliffs as a Source of Sediment

The Needles to the north of the study area act as a total barrier to sediment transport (Bray et al., 2004); the input of beach grade sediment from the chines is considered insignificant (Flint, 1982), and there is little evidence of onshore sediment transport to the beach Posford Duvivier (1999); therefore the major input of sediment will be from cliff erosion. Estimating the mass flux of sediment from cliff erosion requires knowledge of the long-term cliff recession rates, cliff face area, stratigraphy and sediment composition (Colman and Foster, 1994).

The contribution of beach-sediment from a unit length of cliff can be calculated using the following general equation (Young and Ashford, 2006):

$$Q = R_l \times H_c \times K \qquad\qquad (3.10)$$

Where Q = average annual cliff sediment yield, R_l = linear rate of cliff retreat, H_c = average cliff height and K = Composition Factor, indicating the percentage of cliff material that will be retained on the beach, calculated using the LCD, i.e. the smallest grain size stable on the beach. Defined as the grain size for which 95% of the sediment is coarser (i.e. the D_{95}), (Limber et al., 2008). This simple equation (Equation 3.10) assumes simple geology with one or two different lithologies, horizontally bedded. Where the geology is more complex, i.e. dipping beds and unconformities, the equation and associated methodology needs refining.

In areas of complex geology Equation 3.10 is not sufficient to calculate the beach grade sediment input to the system. A new method was developed and is presented here which involves dividing the cliff face into differing lithologies with different particle size distributions. When considering a large or complex length of coastline it is common practice to divide that coastline into more manageable sections. In the case of this study the coastline was divided into 68 segments using the Environment Agency beach profiles and Compton Chine as boundaries, creating sections varying between 70 and 270 m (av. 175 m) Figure 3.3. The calculations are based on the total eroded volume for each segment. For each segment the following steps are carried out:

1) The total volume of sediment eroded annually is calculated by multiplying long term recession rates with average cliff height and segment width (Step 1).

2) The lithology was defined through field measurements and presented as a cliff cross section. These cliff sections are used to calculate the percentage of each segment that is composed of each lithological unit within it, a.k.a. the Lithology Contribution Factor (A), expressed as a value between 0 and 1 (Step 2).

3) The Composition Factor (K) of each lithology is calculated from comparison of the Particle Size Distribution of beach and cliff samples. Also expressed as a value between 0 and 1 (Step 3).

4) Beach grade sediment input for each segment is calculated from the volumes, lithology are composition factors using Equation 3.11 (Step 4):

$$Q_{Beach\ Grade} = \Sigma(Q_{total} \times K_i \times A_i) + (Q_{total} \times K_{ii} \times A_{ii}) + \cdots (Q_{total} \times K_n \times A_n) \qquad (3.11)$$

Where: $Q_{Beach\ Grade}$ = volume of beach grade sediment produced by a segment

Q_{total} = total volume of sediment produced by the same segment

$K_{...}$ = Composition Factors of the lithologies in that segment respectively

$A_{...}$ = Lithology Factors of the lithologies in that segment respectively

i.e. The sum of the beach grade sediment from each lithology within a segment.

The following sections cover these steps in greater detail

Step 1: Total eroded cliff volume

The average annual input from an eroding cliff was calculated using the following simple Equation:

$$Q_T = \bar{H} \times \frac{\overline{R_{CT}+R_{CB}}}{2} \times W \qquad (3.9)$$

Where Q_T = Total average annual eroded cliff volume for a segment, $\bar{H}$ = average cliff height for a segment (m), $\overline{R_{CT}}$ and $\overline{R_{CB}}$ = average cliff top and cliff base recession rates (m a^{-1}) respectively for a segment, and W = width of a segment.

Cliff height is measured from Mean High Water Spring (MHWS) tidal level to the cliff top, the MHWS level being equivalent to the cliff platform junction. Cliff top elevation for each transect was extracted from 2007 LiDAR data provided by the Channel Coastal Observatory (CCO), which has an accuracy of ± 0.15 m. The MHWS tidal level for each transect was extracted from a tidal surfaces produced in ArcGIS from point values at Freshwater and Ventnor Figure 3.8. The error associated with the tidal surface is ± 0.5m, giving an overall error on cliff elevation of ± 0.65m. Using an average of the cliff top and base recession rates takes into account steepening or flattening of the cliff slope over the study period, in terms of eroded volumes. Figure 3.21 shows the potential variations in calculated cliff volumes using the cliff top or base recession rates alone compared to an average of the two.
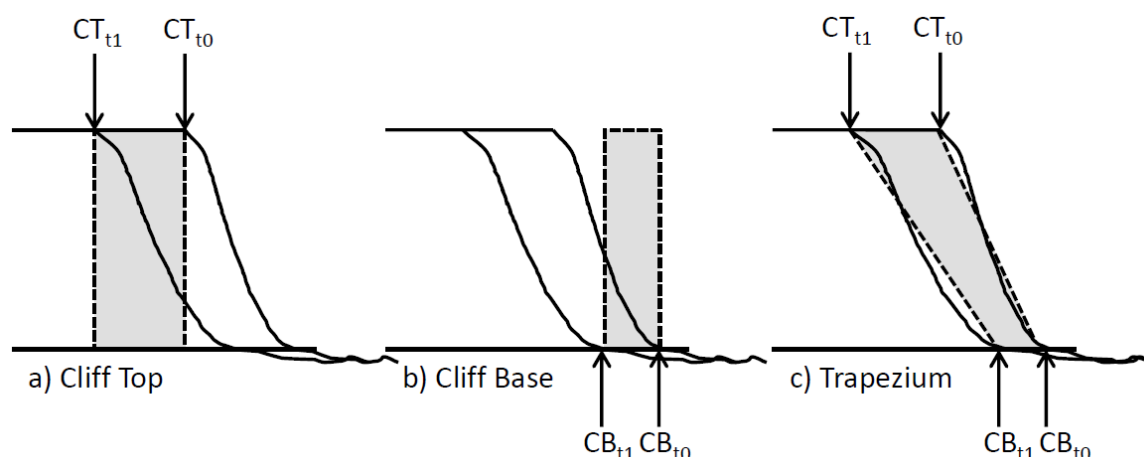
Figure 3.21: Potential variations in volumes calculated using a) Cliff top, b) Cliff base and c) Trapezium using both cliff top and cliff base to take into account steepening or flattening of the cliff face.

Step 2: Dividing Segment by Lithology

It is necessary to identify and quantify the contribution from individual beds or units. This is primarily related to the fact that each bed will have a unique Composition Factor (K) and therefore their volume contribution must be calculated separately. The first step is to create a geological cross section of the cliff face that includes all the major lithological units. The method used to create the cliff section is presented in Section 3.3.1. The second set involves the use of Arc GIS9.3 to calculate the percentage of each segment occupied by each lithology.

Once created the cliff sections were imported in to ArcGIS 9.3 where the polygon tool was used to create a shape feature for each segment (Figure 3.22a), i.e. each segment was traced creating 68 polygons, one for each segment. These features were then converted to rasters, to give a total segment raster value. A raster is a cell of a defined size, in this case 1x1, within a grid that has a value which represents the lithology. Since the volume of each segment is already known, the scale of the cliff sections and the cell size is not important. The individual beds were also traced into shape features and converted to rasters (1x1). Where the beds spanned more than one segment the polygons were divided at the boundaries, so each area defined by a solid black line in Figure 3.22b is an individual feature. This allowed the proportion of different lithologies found in each segment to be calculated. It is the proportion of the segment occupied by the various lithologies that is calculated in this process.
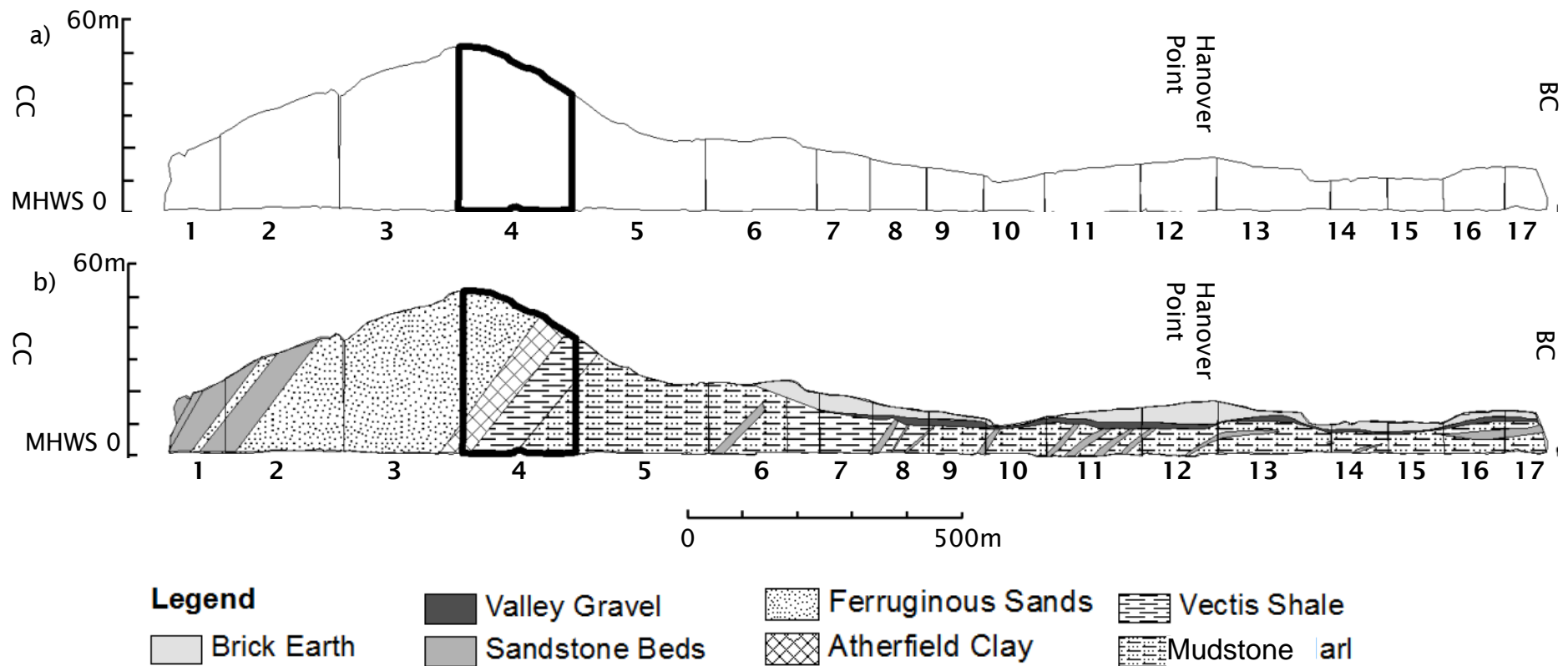
Figure 3.22: Cliff section between Compton Chine (CC) and Brook Chine (BC), created in ArcGIS 9.3. a) The cliff segments represent 100% of their volume calculated using Equation 1. b) Cliff segments divided into different lithologies

Giving the Lithology Contribution Factor (A), a number between 0 and 1 that represents the proportion of the total eroded volume contributed by a lithology within a segment. For example Table 3.15 shows the raster values and corresponding cliff face area proportion and Lithology Contribution Factor (A) of segment 4 (Figure 3.22b). These calculations were carried out for the various lithologies in each segment ready for the composition factor to be added to the calculation.

Table 3.15: Raster values and corresponding cliff face area percentages for Segment 4 (highlighted in Figure 3.22a and b)

	Total	Ferruginous Sand	Atherfield Clay	Wessex Mudstone	Vectis Shale
Raster Value	553954043	184665824	138457482	71480255	159350482
Cliff Face Area (%)	100	33.3	25.0	28.8	12.9
Average Annual Volume Eroded (m^3 a^{-1})	5008	1970	1252	646	1441
Lithology Contribution Factor (A)	n/a	0.33	0.25	0.29	0.13

Step 3: Composition Factor

The Composition Factor (K) is a number between 0 and 1 which represents the proportion of cliff sediment that exceeds the LCD and therefore will be retained on the beach. To calculate K for a lithological unit or formation the particle size distribution was determined from the analysis of cliff samples. The K of each lithology will vary with LCD. Several samples were taken, from each significant bed in each geological formation to determine the particle size distribution (PSD) of the cliff material, through wet sieving (Table 3.16). The number of samples taken varies in relation to the variability in lithology within each formation, and the percentage of the cliff face taken up by each formation. The samples were sent to the Surrey Geotechnical Consultants laboratory for grain size analysis.

The LCD varies alongshore; therefore K is continuously variable based on the LCD which is averaged over three sections of coastline, divided based on abrupt changes in beach grain size and hence LCD and Composition Factor. The sections are 1) Compton Chine to Marsh Chine, 2) Marsh Chine to Atherfield Point and 3) Atherfield Point to Whale Chine. The sections are marked on Figure 3.3. The

average littoral cut off diameter for each section was used to calculate the Composition Factor for each lithological unit within each segment.

Table 3.16: Number of samples taken for grain size analysis from each formation lithology

Formation	Lithology	Percentage of total cliff face area	Number of Samples
Wessex	Mudstone	52.3	4
Wessex	Sandstones	5.13	3
Vectis	Shale	11.8	4
Vectis	Sandstones	3.70	4
Atherfield Clay	Clay	9.76	2
Atherfield Clay	Sandstone	1.97	3
Ferruginous Sand	Sandstone	14.1	8
Brick Earth	Sandstone	4.00	4
Valley Gravel	Breccia	1.46	4

Step 4: Beach Grade Volume Calculations

The final step is to calculate the volume of beach grade sediment produced by each lithology through cliff recession and sum these values to get the total input from that segment. This is achieved by multiplying the total volume of sediment produced by the segment with the corresponding Lithology and Composition Factors as shown in Equation 3.12:

$$Q_{Beach\ Grade} = \Sigma(Q_{total} \times K_i \times A_i) + (Q_{total} \times K_{ii} \times A_{ii}) + \cdots (Q_{total} \times K_n \times A_n)\ (3.12)$$

Where $Q_{Beach\ Grade}$ = volume of beach grade sediment produced by a segment, Q_{total} = total volume of sediment produced by that segment, $K_{\dots}$ = Composition Factors of the lithologies in that segment respectively and $A_{\dots}$ = Lithology Contribution Factors of the lithologies in that segment respectively i.e. the sum of the beach grade sediment from each lithology within a segment.

3.6.2   Subaqueous Cliff/ Shore Platform as a Source of Sediment

The final part of this method looks at the contribution made by the sub- aqueous cliff and shore platform. Most sediment budget studies do not take account of this sediment source. There are some exceptions including Mason (1985), who simply assumed parallel retreat of the cliff and platform and that the platform slopes at 3°

for 100m - this being the base of any erosion. The value of 100m was not justified and is arbitrary. This method is not suitable for the study site since the platform/shoreface slope is not uniform alongshore.

Newsham et al. (2002) present a method more appropriate for this site which involves the creation of a Digital Elevation Model (DEM) that is migrated parallel to the shoreline and compared to the original within a GIS programme. Figure 3.23 shows a horizontal section through the DEM and migrated DEM, demonstrating the change in elevation that represents the sediment input.

A = The original surface is above the migrated surface. Gives correct volume calculation.

B = The migrated surface is above the original surface. Sediment previously removed from these areas.
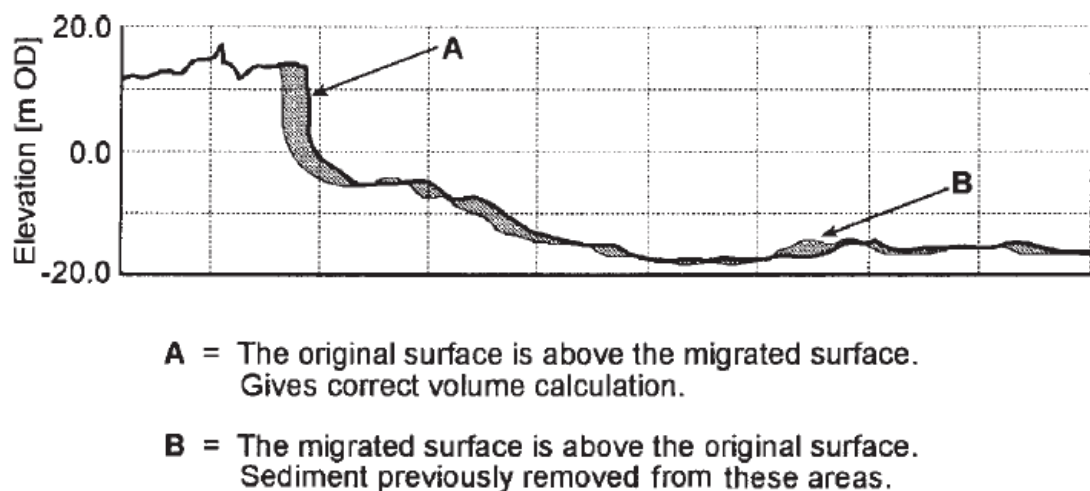
Figure 3.23: Horizontal section through the original DEM. The change in elevation due to the lateral migration is indicated by the cross-hatched area and represents the sediment yield. Figure taken from Newsham et al. (2002).

The seaward extent of the shoreface contribution was taken to be 2.5 km by Newsham et al. (2002) where a prominent break of slope exists. Since no break of slope exists along the southwest coast the sub aqueous cliff/ shore platform contribution was assumed to be from the cliff platform boundary (i.e. mean high water springs) out to the depth of closure. The depth of closure was chosen as a limit to shore platform erosion because the movement of surficial sediment over a shore platform is considered to be a significant factor in their erosion (Skafel and Bishop, 1994). Therefore below the depth of closure, the depth below which no change in beach profile occurs, negligible sand movement and thus platform erosion will occur.

The depth of closure was calculated using Equation 3.13, from Hallermeier (1981):

$$h_{in} = 2.28H_s - 68.5\left(\frac{H_s^2}{gT^2}\right) \qquad (3.13)$$

Where, Hs is the effective wave height just seaward of the breaker zone that is exceeded for 12 hours per year, i.e. the significant wave height with a probability of yearly exceedance of 0.137%, T is the wave period associated with Hs, and g is acceleration of gravity.

Wave data from the Met Office provided values of H_s = 5.5 m and T = 10 s, giving a depth of closure of 10.4 m. A DEM from MHWS out to 10.4 m was created in ArcGIS9.3. The model data was migrated 50 m to simulate 100 years of cliff recession, n.b. the shore line is eroding at a long-term average rate of 0.5 m a^{-1} (Stuiver, 2010). The raster calculator function was used to subtract the original DEM from the migrated one. The change in elevation was converted into a volume by multiplying the value with the cell dimensions. The shoreface was divided by the subsections identified through the changes in beach sediment LCD as shown in Figure 3.24, to make the results comparable with the cliff volume contributions, and further divided into their different lithologies using marine geology maps.
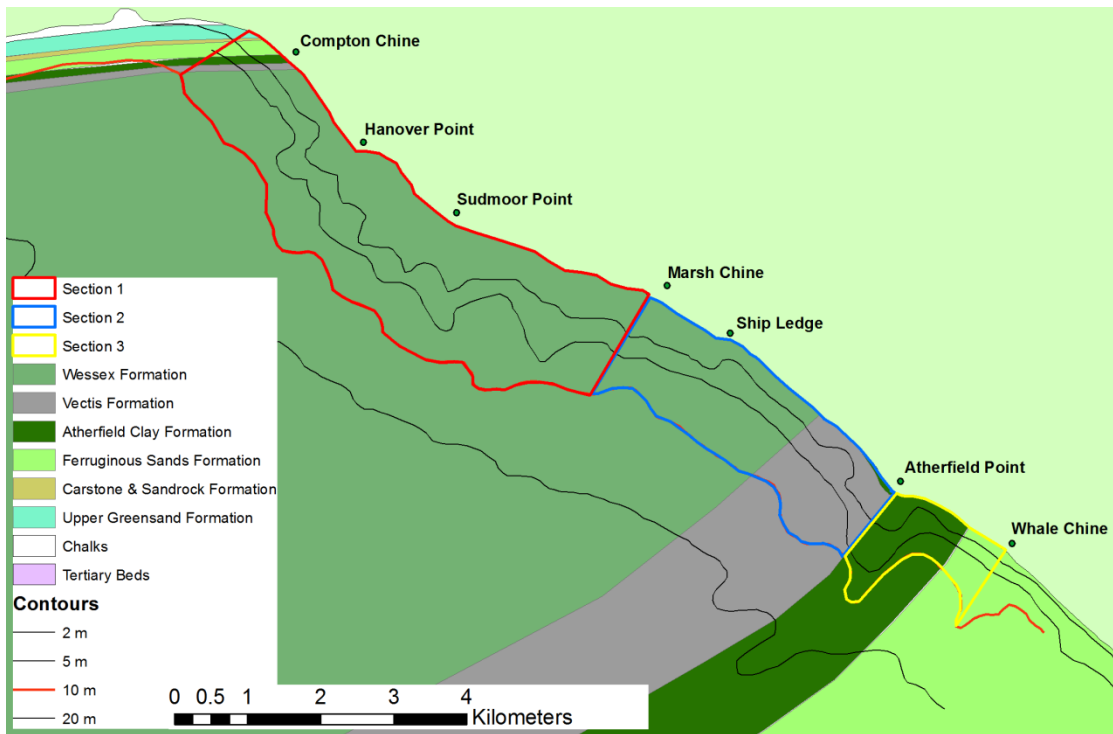
Figure 3.24: Map showing the division of the platform by LCD sections for sediment input calculations. The offshore extent of the areas shown is related to the 10 m depth contour.

3.6.3   Potential Longshore Sediment Transport

Potential longshore sediment transport is an important part of a sediment budget. Two methods were used in this study; both only give an approximation of the true values but do provide a reasonable indication of it. The first method employed was simply to assume a steady beach volume over time and that all sediment entering a beach cell, from both cliff erosion and longshore transport in, would leave as longshore transport out. The beach cells were defined by the Environment Agency profiles (Figure 3.3). This method was carried out using the Sediment Budget Analysis System (SBAS Rosati and Kraus (1999)) by force balancing all beach cells.

The second method used the output from RCPWAVE, i.e. the wave height, wave direction and water depth at each station point, these are not necessarily on the beach but the highest rates of longshore transport occur in the intertidal zone (Van Rijn, 1993). To get a representative value for each beach cell or segment (as defined by the EA profiles Figure 3.3) the average values for each segment were used in the following calculations. Potential longshore sediment transport rates for sand were calculated using the method of Komar and Inman (1970):

$$I_l = 0.77\ EC_g sin\alpha_b cos\alpha_b \qquad\qquad (3.14)$$

Where I_l = Immersed weight sediment transport rate (m³s⁻¹), E = Wave energy density, C_g = Wave group celerity and α_b = Wave incident angle at the break point.

Wave energy density is calculated using Equation 3.15:

$$E = 1/8\rho g H^2 \qquad\qquad (3.15)$$

Where ρ = Density of sea water (1028 kg m⁻³), g = Acceleration due to gravity (9.81 m s⁻¹) and H = Wave height

And wave group celerity (C_g) is equal to wave celerity (C = wave length/wave period) multiplied by n which is calculated using Equation 3.16:

$$n = 1/2(1 + (\frac{4\pi d/L}{\sinh(4\pi d/L)})) \qquad\qquad (3.16)$$

Where d = Water depth and L = Wave length.

To convert the immersed weight sediment transport rate to a volumetric transport rate Equation 3.17 was used (Aagaard et al., 2004):

$$Q_l = \frac{I_l}{(\rho_s - \rho)g a'} \qquad (3.17)$$

Where Q_l = Volumetric sediment transport rate (m³ s⁻¹), ρ_s = Sediment density (2650 kg m⁻³) and a' = Pore space factor (0.6, for medium sand)

This potential transport rate is given in m³ s⁻¹ and is converted to m³ day⁻¹ or m³ a⁻¹ by multiplied by the number of seconds in a day or year respectively. However due to the changing tidal levels the beach will not be subject to the forcing of the waves for 24 hours a day. To give a more accurate estimate of the potential transport rate these values were halved, making the assumption that transport of the beach sediment will only take place when the tidal levels are above a mid-tide level. Along much of the coastline the mid-tide level and below is taken up by the shore platform and no sediment is present.

3.7 Multivariate Statistical Analysis

To determine the dominant controls on cliff recession rates from the results produced using the methodology outlined in this chapter a multivariate statistical approach was required. Therefore a Principal Component Analysis (PCA) was carried out using PAST (PAleotological Statistics) Version 3.0 (Ryan et al., 1995). A PCA takes the multivariate data and creates hypothetical variables, or components, that account for as much of the variance in the data as possible (Davies, 1986). The PCA finds the Eigenvalues of the correlation matrix. Using correlation normalises the variables by dividing by their standard deviations.

Results used in the PCA were extracted at the 68 EA profiles for the 15 parameters listed in Table 3.17. The data included both numerical and categorical variable, e.g. beach width and geology respectively. The categorical variables are entered into the PCA in a binary format. Meaning that each category is represented in its own column, e.g. Vectis Shale, if the geology at the profile location is Vectis Shale a 1 is entered, if it is not a 0 is entered. This process is repeated for each geological formation, cliff morphology and level of cliff coherence respectively. In total 30 columns of data were entered in to PAST for the PCA.

Table 3.17: Multivariate data input to PAST for Principle Component Analysis

Input	Data
Cliff base recession rate (CBRR) (m a^{-1})	Numeric
Beach Wedge Area (BWA) (m)	Numeric
Platform Width (m)	Numeric
Beach Width (m)	Numeric
Beach Slope (°)	Numeric
Backshore Median Grain Size (Phi)	Numeric
LCD (Phi)	Numeric
Sorting (Backshore)	Numeric
Skewness (Backshore)	Numeric
Kurtosis (Backshore)	Numeric
Cliff Height (m)	Numeric
Wave Energy Density (KJ m^{-1}) (common waves from 225, 240 & 255° and 5:1 year & 1:50 year storm waves)	Numeric
Geology (WM- Wessex, VS-Vectis, AC Atherfield Clay and FS-Ferruginous Sand Formations)	Binary
Cliff morphology (CBU a to e)	Binary
Cliff coherence (C1, C1/C2, C2, C2/C3)	Binary

4. Geological and Geotechnical Assessment

The aim of this research is to evaluate the relative role of geological and geotechnical controls, wave energy concentration and sediment volume & supply on headland formation and evolution on soft rock, cliffed coasts. The geological and geotechnical controls will be considered in this Chapter. To determine the importance of variations in the cliff and platform lithology that lithology must first be described and defined. Section 4.1 provides an overview of the geology and geomorphology of the cliffs. The geological structure of the study frontage will be considered in Section 4.2, before the seabed geology and shore platform morphology is described in Section 4.3. Finally the geotechnical properties of the cliffs and shore platforms are explored in Section 1.1.

4.1   Cliff Geology and Geomorphology

The soft rock geology that outcrops between Compton Chine and Whale Chine are Lower Cretaceous in age (Figure 4.1 and Table 4.1). The observed variations in cliff morphology are due to a combination of cliff height, surface and ground water pathways, the dip and strike of the beds and cliff lithology, in particular the presence or absence of supportive sandstone beds (Jenkins et al., 2011). Figure 4.2 defines the range of cliff morphologies or Cliff Behaviours Units (CBU) present on the coastline, their distribution is indicated by the coloured bar below the cross sections (created in ArcGIS from the results of the geological mapping) in Figure 4.3.

Superficial Deposits

- Beach deposits
- Blown Sand
- Peat
- Alluvium
- River Terrace Deposits

Bedrock Geology

- Teriary Beds
- Upper Greensand Formation
- Gault Formation
- Carstone Formation
- Sandrock Formation
- Ferruginous Sand Formation
- Atherfield Clay Formation
- Vectis Formation
- Wessex Formation

The Needles

Compton Chine
Compton Bay

Hanover Point

Brook Bay

Sudmoor Point

Brighstone Bay

Ship Ledge

Atherfield Point

Whale Chine

Chale Bay

Blackgang Chine

0   2   4   8
Kilometers

Figure 4.1: Surficial deposits and bedrock geology of the Southwest Isle of Wight. (Source: British Geological Survey, Copyright NERC).

Table 4.1: The geological succession seen on the southwest coast between Compton Chine and Whale Chine. (From Insole et al. (1998) and Bird (1997)).

GROUP	FORMATION	MEMBER	LITHOLOGY
	River Terrace Deposits	Brick Earth	Windblown silt
		Valley Gravel	Coarse angular flint gravel in a sandy matrix
Lower Greensands	Ferruginous Sands	Members XIV &XV	Sandstone
		New Walpen Chine Member?	Fine to Medium Sand with pebble bed at base
		Old Walpen Chine Member	Laminated Sands and Muds
		Unnamed Member XI	Muddy Sands
		Unnamed Member X	
		Ladder Chine Member	Red Sandstone II
		Unnamed Member VIII	Muddy Sands and Sandy Clays with concretions
		Whale Chine Member	
		Unnamed Member VI	
		Unnamed Member V	
		Unnamed Member IV	Red Sandstone I
	Atherfield Clay	Upper Lobster Bed	Alternating Muds and Sandy Silts
		Crackers	Fine Sand with Concretions
		Lower Lobster Bed	Clay
		Chale Clay	
		Perna Bed	Calcareous Sandstone & Sandy Clay
Wealden Beds	Vectis	Shepherd's Chine	Inter-bedded Shale and Silt
		Barnes High	Channel Sandstone
		Cowleaze Chine	Inter-bedded Shale and Silt
	Wessex		Variegated Mudstone inter-bedded with Channel Sandstones
N.b. The members of the Ferruginous Sands, divided by fossil content not lithology, are not all present in Compton Bay and the youngest seen west of Whale Chine is member VIII.			
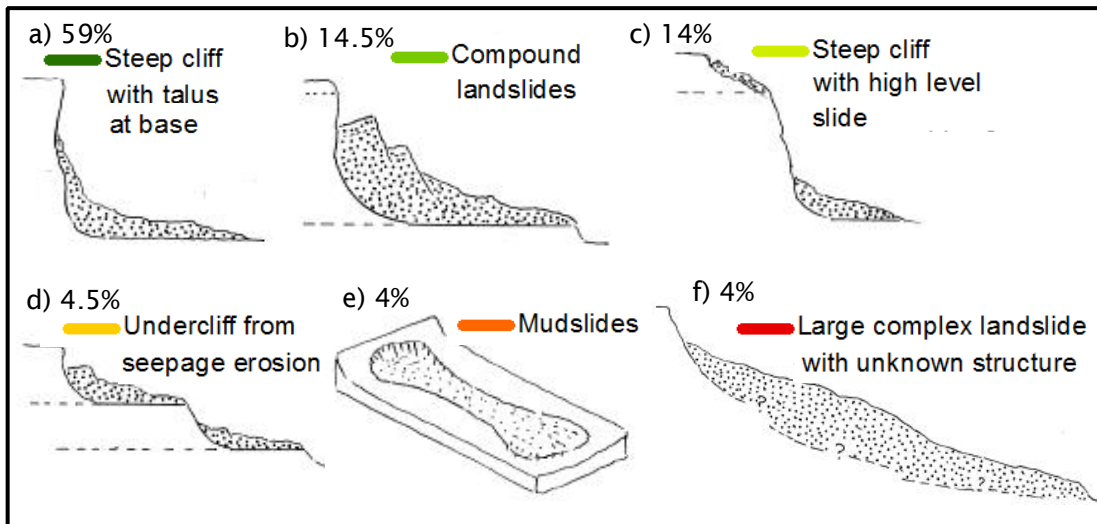
Figure 4.2: Cliff morphologies present on the southwest coast of the Isle of Wight. The percentages indicate the occurrence of the CBU by length of coastline. The colours refer to the coloured bars on Figure 4.3 below the cross sections indicating the morphology of the cliffs. Classification devised from the literature (Barton and Coles, 1984, Moore et al., 2002).

Figure 4.2 also gives the percentage occurrence of each Cliff Behavioural Unit by cliff length. The most common cliff morphology is CBUa, "steep cliff with a talus at base", covering approximately 59% of the coastline. The secondary morphologies are CBUb "Compound Slides" (14.5%) followed by CBUc "steep cliff with high level landslides" (approx. 14%). The other three morphologies contribute less than 5% of the cliff length each. The geology and associated cliff and platform geomorphology of each Formation are described in turn in Sections 4.1.1 to 4.1.5.
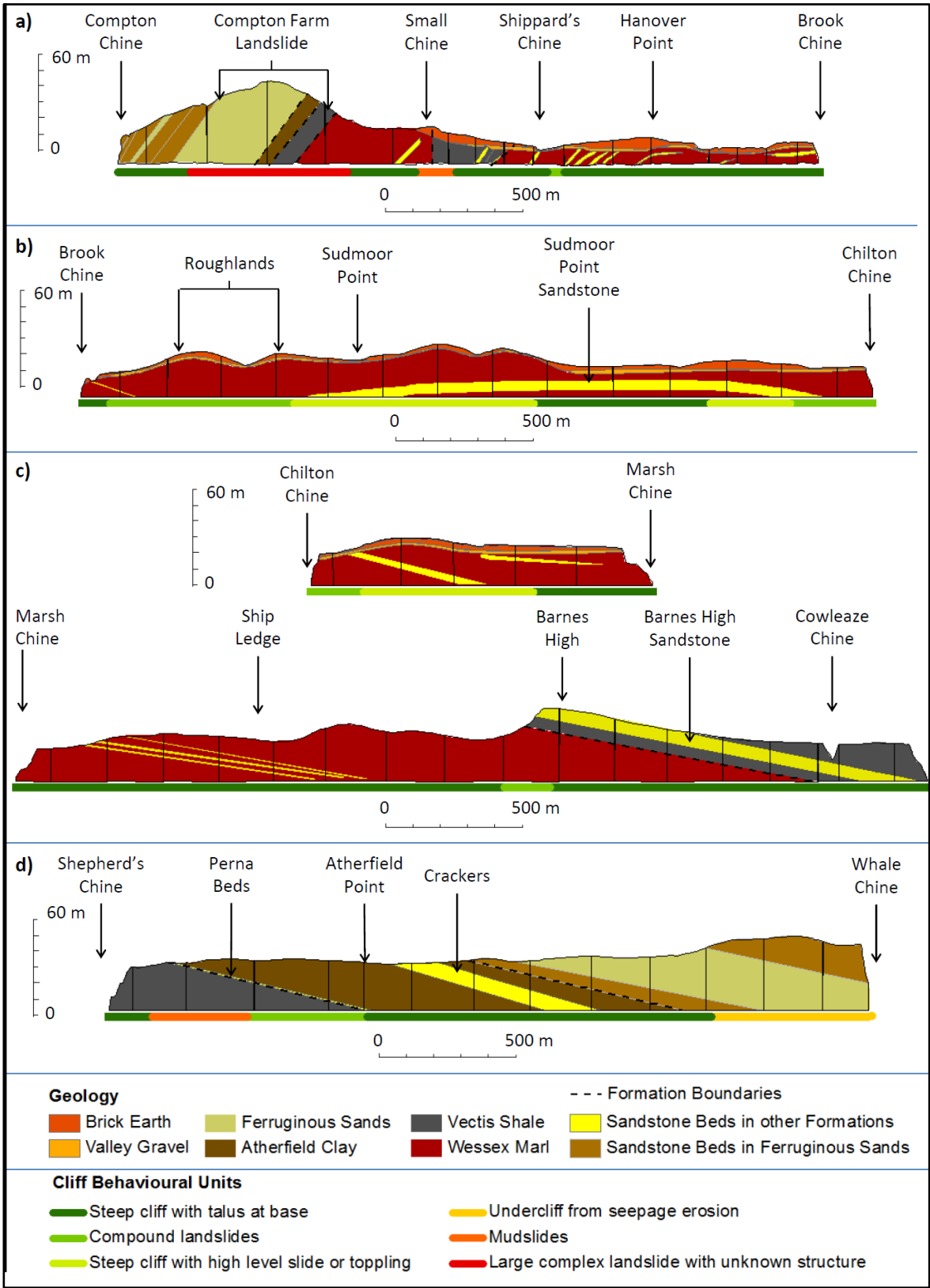
Figure 4.3: Cliff section of study area; a) Compton Chine to Brook Chine; b) Brook to Chilton Chine c) Chilton to Shepherd's Chine and d) Shepherd's to Whale Chine. The coloured bar below the sections indicates the cliff morphology (Figure 4.2)

4.1.1   Wessex Formation

The Wessex Formation represents the oldest beds to outcrop on the Isle of Wight. They dominate the coastline outcropping from around Barnes High in the south to Shippard's Chine in the North. A small section is repeated in Compton Bay by a fault running though the Small Chine landslide, the succession returns to the Vectis Shales on the southern edge of the Compton Farm Landslide (Figure 4.3a). Laid down in a fluvial environment the Wessex Formation consists of two distinct lithologies; the red, green and purple variegated mudstones represent the overbank deposits, while the irregular, laterally discontinuous sandstones are former channel sand deposits (Daley and Stewart, 1979, Insole et al., 1998, Radley and Allen, 2012).

The Wessex Formation displays three dominant cliff morphologies. The most common of which is CBUa "Steep cliffs with talus at base" (Figure 4.4, Figure 4.2 and 4.3), this covers much of the Wessex North of Brook Chine and South of Marsh Chine.
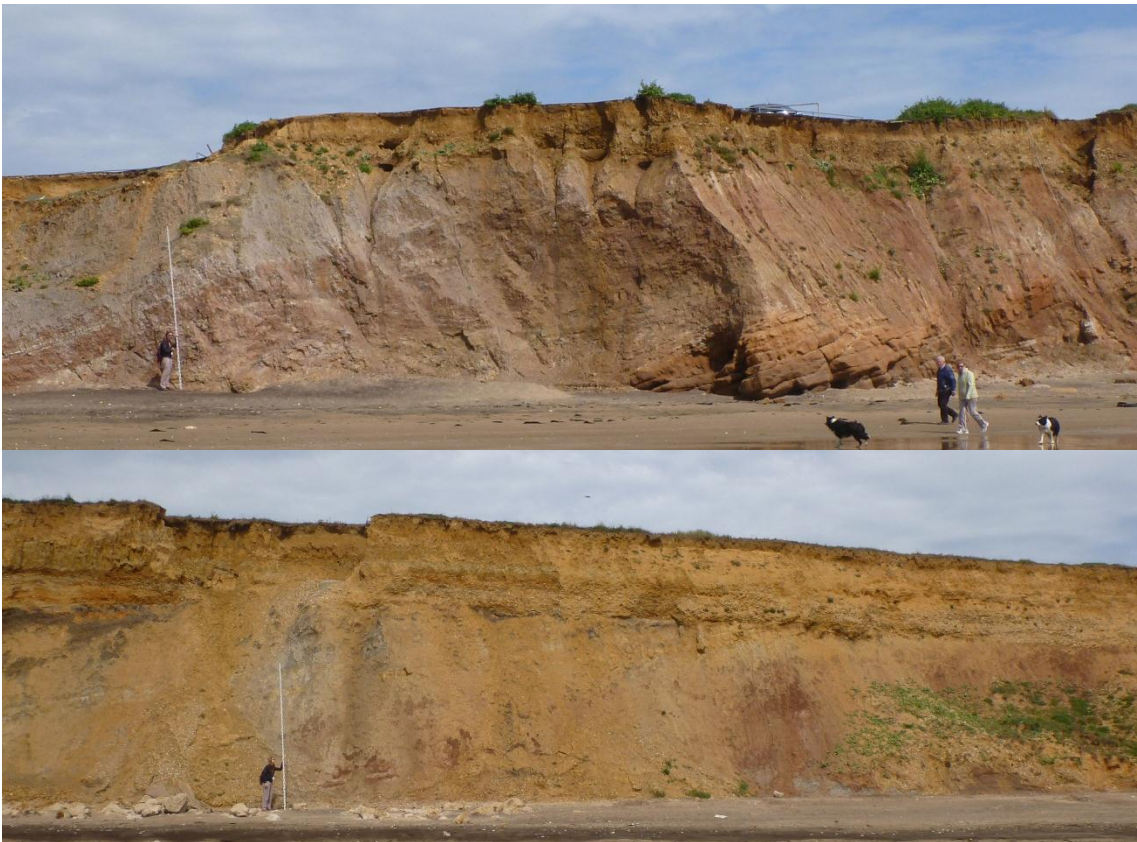
Figure 4.4: The steep low cliffs of the Wessex Formation (CBUa). The measuring staff is 5m long. (Source: Original Photograph).

The second morphology present is CBUb "Compound slides", the most notable of which is known as Roughlands, a landslide feature covering an area of approximately 58,500 m². Smaller compound slides are seen around Chilton Chine, Shippard's Chine and north of Barnes High. These compound slides appear to occur in areas with no supportive sandstones present in the cliff.
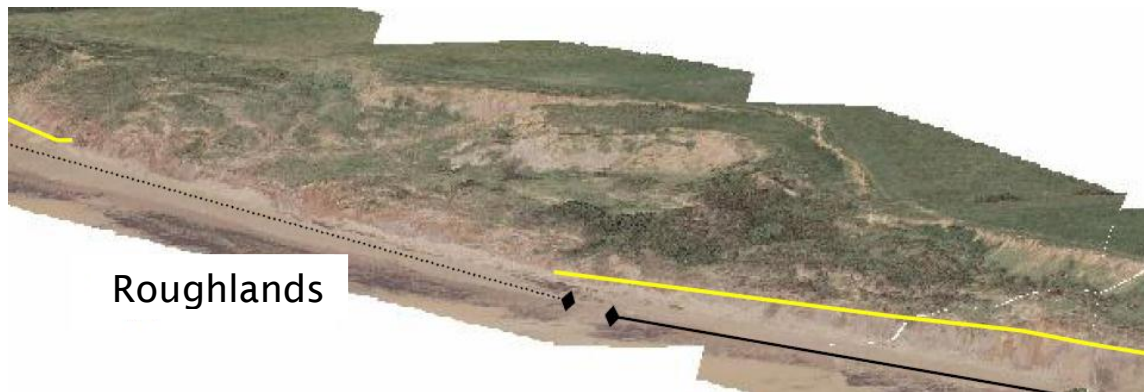
Roughlands

Figure 4.5: Roughlands landslide, the most notable example of a compound landslide (CBUb) within the Wessex Formation (image was created by draping the 2008 aerial photographs over the 2007 LiDAR data provided by CCO in ArcGIS 9.3)

Finally CBUc (Figure 4.2 and 4.3) occurs at either end of the Sudmoor Point Sandstone and between Chilton and Marsh Chines, where the near horizontal sandstone stabilises the lower half of the cliff only allowing landsliding above that sandstone.

Figure 4.6: An example of a steep cliff with high level sliding (CBUc) in the Wessex Formation to the south eastern end of the Sudmoor Point Sandstone. The measuring staff is 5m long. (Source: Original Photograph).

The Wessex Formation makes up approximately 57% of the cliff face by area and 91% of the intertidal platform by surface area across the study site. (n.b. the area of intertidal shore platform was estimated from the 1981 OS map in ArcGIS 9.3. the 1981 represents the most recent map of the area). The geology and geomorphology of the shore platform is explored in detail in Section 4.3.

4.1.2   Vectis Formation

The Vectis Formation overlies the Wessex Formation and is seen in the cliffs at three locations; their best exposure is in Brighstone Bay between Barnes High and Atherfield Point (Figure 4.3c-d); the other exposures are in Compton Bay between Shippard's Chine and Small Chine and in the Compton Farm Landslide, where its exposure is poor (Figure 4.3a). It contributes 15.5% of the cliff face area and 0.3% of the intertidal shore platform area (3.7% of the cliff and all the shore platform is made up by the Barnes High Sandstone).

The base of the Vectis Formation marks the start of the early Cretaceous marine transgression, when the depositional environment changed from fluvial to a brackish lagoonal environment. The formation is divided into three members; the Cowleaze Chine, Barnes High Sandstone and Shepherd's Chine Members (Table 4.1). The Cowleaze Chine and Shepherd's Chine Members consist of a series of shales, inter-bedded with thin beds of siltstone, sandstone, ironstones and limestone (White, 1921). The Barnes High Member sits between the Chine Members; it is a yellow-orange, iron stained sandstone coarsening upwards in a single unit approximately 6m thick (Stewart et al., 1991). It is thought to represent a composite tidal sand bar formed within an incised estuarine valley (Yoshida et al., 2001). The Vectis Formation is more prone to instability than the Wessex. However along much of its exposure the cliffs are steep with talus at the base, i.e. CBUa (Figure 4.2 and 4.3), this is most likely due to the stabilising influence of the Barnes High Sandstone. There are three areas where the Vectis Formation deviates from CBUa. In each case the dominant failure mode is mudsliding (CBUe, Figure 4.2 and Figure 4.3):

1) Small Chine Landslide, Compton Bay (Figure 4.7a, Figure 4.3a); where faulting has repeated the Wessex Formation creating a zone of weakness around a small chine. The presence of water and weakness in the cliff has led to the formation of localised mudslides (Figure 4.2e)

Figure 4.7: Examples of mudslides (CBUe) found within the Vectis Formation at a) Small Chine Landslide and b) Compton Farm Landslide (Source: Original Photographs)

2) Compton Farm Landslide, north end of Compton Bay (Figure 4.7b, Figure 4.3a); A Large Complex landslide with unknown structure covering an area of 57,000m². N.b. It also involves the Atherfield Clay and Ferruginous Sand Formations, but mudsliding is apparent where the Vectis Shales outcrop.

3) Shepherd's Chine to Atherfield Point (Figure 4.8, Figure 4.3d). The area to the west, which is predominantly the Vectis Shales, fails though mudslides (Figure 4.2e). As the Atherfield Clay becomes more dominant towards the headland compound slides become apparent (Figure 4.2b).
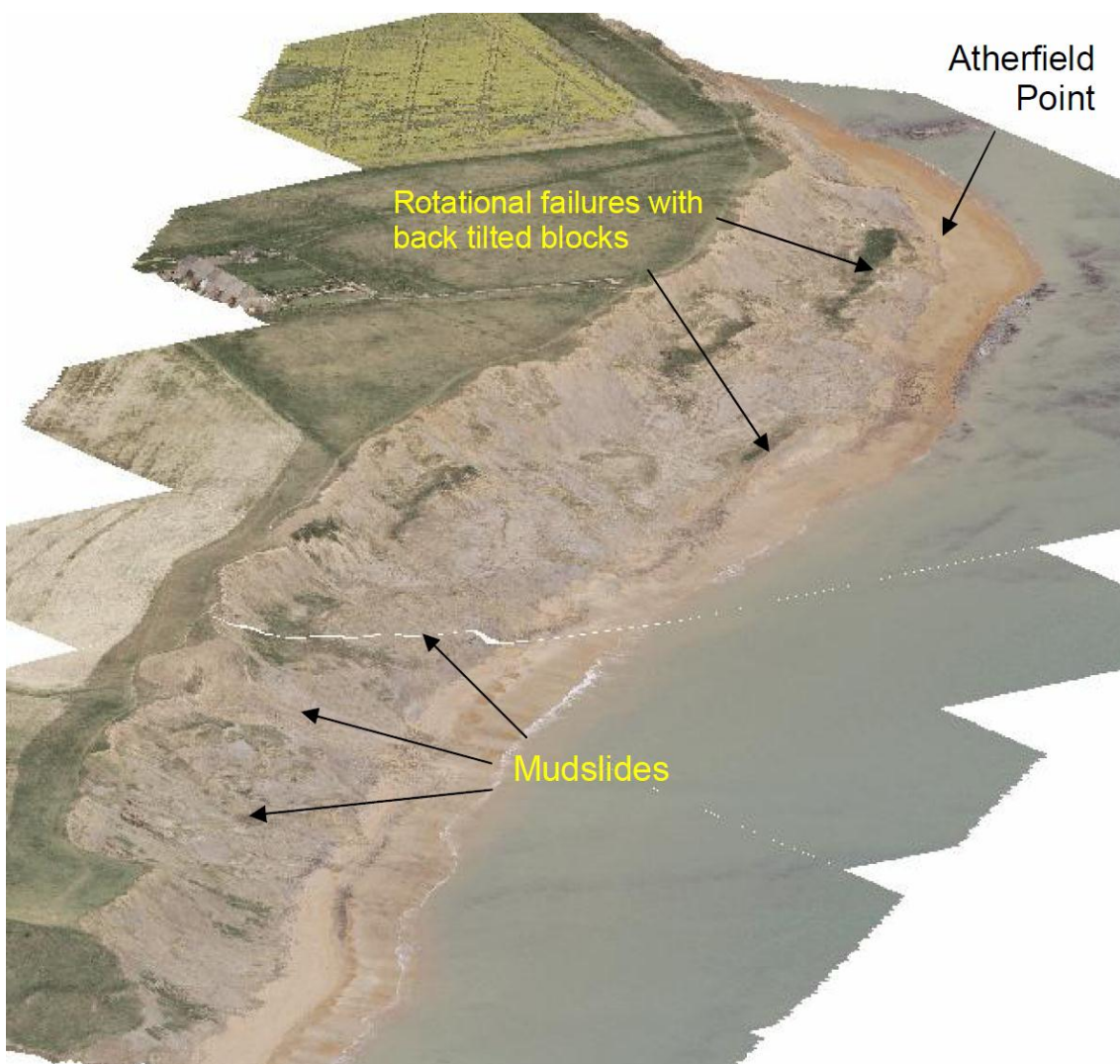
Figure 4.8: Extensive mudslides (CBUe) within the Vectis Formation south of Shepherd's Chine (Image was created by draping the 2008 aerial photographs over the 2007 LiDAR data provided by CCO in ArcGIS 9.3)

4.1.3   Atherfield Clay Formation

The Atherfield Clay Formation represents the youngest beds of the Lower Greensand and denotes the switch from a lagoonal to an open marine environment (Jackson et al., 2005). These beds can be seen in two locations; in the Compton Farm Landslide where they are poorly exposed in a large scale landslide, CBUf, and at Atherfield Point. The cliffs remain relatively steep where only the Atherfield Clay and Ferruginous Sands are exposed in the cliff, CBUa, but display compound slides when overlying the Vectis Shales, CBUb (Figure 4.8, Figure 4.2 & Figure 4.3). Where present outside of the study area the Atherfield Clay Formation is synonymous with landsliding, at Redcliff in Sandown Bay, Isle of Wight and where exposed inland in Sandgate, Kent (Palmer, 1991). The formation is divided into five different members, the lithological succession of which is shown in Table 4.1, combined they represent 12% of the cliff face area. The Perna Beds, which form Atherfield Ledge (Figure 4.19), consist of two thin beds, each less than 1 m thick.

Above the Perna Beds are the Chale Clay and Lower Lobster Beds, both are clay, although the latter is siltier in places. They are difficult to distinguish in the field since they were separated on the basis of fossil content and for the purposes of this study they will be considered as one lithology. The crackers are named for the two layers of bioturbated calcareous silty sand concretions contained within the layers of fine sand (Insole et al., 1998). It is possible that the Cracker Beds offer some support and drainage to the clays, producing the steep cliffs that exist across their exposure. Finally the Upper Lobster Beds consist of three muddy layers alternating with two sandy layers totalling approximately 9.5 m and 5.5 m respectively. None of these beds form significant intertidal platforms, some narrow ridges of the cemented Cracker stones are visible on the beach but do not maintain their elevation offshore.

4.1.4   Ferruginous Sand Formation

The Ferruginous Sands are formed from alternating layers of dark silty clays and muddy glauconitic sands, laid down in a shallow marine shelf environment (Insole et al., 1998). They are exposed at either end of the study site making up 14% of the cliff face area (Figure 4.3), to the north of Compton Bay and in Chale Bay between Atherfield Point and Whale Chine (in fact they extend beyond the study area to

around Blackgang Chine). In Compton Bay and close to Atherfield Point they form fairly stable, precipitous cliffs (CBU a, Figure 4.9a). Closer to Whale Chine they have formed a debris bench or undercliff through seepage erosion (CBU d, Figure 4.9b ; Figure 4.2 and Figure 4.3), in this area the recession of the cliff top is controlled by the rate of ground water out flow (Hutchinson, 1965), not the rate of cliff base erosion.
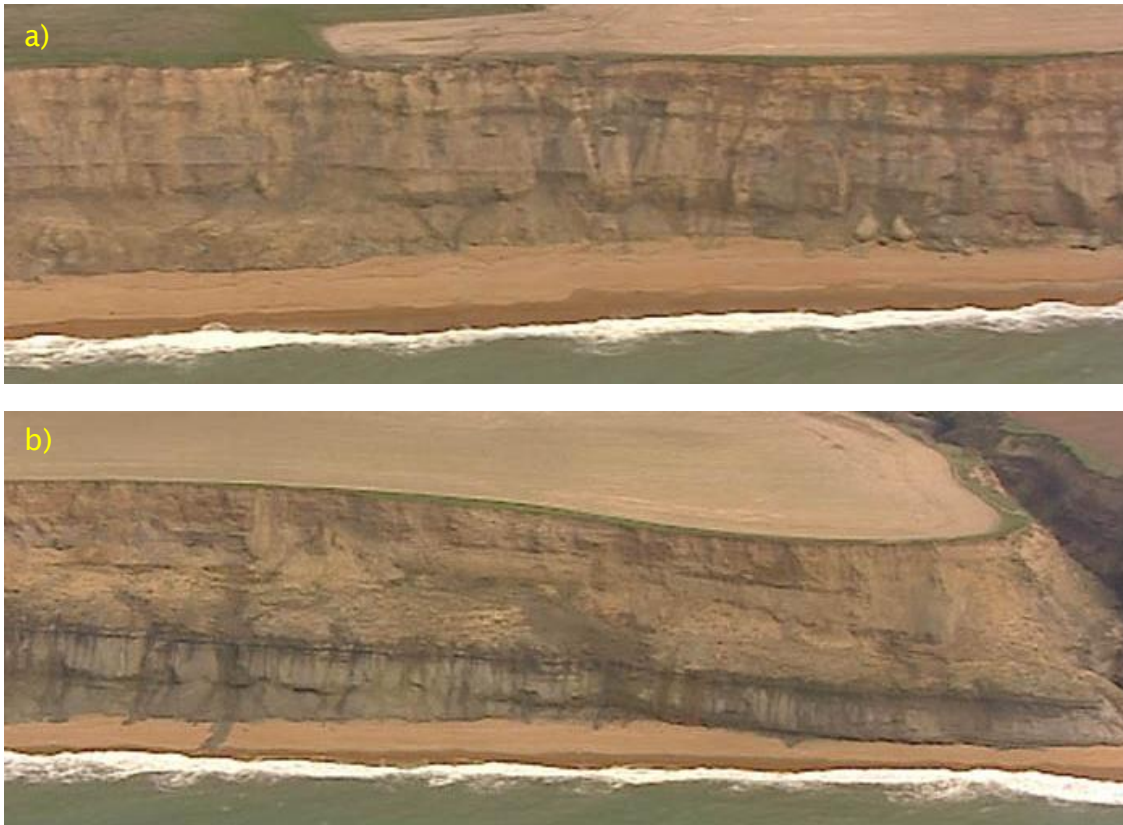
Figure 4.9: Examples of the typical cliff morphology seen in the Ferruginous Sand Formation, a) Steep cliffs with talus at the base (CBUa) and b) benched cliff formed through seepage erosion (CBUd) (Source: Future Coast DEFRA (2002))

As with the Atherfield Clay Formation many of the divisions of the Ferruginous Sands were devised in relation to fossil content but will simply be divided by lithology for this study (Table 4.1). Between Atherfield Point and Whale Chine three subdivisions can be readily identified. The first corresponds to unnamed member IV, a group of bioturbated reddish brown sandstones (White, 1921). The next incorporates unnamed members V and VI and Whale Chine Member and can be described as grey-green bioturbated, glauconitic muddy sandstones. Finally unnamed member VIII; a series of grey to brown muddy sands that form the top of the walls of Whale Chine (Insole et al., 1998). In Compton Bay the individual

members are not easily identified and the succession is incomplete. The beds present include several grey fine grained silty sand, coarse red sandstones and a thin clay bed.

4.1.5   River Terrace Deposits

The extent of the Pleistocene alluvial deposits of Brick Earth and Valley Gravel along the coastline is shown in Figure 4.1 and Figure 4.2. Today they occupy the cliff top from around Small Chine in Compton Bay to Marsh Chine in Brighstone Bay and represent the final 5.5% of the cliff face area. In the late 18th Century according to Codrington (1870) they extended from Compton, beyond Whale Chine to Blackgang Chine. This indicates that the length of exposure has decrease from approximately 15.5km to approximately 5.5km in the last 140 years. This represents a reduction of gravel input to the beach of approximately 65%. The Valley Gravels are intermingled with the Brick Earth in places and are thought to have been deposited by the Western Yar at a time when the river was much bigger than it is today and drained a large area to the south which has long since been eroded (White, 1921, Leighton, 1891). The Brick Earth is a superficial, structureless, windblown deposit originating under periglacial conditions from sparsely vegetated outcrops of unconsolidated sand silt and clay formations and laid down over the Valley Gravels (Bird, 1997). The gravel consists of angular flints, with chert and ironstone; it is overlain by evenly bedded Brick Earth (Codrington, 1870). The Valley Gravels are an important source of beach gravel.

4.2   Structural Geology

In addition to the lithology, the structural geology of the southwest coast is fundamental to the control of shore platform formation and evolution. The variations in the dip of the beds also control the morphology of the platforms. As such it is vital to gain an understanding of the structural geology of this coastline. The southwest coast represents a section through the northern limb of the Brighstone Anticline, an asymmetrical anticline plunging to the southeast (Figure 4.10). The Brighstone Anticline was created by compressional forces associated with the north-south convergence in the Alps during the early Oligocene to early Miocene. The compressional forces reactivated and reversed several faults previously created by extensional forces, including the Needles Fault and the

Sandown Fault (Figure 4.10 Evans et al. (2011)). The overlap of these fault zones created a relay ramp in the folds, with both the Sandown and Brighstone anticlines petering out towards the centre of the island where the compressional forces were spread across the two fault zones.

The axis of the Brighstone Anticline is curvilinear, lying just offshore of the Needles and Freshwater Bay it bends round to run roughly parallel to the southwest coast appearing onshore around Chale (Evans et al., 2011). The angle at which the anticline plunges increases to the west as the influence of the Sandown Fault disappears increasing the dip of the beds of the northern limb, from east to west (Figure 4.11). This change in the dip and plunge of the anticline along with the relative orientation of the coastline with respect to the axis is reflected in the dip seen in the cross sections (Figure 4.3a).
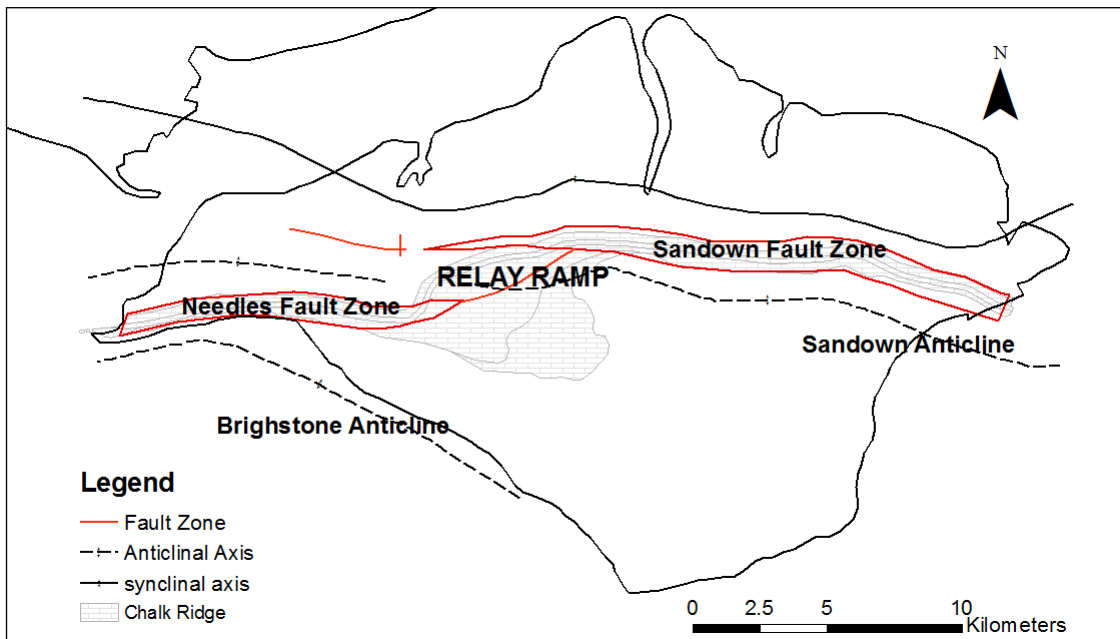
Figure 4.10: Structural geology of the Isle of Wight. Adapted from Evans et al. (2011).

To the north of Hanover Point the apparent dip is approximately 12° to the northwest, while the actual dip is around 20 to 40° to the north to north-northeast (Figure 4.11). This is a result of the deviation of the coastline orientation from that of the fold axis. The abrupt change in apparent dip at Hanover Point to near horizontal comes as the coastline turns to run parallel to the fold axis. The apparent folding of the Sudmoor Point Sandstone has misled geologists in the past to assume the axis of the fold made landfall in this area (White, 1921).
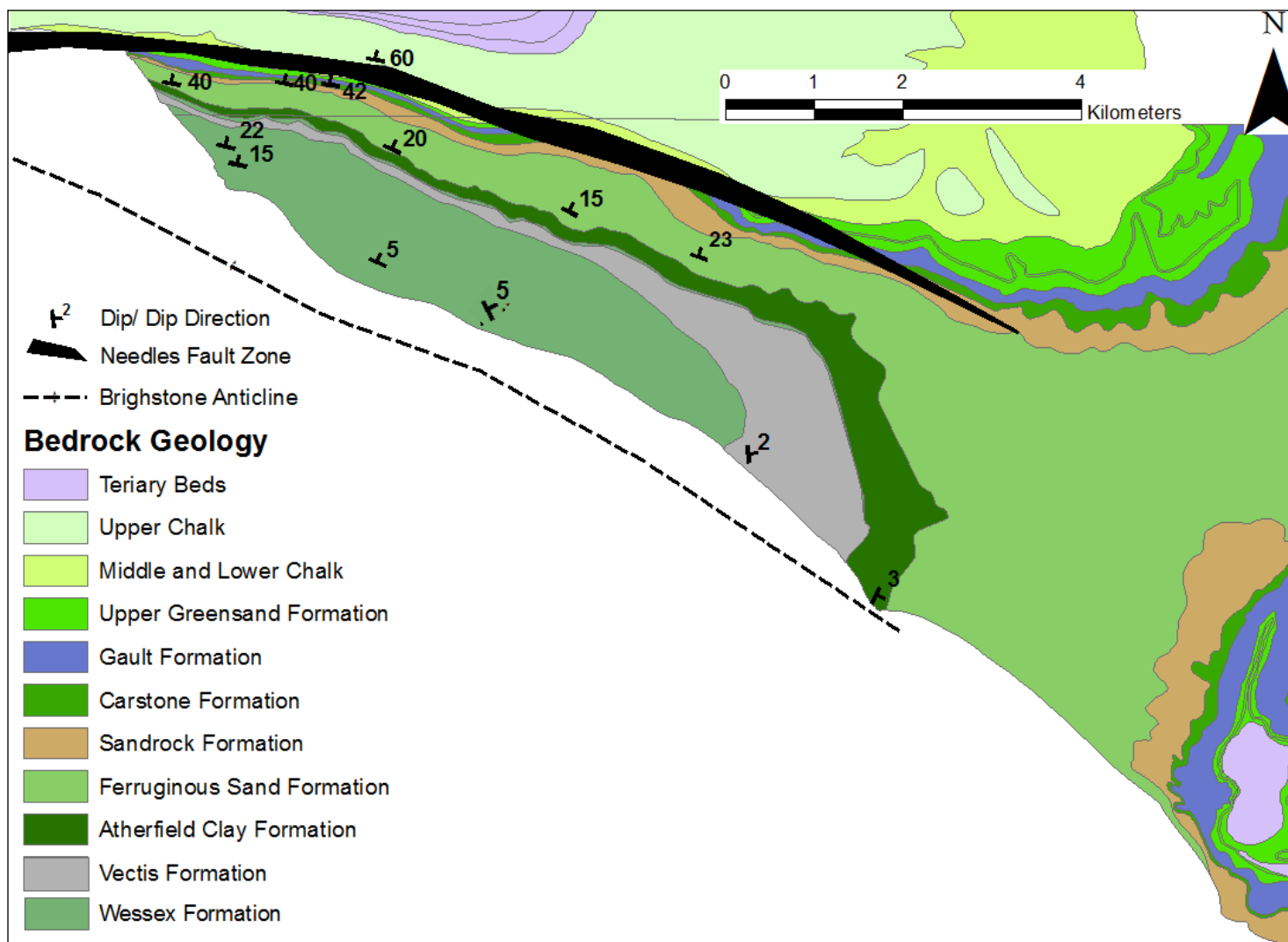
Figure 4.11: Geological structure of the Isle of Wight (Fault zone and fold from Underhill and Paterson, 1998, dip measurements from BGS map, 1975).

Therefore, it is important to be aware of the difference between the bed geometry of the channel sandstones and the actual dip of the beds. The sandstones are unlikely to have been deposited in a horizontal channel, the lobate nature of these deposits also distorts the geometry and apparent dip of the beds. Beyond Sudmoor Point the apparent dip of the bed switches to the south east at 2 -2.5° and more likely reflects the plunge of the anticline than the dip of its northern limb. These changes in dip and apparent dip are very important when considering planform evolution and cliff stability. It is of particular importance in terms of the dip and strike of the platform forming beds, which are thought to control the formation and migration of headlands as the cliff line recedes.

4.3   Seabed and Platform Geology and Geomorphology

The seabed and platform geology of the southwest coast is described here. The seabed geology is shown in Figure 4.12. The offset in the boundaries between the formations on land and on the sea bed are a reflection of the dip of the beds. to the north of the study area the sea bed geology is almost aligned with that of the land, here the dip of the beds is steep, up to 60°, and the outcrops are narrow. To the south, around Atherfield Point, the dip is much lower (2 to 3°; Figure 4.11) and the off set in cliff top and platform/seabed geology is up to 1km. The off shore bathymetry appears to be controlled by the seabed geology, with steeper shoreface slopes seen where the Vectis and Ferruginous Sand Formations outcrop compared to that seen with the Wessex and Atherfield Clay Formations. This is considered in more detail in Chapter 5.

The shore platform geology and morphology is controlled by the lithology and structural geology in the intertidal zone where the cliff and seabed geology intersect. Only the Wessex and Atherfield Clay Formations produce shore platforms. The most extensive of which is in the Wessex Formation. Along almost the whole length of its exposure, from Ship Ledge to just north of Shippard's Chine, the mudstones and the sandstones of the Wessex Formation form intertidal platforms of varying character. Although predominantly Type A (i.e. gently sloping out to sea, Figure 2.1) the shore platforms within the Wessex Formation can be divided into two characteristic types according to dip, strike and the occurrence of sandstone and mudstone beds. The shore platforms around Hanover Point and extending some 700 m into Compton Bay dip approximately 20° to the north and

show a clear east west strike, they also contain several sandstone beds giving the platform a ridged morphology (Figure 4.13 and Figure 4.14). At one time a large fossil assemblage known as the "Pine Raft" occupied the shore platform at Hanover Point, reports exist of fossilised tree trunks protruding from the cliff base (Bristow, 1862) and strewn across the platform clearly visible at low tide (Norman, 1887). The shoreline has eroded over 100m since these accounts were made, today only a small number of fossilised trees are visible. This may be related to the localised nature of the deposit which now lies further offshore. However erosion by waves and humans is likely to have has an influence. Colenutt et al. (1906) alludes to the removal of block by "many persons" for "various purposes".

In contrast, for the shore platform across the front of Sudmoor Point the bedding within the mudstones is unclear and possibly near horizontal, creating a smooth platform with regular drainage channels (Figure 4.15). To the southern end of the Wessex platforms the strike becomes visible once more; the shallow dip of 2 to 3° to the south east represents the plunge of the anticline (Section 4.1.6). One location this strike is most apparent is at Ship Ledge, where the shore platform becomes more prominent and marks the location of the potentially emerging headland (Figure 4.16). The swath bathymetry in Figure 4.17 shows the offshore extent of these platform forming beds.

Within the Atherfield Clay Formation there are two thin beds that produce the shore platform at Atherfield Point. The lower bed of sandy clay 0.85 m thick forms the majority of the platform (Figure 4.18). The overlying calcareous sandstone is 0.54 m thick (Simpson, 1985) and forms the eastern edge of the platform in-situ, while the remainder of the platform and beach to the west is strewn with disarticulated blocks approximately 0.5 m^3 in size (Figure 4.19). The dip of these beds is 2 to 3° to the southeast, and strike to the southwest approximately 90° to the coastline. The swath bathymetry in Figure 4.18 shows the offshore extent of these beds. The thickness of the Perna bed Sandstone has been found to vary over its exposure within the ledge, measurements by Fitton (1847) revealed the sandstone bed to be 0.75 m, indicating a reduction in the thickness of the platform exposed at the landward edge of the platform of 0.21 m between 1847 and 1985. This represents a lateral variability in the thickness of the bed.
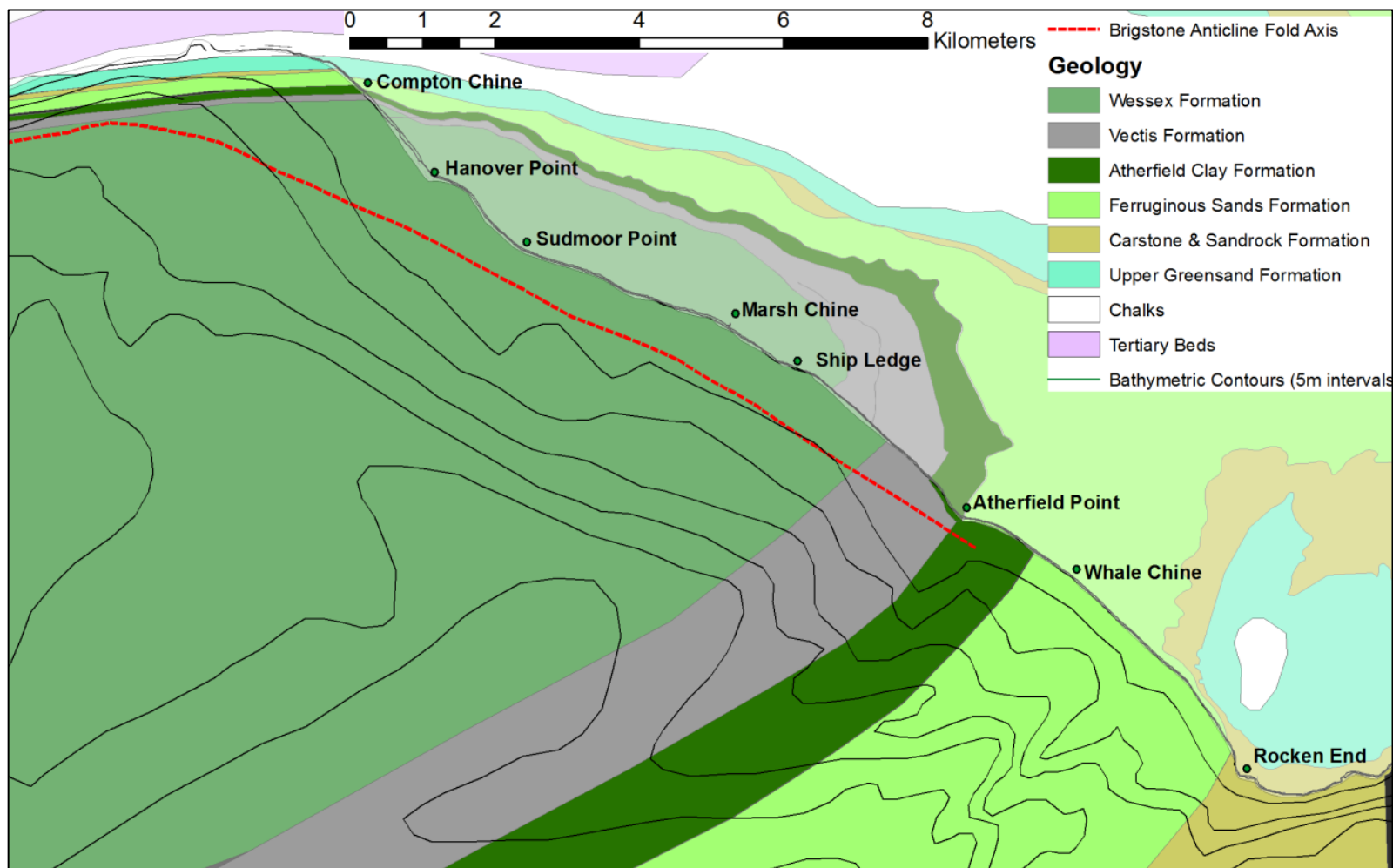
Figure 4.12: Map showing the seabed geology off the southwest cast and how it relates to the geology of the Island itself (the colour of the land based geology has been subdued to delineate the two)

Figure 4.13: Photograph of the shore platform fronting Hanover Point taken from the cliff top. Note the ridged morphology and in particular the prominent sandstone beds. (Source: Original Photograph)
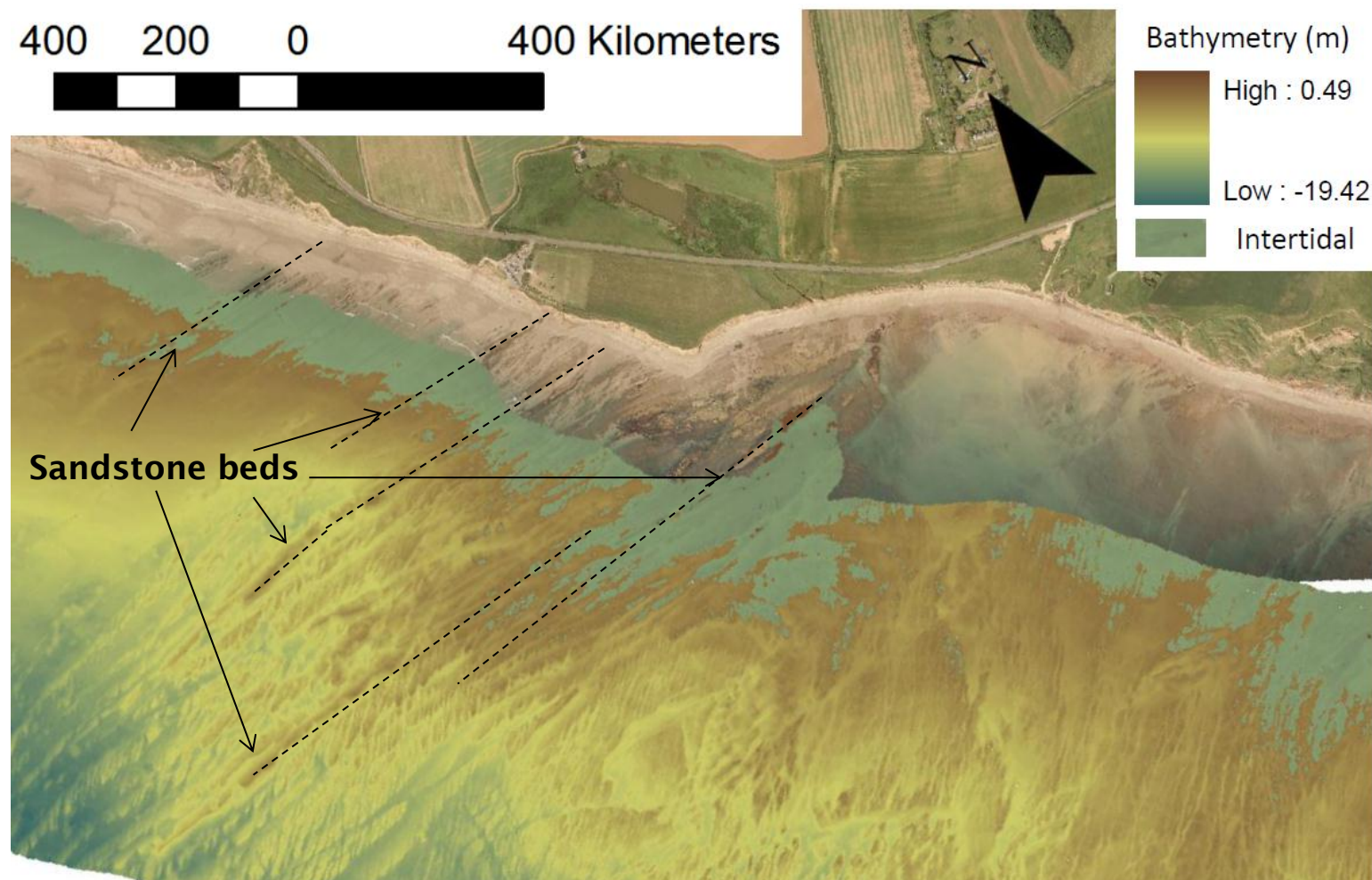
Figure 4.14: Aerial photograph of Hanover Point and its associated shore platform from 2001 overlain by swath bathymetry from 2010. Note the prominent sandstone ridges outcropping in the intertidal and nearshore area. (Data Source: Channel Coastal Observatory)

Figure 4.15: Photograph of the mudstone platform fronting Sudmoor Point, taken at beach level. Note the horizontal nature of the platform bedding. (Source: Original Photograph)
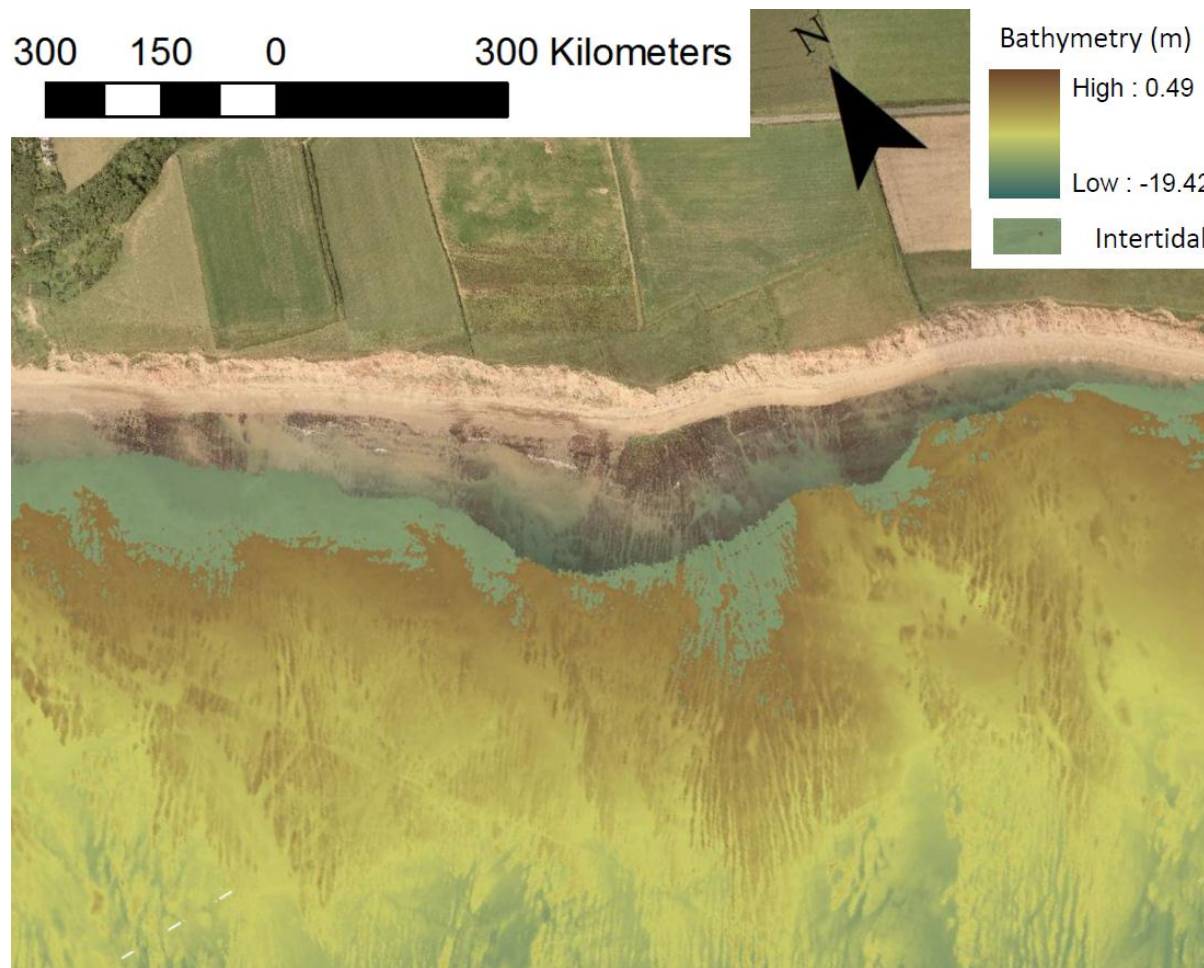
Figure 4.16: Aerial photograph of Ship Ledge and its associated shore platform from 2001 overlain by swath bathymetry from 2010. (Data Source: Channel Coastal Observatory)

Figure 4.17: Photograph of Ship Ledge taken at beach level. (Source: Original Photograph)
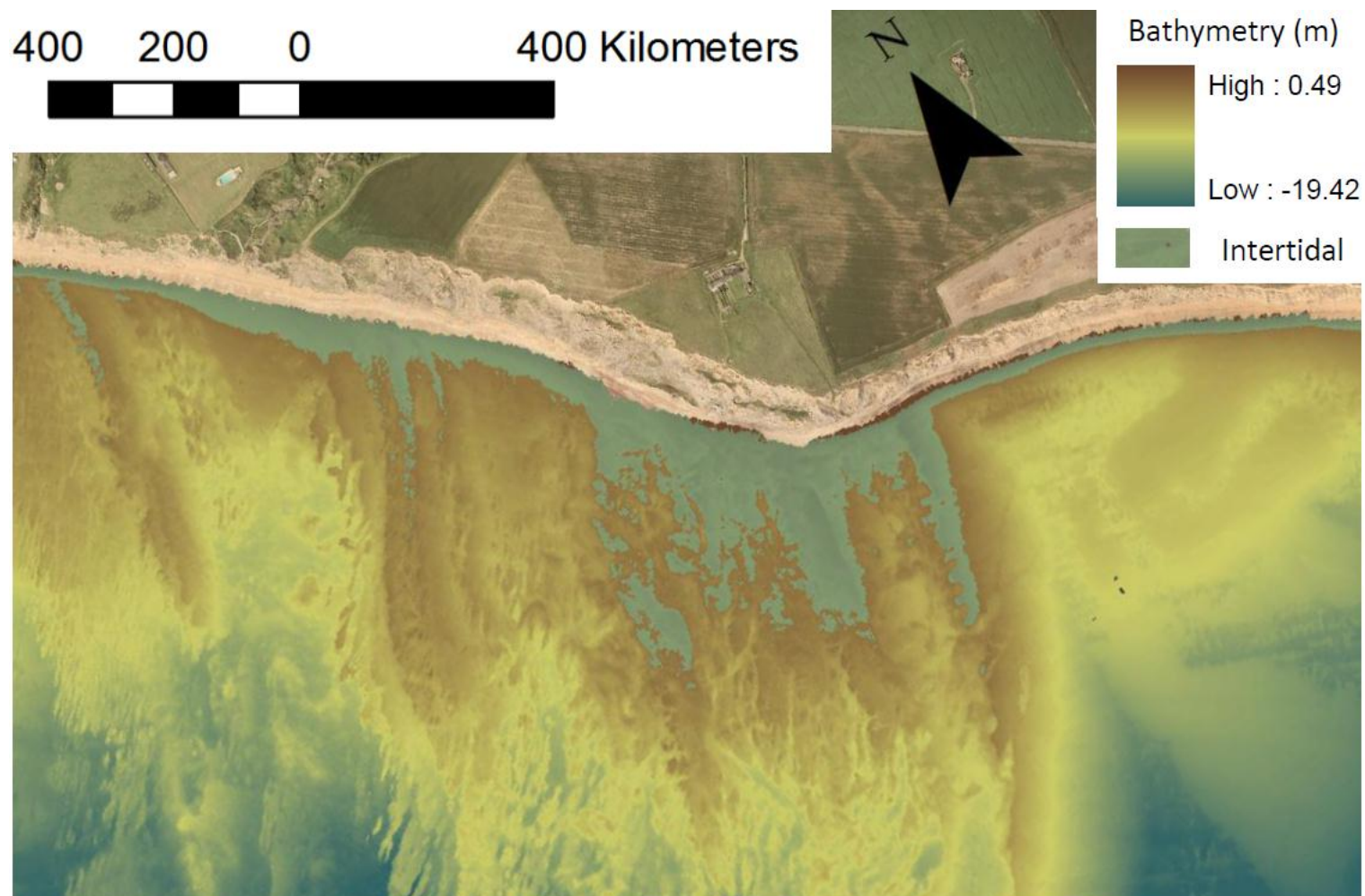
Figure 4.18: Aerial photograph of Atherfield Point and its associated shore platform from 2001 overlain by swath bathymetry from 2010. Note the offshore extent of the intertidal. (Data Source: Channel Coastal Observatory)
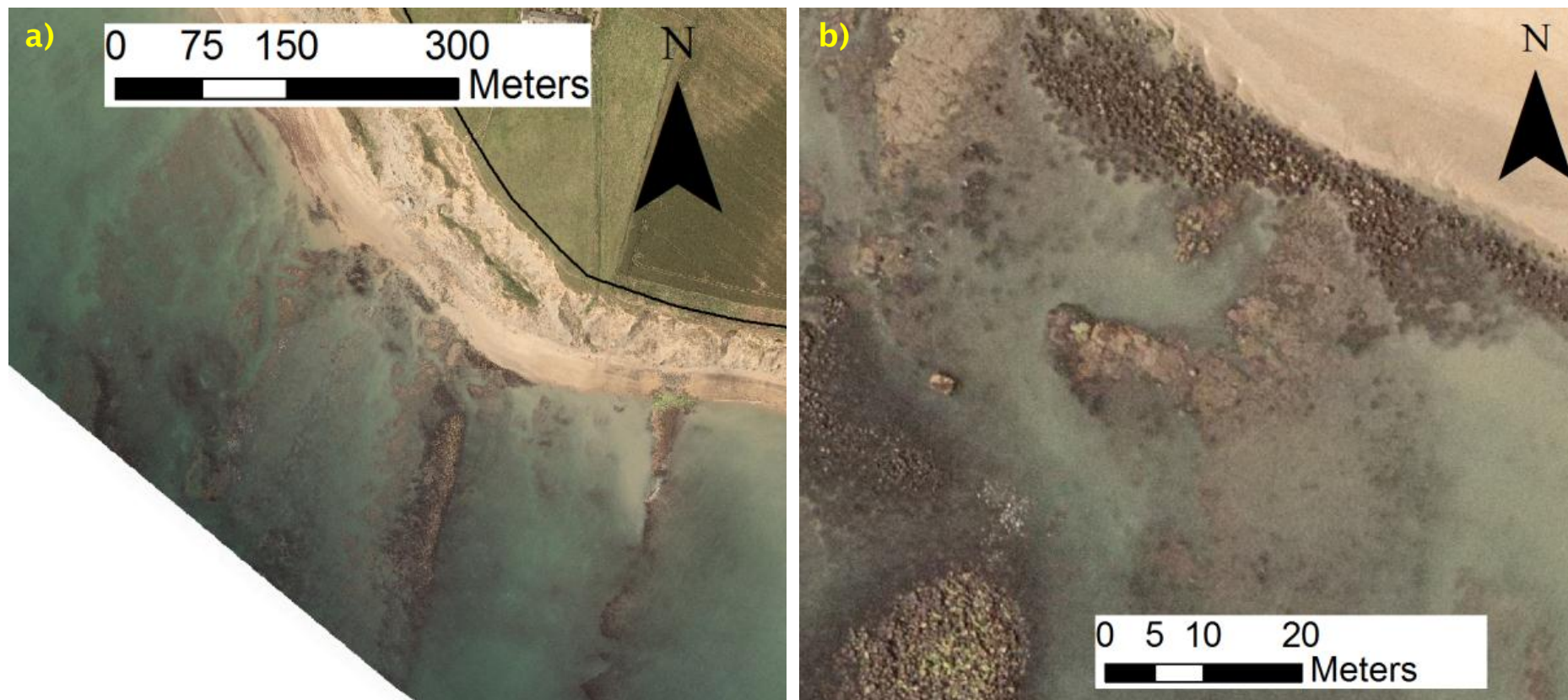
Figure 4.19: Aerial Photograph of a) Atherfield Point and Ledge and b) a close up of Atherfield Ledge showing the blocks of calcareous sandstone on the clay platform, both from 2005. (Source: Channel Coastal Observatory)

4.4 Geotechnical Assessment

The purpose of the geotechnical assessment was to determine if variations in geotechnical strength and properties can be correlated with recession rates or headland location. The lithology exposed within the study area falls under the category of hard soils/soft rock behaving neither completely as a soil or a rock. Assessment of the geotechnical properties of the cliff base and platform were made along the length of the coastline. Samples were collected and analysed from each of the clay rich formations for clay content and mineralogy. Observations of the mass properties of the various lithologies were also made.

4.4.1 Cliff and Shore Platform Coherence

An assessment of cliff and platform coherence was made through a visual appraisal technique developed by Soares (1993). It relates the coherence of hard soils/soft rocks, as classified with simple field test, to their typical compressive strength in MPa. Measurements of cliff coherence were made on the cliff base, within 50cm of the cliff/beach junction, at least every 50m alongshore. At certain locations it was not possible to access the intact, in-situ cliff base material. At these points assessment was made from the talus or rotated blocks of intact material found at the cliff base. To distinguish between measurements made at each of these cliff states, the results have been marked with different symbols in Figure 4.20. The talus measurements are not included in the results so as not to distract from the in-situ results, the coherence of the talus did not exceed C3 (Less Coherent). For talus coherence results see Appendix 3. Platform coherence was measured every 50 to 100m where present on the foreshore. The results of the geotechnical assessment are presented in Figure 4.12.

The coloured bar at the base of the graphs indicate the geological formation. The majority of intact in-situ cliff material has an intermediate level of coherence irrespective of its lithology (C2, Figure 4.20a). Deviations from intermediate coherence are seen at the far ends of the study frontage in the Ferruginous Sands, along with some channel sands within the Wessex and Vectis Formations, with a lower level of coherence (C3/C4). Greater coherence (C1) of the cliff base is seen at four locations along the frontage.
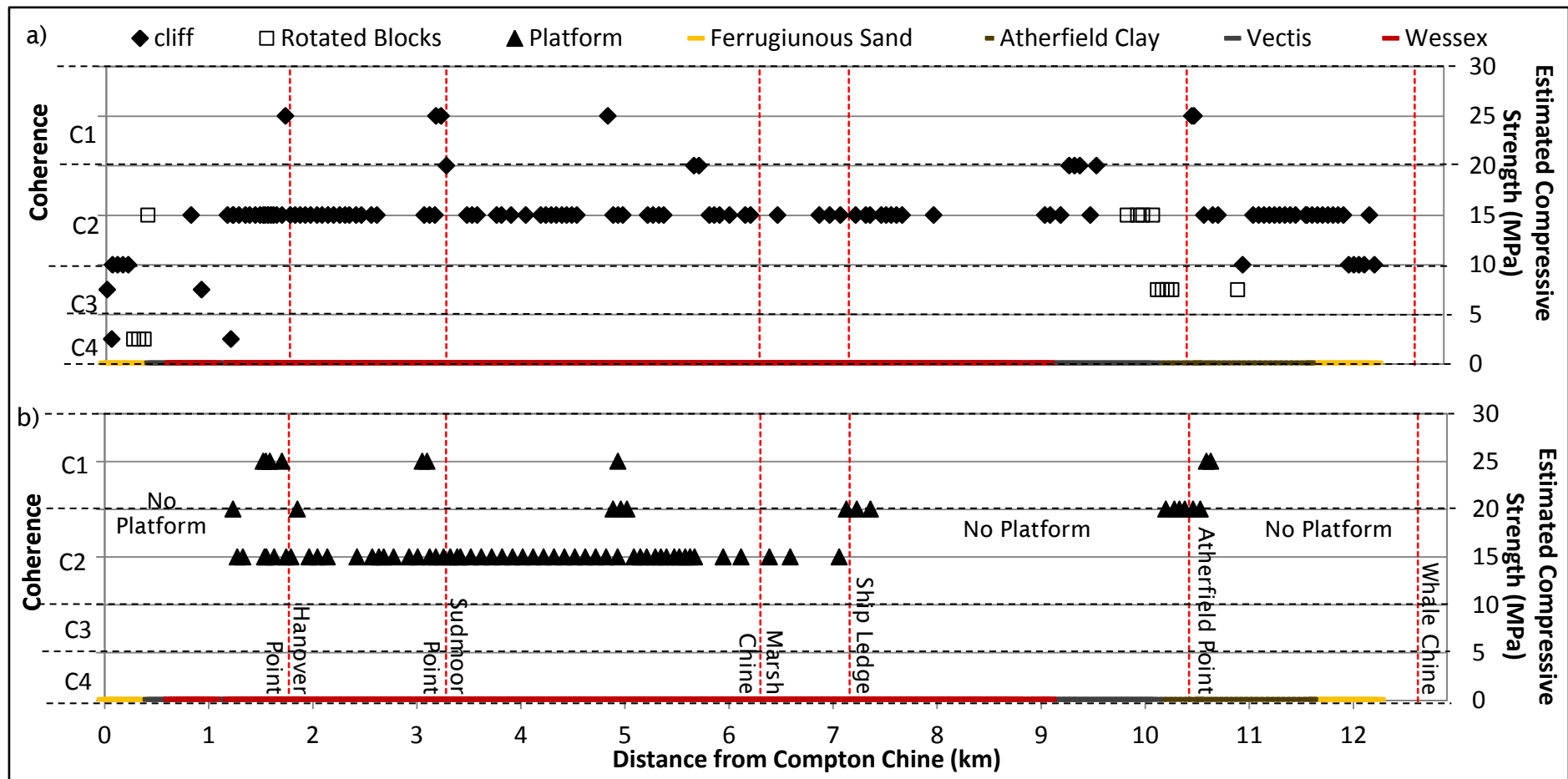
Figure 4.20: Results of the geotechnical assessment of a) cliff base coherence and b) Platform coherence. C1 to 4 represent the coherence levels described in Table 3.7. The coloured bar along the base of the graph indicate the geological formation.

These match up with the coherent (C1) beds observed in the shore platform, although due to the dip of the beds they do not match up exactly. Three of the measured areas of coherent beds coincide with the headlands. It is important to note that the measurements were taken for the cliff base only, had measurements been taken further up the cliffs these coherent beds would not be observed at the headlands due to the dip of the geology. The final area of increased coherence is due to the southern end of the Sudmoor Point Sandstone crossing the beach and intertidal zones.

The majority of the platform is formed from the Wessex Mudstones, with only the platform at Atherfield Point representing the Perna Beds of the Atherfield Clay Formation; the Vectis Shales and Ferruginous Sands fail to form significant intertidal shore platforms. Figure 4.20b shows shore platform coherence along the southwest coast. As with the intact in-situ cliff material the majority of the platform material is of intermediate coherence (C2), with deviations to coherent (C1) where sandstone beds outcrop. The Wessex Sandstones appear at Hanover Point and either side of Sudmoor Point (signifying the locations where each end of that Sandstone crosses the intertidal zone).

The calcareous sandstone of the Perna Beds forms the platform on the eastern side of Atherfield Point and blocks of the sandstone are seen strewn across the clay platform the width of the headland (Figure 4.19b). There are also a number of locations where the coherence of the platform was found to be border-line between coherent (C1) and intermediate (C2), most notable of these are in the vicinity of Atherfield Point and Ship Ledge. These areas of platform potentially have an increased coherence due to an increased silt content combined with greater cementation. Cement will penetrate into coarser sediment more readily than that with a finer grain size. The cause of this apparent increase in coherence and the reason the Vectis Shale and Ferruginous Sands fail to form intertidal platforms is explored below with consideration of clay content and mineralogy. These results indicate that there is some variation in cliff strength at the headlands. However these results only apply to the cliff base, further up the cliffs these patterns of coherence may not be observed. The strength measured at the cliff base is closely related to that of the shore platforms. It would be expected that the areas of shore platform with greatest coherence will exhibit higher elevations.

4.4.2   Clay Content and Mineralogy

A small number of samples were collected for clay content and mineralogy analysis from each of the clay rich geological formation (for more details see Section 3.2.2). The Ferruginous Sands samples were not tested for clay mineralogy since initial results showed that on average they consist of 87% sand and much of the <63 μm fraction is silt. The absence of shore platforms within the Ferruginous Sands, may be due to the lack of cohesive or cemented material within them. As with many unconsolidated marine sandstone their tensile strength is greatly reduced when saturated, by submergence in the intertidal zone (Collins and Sitar, 2008), leading to rapid disaggregation and erosion. The results of the grain size analysis are shown in Figure 4.22 to 4.24 one formation at a time. The results for the Wessex mudstones (Figure 4.22) are taken from the work of Redshaw (2013). They are divided into the three characteristic lithofacies outlined in that work based on colour mottling, reflecting changes in geochemistry, namely the massive red mudstones, the varicoloured mudstones and the plant debris beds.
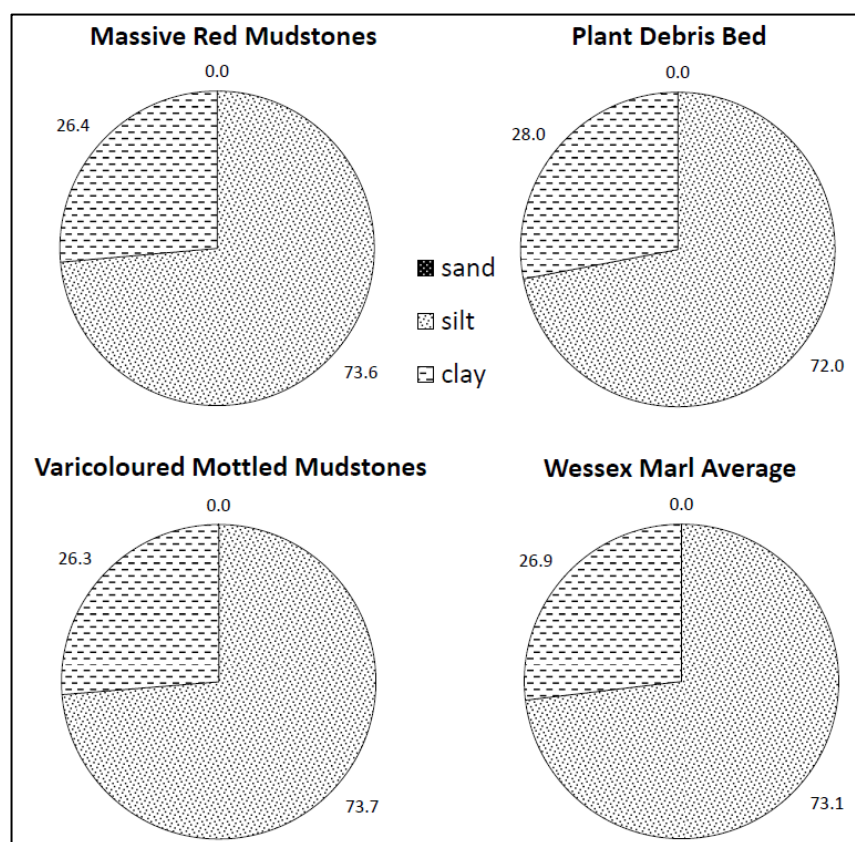
Figure 4.21: Grain size analysis of the Wessex Mudstones

The results show a uniform PSD across the lithofacies all with a high silt content (over 70%). This high silt content was questioned by (Redshaw, 2013) suggesting that the result was due to clay flocculation. This was confirmed through observations with a Scanning Electron Microscope.
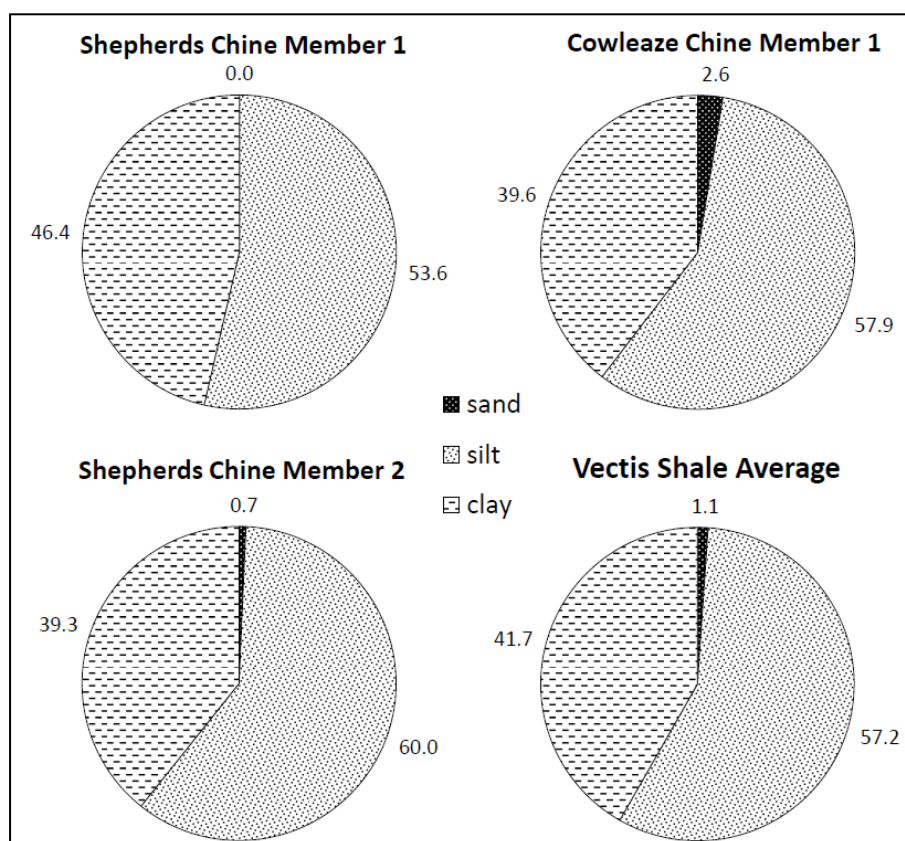
Figure 4.22: Grain size analysis of the Vectis Shales

The Vectis Shales show a higher proportion of clays than the Wessex Mudstones (Figure 4.22). There is some variation between samples, with sample 1 from the Shepherd's Chine Member having a 5% greater clay content than the other two samples. The Chale Clay samples both showed and approximate 50/50 split between silt and clay while the Lower Lobster bed sample had lower clay content. This reduces the average clay content for the Formation as a whole (Figure 4.23). There is a large difference between the clay content measured within the Perna Clay bed (Figure 4.24). The sample collected from the cliff base has a 29% higher clay content than the sample collected from the platform. This may indicate a fining upwards of the Perna Bed. Despite some variability within formations, overall the results show that the formations with the highest proportion of clays

are those that do not form shore platforms, i.e. the Atherfield Clays and Vectis Shales, as would be expected.
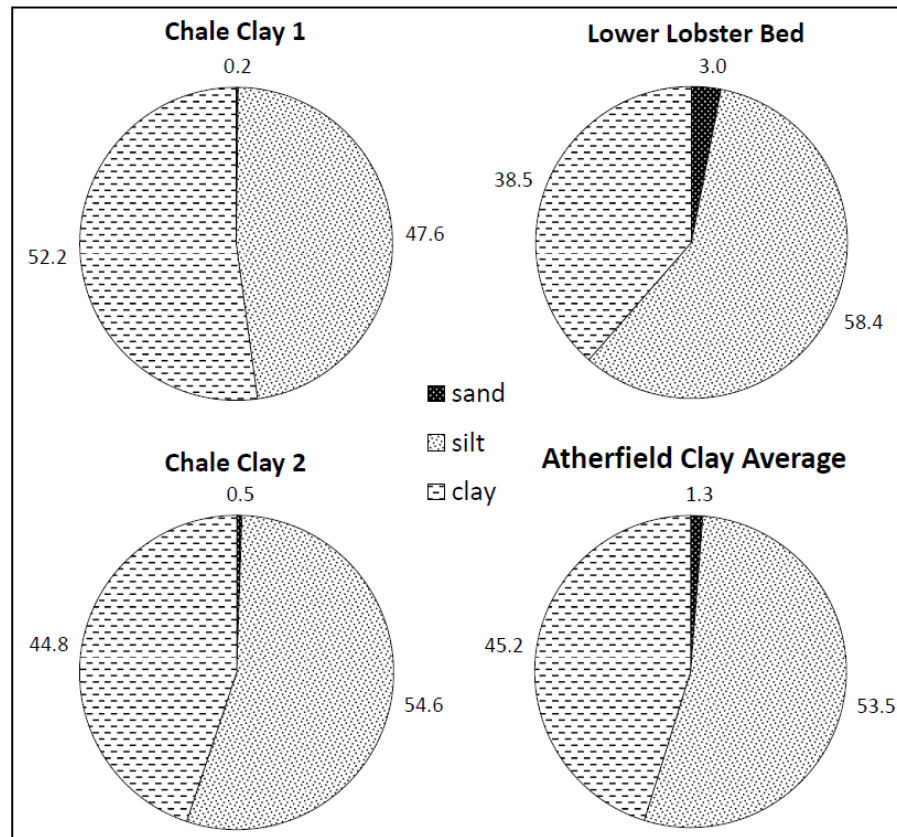
Figure 4.23: Grain size analysis of the Atherfield Clays
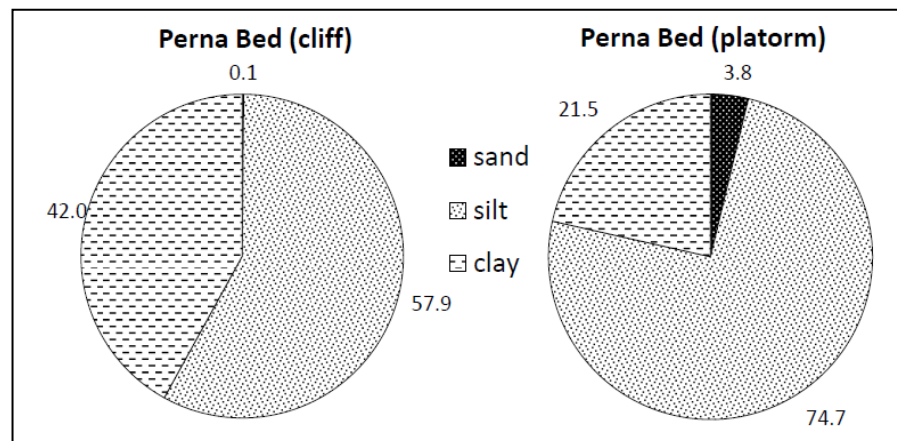
Figure 4.24: Grain size analysis of the Perna Clay

It is also expected that soils/soft rocks with a high proportion of swelling clay minerals, such as Smectite, would have lower shear strength and cohesion, i.e. the component of shear strength independent of inter-particle friction (Hajdarwish et al., 2013). It would follow that the platform forming beds found along the study sight would have a lower proportion of those swelling minerals. The results of the

X-Ray Diffraction of the clay minerals are shown in Figure 4.25 to 4.26. The clay mineralogy within the Wessex Mudstones is highly variable. Most notably the plant debris bed sample contains 34.2% Smectite compared to 21.4% in the varicoloured mudstones and only 7.1% in the red mudstones. This variation correlates with the occurrence of shore platforms, i.e. the dominant platform forming lithofacies within the Wessex is the red mudstones.
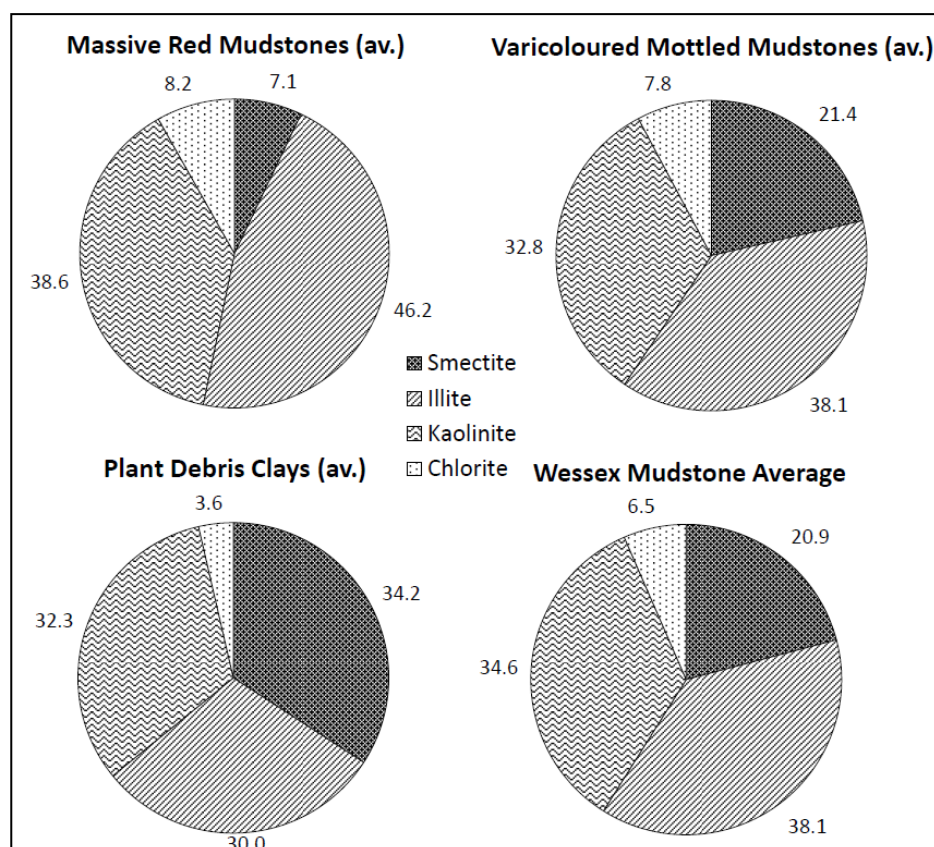
Figure 4.25: Clay Mineralogy of the Wessex Mudstones

In contrast to the Wessex Mudstones the Vectis Shales and the Atherfield Clays show relatively uniform levels of Smectite, around 15 % in the Shales (Figure 4.26) and 8% in the Clays (Figure 4.27). Of the two Perna Clay samples only the cliff sample was analysed for clay mineralogy, no clay could be recovered from the platform sample. The cliff sample shows 20.4% Smectite content (Figure 4.28).
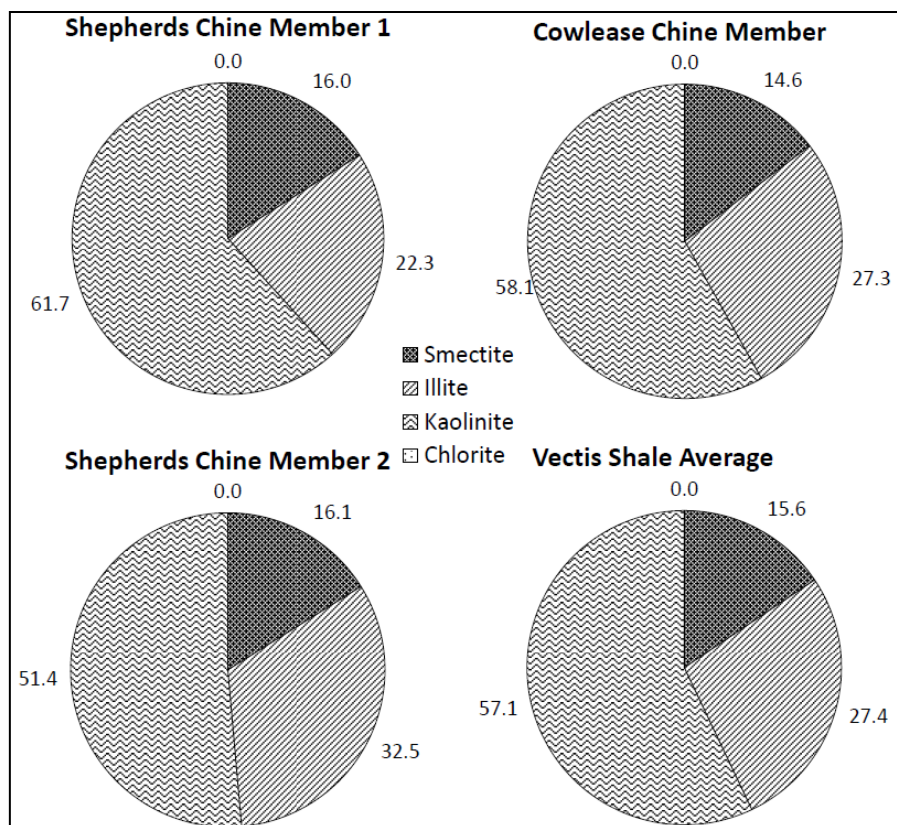
Figure 4.26: Clay Mineralogy of the Vectis Shales
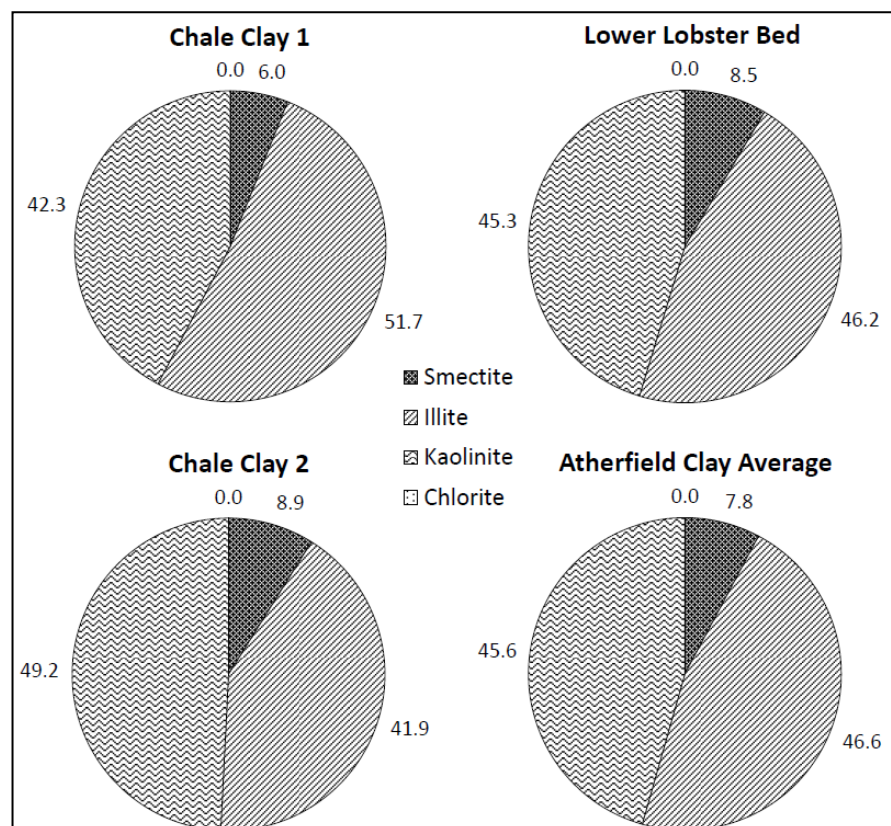
Figure 4.27: Clay Mineralogy of the Atherfield Clays
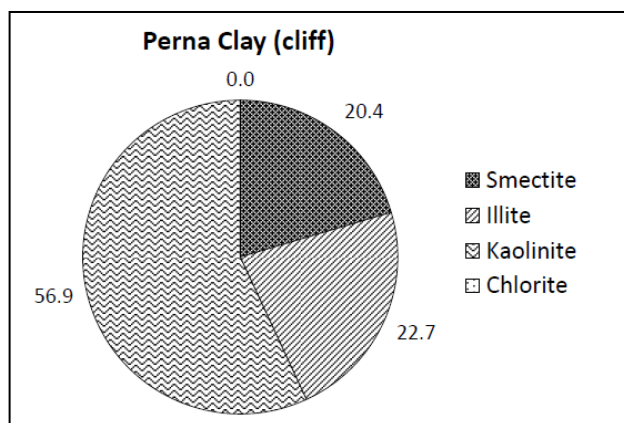
Figure 4.28: Clay Mineralogy of the Perna Clay cliff sample

Overall the analysis revealed a higher proportion of swelling minerals in the platform forming lithologies than the non-platform forming ones. This result was not expected, since high swelling clay content is associated with reduced rock strength. However the small sample size, particularly when considering the Perna Clays and the variability within formations means these results are far from conclusive. A study by Rust and Gardener (2002), investigating a small landslide which is threatening the car park at Compton Bay, found much higher levels of swelling clays in the Vectis Shales, with 57% Smectite + Vermiculite. They also found higher clay size content in the Shales of 59%. As with this study only a small number of samples were taken. The heterogeneous nature of these clay rich lithologies means that to gain a true picture of the particle size distribution and clay mineralogy of these lithologies many more samples must be collected and analysed. This is beyond the scope of this project.

4.4.3   Mass Properties

The clay content and mineralogy give some clues as to the platform forming potential of the various lithologies present but do not fully explain the variations seen in the field. The coherence of the lithologies appears to be uniform along the coast at a small (cm) scale. The mass properties of the lithologies consider their strength and erosional processes at a larger scale. The Wessex mudstones are massively bedded, i.e. there are no regular bedding planes creating planes of weakness. Rust and Gardener (2002) noted that the mudstones were remarkably resistant to erosion and behaved in a non-plastic way even when saturated. Their analysis of the Mudstones in Compton Bay showed low clay content (30%) and a high quartz content (60% mainly as silt). This combined with their observation of a

distinctive pattern of fine fractures, providing a degree of permeability was given as an explanation for the steepness of many of the low cliffs where it outcrops and the extensive intertidal platforms they form.

A study by Kollios (1993) found that the freshly exposed mudstone has an adequate factor of safety against failure in the short term. However, with the reduction of internal stresses and exposure to the environment the mudstone dries out and cracks. This allows ground and surface water to penetrate deeper into the mudstone where chemical weathering takes place. The combination of these wetting and drying cycles and chemical weathering forms a surface layer of hard blocks of disaggregated mudstone. The mudstones of the Wessex Formation act in a similar way. Observations of the cliffs within the study area revealed the disaggregated blocks present to be less than 20 mm^2 (Figure 4.29a).
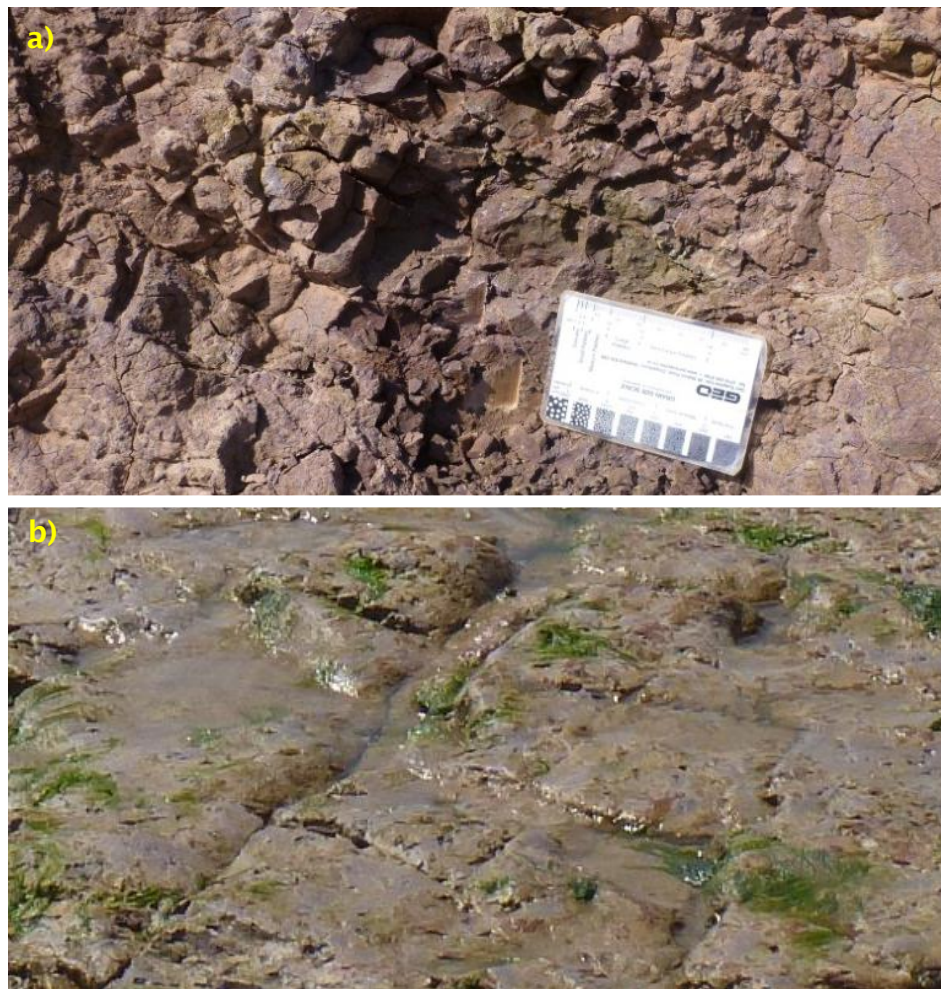
Figure 4.29: The Wessex Mudstone, note the different style of weathering seen in a) the cliff and b) the platform. The grain size card in the photographs is 8.5 x 5.5 cm. (Source: Original Photographs)

The shore platforms in the mudstone do not behave in the same way, the shorter period over which they are exposed to the air prevents them fully drying out (Figure 4.29b). Also their increased exposure to waves means any weathered material will be removed regularly preventing build-up of a weathered layer (Davidson-Arnott and Langham, 2000). Field observations also showed the shales of the Vectis Formation are thickly laminated (6 - 20 mm) to thinly bedded (20 - 60 mm), in places especially where siltier bands exist, making them more susceptible to weathering and erosion. These shales are sometimes known as paper shales (White, 1921) due to their tendency to split into very thin sheets, like paper on weathering. The shales weather into thinly laminated (6 to 1 mm) hard lumps 2 to 3 cm across (Figure 4.30).

Figure 4.30: Photographs of the Vectis Shales showing a) weathered "paper shales" and b) unweathered samples in the cliff. The pen is 14 cm long and the black end is 1.5 cm long, and the grain size card is 8.5 x 5.5 cm.

Rust and Gardener (2002) found the shales had a larger proportion of clay than the mudstones (i.e. 59 % compared to 32 %). The high clay content combined with the

tendency to split parallel to the bedding plane may explain the lack of intertidal platforms in the Vectis Formation, with the fissile nature of the shales being the dominant control. It may also contribute to the slight increase in the average annual recession rate for the Vectis Formation compared to the Wessex Formation (Figure 7.9). And contribute to the increased occurrence of mudslides and compound slides, seen in the shales, compared to the mudstones (Figure 4.2 and Figure 4.3).

The character of the Perna Clay is similar to that of the overlying Chale Clay, both are massively bedded and weather in a comparable way to the Wessex Mudstones. Figure 4.31a shows an area of Chale Clay; the darker area shows a fresh exposure while the lighter area is weathered. The are no regular bedding planes present. However these beds fail to form an intertidal platform due to their well jointed nature and an abundance of small and large scale fissures.

Figure 4.31: Photographs of a) the Chale Clay in the cliff and b) the Perna clay on the shore platform. The grain size card is 8.5 x 5.5 cm (Source: Original Photograph).

The increased clay content may also play its part. Figure 4.31b show the shore platform of Atherfield Ledge formed from the Perna Clay. The high sand and low cement content of the Crackers (excluding the nodules) and Upper Lobster Beds cause them to act much like the Ferruginous Sands, losing tensile strength when saturated, explaining why they fail to form intertidal platforms.

4.5   Summary

The geology of the southwest coast of the Isle of Wight is complex, both in terms of the individual formations which contain a number of laterally discontinuous beds, and in terms of the structural geology. Within the Wessex and Vectis Formations the channel and tidal sand bar sandstones offer support to the cliffs. The majority of the intertidal shore platforms (91%), including those fronting Hanover and Sudmoor Points and Ship Ledge are formed from the Wessex Formation. The platform fronting Hanover Point once contained a large fossil assemblage or plant debris bed known as the Pine Raft. Over time this fossil assemblage has been eroded by waves and fossil hunters, potentially reducing the protection afforded to the headland. The remainder of the platform is formed from the Perna Beds (9%) of the Atherfield Clay Formation, these beds are both less than 1 m thick and there is evidence of some reduction in their thickness over the study period. The laterally discontinuous nature of the lithology is likely to promote changes in cliff face exposure and the associated recession rates along the entire coastline as the cliff line retreats.

Table 4.2 summarises the geological, geomorphological and geotechnical properties of the four major geological formations found on the coastline and defines there platform forming capacity and relative resistance. The majority of intact, in-situ cliff samples have intermediate levels of coherence irrespective of their lithology. Variations are seen at the headlands where coherent beds outcrop at the platform and cliff base level; however the cliff material above does not show the same level of coherence. Reduced levels of coherence are observed in the poorly cemented sandstones within the Ferruginous Sand Formation and in some of the channel sands of the Wessex and Vectis Formations. This is reflected in the lack of intertidal platforms formed from the Ferruginous Sands, due to their poorly cemented nature they lose tensile strength when saturated, rapidly disaggregating.

Table 4.2: Summary of the geology, geomorphology and geotechnical properties of the southwest coast

Formation	Lithology	Coherence	Mass Properties	Dominant CBUs	Platform Forming?	Relative Resistance
Ferruginous Sands	Sandstones and sandy clays	C4 to C2/3	Poorly consolidated	CBUd	No	Low
Atherfield Clay	Sandstones	C2	Poorly consolidated	CBUa & CBUb	No	Low
	Chale Clays	C2	Massive		No	Low
	Perna SST	C1	Well cemented	N/A	Yes	High
	Perna Clay	C1/C2	Massive		Yes	High
Vectis	Sandstones	C1/C2	Well cemented to poorly consolidated	CBUa	No	High to Low
	Shales	C2	Fissile	CBUe	No	Low
Wessex	Sandstones	C1 to C2	Well cemented to poorly consolidated	CBUa &CBUc	Yes	High to Low
	Mudstones	C2	Massive		Yes	High

All the platforms show intermediate coherence or higher. Again the locations of the headlands are marked by an increase in coherence. Only the Wessex Formation and the Perna Beds of the Atherfield Clay Formation form significant intertidal platforms. To understand why these variations occur, consideration of the clay content, clay mineralogy and mass properties of the platform forming beds were made and compared with the non-platform forming beds. This showed that the mass properties of the rock to be the dominant control on their platform forming potential.

The mass properties of the beds are strongly related to their depositional environments. For example the Wessex Mudstones were laid down rapidly, forming a massive structure with few regular planes of weakness that can be utilised by wave energy. In contrast the Vectis Shales were laid down slowly allowing time for the clay minerals to align, producing a fissile rock which disaggregates rapidly when saturated. In term of the mudstone weathering the regular submergence of the platforms prevents them from drying out; this reduces their weathering as the dominant mode of cliff weathering is through a continued cycle of wetting and drying. Structural controls on the morphology and elevation of the shore platform were also found to be important, along with the resistance of the underlying beds to erosion and the orientation of the beds in relation to the direction of incoming waves.

5. Longshore Variations in Wave Conditions

As outlined in Chapter 2 the evolution of a headland, once formed, is thought to be controlled by the balance between the ability of the shore platform to attenuate wave energy and the refraction of wave energy towards the headland due to the presence of the intertidal shore platform. This relates to an objective of this project which is to "Examine the longshore variations in near shore bathymetry and consider how those variations influence the distribution of wave energy along the shoreline". To achieve this objective a simple wave refraction model (RCPWAVE) was used (Section 3.3). Wave energy reaching the cliff toe is controlled by both the wave climate and the bathymetry those waves pass over to reach the shore. Therefore a brief description of the wave climate and nearshore bathymetry of the southwest coast is presented in Section 5.1, before the results of the wave refraction modelling are presented in Section 5.2. The longshore variation in wave energy for common and storm waves are presented in Section 5.2.1 and 5.2.2 respectively.

5.1   Wave Climate and Bathymetry

The southwest coast of the Isle of Wight is exposed to a high energy wave climate. Its large fetch of over 4000 km brings Atlantic Swell waves and the coastline is fully exposed to local storm waves approaching from the southwest (Figure 5.1). The dominance of these south-westerly waves is reflected in the data provided by the Met Office (Figure 5.1) with 74% of all waves approaching from the southwest. The prevailing nature of the south-westerly waves appear to be very effective in maintaining the alignment of the shoreline (May, 2007), the coastline between Compton Chine and Rocken End is broadly drift aligned although the degree of alignment varies locally (Figure 5.2). The southern end of each bay shows the greatest alignment to waves approaching from 240°, while the greatest deviation from that alignment is found in the northern ends of each bay.
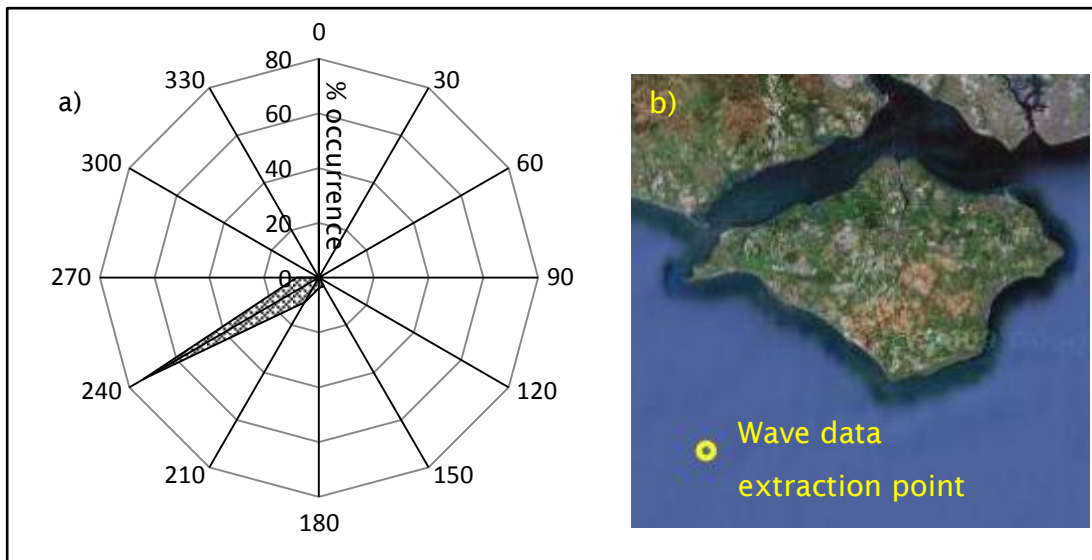
Figure 5.1: a) Wave rose showing percentage occurrence for all offshore waves with the potential to reach the shoreline over a 10 year period, from Met Office 12km Grid wave model. b) Location data was extracted from the model (50.506° n, 1.573° w)
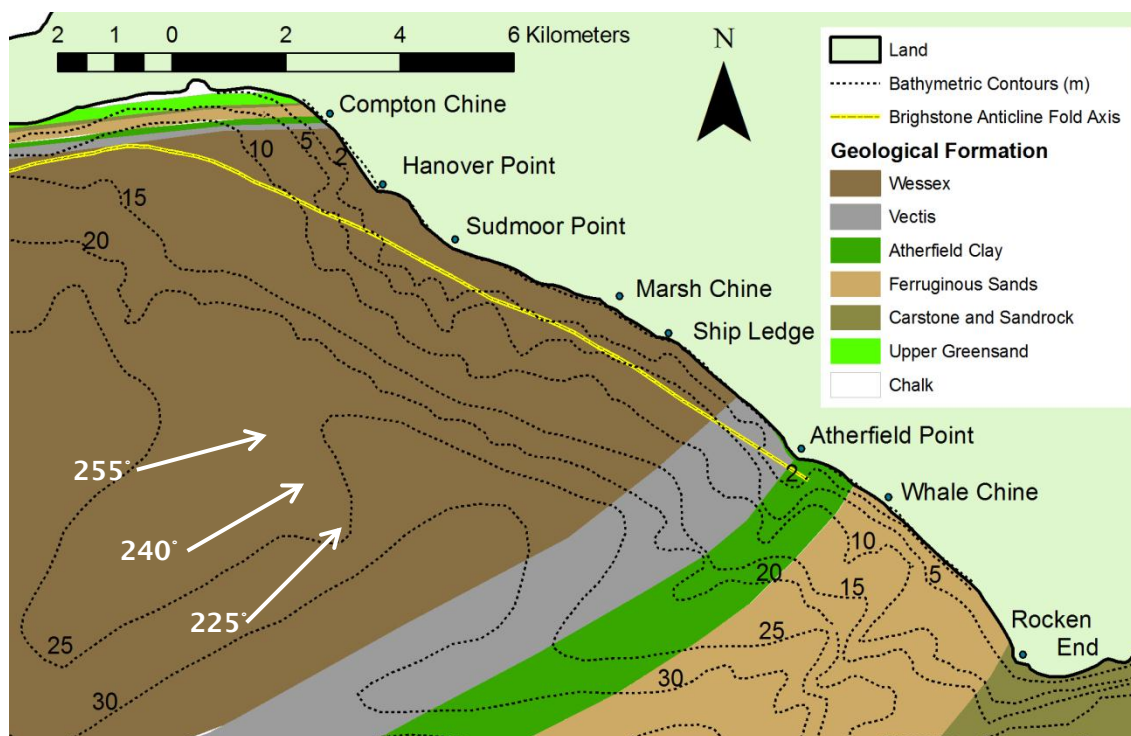
Figure 5.2: Depth contours and geology of the southwest coast of the Isle of Wight. The marine geology was adapted from Underhill and Paterson (1998). The white arrows indicate the various angles of wave approach used in the refraction modelling.

Figure 5.2 shows an approximation of the seabed geology adapted from Underhill and Paterson (1998), overlain with bathymetric contours. The landward boundaries between geological formations were taken from the mapping described in Section 3.3, the line of the boundaries offshore are only an approximation, based on

the map presented in Underhill and Paterson (1998). However, the bathymetry of this coastline appears to be strongly influenced by the bedrock geology of the sea bed. For example the landward shift in the 30 m depth contour runs parallel with the Wessex/Vectis boundary. The seaward extension of all contours roughly perpendicular to the coast from Atherfield Point may represent an extension of the Perna Beds and Atherfield Ledge.

Closer into shore the 2 m contour gives a good indication of the location and extent of the intertidal platforms. Broadly speaking the slope of the shoreface increases from north to south, with the exception of the area around Atherfield Point, where Atherfield Ledge reduces the beach slope locally. At the southern end of Brighstone Bay an abrupt increase in the shoreface slope is apparent near the southern edge of the Wessex Formation beyond Ship Ledge and an increase in wave energy reaching the coast south of this may be expected. The shoreface is at its steepest in Chale Bay where the Ferruginous Sands dominate. The reasons for these variations in shoreface slope with changes in lithology are outlined in Chapter 4. The high clay content and mass properties of the Vectis Shales cause them to disaggregate more readily than the Wessex Mudstones when saturated, while the Ferruginous Sands lose their tensile strength (Collins and Sitar, 2008).

5.2   Model results

A number of wave conditions were chosen to represent commonly occurring waves and common and rare storm waves, these were (n.b. Hs – Significant wave height and Tp – Peak wave period):

- Common Waves (35:1year):   Hs - 1.0 m,   Tp - 5.5 s

- Common Storm Waves (5:1 year):   Hs - 3.5 m,   Tp - 6.5 s

- Rare Storm Waves (1:50 year):   Hs - 6.01 m,   Tp - 8.1 s

These waves were subjected to two separate sets of bathymetry data one synthetic, created from equilibrium profiles and the current (2011) cliff base position, and one based on observed data. See Section 3.4 for more details.

5.2.1   Common Waves

Common waves have been defined as the wave conditions (Hs-1m, Tp-5.5) that will occur on average 35 times in 1 year (35:1 year); that is equivalent to once every 10.4 days. Three wave directions were used 225°, 240° and 255°. These waves were propagated over a simplified bathymetry constructed from a series of equilibrium profiles, using the 2011 cliff base as the shore line position (Figure 5.3a). The results show wave concentration at the headlands as would be expected, with the greatest concentration occurring at the most pronounced headlands, i.e. Hanover and Atherfield Point. The angle of wave approach influenced the amount of wave energy reaching the shoreline. The wave energy density at the shoreline was greatest for wave approaching at 225°, closely followed by those approaching from 240°, with wave from 255° on average delivering approximately 325 KJ m^{-2} less power to the shoreline. The peaks in wave energy for those waves are also lower. This is likely to be due to the extra distance these waves have had to travel to reach the shoreline. It must be noted that the depth of the stations at which the results were extracted vary along shore, in particular in Chale Bay where the shoreface steepens (Figure 5.3c). Therefore some of the noise in the wave energy distribution can be attributed to these variations. However where clear peaks in wave energy exist as outlined below these variations can be considered to be real.

Figure 5.3b shows the patterns of wave energy distribution when waves are propagated over the complex real world bathymetry. Under these conditions the pattern of wave concentration changes, not only in the longshore but also in terms of the various angles of wave approach. These changes can be directly related to the near shore bathymetry shown in Figure 5.2. The peaks in wave energy density along the coast, starting in the northwest and continuing to the southeast are as follows:

- Hanover Point: Common waves from all directions show a peak in wave energy around Hanover Point. In contrast to the results shown in Figure 5.3a the greatest peak comes from the 255° waves and the smallest form the 225° waves. This can be explained by the bathymetry around Hanover Point, in particular the 2 and 5 m contours, which run parallel to the shoreline for much of Compton Bay extending seawards around the headland itself.
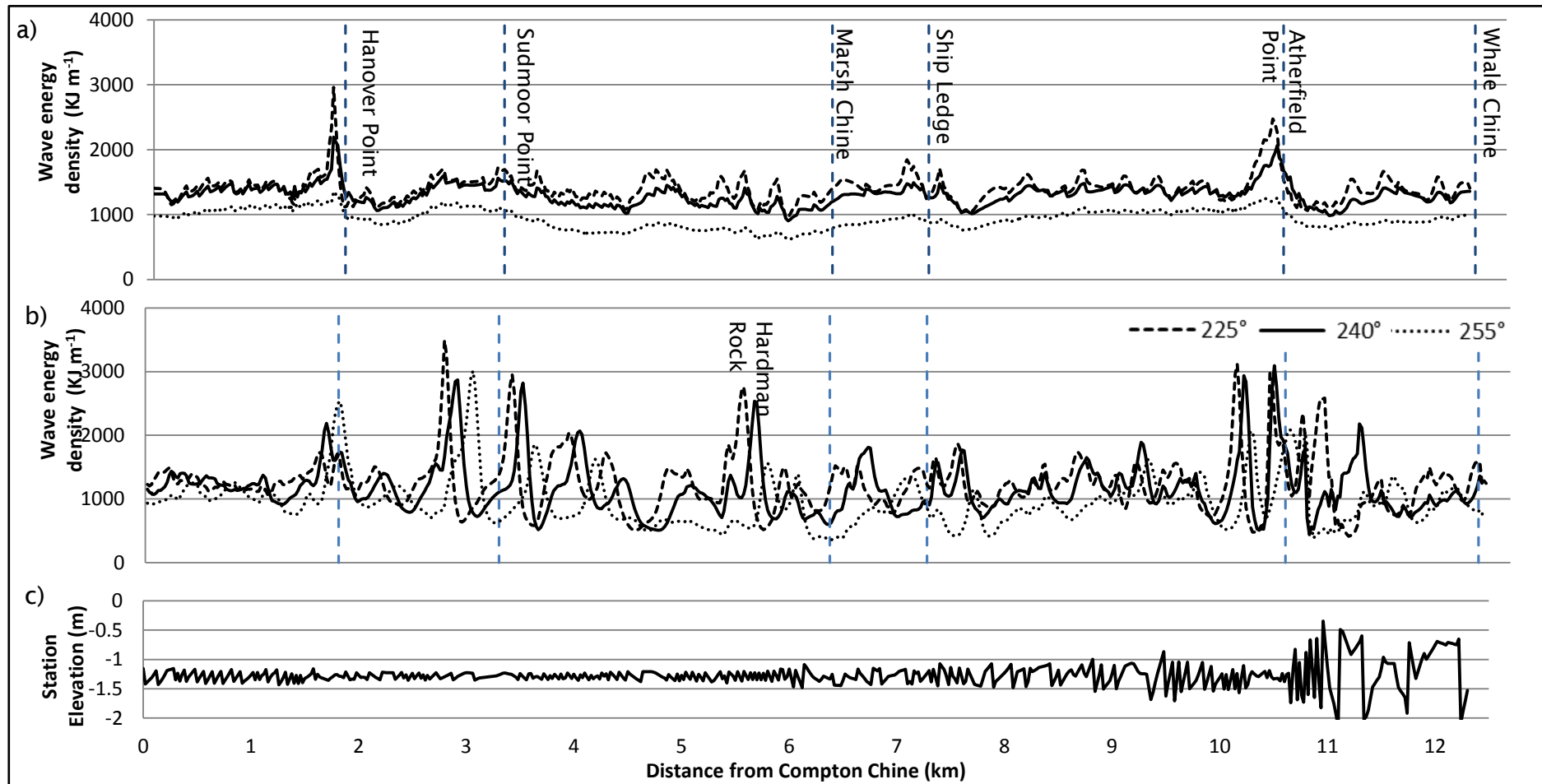
Figure 5.3: Wave energy density at the shoreline for common waves Hs:1m, Tp:5.5s from 225°, 240° and 255° propagated over: a) Simplified bathymetry, shore parallel equilibrium profiles and b) Real world bathymetry, c) shows the longshore variation in station elevation.

This will allow wave approaching from 255° to proceed to the shoreline with less attenuation than those from 240° or 225°, which have to cross the extensive platforms found to the south of Hanover Point.

- Sudmoor Point: Peaks in wave energy occur either side of the location chosen to define the apex of Sudmoor Point. However, defining the apex of such a rounded headland is arbitrary, and the three decreasing peaks in wave energy across Sudmoor Point can all be attributed to the headland. These peaks are related to variations in the elevation of the shore platform fronting Sudmoor Point, as described by the 5 and 2m contours in Figure 5.2. The concentration of wave energy around Sudmoor Point using the complex geology compared to the simplified equilibrium results is testament to the prominence and significance of the extensive elevated platform in that area.

- Hardman Rock - The seaward extension of the 10m depth contour between Sudmoor Point and Marsh Chine is caused by a feature known locally as Hardman Rock (Figure 5.2) and is responsible for the peak in wave energy density seen at 5.5km southeast from Compton Chine (Figure 5.3b).

- Atherfield Point - Under each of the angles of wave approach the concentration of wave energy around Atherfield Point is in the form of a double peak (Figure 5.3b). This double peak mirrors the two narrow extensions of the 10 and 20m contours seen in Figure 5.2. As with Sudmoor Point the peaks in wave energy are not directed solely at the apex of the headland, but across an area 500m either side. The largest peak in wave energy approaching from 240° is within 150m of the apex on the northwest side.

These results show that under common wave condition wave energy concentration at the shoreline is strongly controlled by variations in nearshore bathymetry, in particular the 2 to 10m contours (Figure 5.2).

5.2.2   Storm Waves

The increase in wave height and period used to represent storm waves had an interesting influence on wave energy concentration over the simplified, equilibrium bathymetry. There is no observable pattern in wave energy concentration with either the 5:1 year or the 1:50 year storm events (Figure 5.4a and Figure 5.5a). It would appear that beyond a critical threshold the subtle variations in bathymetry imposed by the coastal outline no longer cause refraction towards the headlands. The noise in the data seen in Figure 5.4 and 5.5 is related to the longshore variability in station depths shown in Figure 5.4c and 5.5c. Interestingly the wave energy reaching the cliff base for the 5:1 year storm waves and the 1:50 year storm waves is very similar despite the 2.51m difference in initial wave height. This is likely to be a result of the larger waves "feeling bottom" further offshore, where the bathymetric variations are smaller and the wave energy can be dissipated over a wider area. Linear wave theory dictates that waves cease to be "deep water waves" once the water depth falls below half their wave length. For the 5:1 year and 1:50 year storm waves this occurs at 33m and 51.2m respectively, while common waves "feel bottom" at 23.6m. This means that the storm waves are feeling bottom from the edge of the model. The bathymetry beyond the 30m contour is reasonably uniform and therefore it was not necessary to extend the model dimensions.

Overall the wave energy reaching the wave stations (positioned at approximately 1.5m water depth alongshore) is greater under storm wave conditions. This is not only by virtue of the larger waves providing more energy, but is also related to the increased water depths associated with storm surges, allowing larger waves to reach the same point in the cross-shore. When propagated across the real world bathymetry the storm waves show a large increase in wave energy south of Atherfield Point (Figure 5.4b, Figure 5.5b), coinciding with the exposure of the Ferruginous Sand Formation and the increase in shoreface gradient (Figure 5.2). Again the increase in water depth close to the shoreline allows a greater proportion of the wave energy to reach the shoreline without being dissipated this effect may have been exaggerated in the data due to the increased variability in station depths in Chale Bay (Figure 5.5c).
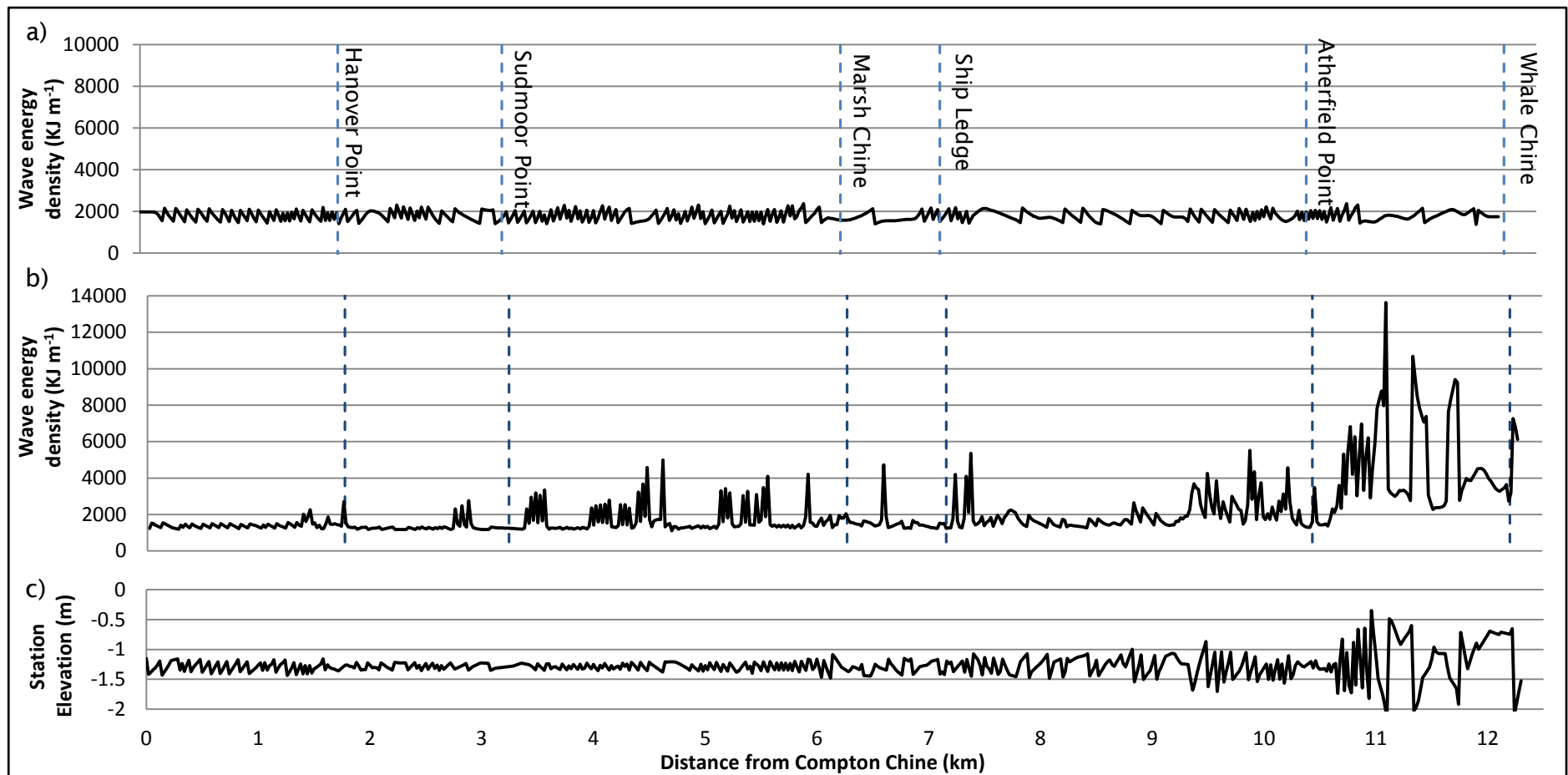
Figure 5.4: Wave energy density at the shoreline for 5:1 year storm waves Hs: 3.5m, Tp: 6.5s from 240° propagated over a) Simplified bathymetry, shore parallel equilibrium profiles and b) Real world bathymetry, c) shows the longshore variation in station elevation.
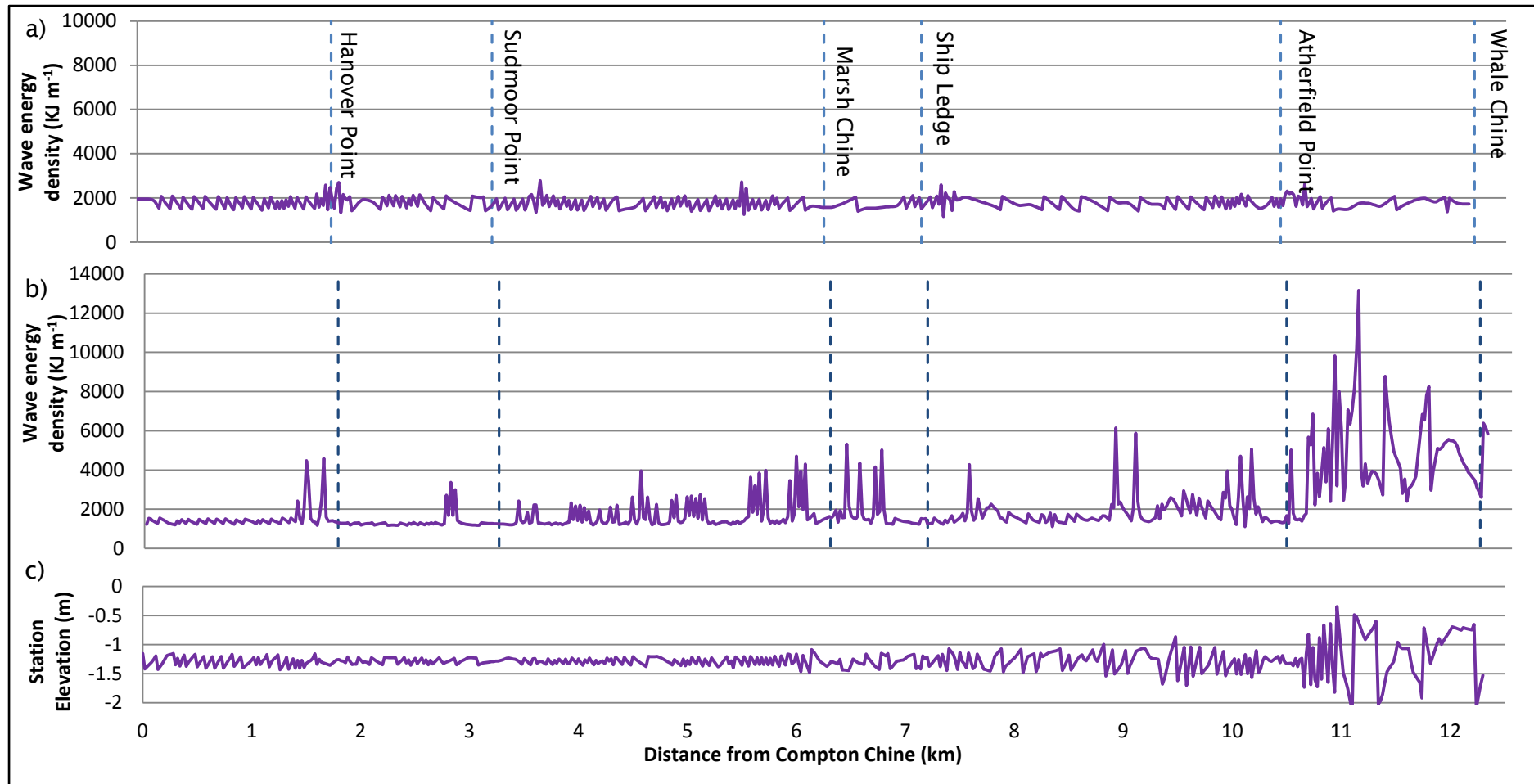
Figure 5.5: Wave energy density at the shoreline for 1:50 year storm waves Hs: 6.01m, Tp: 8.1s from 240° propagated over a) Simplified bathymetry, shore parallel equilibrium profiles and b) Real world bathymetry, c) shows the longshore variation in station elevation.

However the increase in energy density seen under the real world bathymetry exceeds the variations seen under the simplified bathymetry indicating that the increase in Chale Bay is genuine. The other, smaller peaks in wave energy vary slightly between the two storm wave types. Both show peaks in wave energy either side of Sudmoor Point in similar locations to those seen under common waves.

The 5:1 year storm waves create a peak in wave energy at Hanover Point (Figure 5.4b) while the 1:50 year storms cause a larger peak just to the north of the headland (Figure 5.5b). Many of the smaller peaks occur in the area south of Sudmoor Point to 500m south of Ship Ledge and the north of Atherfield Point for around 1.5 km. They are potentially related to the refraction of wave energy over the seaward extension of the 25m and 30m depth contours (Figure 5.2), due to the position of the Wessex Mudstone and Perna Beds respectively.

The smaller peaks in wave energy around Hanover and Sudmoor Points indicate that the shallower depth contours do have some influence on wave energy concentration in storm wave conditions. Although when compared to the peaks observed in Chale Bay it is clear that the greater depth at which these wave "feel bottom" has a strong influence on the amount of energy reaching the cliff base.

5.3   Summary

The aim of this chapter was to determine the influence of waves; including the variations in shore platform elevation and nearshore bathymetry have on the concentration of wave energy along the coast line. Under commonly occurring wave conditions (35:1 year events) wave energy concentration is seen at and around the prominent headlands of Hanover, Sudmoor and Atherfield Point. The pattern is not as clear as that seen when waves were subjected to a simplified, idealised bathymetry, demonstrating the influence of the complex bathymetry. However it does show that at least under current conditions the greatest levels of wave energy density are not found in the bays, indicating that the bays and hence the headlands are not a result of longshore variations in wave energy concentrations but exist despite them.

Under storm wave conditions no significant concentration was seen at the headlands for simplified bathymetry, with the larger waves simply breaking further offshore where the bathymetry is more uniform. Some concentration was

seen around Hanover and Sudmoor Points for the real world bathymetry but these peaks were secondary to those seen in Chale Bay. The increase in beach slope in Chale Bay allowed greater levels of wave energy to reach the shoreline south of Atherfield Point.

The results of this chapter indicate that there is some concentration of wave energy towards the established headland. The influence this concentration has on headland formation cannot be determined without consideration of cliff recession rate, for these considerations see the results presented in Chapter 7, Section 7.2.2.

6. Beach and Shore Platform Characteristics

The third objective of this project was to "Study the interaction between beach volumes, sediment budget and cliff recession rates, in the presence of intertidal shore platforms and the influence these features have on local recession rates." To achieve this, the first step was to look at the basic sediment characteristics (Section 6.1.1 and 6.1.2). The next was to consider the beach dimensions, its width and volume, and how it interacts with the intertidal shore platforms (section 6.1.3). Finally the sediment supply and dynamics were considered in terms of a simple sediment budget with consideration of the longshore sediment transport potential (Section 6.2).

6.1   Sediment Characteristics

6.1.1   Grain Size

The southwest coast can be divided into three distinct subsections according to abrupt changes in median grain size (Figure 6.1, Figure 6.4). These subsections are marked in Figure 3.3 and include:

1)   Compton Chine to Marsh Chine

2)   Marsh Chine to Atherfield Point

3)   Atherfield Point to Whale Chine

These abrupt changes in grain size are unusual; particularly between subsections one and two which occurs in the middle of Brighstone Bay. Typically the changes in grain size along a bay will be a gradual progression (Celikoglu et al., 2004).

The average median (φ 50) grain size within Section 1 is the same for the foreshore and back shore samples (where present on the foreshore) at 1.9φ (0.266 mm). The change in grain size between Sections 1 and 2 occurs at different locations for the foreshore and back shore samples. The median foreshore grain size increases to -3.3φ (9.67 mm) at Ship Ledge, while the back shore grain size increases to -3.9φ (14.8 mm) around Marsh Chine (Figure 6.1).
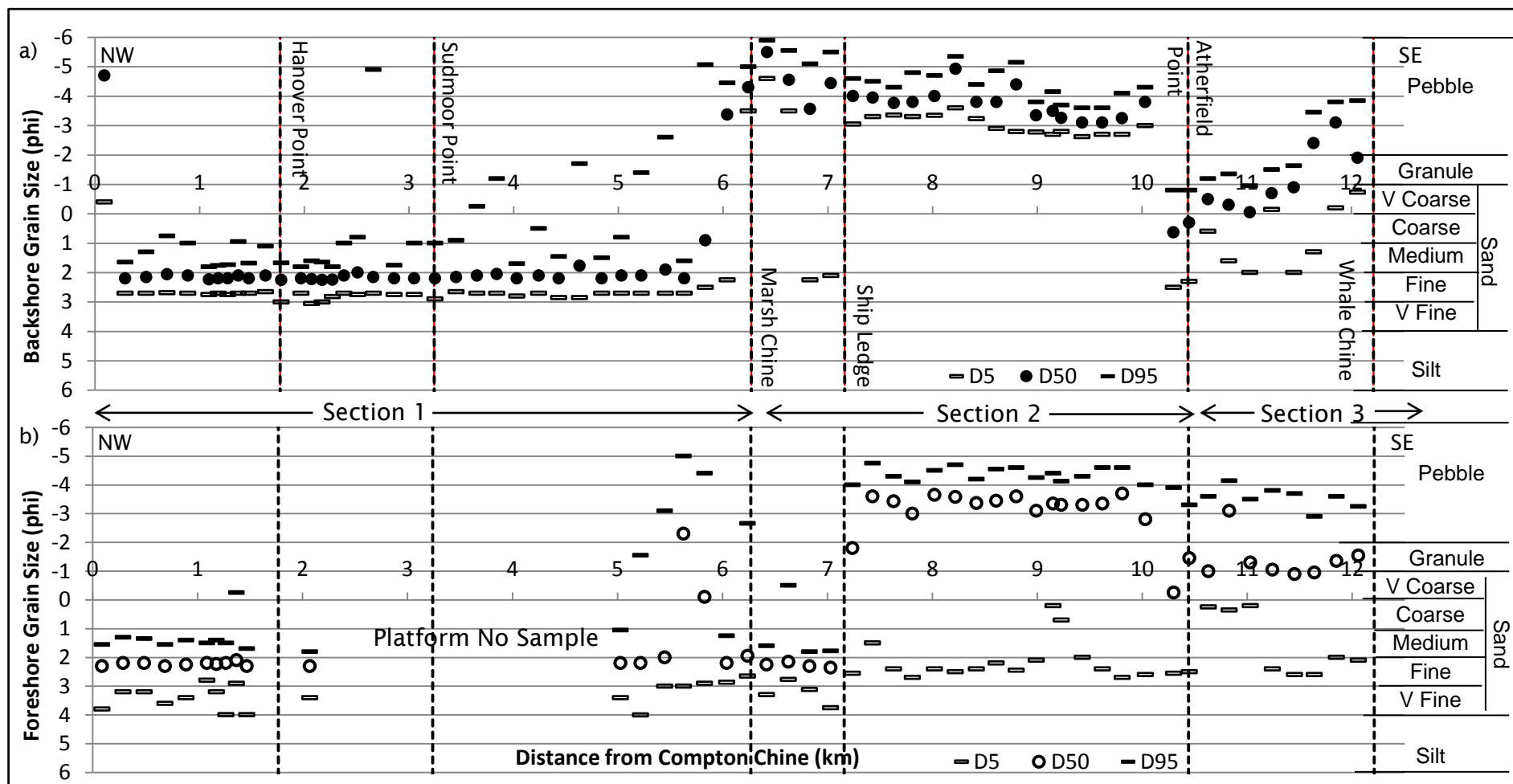
Figure 6.1: a) The backshore median (D_{50}) grain size, with D_{95} and D_5; b) The foreshore median (D_{50}) grain size, with D_{95} and D_5 (which represent the upper and lower limits of the littoral cut-off diameter respectively)

Once the transition is made the $\Phi 50$ and indeed the $\Phi 5$ & $\Phi 95$ remain uniform alongshore until the next transition around Atherfield Point. The average $\Phi 5$ of the foreshore samples only increased slightly from its value in the previous Section from an average of around 3.3φ (0.1mm) to 2.1φ (0.23mm). This increase in $\Phi 5$ indicates an offshore loss of beach material during longshore transport across the transition from one Section to another.

Approximately 100m west of Atherfield Point the final abrupt change in grain size distribution occurs. The average $\Phi 50$ drops from -3.3φ (9.67mm) to -1.3φ (2.44mm) and -3.9φ (14.8mm) to $-0.9\ \varphi$ (1.86mm) for the foreshore and back shore respectively (Figure 6.1). Beyond Atherfield Point towards Whale Chine into Chale Bay, the foreshore $\Phi 50$ remains reasonably uniform, as does the $\Phi 95$. There is a localised increase in the littoral cut-off diameter for the three profiles east of Atherfield Point. The backshore sediment distribution however, shows an increase in all three grain size indicators towards Whale Chine. The beach continues past Whale Chine the entire length of Chale Bay to Rocken End (approx. 3.5km). The beach sediment in the southern part of Chale Bay was not sampled for this study (due to access problems) but analysis of samples collected in 1992 showed a similar pattern between Atherfield and Whale Chine, i.e. an increase in mean grain size towards Rocken End. As is more typical for a headland bound bay, although much of the coarsening had occurred up to Whale Chine (Rix, 2000).
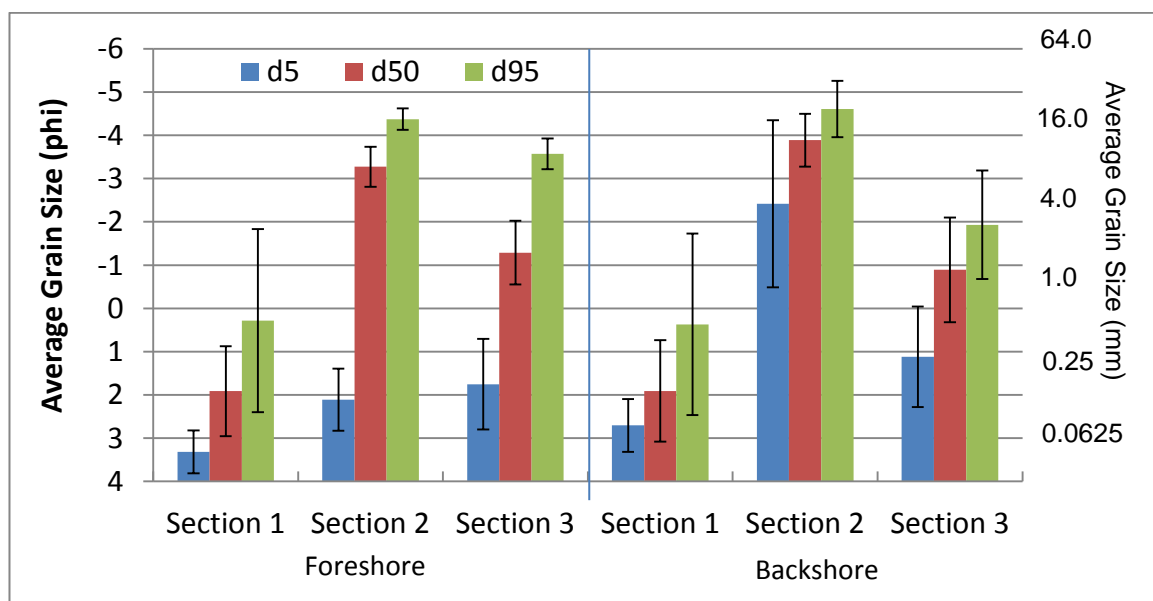
Figure 6.2: Graph showing the variations in average Φ_5, Φ_{50}, Φ_{95} across each section for a) Foreshore and b) Back shore samples. Error bars show one standard deviation around the mean.

Figure 6.2 summarises the change in average $\Phi5$, $\Phi50$, $\Phi95$ across each Section for a) foreshore and b) back shore samples. In general the lowest and highest values of each parameter are found in Sections 1 and 2 respectively. One notable exception to this rule is seen in the foreshore $\Phi5$ or littoral cut off diameter which is the measure of the finest grain size stable on the beach under the prevailing wave condition at the time of sampling. The average littoral cut-off diameter of the foreshore increases from Section 1 to 3, implying that the net longshore transport is to the south east, so as sediment is transported along the coast progressively coarser fine material is lost offshore.

6.1.2   Skewness and sorting

The skewness and sorting of the sediment samples are shown in Figure 6.3 as along shore variations and in Figure 6.4 plotted against D_{50}, give an insight into the beach system. Typically beach sands exhibit a negative skew, i.e. a predominance of coarse grains, i.e. the mean grain size is larger than the median (Bird, 2008). The majority of the back shore samples prior to the increase in $\Phi50$ at Marsh Chine display a positive skew. This may reflect the fine grained nature of the cliff material entering the beach and the low frequency with which the backshore is exposed to wave action, i.e. there is a lag between the fine grained material entering the backshore beach and wave action completely removing it.

The increase in grain size at the transition from Section 1 to 2 coincides with an increase in the negative skew and reduction in the positive skew of the foreshore and backshore samples respectively (Figure 6.3). The skewness of both the foreshore and backshore samples becomes closer to zero in Chale Bay, although the backshore on the whole remains negatively skewed, a state typical of beach sediment (Pethick, 1984). The bulk of both the foreshore and backshore samples northwest of Marsh Chine are well sorted to some degree, becoming poorly sorted as the median grain size begins to increase. The increase in the average grain size of the back shore samples around Marsh Chine coincides with their overall improved sorting (Figure 6.4a). The opposite is true for the foreshore samples which have become poorly sorted south east of Marsh Chine. The sorting of the foreshore samples improves around Atherfield Point and again towards Whale Chine, while the sorting of the backshore samples becomes increasingly poor towards Whale Chine (Figure 6.3).
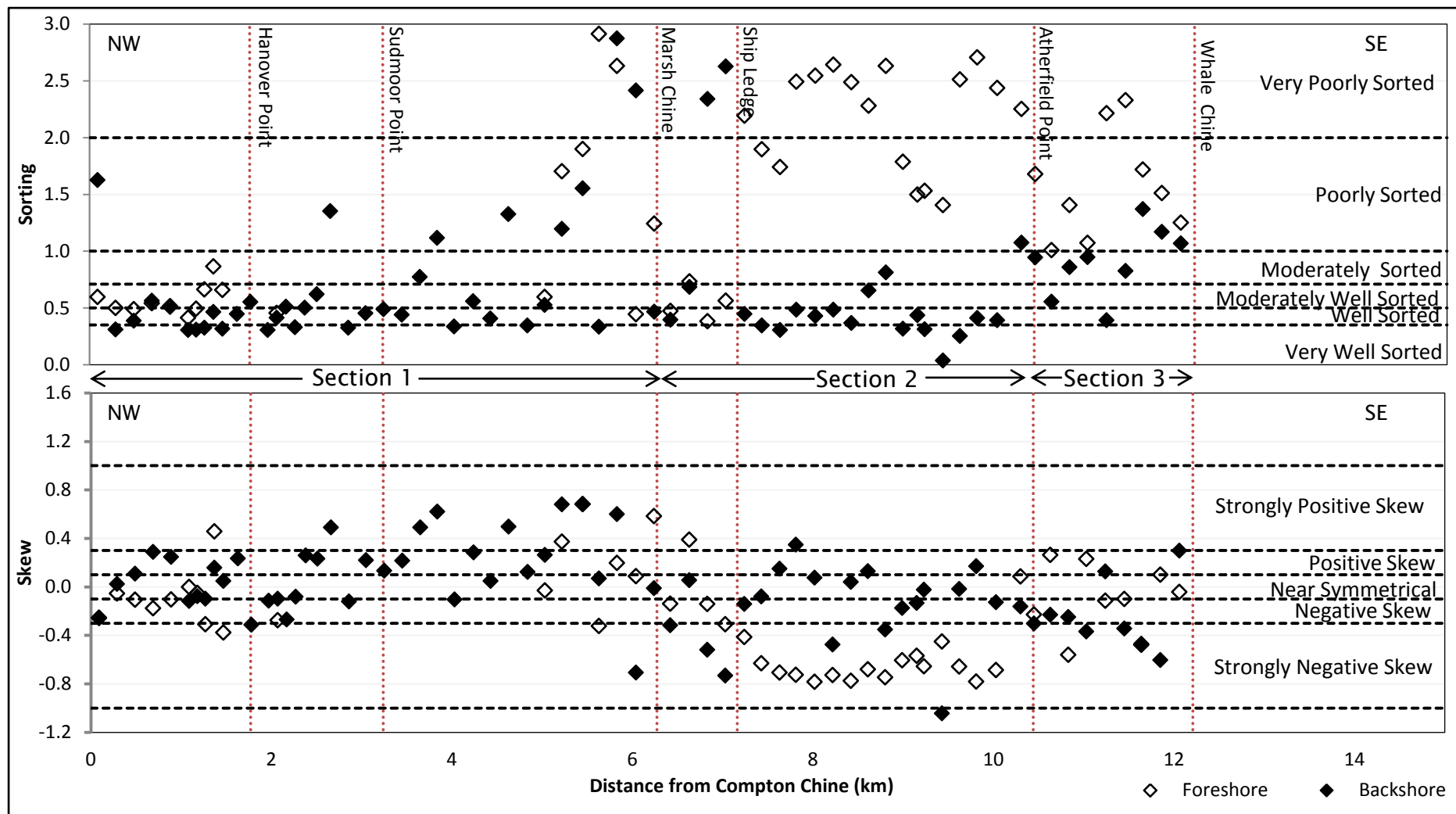
Figure 6.3: a) Sorting and b) Skewness of beach samples collected along the southwest coast of the Isle of Wight
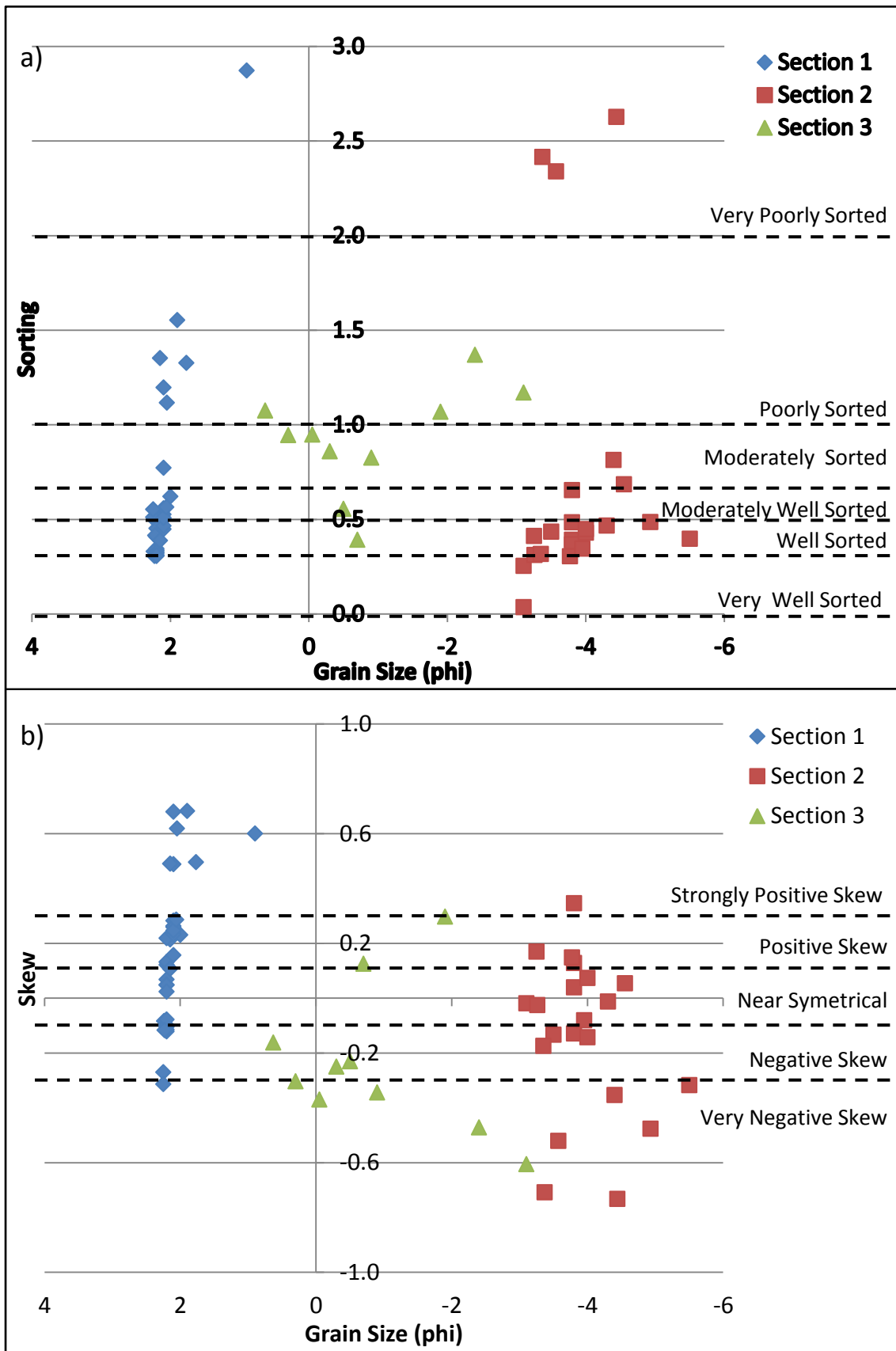
Figure 6.4: Bi-plots showing the backshore D_{50} vs. a) Sorting and b) Skew, samples are divided into the beach sections defined in section 6.1.1

On average across all three sections the skew of the beach sediment is negative apart from the back shore of Section 1 (Figure 6.5). As discussed previously this could be due to the high proportion of fine material entering the system from the cliffs combined with the dissipative nature of the beach in this area (i.e. Compton to March Chine). On average the greatest negative skew was found in the foreshore samples of Section 2. This is congruent with the greatest grain size for both foreshore and backshore samples, the high negative skew is due to the dominance of cobble size sediment. The sorting of backshore samples is consistently better than that of the foreshore samples (Figure 6.5). In Section 2 and 3 this may be related to the greater energy required to shift the gravels on to the back shore.
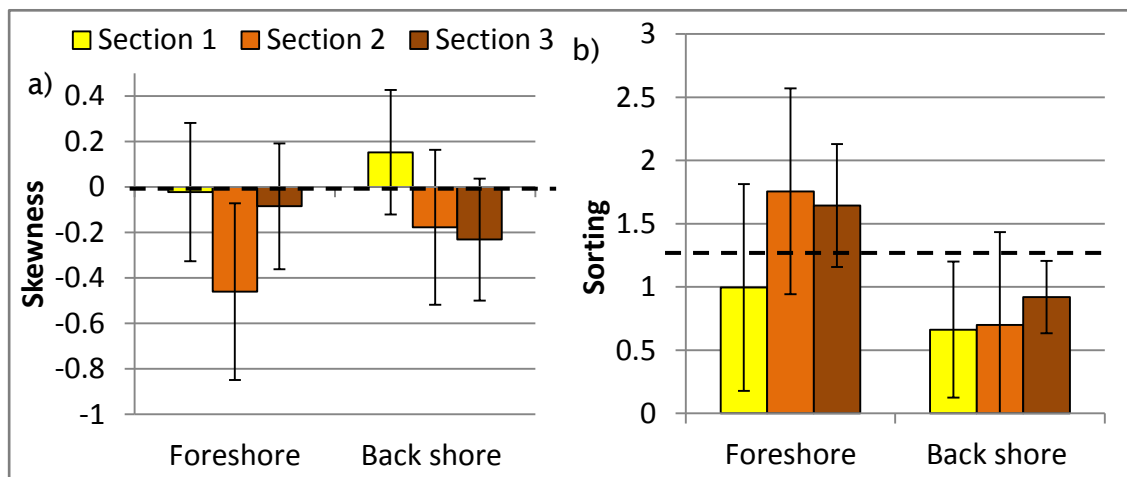
Figure 6.5: The variation in a) mean skewness and b) mean sorting across each section. Error bars show the standard deviation around the mean.

6.1.3 Beach Parameters

The character of the beaches and intertidal shore platforms vary across the study frontage, changing from a dissipative form north of Marsh Chine (Figure 6.6) to a reflective form south of the chine (Figure 6.6). This sudden change in beach form is due to the abrupt change in grain size described above, with an increase in grain size leading to an increase in the angle of internal friction and hence beach slope. This can be seen in Figure 6.7 where the D_{50} grain size is plotted against beach slope, showing the increase in beach slope coinciding with the increase in D_{50} grain size. Samples are separated into the beach sections defined in Section 6.1.1.
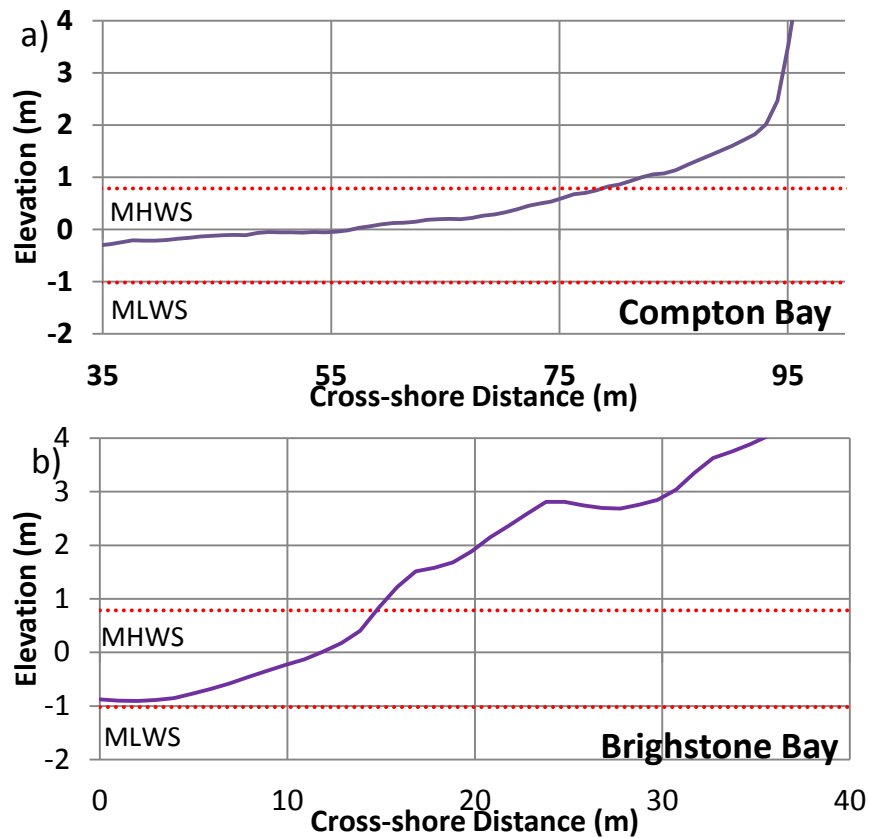
Figure 6.6: Examples of each profile forms; a) dissipative beach north of Marsh Chine, and b) reflective beach south of Marsh Chine
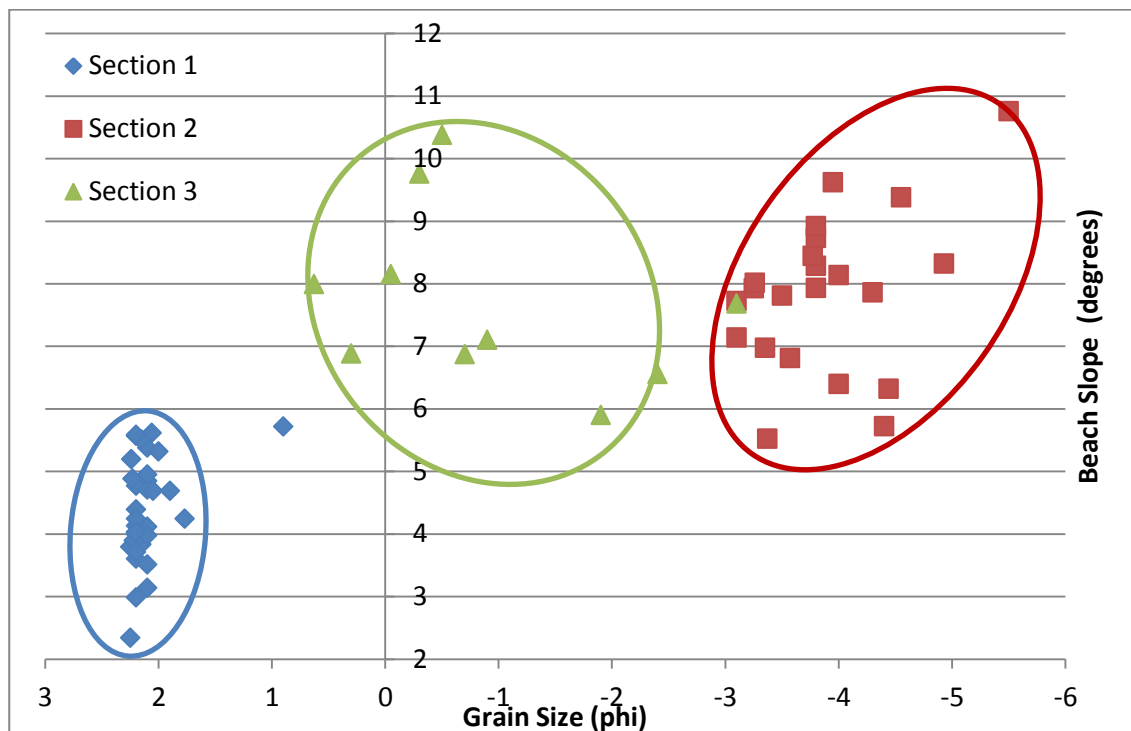
Figure 6.7: D$_{50}$ grain size vs. beach slope, samples separated by beach section showing an increase in beach width coinciding with an increase in beach slope

It may be expected that the change from a dissipative to a reflective beach form would be reflected in a decrease in the beach width at Marsh Chine (Figure 6.8a). Beach width is defined as the width from the cliff beach junction to Mean Low Water Spring tidal level and extracted from historic OS maps and aerial photographs (see Section 3.4.4 for full details). Although there is a marked decrease in beach width at Marsh Chine, from approximately 60m to 35m, the most significant decrease in beach width comes in Compton Bay. Approximately 1km south of Compton Chine, beach width drops from around 80m to 30m (Figure 6.8a). To understand this apparent discrepancy the width and elevation of the shore platform must be considered. Figure 6.8b shows the intertidal platform width along the study frontage, the drop in beach width coincides with the increase in shore platform width. Then, from Sudmoor Point the beach width increases towards Marsh Chine as the elevation of the intertidal shore platform decreases (Figure 6.6a). These inverse variations can be explained by the interaction between the two features; since the profile of a shore platform will develop to mimic the equilibrium beach profile, thus reducing their capacity to store beach sediment (Trenhaile, 2004).

It is worth noting that the overall platform width has reduced over the study period as indicated by the changes between the 1909 and 1975 OS maps. Changes to the Beach Wedge Area (BWA) alongshore are more closely related to variations in grain size (Figure 6.6b), with an increase in BWA coinciding with the increase in backshore grain size around Marsh Chine (Figure 6.1a). There are four areas where the BWA falls below $10m^3m^{-1}$. The largest of which is between Hanover Pont, across the front of Sudmoor Point, to around 600m north of Marsh Chine, this area also displays low beach and high platform widths. The other drops are over shorter distances at Atherfield Point, Ship Ledge and in Compton Bay at the southern end of a large landslide. The locations of these dips in BWA indicate potential barrier to longshore transport, potentially caused by the headlands and associated platforms or in the case seen in Compton Bay by talus build up from the landslide blocking movement.
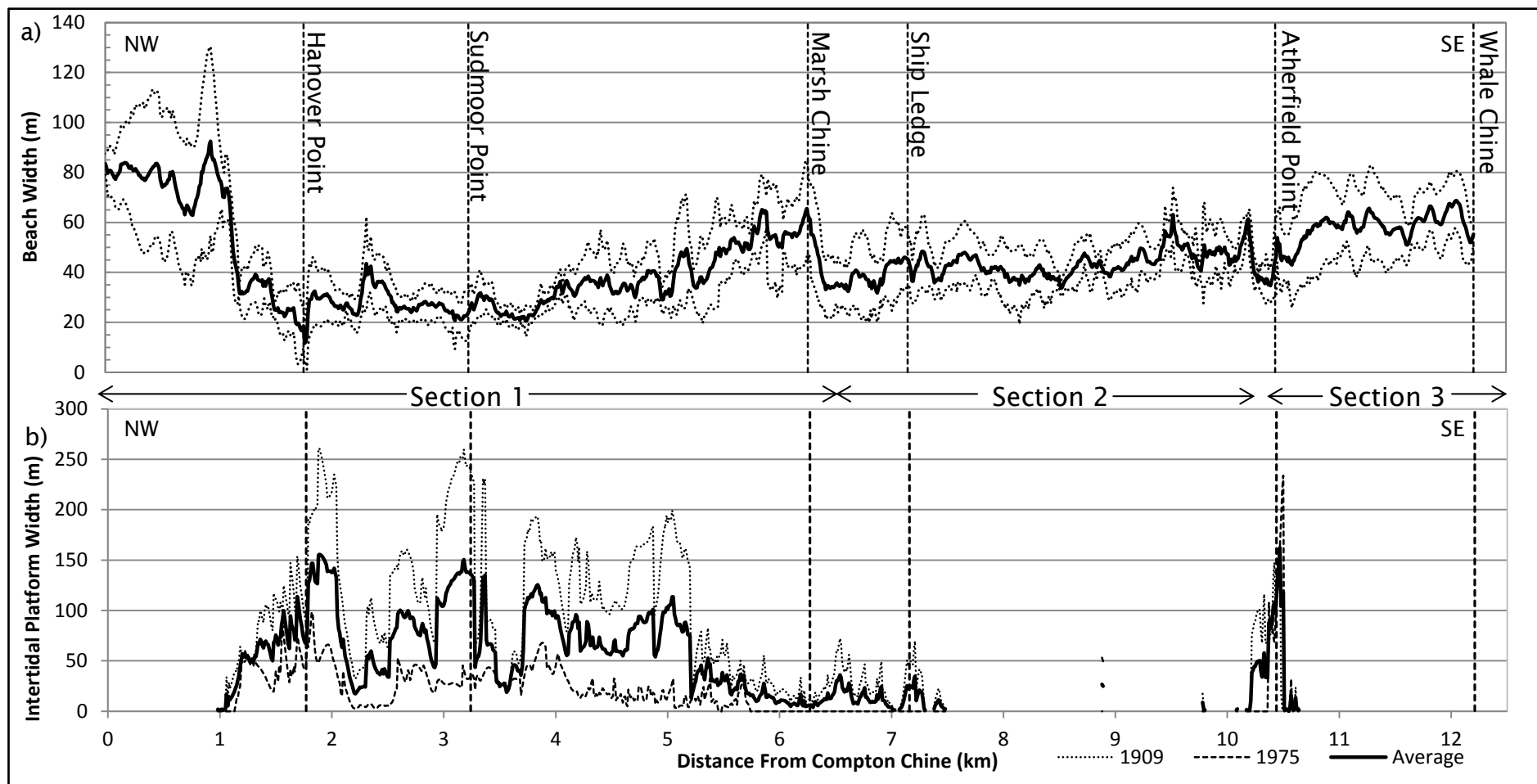
Figure 6.8: a) Average beach width (from 1866, 1909, and 1975 OS Maps and 2008 aerial photographs), dotted lines indicate one standard deviation either side of the mean, b) Average Platform Width (from 1909 and 1975 OS maps).
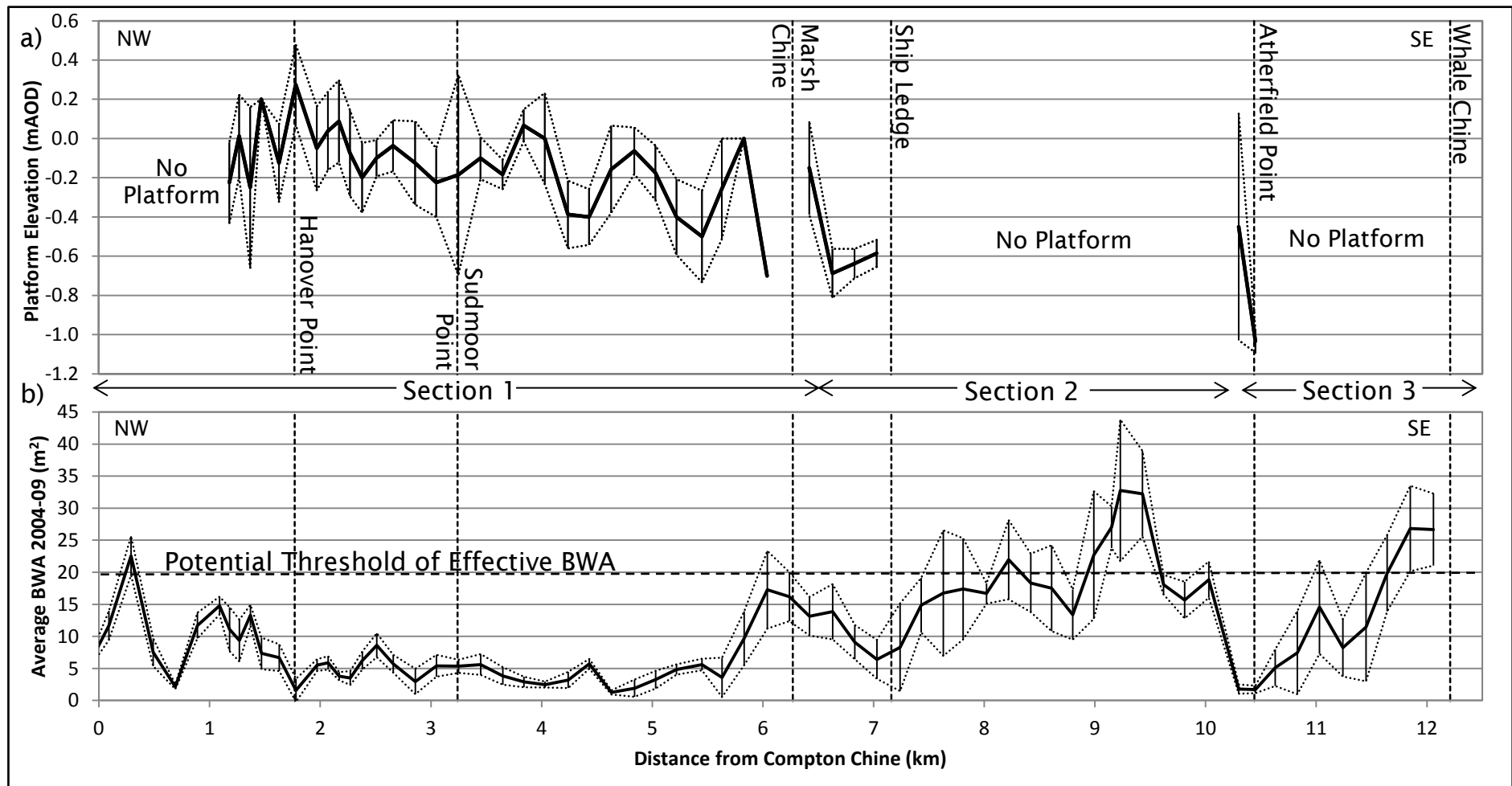
Figure 6.9: a) Shore platform elevation at the landward limit of exposure (1991- 1998). In both charts the dotted line shows one standard deviation either side of the mean; b) Average Beach Wedge Area (BWA) 2005, and 2007-2009.

6.2   Sediment Budget

A sediment budget provides an insight into the evolution of the beaches over time by describing the sources, pathways and sinks of sediment within a defined system (Kana, 1995). The southwest coast of the Isle of Wight has a strongly defined transport divide to the northwest in the form of the Needles, in terms of sediment input to the study area the Chalk cliffs between the Needles and Compton Chine provide an insignificant amount of beach grade material (Bray et al., 2004, Rix, 2000). The main source of sediment is from erosion of the cliffs between Compton Chine and Whale Chine. The sea bed is also a potential source of sediment and will be considered below. The major sinks are offshore and longshore sediment transport. The following Sections will look at the cliffs as a source of sediment (6.2.1); and consider the patterns and rates of sediment transport through the development of a simple sediment budget (6.2.3).

6.2.1   Cliffs as a Source of Sediment

The cliffs of the southwest coast erode at an average rate of approximately 0.5 m a^{-1} (Stuiver, 2010). The input of beach grade material from recession is controlled by the percentage of that cliff material that exceeds the Littoral Cut-off Diameter (LCD). The cliffs vary in height, slope, grain size distribution and average annual recession rate alongshore, as does the LCD (Figure 6.10). This means there will be an offshore loss of sediment with littoral drift across beach sections. Table 6.1 shows variations in the percentage of cliff sediment greater than the littoral cut off diameter of the adjoining beach. Where the lithology is not present in a section the table is marked n/a. The mudstones and shales produce less than 5% beach grade material, even in Section 1 where the LCD is lowest. The Composition Factor decreases from Section 1 to 3 as the LCD increases, until in Section 3 the input of sediment is from the Ferruginous Sands alone and only at a rate of 8%.
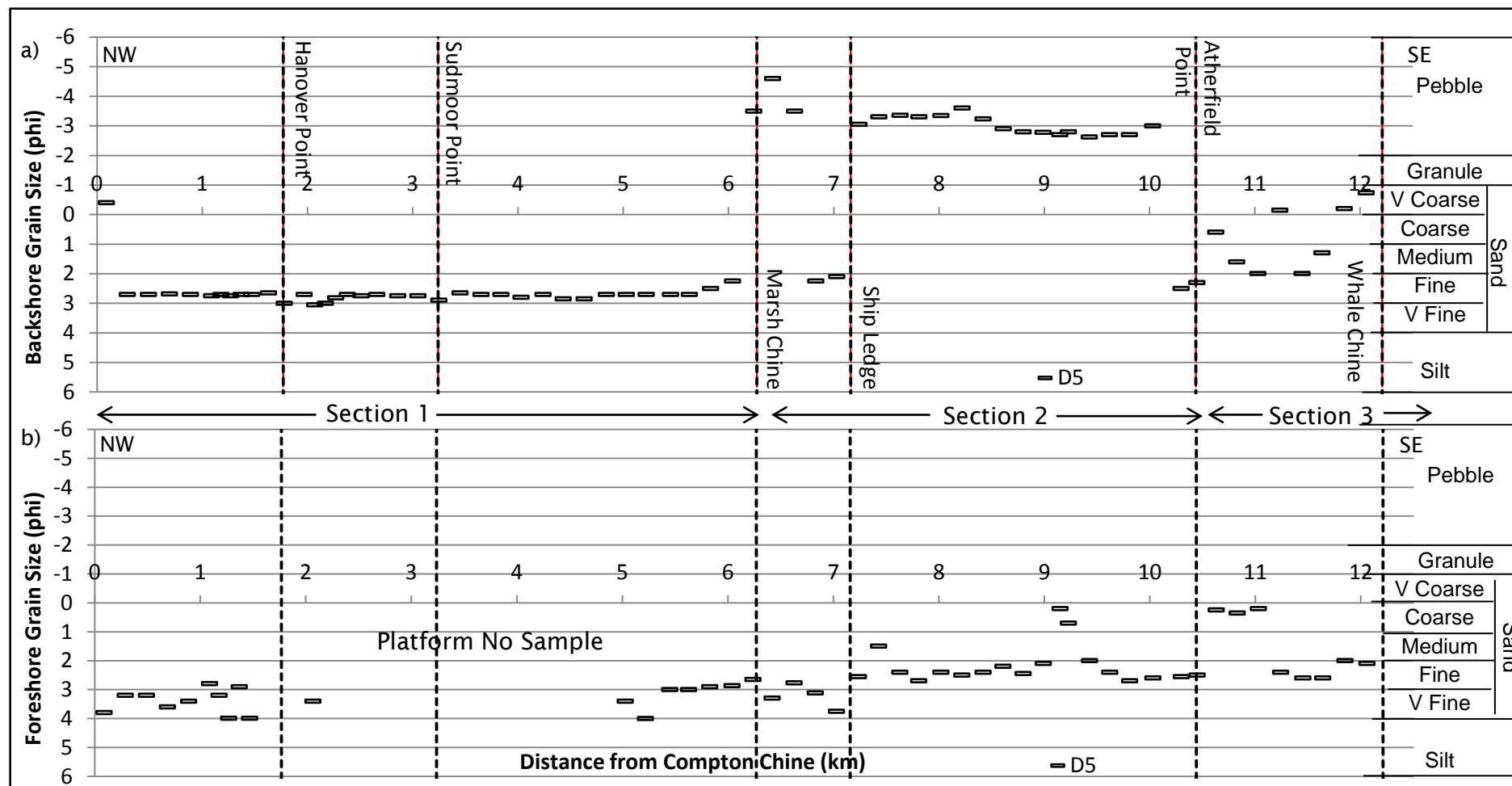
Figure 6.10: Variations in the Littoral Cut-off Diameter (LCD) alongshore

Table 6.1: Variations in averaged Composition Factor (K) for each lithology in each section. n/a denotes a lithology is not present in that section. The Composition Factor refers to a value between 0 and 1 which describes the percentage of the cliff material that will remain on the beach, i.e. beach grade material.

Formation	Member/Lithology	Composition Factor (K)		
		Section 1	Section 2	Section 3
River Deposits	Valley Gravels	0.80	0.72	n/a
	Brick Earth	0.45	0.25	n/a
Ferruginous Sands	Various Sands	0.69	n/a	0.08
Atherfield Clay	Clay	0.15	n/a	0.00
	Crackers	n/a	n/a	0.00
Vectis	Shale	0.03	0.003	n/a
	Sandstone	0.96	0.54	n/a
Wessex	Mudstone	0.05	0.02	n/a
	Sandstone	0.49	0.09	n/a

Figure 6.11a shows the total average annual input of sediment along the coastline compared with the average annual input of beach grade material. Volumes have been normalised by dividing the volume input of each segment by its width, so values are in m^3m^{-1}. The variations in the total input are caused by changes in cliff elevation and slope. It is clear from this graph that a large proportion of the cliff material entering the beach system from cliff erosion each year is lost offshore (87% is lost). The Ferruginous Sands provide the greatest proportion of beach grade sediment, to the north of the study area where they outcrop, in Compton Bay. However, the increase in littoral cut off diameter in the southern end of the frontage means that a large proportion of the sediment produced by the Ferruginous Sands in Section 3 (Chale Bay) is lost offshore. The input of beach grade sediment between 8 and 9.4km in Section 2 is a product of the Barnes High Sandstone. Similarly the increase between Sudmoor Point and Marsh Chine is related to the Sudmoor Point Sandstone. The errors on the sediment inputs presented as dotted lines in Figure 6.11 were calculated using the measurement errors on each component of the calculation, i.e. cliff height, recession rate and LCD. The mean values plus or minus their individual errors were used to calculate the maximum and minimum volumes respectively. The error in LCD translates to a large error range in beach grade input in areas where the LCD is close to the median grain size in well sorted lithologies such as the Ferruginous Sands in Section 3.
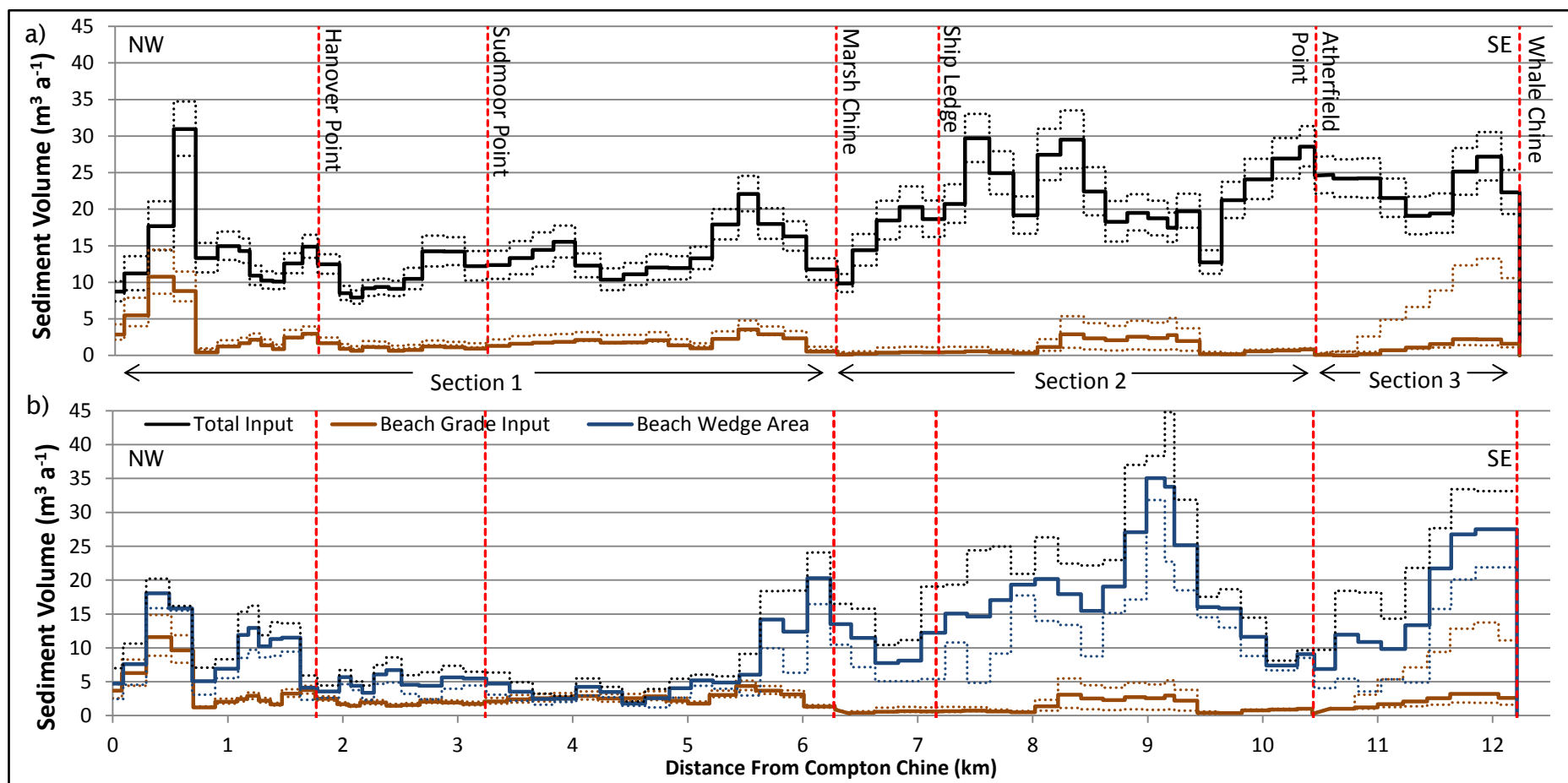
Figure 6.11: a) Average annual total sediment input and b) Average Beach Wedge Volume (2004-2009) compared with the average annual beach grade sediment input along the southwest coast. Dotted lines show the errors (see text for details)

Figure 6.11b compares the average annual input of sediment with the beach wedge volume (BWV), i.e. the volume of sediment above MHWS tidal levels. In essence the BWV is the same as the BWA in this instance, as the sediment input and BWV are both expressed as a volume per metre of coastline (i.e. m^3m^{-1}) equivalent to m^2. It is important to note that the BWV is not a true measure of beach volume, only an approximation, as the volume of beach material below MHWS tidal levels is not considered. The correlation between BWV and sediment input is poor, except for the north end of the large landslide in Compton Bay at 0.29 to 0.9 km where the high beach grade sediment input from the Ferruginous Sands is prevented from moving down drift by the talus of the aforementioned landslide creating a partial transport boundary. There is only one area where the average annual input of sediment comes close to the average BWV, between Sudmoor Point and Marsh Chine (3.65 km and 4.63 km from Compton Chine). This is related to the low beach volumes and high sand content of the Sudmoor Point Sandstone.

The distribution of gravel in the cliffs and on the beach raises some interesting questions. Figure 6.12a shows the distribution of the average annual gravel input along the coast, while Figure 6.12b shows the percentage of beach material greater than – 3, -4 and -5 phi respectively (i.e. gravel). The source of gravel from the cliff is contained entirely within beach Section 1, while the majority of gravel on the beach is found in beach Sections 2 and 3 (Figure 6.12b). There is evidence from the literature that the current pattern of sediment distribution on the beach has been in place for at least the last 130 years. An account of the coastline from Jenkinson (1879) describes a similar pattern of gravel distribution, with a firm sand backshore north of Marsh Chine and a gravel beach between Marsh Chine and Atherfield Point. The distribution of sediment in the cliffs however has not remained constant. For example the channel sands within the Wessex and Vectis Formations can be important sources of beach grade material but they are laterally discontinuous and as such are a finite sediment source, e.g. the Sudmoor Point and Barnes High Sandstones. Potentially the most significant example of this was outlined in Section 4.1.5; there is evidence the River Terrace Deposits extended as far south as Blackgang Chine and as far north as Compton Chine. This represents a significant loss of sediment input. However a beach is a sink and can represent decades if not centuries of sediment input.
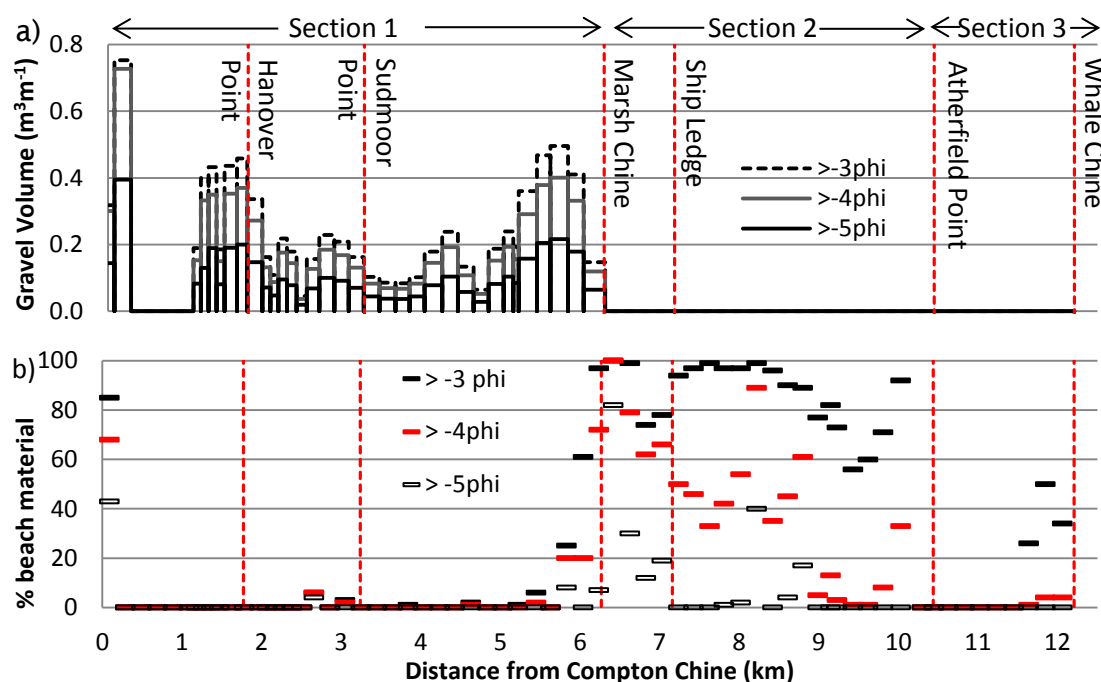
Figure 6.12: a) Average annual gravel input along the south west coast; b) percentage of beach material greater than -3, -4 and -5 phi respectively (i.e. gravel).

An alternative explanation for the disproportionately high level of gravel on the beach compared to the apparent source in the cliff combined with its well-rounded nature implies that the majority of the gravel comes from the seabed and is transported to the beach through onshore sediment transport (Brampton et al., 1998), an implication that will be discussed below (Section 6.2.2).

6.2.2 The Sea Bed as Source of Sediment

Reports of occasional rapid changes in beach volume and composition are scattered throughout the literature. Colenutt (1938) stated that the coarse sandy beach at Brook Green had on occasion been replaced by well graded, polished gravel, Kay (1969) inferred the pebbles of Chale Bay had recently (in the 60's) decrease in size. Brampton et al. (1998) referred to talk by locals of major changes in gravel volumes on the beach after storms implying an off shore source of sediment, but their investigation found little sediment mobility immediately offshore. A sediment mobility study by Posford Duvivier and BGS (1999) found no direct evidence of offshore or onshore transport of gravel. Modelling of onshore orthogonal sediment transport running across offshore coarse sediment stores by Rix (2000) showed that all the waves considered (ranging from Hs - 1 m Tp - 5.5 s to Hs - 6.02 m Tp - 8.1 s) were capable of moving coarse sediment particles (up to 8 mm) towards the

shoreline. The average size of the gravels within section 2 and 3 are approximately 16mm (-4phi) and 4mm (-2phi) respectively (Figure 6.12b).
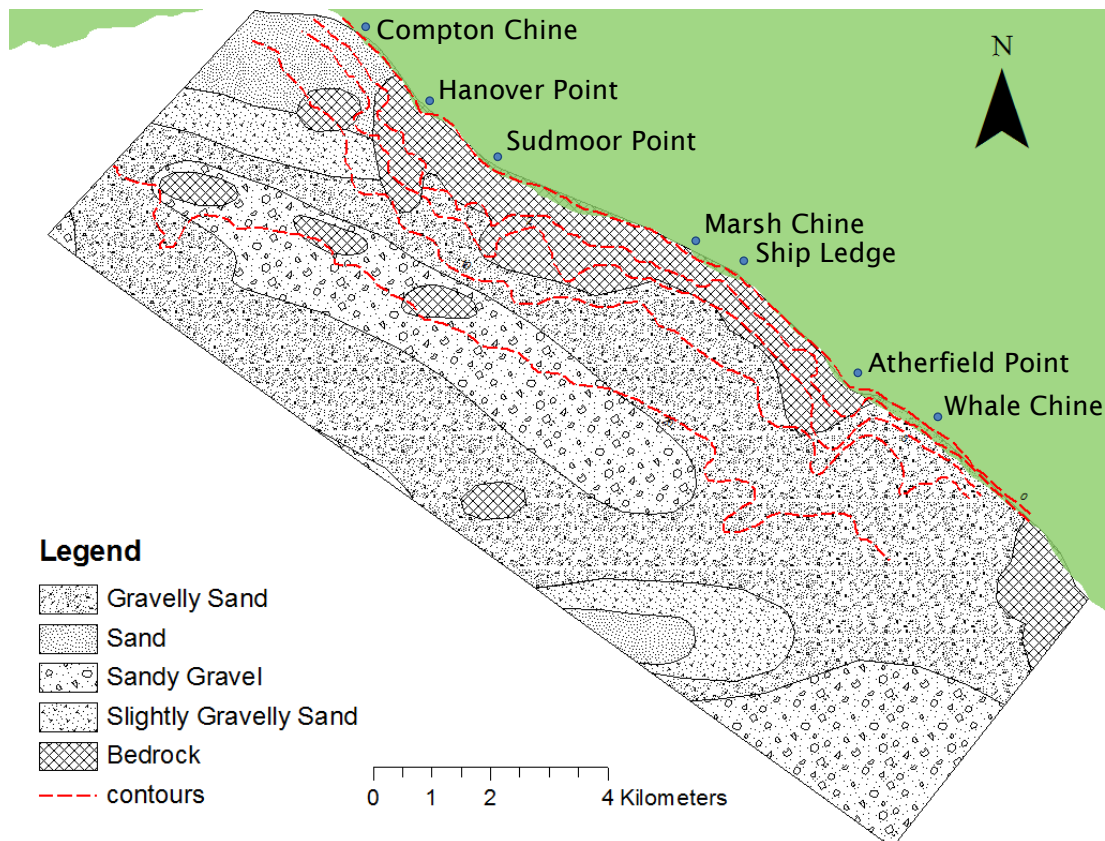
Figure 6.13: Seabed sediment off the southwest coast of the Isle of Wight, with depth contours. Data taken from the British Geological Survey Digital Map collection, Depth contour taken from the Admiralty Chart (SC5600.2)

Figure 6.13 shows the seabed sediment distribution along the south west coast of the Isle of Wight. The majority of the nearshore, i.e. between Shippard's Chine Car Park to just east of Atherfield Point, is exposed bedrock. Onshore transport of sediment is less likely in these areas. To the north of the Car park up to Compton Chine the seabed is covered in sand, coinciding with the wide sandy beach of Compton Bay. In the south along much of the length of Chale Bay the seabed is covered by gravelly sand. It will be in these areas that most potential for onshore transport exists. The sea bed is unlikely to be a significant source of sediment to the sediment budget due to the limited nearshore seabed sediment cover.

6.2.3   Longshore Sediment Transport

A review of the literature indicates that the consensus of opinion is that the dominant longshore transport is from the northwest to the southeast (Barrett,

1985, Brampton et al., 1998, Colenutt, 1938, Rix, 2000). Evidence of this can be seen in variations of the BWA, gravel size and roundness. Increases in BWA to the west of littoral drift barriers are seen at Atherfield Point, Hanover Point and the eastern edge of the Compton Farm Landslide. The winnowing of progressively coarser sediment, represented by the increase in LCD, and the reduction in gravel angularity from west to east also implies transport in that direction (Bray et al., 2004, Rix, 2000). An initial estimate of sediment transport rates was calculated assuming stable beach volumes, i.e. the transport out of a beach segment is equal to the transport in plus the input from cliff erosion. These calculations were carried out in SBAS, the Sediment Budget Analysis System developed by Rosati and Kraus (1999) for the US Army Corps of Engineers, by force balancing each beach segment. The results are shown in Figure 6.14 where they are compared with the potential sediment transport rates for sand calculated using the Komar and Inman (1970) equation (Equation 3.12) and results from the wave refraction analysis (Chapter 5).

Figure 6.14 shows the long shore variations in potential sediment transport under a number of representative wave conditions, calculated using the Komar and Inman (1970) equation, compared with the estimates calculated through force balancing of sediment cells in SBAS (Section 3.6.2). The transport rate per day was calculated assuming that transport is only possible when the water level is above a mid-tide level (i.e. only 12 hours a day). The dominant direction of longshore transport is to the southeast, however reversals are seen between Sudmoor Point and Marsh Chine and southeast of Atherfield Point. The estimates of longshore sediment transport from the force balancing of cells show no reversals as all sediment was assumed to move down drift or offshore. The overall trend shows a steady increase in transport rates along the coast with two sharp drops at Marsh Chine and Atherfield Point, where the LCD increases and sediment previously assumed to be transported along the coast is lost offshore. The sediment budget calculated within SBAS by force balancing cells, based on the premise that transport out of a cell is equal to transport in plus input from cliff erosion, is presented in Figure 6.15.
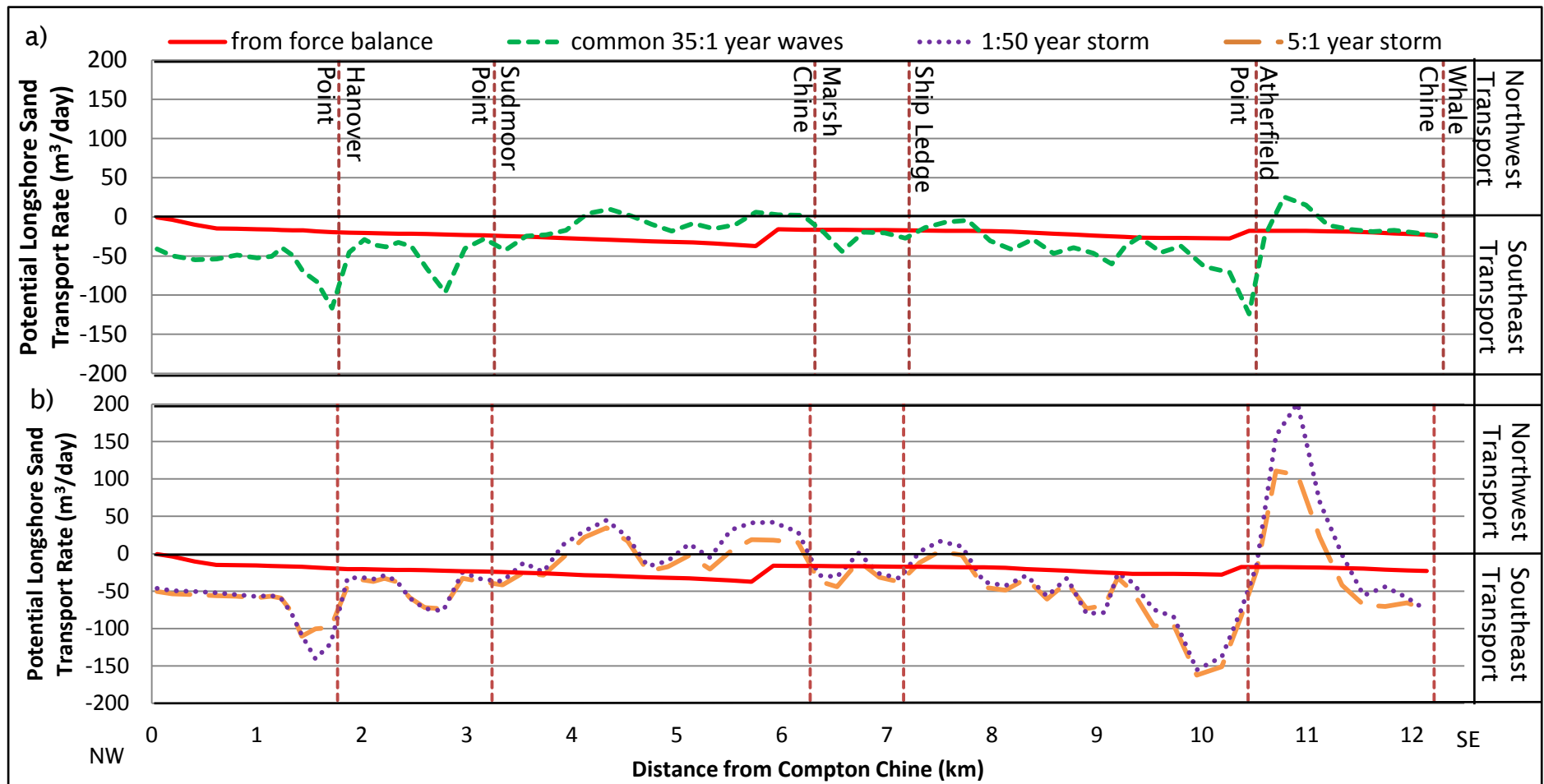
Figure 6.14: Potential longshore transport (assuming transport only occurs for 12 hours a day) under a) common wave which occur 35 times in 1 year and b) storm waves compared with estimated based on stable beach volume calculated in SBAS.
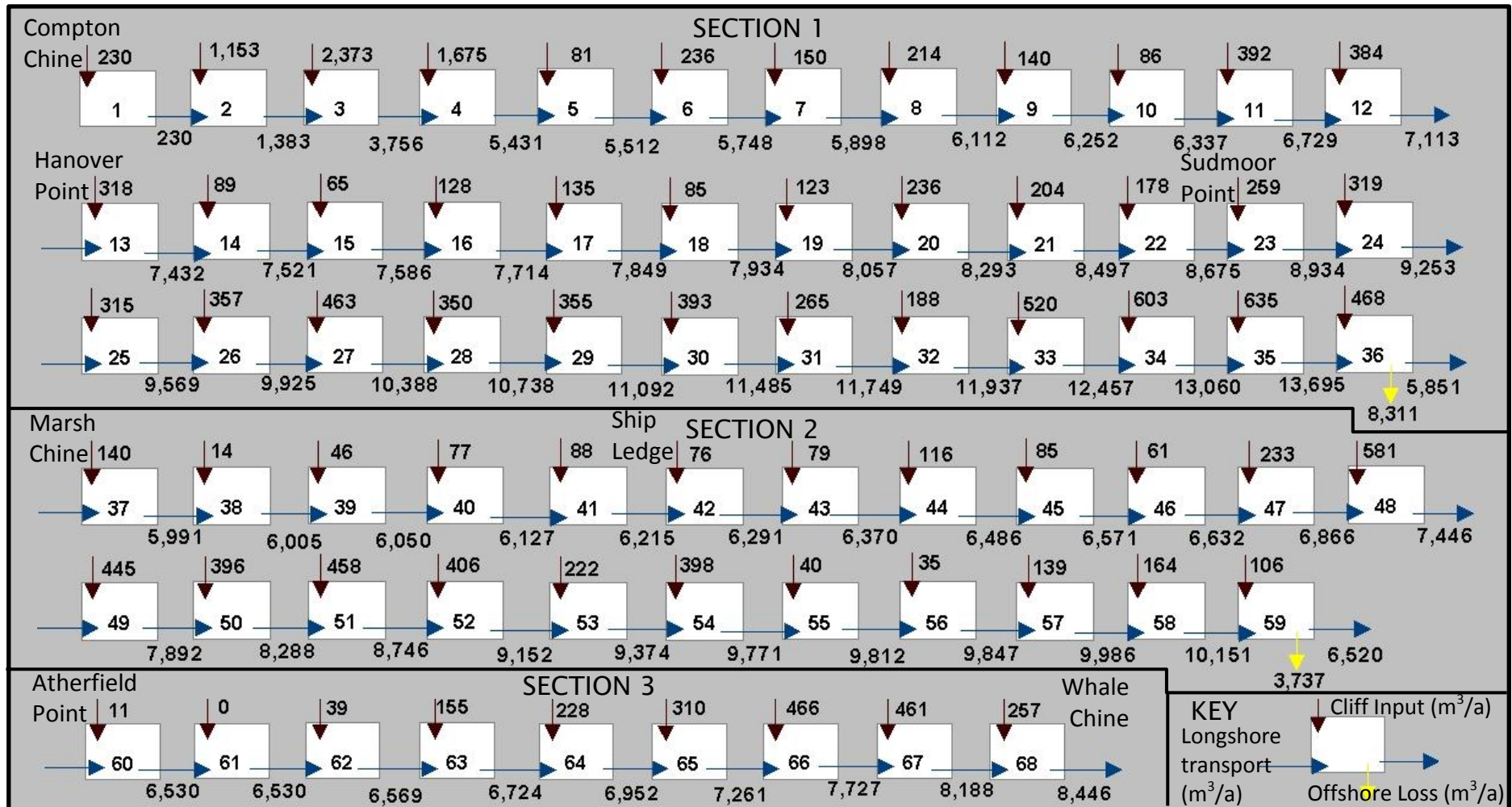
Figure 6.15: Sediment budget for the southwest coast of the Isle of Wight, longshore transport is based on the premise that transport out is equal to transport in plus the input from cliff erosion.

The pattern of potential sediment transport for all waves is broadly similar, with the majority of transport from the northwest to the southeast apart from three zones of reversal. The first is between Sudmoor Point and Marsh Chine and the second and third are found down drift of Ship Ledge and Atherfield Point respectively. Rix (2000) found local reversals of longshore sediment transport direction down drift of Atherfield Point under certain wave conditions; she did not find reversals between Sudmoor Point and Marsh Chine or south of Ship Ledge but did report reversal downdrift of Hanover Point. Peaks in the potential transport to the southeast are found updrift of all the established headlands, due to refraction of wave energy over the shore platforms fronting the headlands, towards the aforementioned headlands.

6.3   Summary

The character of the shore platforms, beaches their sediments and sources change along the study frontage. Figure 6.16 summarises the longshore variations in beach and sediment parameters. It highlights the interconnected nature of these variations, for example beach width is greatest in Compton Bay where no intertidal platform is present and the input of beach grade sediment is greatest. The beach width also drops to its lowest levels at Hanover Point where inputs are low, potential transport rates are high and platform elevation is at its highest. South from Hanover Point the beach width increases as the platform elevation decreases until Marsh Chine (Figure 6.8 and 6.6). Around Marsh Chine the beach width decreases as the BWA and backshore grain size increases forming a steeper back shore profile. BWA drops again at Atherfield Point, along with a small drop in beach width in the presence of the intertidal platform and the drop in grain size.

Values of BWA only exceed the 20 m^2 threshold defined by Lee (2008) in three locations (Figure 6.6). It could be argued that the higher energy wave conditions the southwest coast is subjected to in comparison with that of Norfolk and Suffolk, where the value of 20 m^2 was calculated, would lead to a higher threshold value for an effective BWA. The Norfolk coast is exposed to waves generated in the North Sea sheltered from the prevailing wave from the SW generated across the North Atlantic which the southwest coast are exposed to. With the increased exposure of the southwest coast the BWA threshold must be increased. The results indicate that the beach offers little or no protection to the cliff toe along the entire coast,

particularly to the north of Marsh Chine.
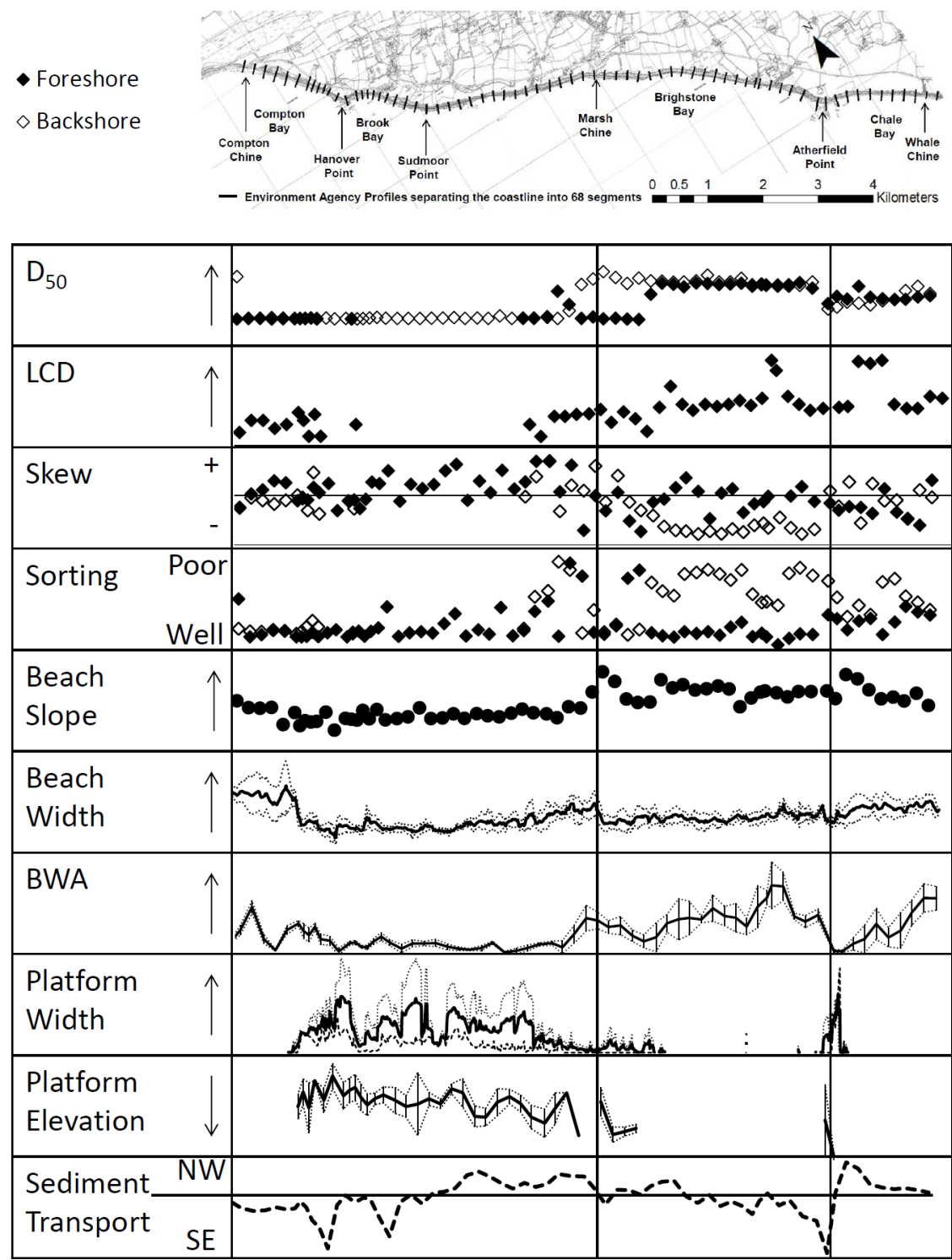
Figure 6.16: Summary of beach sediment, morphology and platform properties.

The sediment budget highlights the variation in sediment input along the coast; the majority of the sand is supplied from the Ferruginous Sands in the far north and south of the study area. The levels of the sandy beaches reflect this pattern.

There is some evidence of partial transport barriers to sand at the eastern edge of the Compton Chine Landslide and Hanover Point. The input of gravel from the cliff is predominantly to the north of Marsh Chine, while the gravel beaches are found to the south. In the past the gravel source in the cliff extended to the south beyond the limits of the study area; it is also possible that Atherfield Point acts as a barrier to the littoral transport of gravel. There is some evidence for onshore transport of gravel but, as yet no quantitative data. Since the evidence for onshore sediment transport points towards rapid, short lived changes to the beach sediment it is not necessary to consider this transport path in detail over the timescales involved in this project.

Although the values of BWA have only been calculated for a short period (2004 to 2009) the calculation of beach width was made using maps and aerial photographs over the whole study period. Some variability in the beach levels was observed, indicated by the standard deviation around the mean shown in Figure 6.8, but the overall patterns of beach width are consistent over the study period. This combined with accounts from the literature describing sediment distribution as it exist today has led to the assumption that beach levels have been stable over the two hundred years. This has allowed estimates of longshore sediment transport to be made by simply taking the longshore transport out to be equal to the longshore transport in plus the input of beach grade material from the cliff. When compared to calculations of potential longshore transport these estimates have both over and underestimated the transport rates in certain areas. The reversal of the potential transport rates between Sudmoor Point and Marsh Chine and down drift of Ship Ledge and Atherfield Point were also missed. This implies that the sediment could, and is likely to be moving in both directions along this shoreline. The extended area of transport reversal across Sudmoor Point may contribute to the low sediment volumes in that area. Overall, it seems that the coastline is broadly drift aligned and the potential for sediment transport is low, with peaks seen updrift of all the headlands, including Ship Ledge, and reversals noted downdrift of the same headlands, except Hanover Point.

Overall the sediment budget has highlighted the importance of changing cliff face exposure over time. The inferred change in the gravel input to the coast over the last 160 years represents a significant change to the sediment budget of the coastline. It has also shown that the input of sediment along the coastline is very

low, indicating that the current situation, whereby the beach has little or no influence on recession rates is likely to have existed and continue to exist over a timescale of many decades.

7. Coastal Planform Evolution

The previous chapters have presented the results of the geological and geotechnical assessment, the wave refraction analysis and the beach morphology and sediment budget analysis. These results cover the first three objectives of this project with the exception of the influence the variations identified have on the long-term recession rates. An insight into the changes in the coastal planform over the last 440 years can be gained from an analysis of historic maps and recent dGPS surveys. This chapter aims to provide an overview of how the coastal planform has evolved. This will be achieved in two stages. First the persistence of the established headlands between 1570 and 1850 will be considered using historic maps prior to the advent of the Ordnance Survey, which produced the first reliable maps for the Isle of Wight in 1866 (Section 7.1). Secondly a more detailed study of the coastal planform evolution over the last 145 years is presented. Initially the longshore variations in cliff top and cliff base recession rates along the whole coastline are presented (Section 7.2), before consideration of the relationship between the factors outlined in Chapter 2 and presented in Chapters 4 to 6 are made (Section 7.3). Recession rates around each of the headlands, including Ship Ledge will be looked at in detail in Section 7.4. The impact these variations have had on the indentation of the coastline will be investigated in Section 7.5 and finally the development of the headlands including their migration is considered in Section 7.6.

7.1   Persistence of Headlands Pre 1866

To give an indication of how persistent the three established headlands have been over the past 450 years a number of historical maps were studied. One example from each century is presented in Figure 7.1 to Figure 7.4. The oldest map acquired was produced in 1570 by John Rudd for the Burghley Atlas (Figure 7.1). The map shows one pronounced headland separating Compton Bay and Chale Bay. The headland is not labelled but the location towards the southern end of the coastline implies that it represents Atherfield Point. There is no evidence of Hanover or Sudmoor Point.

Figure 7.1: Map of the Isle of Wight produced in 1570 by J. Rudd for the Burghley Atlas
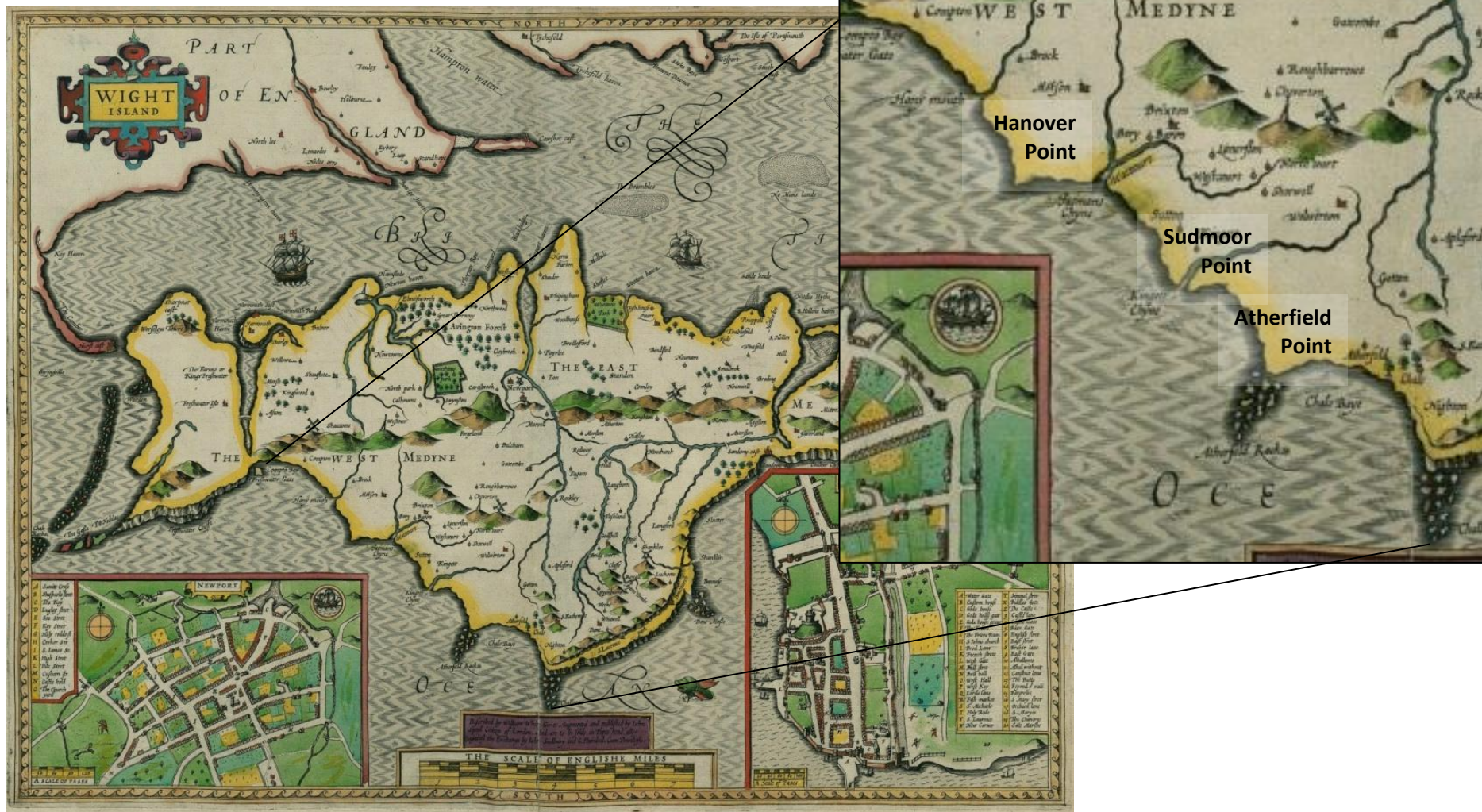
Figure 7.2: Map of the Isle of Wight produced in 1611 by J. Speed

Hanover
Point

Sudmoor
Point

Atherfield
Point

Figure 7.3: A New Map of the Isle of Wight created by Thomas Kitchin in 1760 for the London Magazine.

Figure 7.4: Map of the Isle of Wight produced by J. Walker and Published by Payne and Foss in 1815.

The second map selected was produced in 1611 by John Speed and is shown in Figure 7.2. There are three well defined headlands portrayed by this map. The platform fronting the headland approximately two thirds of the way down the coast is labelled Atherfield Rocks indicating that the headland is indeed Atherfield Point. The northerly headland is not labelled but its position in relation to Brook Village implies it is Hanover Point. The central headland appears to coincide with the outflow of a Chine; it is unclear if this headland represents Sudmoor Point. The third map created in 1760 by Thomas Kitchin more closely resembles the coastline that exists today, with Atherfield and Sudmoor Point labelled and Hanover Point is clearly defined (Figure 7.3). The final map used in this analysis was produced in 1815 by J. Walker and is a close approximation of the 1866 map, with all three headlands visible (Figure 7.4). The persistence of Atherfield Point since 1570 is supported by all the maps considered. The persistence of Hanover and Sudmoor Point however, is less evident. There have been three headlands recorded on the coastline since 1610, this indicating that Hanover, Sudmoor and Atherfield Points, have persisted for at least 400 years.

7.2   Longshore variations in cliff recession rates

The cliff top position in 1866 and 2012 are shown in Figure 7.5a and long-term average annual recession rates of the cliff top from 1866-2012, are shown in Figure 7.5b. While those of the cliff base between 1866-2011 are found in Figure 7.6. The mean recession rate for the whole coastline is indicated in each graph as a solid red line, the dashed red line shows one standard deviation either side of the mean. The mean recession rate of the cliff base and cliff top are very similar at 0.49 m a^{-1} for the cliff top and 0.51 m a^{-1} for the cliff base. The variable nature of cliff morphology and behaviour along the coastline means that the cliff top recession rates (Figure 7.5; Figure 4.2 & 4.3) are more variable than those of the cliff base, particularly in areas which exhibit large scale low frequency landslide events (Figure 7.6) as indicated by the standard deviation of the cliff top recession rates at 0.17 m a^{-1} compared to 0.13 m a^{-1} at the cliff base.
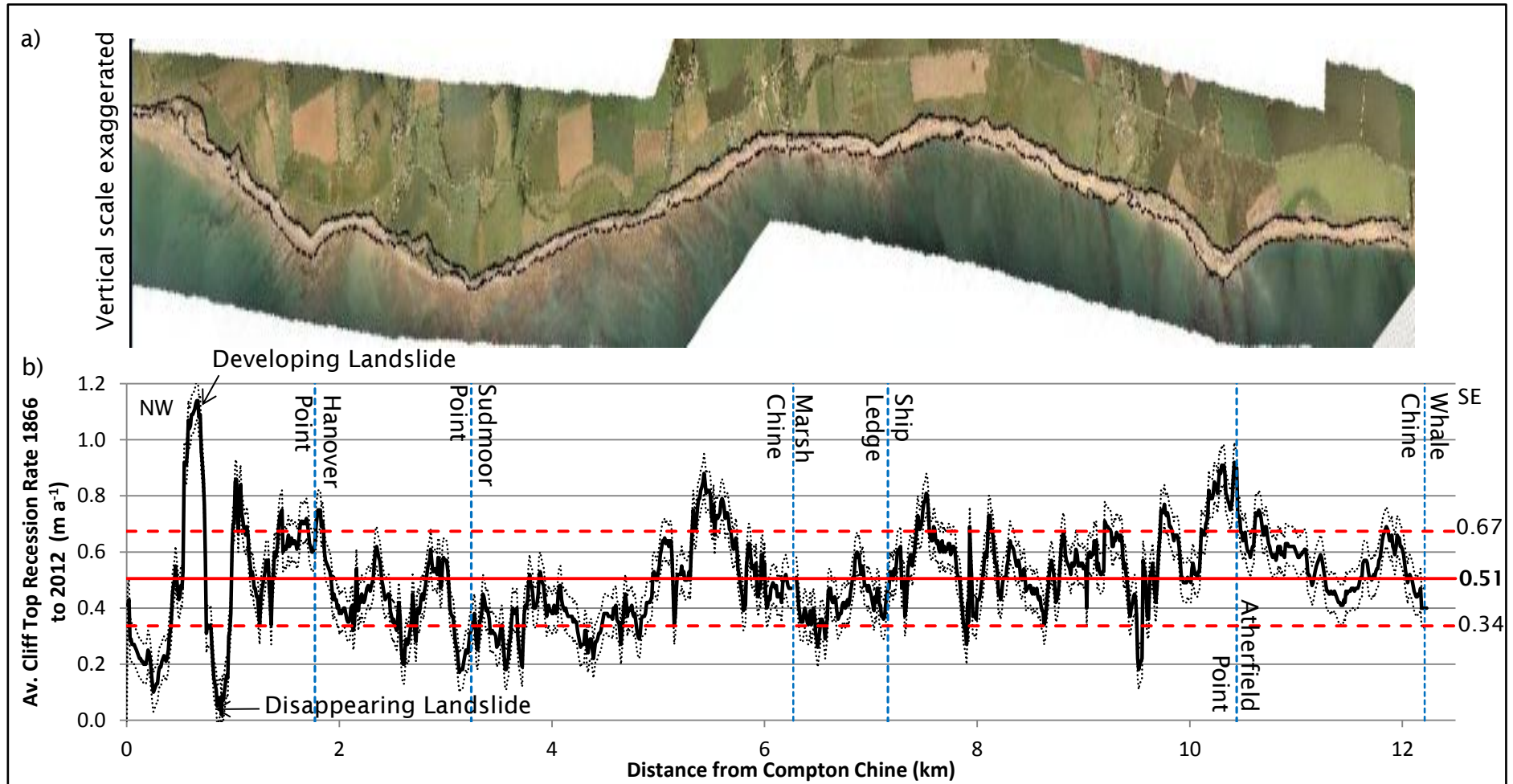
Figure 7.5: a) Aerial photograph with 1866 (dashed) and 2012 (solid) cliff top line imposed and **b)** Average annual recession rate for the cliff top (1866-2012). The dotted black lines mark the error in average annual recession rate calculated using Equation 4.1. The solid red line indicates the average recession rate for the whole study area, while the dashed red lines represent one standard deviation around the mean.
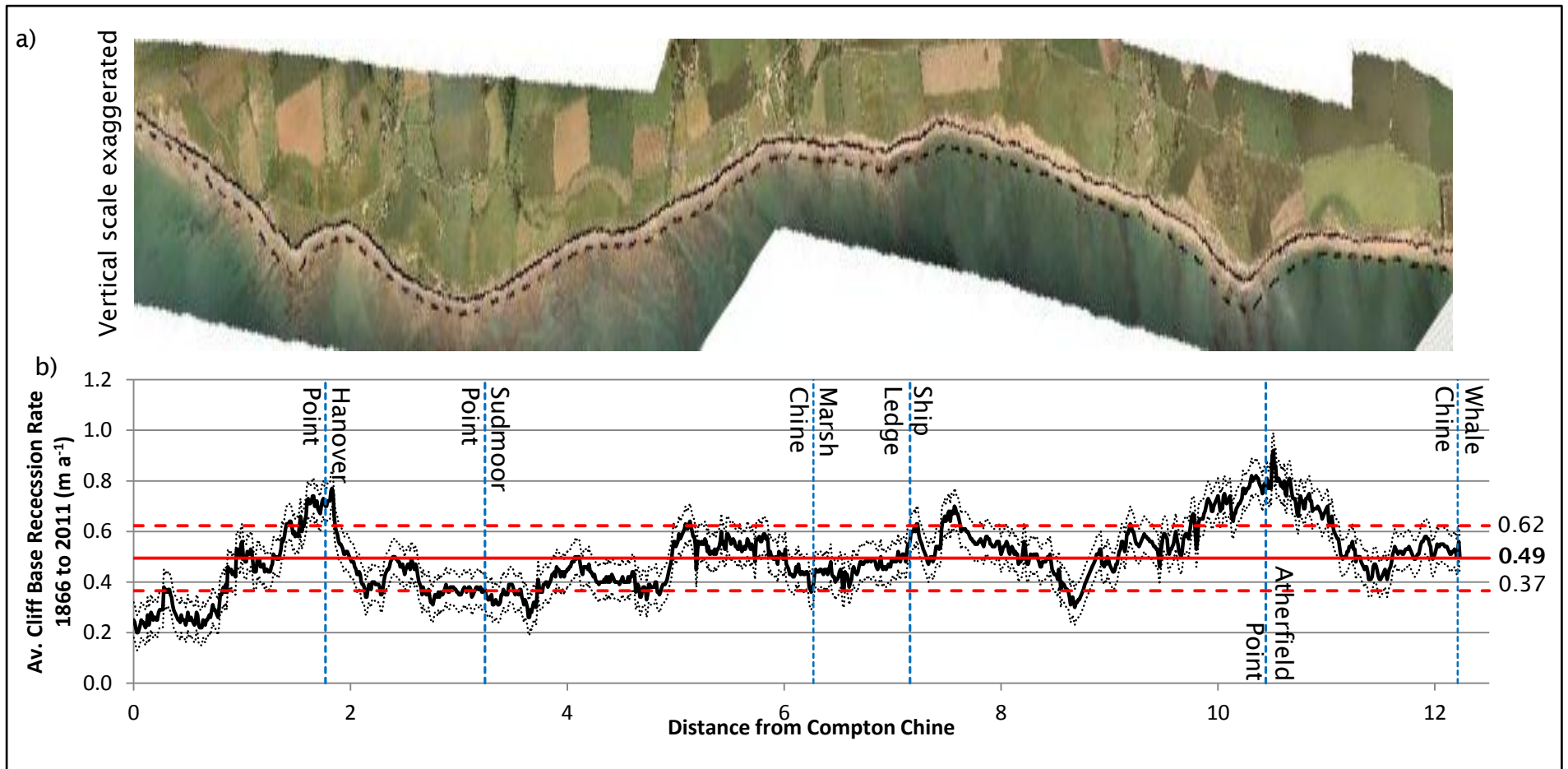
Figure 7.6: a) Aerial photograph with 1866 (dashed) and 2011 (solid) cliff base line imposed and **b)** Average annual recession rate for the cliff base (1866-2011). The dotted black lines mark the error in average annual recession rate calculated using Equation 4.1. The solid red line indicates the average recession rate for the whole study area, while the dashed red lines represent one standard deviation around the mean.

Compton Bay provides a striking example of how cliff top recession rates can be misleading. In 1866 the large complex landslide to the north of Compton Bay was much smaller than it is today, only the rotational failure of the Ferruginous Sands had occurred. Since then the eastern end of the landslide has developed causing the cliff top to retreat at a rapid rate (Figure 7.7). The reason for this change in cliff behaviour is unclear; there may have been a change in the lithology as the cliff retreated or it may be part of a natural cyclical landslide complex. Where landslides are large but infrequent with subsequent landslides occurring once the debris from the previous on is cleared reducing the cliffs stability. The development of this landslide explains the peak in recession rate. Further downdrift (0.88 km from Compton Chine) unique to this location in the coastline, the cliff top recession rate drops to zero while the cliff base recession rate remains at around 0.5 m a^{-1} (Figure 7.8). The cliff top line in 1866 represents the back scarp of a large landslide.
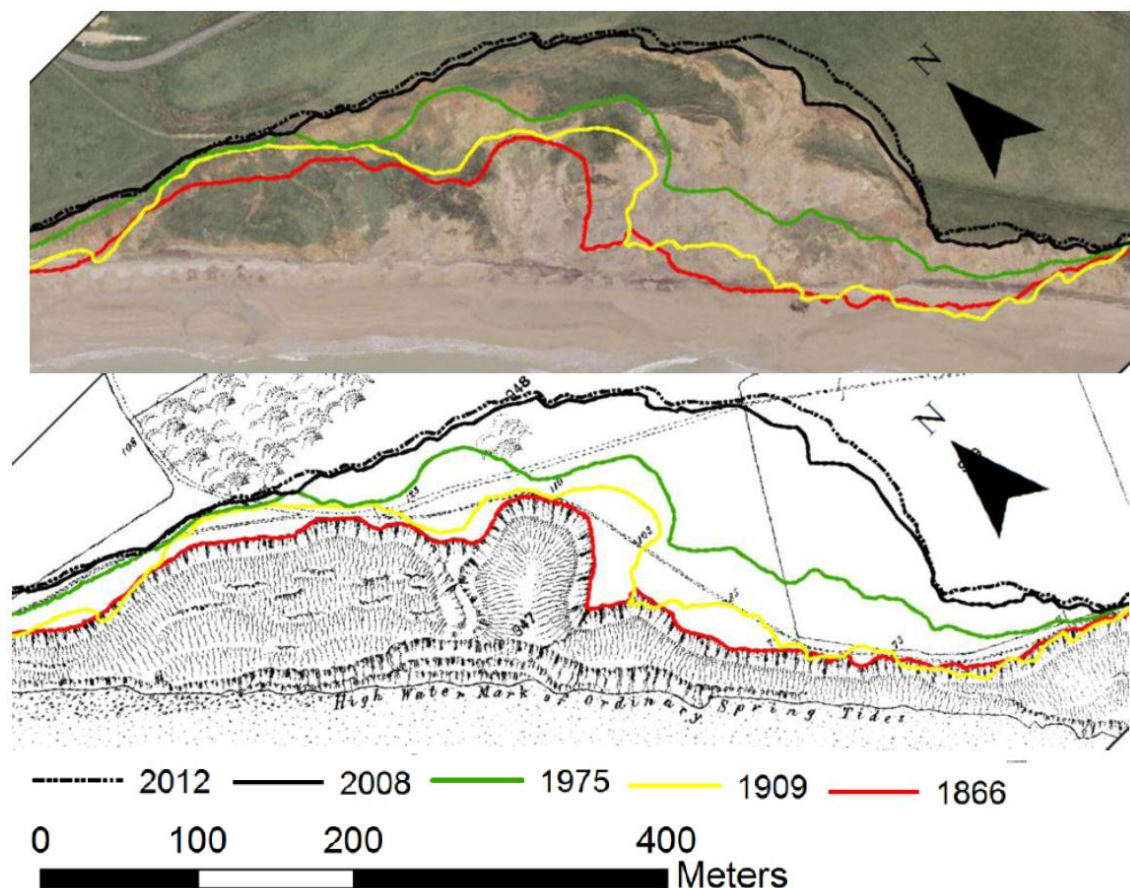
Figure 7.7: Development of the large scale landslide to the north of Compton Bay, location indicated on Figure 7.5
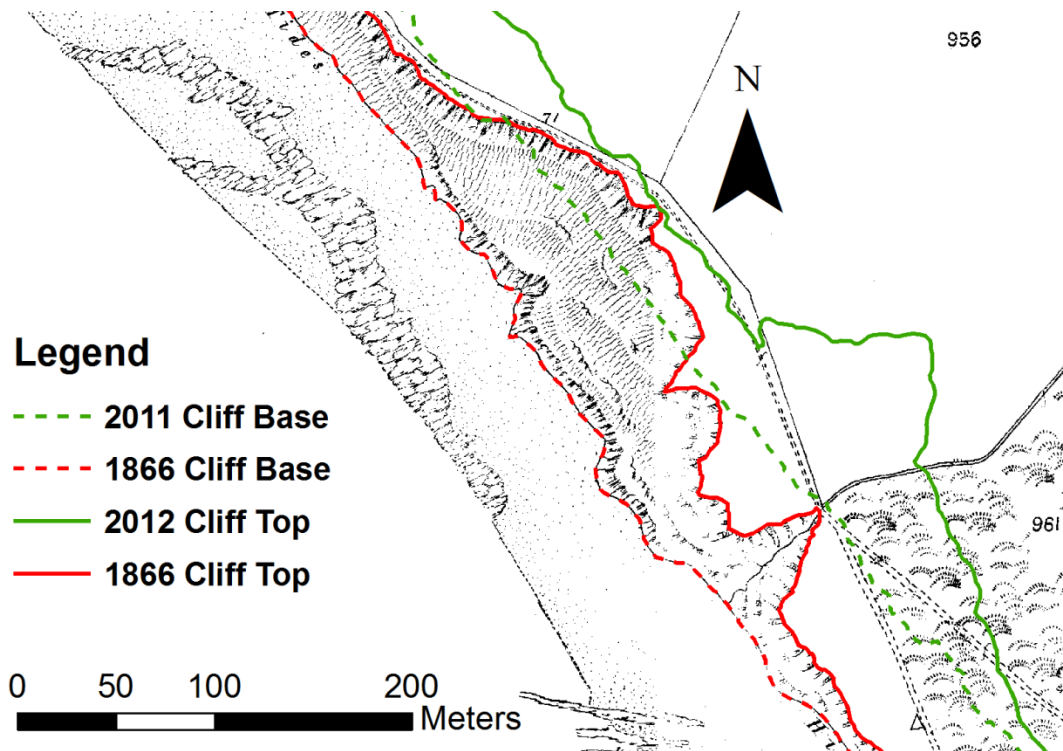
Figure 7.8: The disappearing landslide in Compton Bay, location marked on Figure 7.5

In the intervening years that landslide has been eroded creating a much steeper cliff and leaving the cliff top in the same position. It is thought that here the recession has progressed north of what was probably a slip prone horizon (perhaps of flexural slip origin) as suggested by Redshaw et al. (In Review). Equally the true location of the cliff base line can be obscured by talus and high beach volumes. Therefore care must be taken when analysing recession rates from cliff top and cliff base, to take the cliff geomorphology into account (Figure 4.2 & 4.3).

Table 7.1 shows the changes in average annual recession rate for the whole coastline over the study period. There is a steady increase in the cliff top recession rates over time. However the cliff base recession rates show a more rapid increase in the first three time steps, 1866 to 1975, dropping back down to a lower rate in the most recent period, 1975 to 2011. This most recent rate is higher than the rates at the initial period therefore it can be concluded the recession rates of both cliff top and cliff base have shown an overall increase over the study period. This could be related to rising sea levels over the study period, which is supported by the reduction in intertidal platform width over the study period. Rates of relative sea level rise for the south coast of England over the last 100 years is between 1.21mm a^{-1} to 1.81mm a^{-1} (Haigh et al., 2011).

Table 7.1: Average annual cliff top and cliff base recession rates for the whole coastline over a number of surveying periods.

Survey period	Average Annual Cliff Base Recession Rate (ma⁻¹)	Average Annual Cliff Top Recession Rate (ma⁻¹)
1866 – 1909	0.27	0.34
1909 – 1946	0.55	0.46
1946 – 1975	0.87	0.59
1975- 2011/12	0.49	0.69
1866 – 2011/12	0.49	0.50

The long-term average annual recession rates of the cliff top, ignoring the extreme values around the Compton Farm Landslide, show above average erosion at Hanover Point, north of Marsh Chine, southeast of Ship Ledge and at Atherfield Point, with below average rates across Sudmoor Point and southeast of Marsh Chine. A clearer pattern is seen in the cliff base recession rates. Due to the lower variability seen in the cliff base recession rates when compared to that of the cliff top the cliff base will be used when attempting to determine the influence of the various controls on recession rates presented in Section 7.3 (Figure 7.5 and Figure 7.6). The areas experiencing higher than average rates of erosion between 1866 and 2011 include the north side of Hanover Point, across Atherfield Point and south of Ship Ledge. The main area displaying lower than average recession is across the front of Sudmoor Point. These results indicate that Hanover and Atherfield Points are headlands in decline and that Sudmoor Point is becoming more defined. The role of Ship Ledge is unclear; the recession rates at Ship Ledge are close to the average while the rates just down drift are above average. Closer inspection of the recession rates around the headlands is provided in Section 7.4.

7.3   Controls on Recession Rates

This section considers the relationships between the factors outlined in Chapter 2 as controls on recession rates, and the measured recession rates presented in Figure 7.5b. The cliff base is used due to its lower standard deviation resulting from the lower variability caused by landsliding events seen in the cliff top recession rates. These factors include geology, cliff coherence, wave energy reaching the shoreline, beach width, BWA and shore platform width. It is worth noting that the variations in recession rates from the 1866 OS map to the 2011 survey only represent a relatively short time period in terms of headland formation

and evolution in the geological (millennia) timescale, although it will be of relevance to an engineering (century) time scale.

7.3.1 Geology vs. Recession rates

The aspects of geology that can influence recession rates along a coastline include geology, geomorphology and strength or coherence (as defined by Soares (1993) and described in Section 3.2.2). The influence of longshore changes in these factors on recession rates were considered using the result of the average annual cliff base recession presented in Figure 7.6. Measurements of cliff base recession were made every 10m along the coastline; these results have been divided according to cliff base geology, morphology and coherence.

The average recession rates related to cliff base geology are shown in Figure 7.9. There does appear to be some variation in recession rates with geology. Rates are higher in the Atherfield Clay and Vectis Formations, i.e. 0.11 m a^{-1} greater than the average for the whole coastline, this is greater than the estimated error of 0.08m a^{-1} for the study period (Table 3.8). The mean values for all formations fall within one standard deviation of the whole coast average. The rates of erosion for the Ferruginous Sands and Wessex Formations are much closer to the whole coast average. This may simply be a result of their extensive exposure along the coast, covering 57% of the cliff face by area.

These variations between lithologies have been shown to be statistically significant to the 95% confidence level, with all combinations returning t-values greater than the critical except for the comparison of the Atherfield Clay and Vectis Formations (Appendix 3). The greater rates of recession seen in the Vectis and Atherfield Clay Formations could be related to their tendency to fail in low frequency, large scale events, forming large, complex landslides. In comparison the Wessex and Ferruginous Sand Formations fail in high frequency, low magnitude events (Insole et al., 1998). The relatively long time scale, over which the recession rates were calculated, i.e. 145 years (1866-2011), should reduce the effects of variations in scales of failure. Although statistically significant these variations are small and consideration of the other factors such as beaches and wave refraction must be considered before any firm conclusions on the role geology plays can be made.
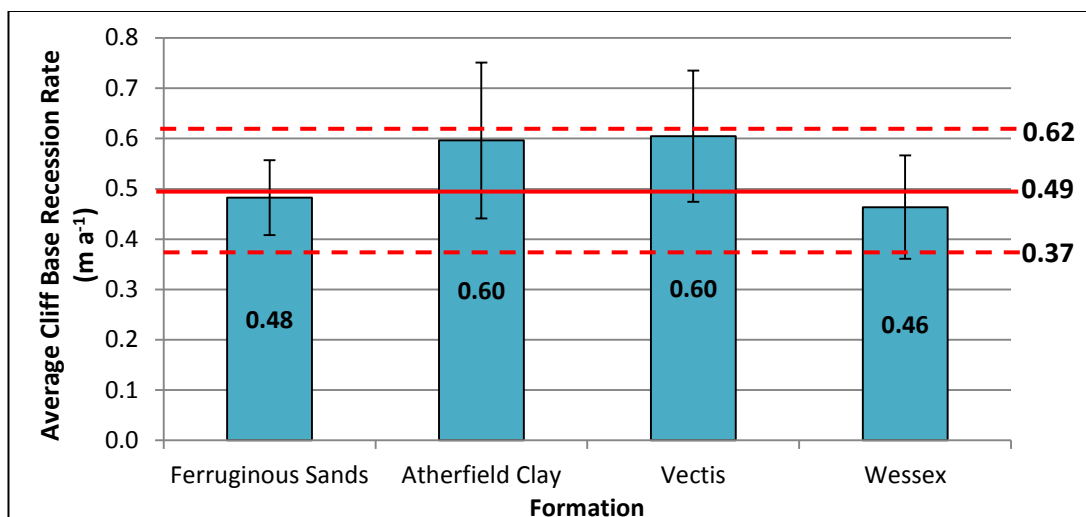
Figure 7.9: Average cliff base recession rates for each geological formation from 1866 to 2011. The error bars represent one standard deviation. The solid red line indicates the average recession rate for the whole study area, while the dashed red lines represent one standard deviation around the mean.

Interestingly the higher rates of recession observed in the Vectis and Atherfield Clay Formations only applies southeast of Hanover Point (Figure 7.10). North of Hanover Point the average cliff base recession rates for all but the Wessex Formation are much lower than the whole coast average. These variations between the north and southeast for the Ferruginous Sands, Atherfield Clay and Vectis Formations have been found to be statistically significant to the 95% confidence level (Appendix 4). The reason for this drop in recession rate is not clear. It may be due to the steeper dip of the beds in Compton Bay increasing cliff stability of the Vectis, Atherfield Clay and Ferruginous Sand Formations (Figure 4.3); the strongly drift aligned nature of Compton Bay; or the Compton Farm Landslide providing talus to protect the cliff base (Figure 7.11). Alternatively these variations could be controlled by the amount of wave energy reaching the cliff base, as the beach slope across Compton Bay is shallow, due to the wide sandy beach, where these beds outcrop, further south the absence of the Wessex Mudstone platforms leads to a steeper shoreface gradient.
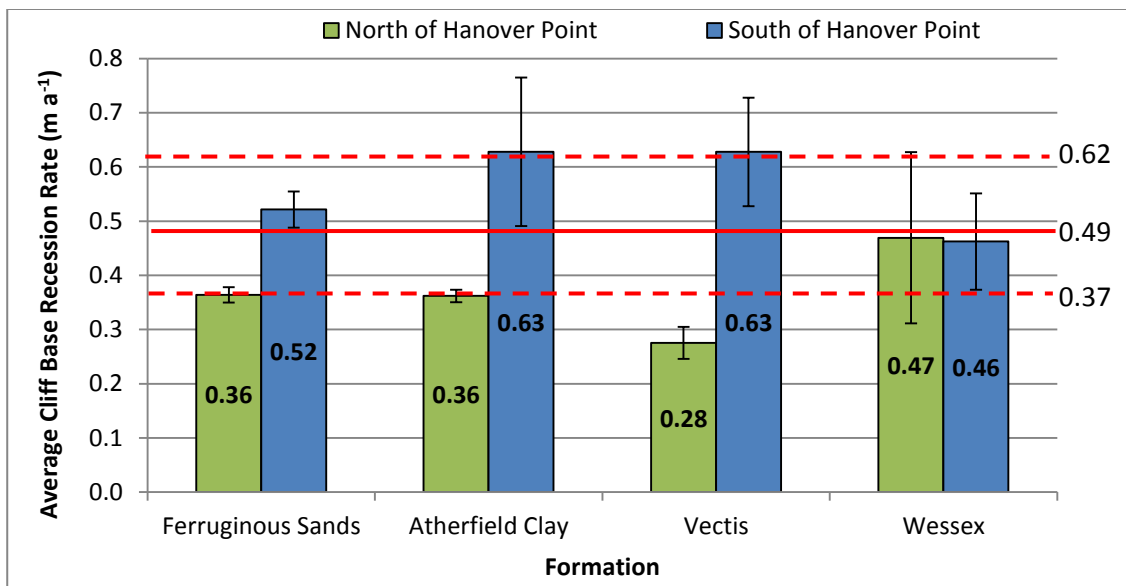
Figure 7.10: Average cliff base recession rates for each geological formation north and southeast of Hanover Point from 1866 to 2011. The error bars represent one standard deviation. The solid red line indicates the average recession rate for the whole study area, while the dashed red lines represent one standard deviation around the mean.
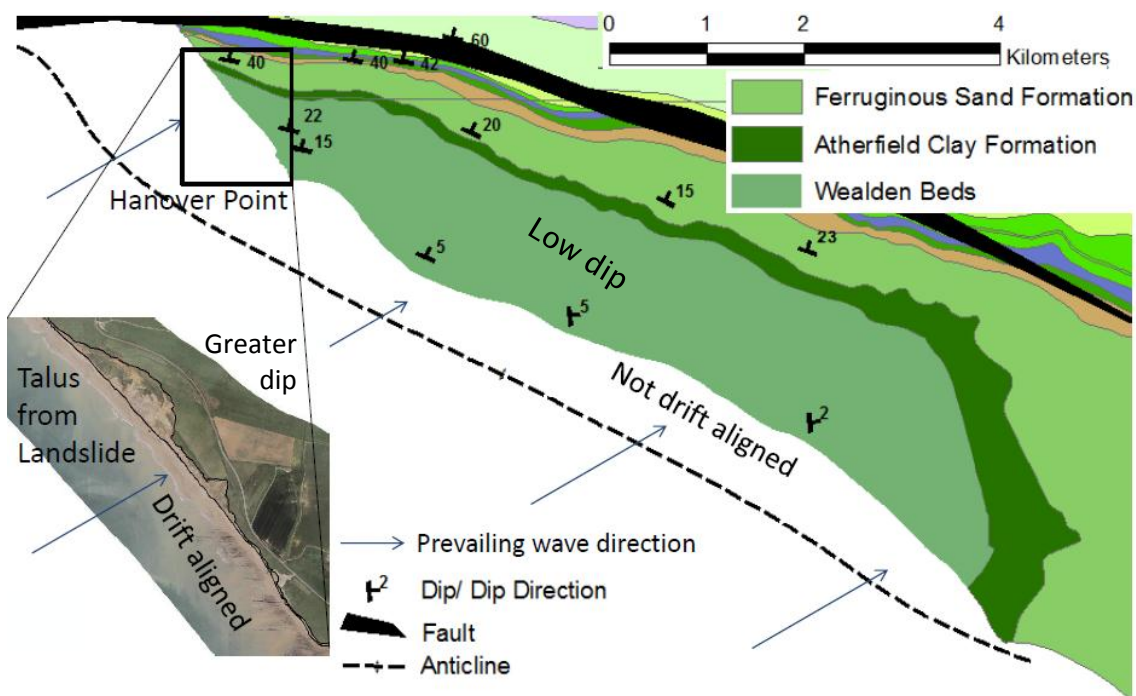
Figure 7.11: Potential explanations for the lower rates of recession north of Hanover Point.

The average cliff base recession rates for each Cliff Behaviour Unit (CBU; Figure 4.2) is shown in Figure 7.12. The highest recession rates are seen where mudslides dominate the cliff. Mudslides are most commonly seen in the Vectis Shales, this is reflected in the higher recession rates measured for the Vectis

Formation (Figure 7.9) particularly those measured southeast of Hanover Point
(Figure 7.10).

The lowest recession rates were found to relate to the large scale landslide with
unknown structure found in Compton Bay. This is consistent with the lower
recession rates reported in Compton Bay for the Vectis, Atherfield Clay and
Ferruginous Sand Formations (Figure 7.10) which make up this landslide. Again
the reason for this relative drop in recession rates is unclear, but is considered to
be related to input of talus from the landslide maintaining the cliff base position.
Incidentally the average cliff top rate of recession across this landslide is greater
than the whole coast average at 0.58 m a^{-1} ± 0.37 m a^{-1}, due to the low slope and
large scale of the landslide and the rapid and variable recession of the back scarp.
The average recession rates of the remaining CBU's fall close to that of the
coastline as a whole. The steep cliffs with high level landsliding found either side of
Sudmoor Point, where the sandstone of the same name dominates the coastline,
display slightly lower than average recession rates.
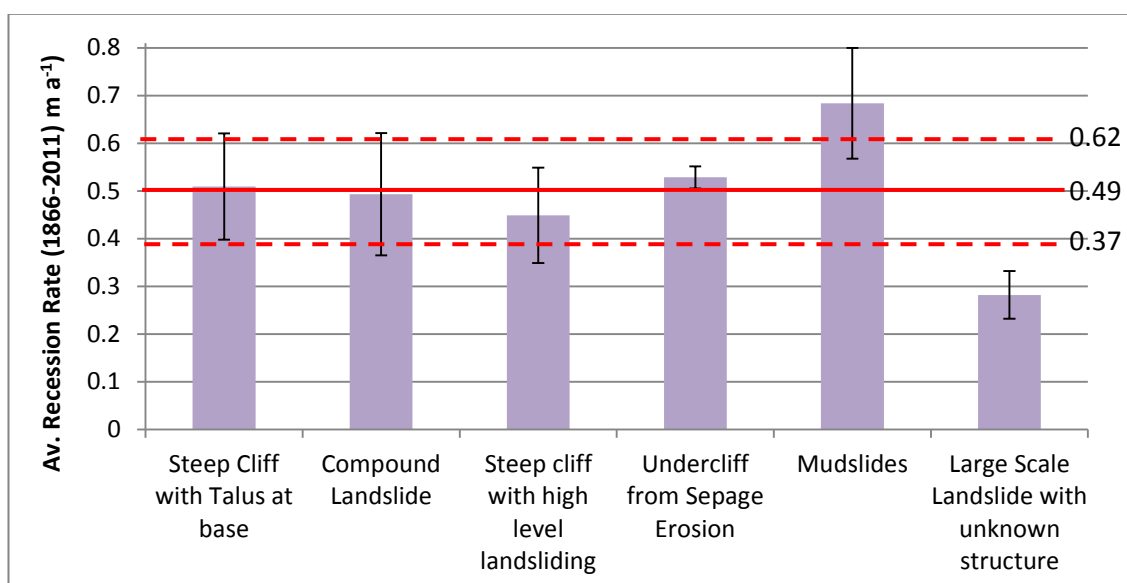
Figure 7.12: Average cliff base recession rates for each Cliff Behaviour Unit (CBU) from
1866 to 2011. The error bars represent one standard deviation. The solid red line indicates
the average recession rate for the whole study area, while the dashed red lines represent
one standard deviation around the mean.

The variations in average recession rates displayed in Figure 7.12 related to cliff
morphology are all statistically significant to the 95% confidence level except for
the difference between CBUa and CBUb. i.e. steep cliff with talus at base and

compound landslides (Appendix 5). However, it is important to consider that the geomorphology of the cliffs is not necessarily consistent over time.

It may be expected that variations in cliff base coherence, used as a measure of cliff strength, would display a negative correlation with recession rates. i.e. decreasing recession rates with increasing coherence. This relationship is not found (Figure 7.13), instead the recession rates are lowest (0.38 m a^{-1}) where coherence is at its lowest (C4), increasing to 0.62 m a^{-1} with a small increase in coherence (C3). These variations can be explained by the location of these measurements (Figure 4.20). The majority of C4 cliff base measurements were made in Compton Bay around the large scale landslide where cliff base recession rates are influenced by the input of talus from the aforementioned landslide. While the C3 measurements came from the area of fallen intact blocks of Atherfield Clay close to Atherfield Point, which as discussed in Section 7.1 is a headland in decline.
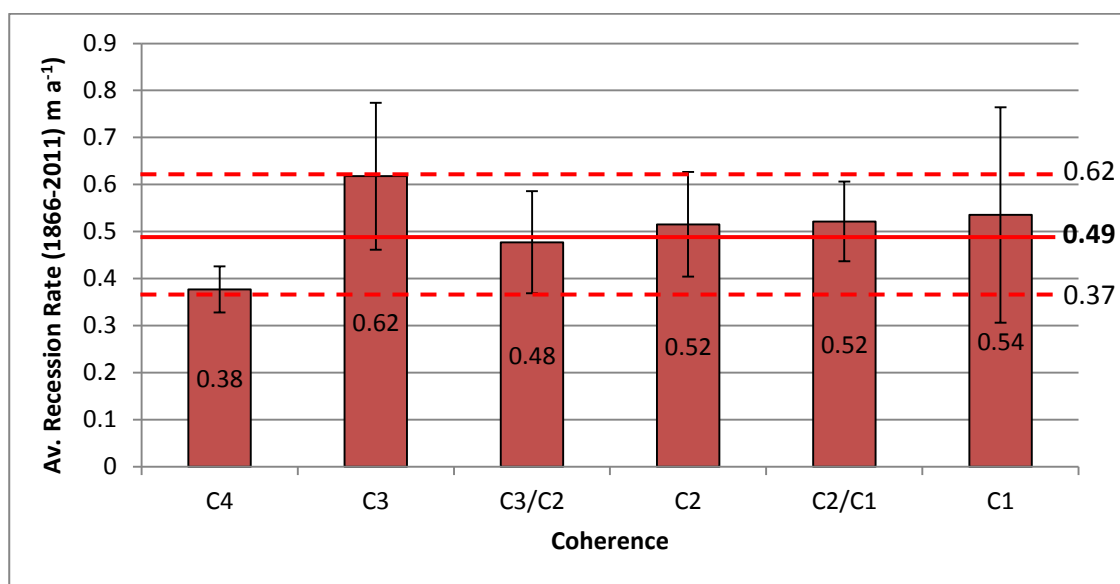
Figure 7.13: Average cliff base recession rates for cliff base coherence from 1866 to 2011. The error bars represent one standard deviation. The solid red line indicates the average recession rate for the whole study area, while the dashed red lines represent one standard deviation around the mean.

For coherence levels of C3/C2 or above, equivalent to a compressive strength of approximately 10MPa according to Soares (1993), the average recession rates remain close to the whole coast average and show little variation. T tests were carried out on the variations in recession rates shown in Figure 7.13. The only statistically significant variations exist between the C4 (non-coherent) cliffs and all other levels of cliff coherence except C1 (coherent). All other relationships are

insignificant to the 95% confidence level (Appendix 6). The coherence measured is that of the intact material whereas in practice the cliff stability and hence recession rates depends on the mass properties of the beds, and any landslide structures. This would explain the lack of correlation with recession rate seen in this study.

7.3.2   Wave Energy vs. Recession Rate

To determine if an observable relationship exists between wave energy reaching the shoreline (as described in Chapter 5) and long-term cliff recession rates, a simple regression analysis was carried out for the wave energy density of each wave condition. The results are summarised on Table 7.2. Despite there being clear concentration of wave energy towards Hanover and Atherfield Points, the headlands in decline under all common wave conditions (Figure 5.3b), no correlation was found between wave energy density and recession rates. This is due to the concentration of wave energy towards Sudmoor Point and Hardman Rock which do not show signs of higher than average recession rates (Figure 7.5). This indicates that the influence of wave energy is secondary to that of the geology.

Table 7.2: Statistical results of linear regression analysis comparing cliff base recession rates with wave energy density at the shore line.

Wave Type	Wave Direction	Wave Height	Wave Period	Water Level	Slope (Y =)	Critical R^2 95%	R^2
Common waves 35:1 year	225°	1 m	5.5 sec	+1.11 m	$5 * 10^{-6} x$	0.073	0.0056
	240°	1 m	5.5 sec	+1.11 m	$7 * 10^{-6} x$	0.073	0.0094
	255°	1 m	5.5 sec	+1.11 m	$5 * 10^{-6} x$	0.073	0.0052
5:1 year storm wave	240°	3.5 m	6.5 sec	+1.46 m	$4 * 10^{-6} x$	0.073	0.045
1:50 year storm wave	240°	6.02 m	8.1 sec	+2.30 m	$4 * 10^{-6} x$	0.073	0.0591

In the case of the 5:1 year and 1:50 year storm waves the major concentration of wave energy was found in Chale Bay south of Atherfield Point (Figure 5.4b). Again no increase in recession rate is obvious in that area and no relationship between wave energy density and recession rates were found for either of the storm wave conditions. Thus there is no correlation between wave energy density and recession

rates for any of the wave conditions. Demonstrated by the low R^2 values, none of which exceeded 0.073, which is the critical R^2 value at the 95% confidence level (Table 7.2).

7.3.3   Beach Dimensions vs. Recession Rate

Two measures of beach size were used within this study, beach width and Beach Wedge Area (BWA). Beach width was taken from a series of OS Maps (1866, 1909 and 1975) and aerial photographs (2008), since little systematic variation in beach width over the study period was observed the widths were averaged to give a long-term measure of beach width. While BWA was calculated from the 2004 to 2009 LiDAR data providing only a snapshot of BWA (Methods: Section 3.4.4; Results: Section 6.1.3, Figure 6.8a and 6.6a respectively).
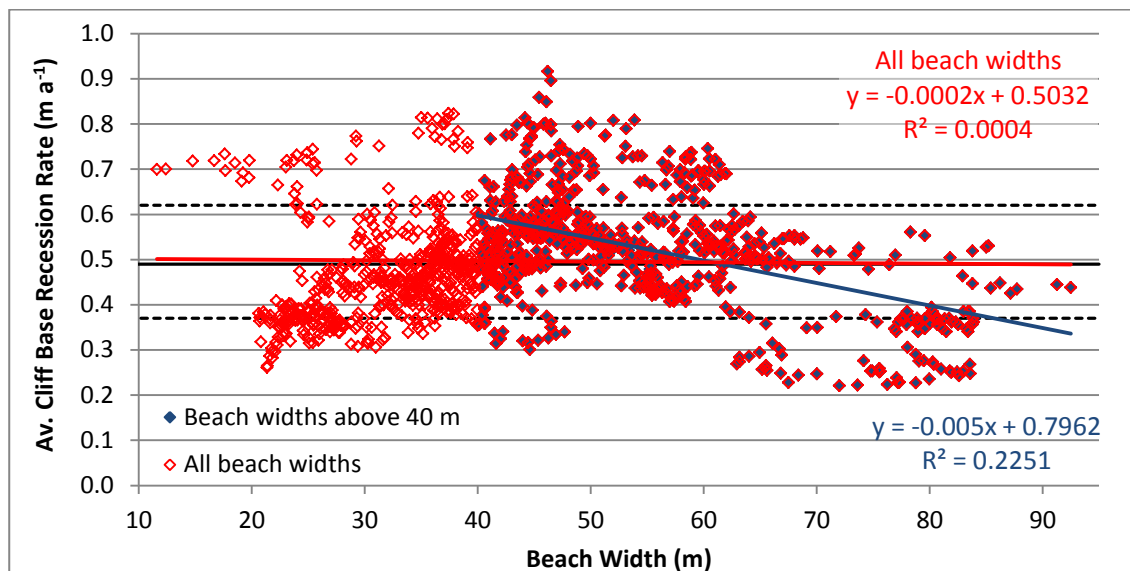
Figure 7.14: Beach width vs. average annual cliff base recession rates (1866-2011) for all beach width (red) and beach widths above 40 m (blue). Trend line for all beach widths is shown in red; the trend line for beach widths above 40 m is shown in blue. The solid black line indicates the average recession rate for the whole study area, while the dashed black lines represent one standard deviation around the mean.

Simple linear regression analysis was used to determine if there was any relationship between beach width/ BWA and recession rates. No correlation was found between beach width and long-term recession rates, the slope of trend line was close to horizontal (y = -0.0002x; Figure 7.14). However when considering the beach widths above 40 m a stronger correlation with recession rate is observed as denoted by the blue trend line on Figure 7.14. This indicates that the threshold of

effective beach width is around 40m. The R² value shows that 23% of the variability in recession rates is controlled by beach width, when beach width exceeds 40 m. However many of the measurements of beach width over 40 m were made in Compton Bay, and described in Section 7.3.1 the talus input from the Compton Farm Landslide is thought to be the dominant control on the reduced rates of cliff base recession in that area.

The relationship between BWA and recession rate is shown in Figure 7.15. As a large BWA is thought to offer greater protection to a cliff, it follows that the relationship between BWA and recession rates should be a negative correlation, i.e. recession rates should fall as BWA increases.
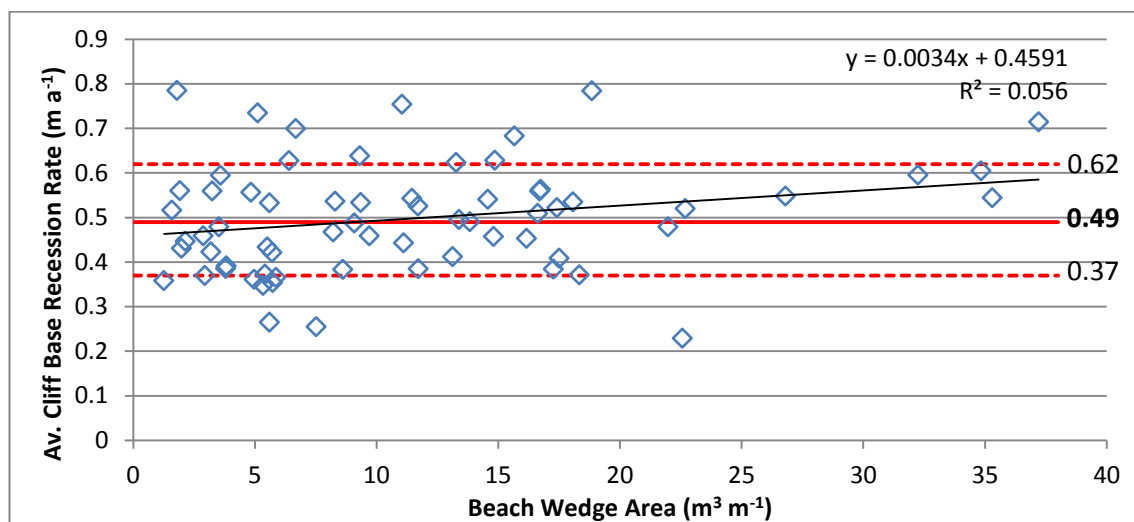
Figure 7.15: Beach Wedge Area (BWA) vs. average annual cliff base recession rates (1866-2011). Simple linear regression indicates a positive correlation with an R² value of 0.056. The solid red line indicates the average recession rate for the whole study area, while the dashed red lines represent one standard deviation around the mean.

The results in Figure 7.15 show the opposite, there appears to be a positive correlation between BWA and recession rates. This discrepancy in the data may be a result of the timescale of the BWA measurements. The recession rates are an average for the last 145 years while the BWA is an average value measured over 5 years between 2004 and 2009, providing only a snapshot of beach conditions. However, the R² values did not exceed 0.06 in either case, suggesting that no relationship exists between beach width, or BWA, and recession rates. However when beach widths below 40m are omitted a negative relationship with recession rate does emerge, explaining 23% of the variation in recession rates. This supports

the argument made in Chapter 6, that on the whole the beach dimensions are insufficient to significantly influence recession rates.

7.3.4   Shore Platform dimensions vs. Recession Rates

Although it is clear that the shore platforms play an important role in the formation and evolution of the subtle headlands on the southwest coast this is not strongly reflected in the results of the linear regression analysis displayed in Figure 7.16.
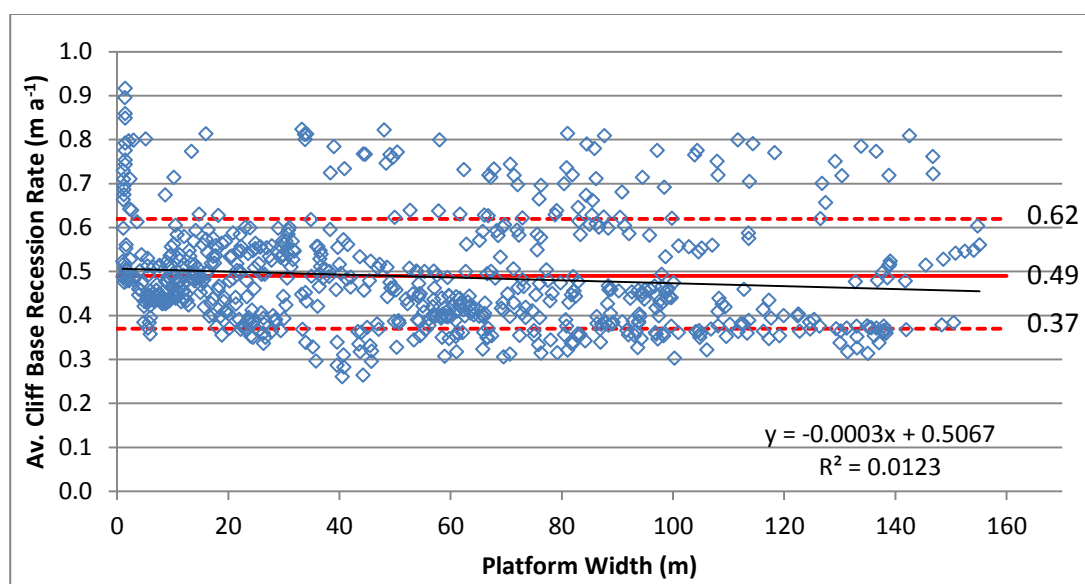
Figure 7.16: Platform width vs. average annual cliff base recession rates (1866-2011). Only measurements from transects that intersected platforms were used in this analysis. Linear regression indicates a slight negative correlation with an R^2 value of 0.0123. The solid red line indicates the average recession rate for the whole study area, while the dashed red lines represent one standard deviation around the mean.

The extent of the exposed shore platform from beach to mean low water, was taken from the 1909 and 1975 OS maps (Methods: Section 3.4.5; Results: Section 6.1.3, Figure 6.8a). There is a slight negative correlation between shore platform width (as shown in Figure 6.8b) and cliff base recession between 1866 and 2011. However the R^2 value of 0.0123 indicated this relationship is not statistically significant. Indeed when comparing average recession rates of the coastline with and without platform the variation is very small. The average cliff base recession rates being 0.49 and 0.51 ma^{-1} for those areas with and without intertidal platforms respectively.

7.3.5   Cliff Height vs. Recession Rates

The final factor considered is cliff height. Typically high cliffs fail through large scale, low frequency landslide events, while lower cliffs recede through high frequency low magnitude events (Hapke et al., 2009). This is because cliff height controls the loading caused by the weight of the overlying strata, higher cliffs have a greater inherent instability (Wolters and Muller, 2008). Therefore we could expect that recession rates will increase with cliff height. The cliffs within the study area are relatively low not exceeding 55m. Correlation with cliff base recession rates shows a weak negative relationship, with recession rates falling as cliff height increases. The correlation has a R^2 value of 0.0224 and is not statistically significant (Figure 7.17).
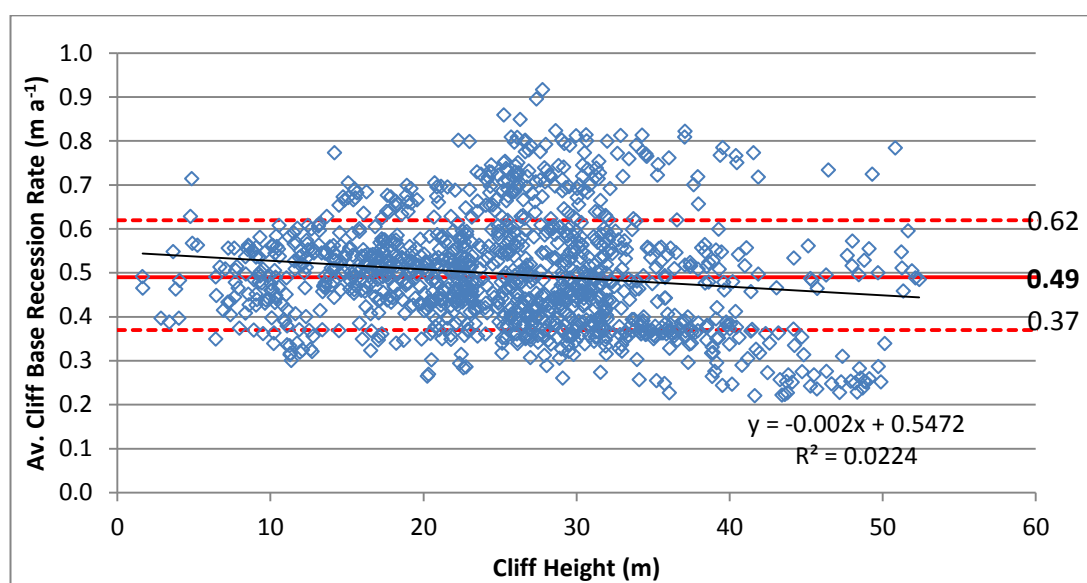
Figure 7.17: Cliff height vs. average annual cliff base recession rates (1866-2011). Simple linear regression indicates a positive correlation with an R^2 value of 0.056. The solid red line indicates the average recession rate for the whole study area, while the dashed red lines represent one standard deviation around the mean.

7.3.6   Multivariate Statistical Analysis

The objective of this study was in part to determine the dominant control on cliff recession rates and by proxy coastline evolution. The three possible controls considered were, geological and geotechnical, beach and platform morphology and wave energy concentration. Since few significant relationships could be drawn from correlation of the various parameters studied and recession rates a Principal

Component Analysis (PCA) was carried out in an attempt to draw out any complex relationships or correlations within the data. The analysis included all the numeric data available plus the morphology, geology and coherence class data as binary inputs (Table 3.17), this made up 30 inputs. The analysis produced 30 principle components that together explain all the variance in the data. The percentage of the variance described by each of the components is shown in Figure 7.18. The first two Principal Components (PC), explained only around 30% of the variance in the data, 20.1% by PC1 and 10.4% by PC2, which is a poor result. The percentage of variance explained by the remaining components continues to decrease.
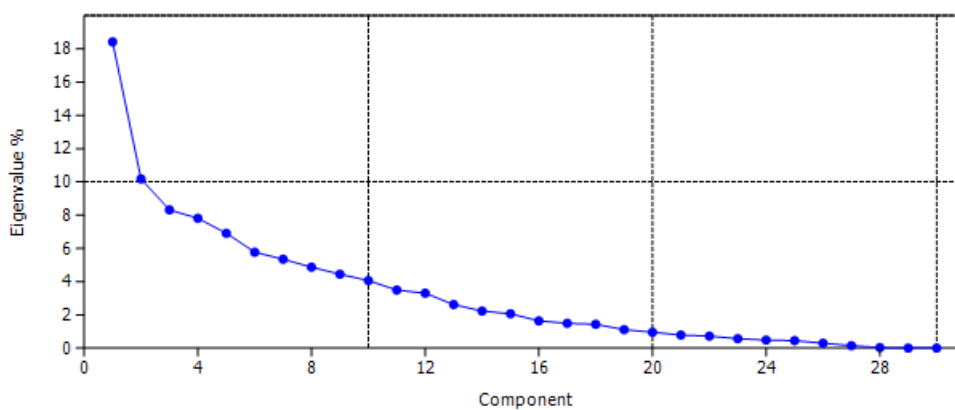
Figure 7.18: Percentage variance, represented by the eigenvalue, for each of the components produced by the PCA.

This demonstrates the complexity of the controls on recession rates within the study area indicating that no one factor has dominance. This complexity is highlighted by comparison with other recession studies. A study by Amin and Davidson-Arnott (1997) in Lake Ontario found that only four variables were able to explain 72% of the variance in recession rates. The high correlation in that study was thought to be due to the uniform geotechnical properties of the cliffs. The complexity of the geology on this coastline may be responsible for the lack of correlation seen in the data.

The loading plots for PC1 and PC2 is shown in Figure 7.19. They give an indication of the main gradients in the data. PC1 is primarily driven by BWA, beach slope and storm waves (positively correlated) and platform width, Wessex Mudstone and grain size parameters (LCD & D50) (negatively correlated. While PC2 is driven by Ferruginous Sands and CBUd, undercliff from seepage erosion (positively

correlated) and CBUa, steep cliff with talus at the base (negatively correlated).
These results show that PC1 is dominated by beach and platform parameters while
PC2 is controlled by lithology and cliff morphology.
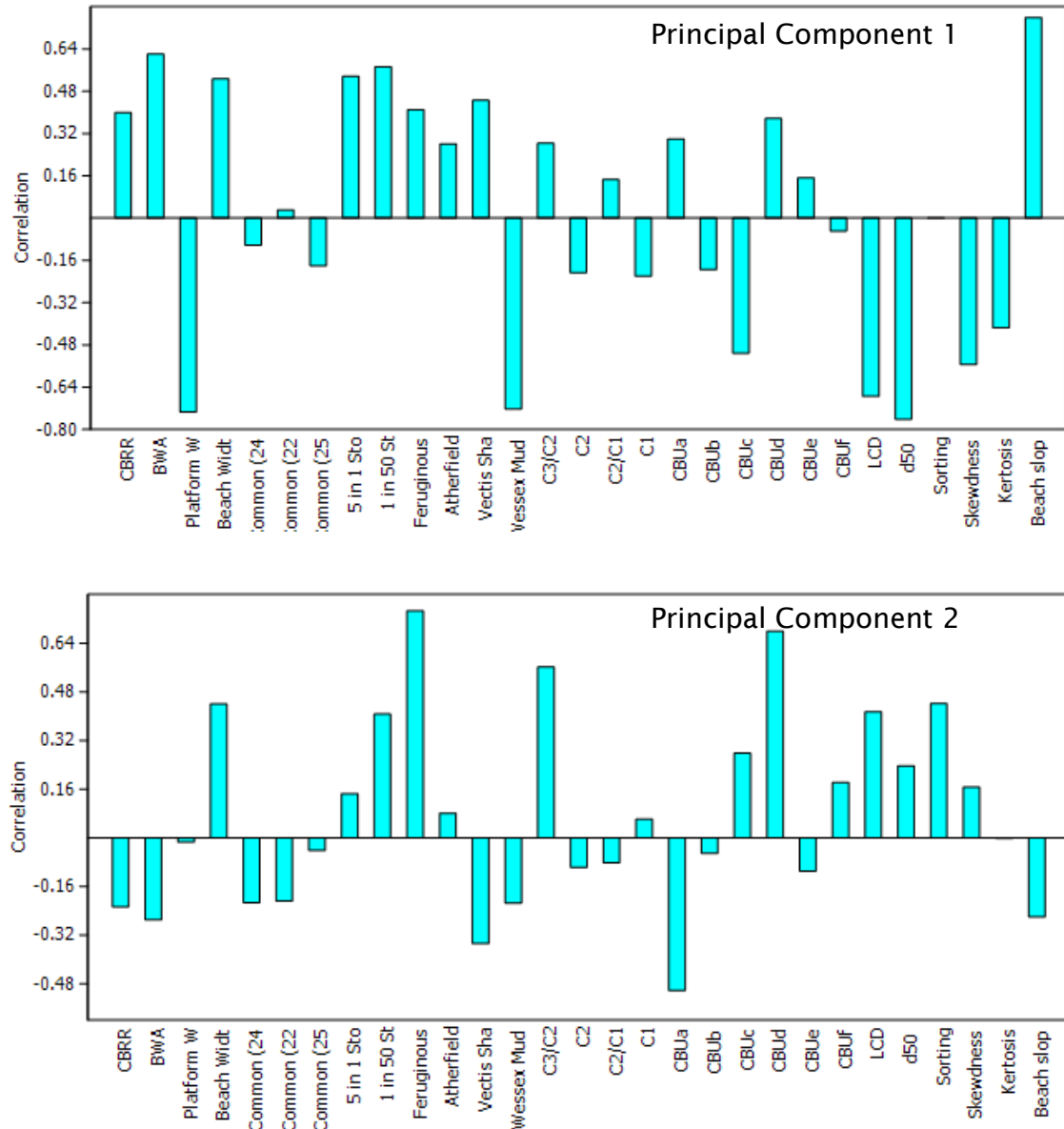
Figure 7.19: Loading plots for Principal Components 1 and 2, showing the main gradients in the data.

These results indicate that the variance in the data comes from a combination of beach and platform parameter, storm waves, lithology and cliff morphology. But no single factor is dominant.

Figure 7.20: Results of the Principle Component Analysis showing the correlation in the data for PC1 and PC2

In terms of what is controlling recession rates the location of the data in Figure 7.20 in relation to CBRR (Cliff Base Recession Rates) must be considered. The Vectis Formations and their associated mudslides (CBUe) along with an intermediate coherence (C2), beach slope and BWA are related to an increase in recession rates. Conversely CBUc (steep cliffs with high level sliding), the grain size parameters and coherent cliffs (C1) are associated with reduced recession rates. The beach width and cliff height vectors lie at right angles to CBRR, indicating that they have no relationship to recession rates. This analysis confirms the individual regression analysis results, showing that no one factor has a dominant control on recession rates.

7.4   Variations of Recession Rates around the Headlands

To gain a simplified view of the pattern of recession rate around the headlands the results from the transects cast at 5 m intervals were averaged at the headlands and up drift and down drift in 300m long sections. In the case of Atherfield Point and Ship Ledge the width of the headland was defined by the longshore width of the intertidal platforms fronting them at 300m and 200m respectively. For Hanover Point and Sudmoor Point where the intertidal platform extends beyond the headland itself, the transects that crossed the apex of the headland where chosen, extending 200m across Hanover Point and 300m across Sudmoor Point. The greater distance across Sudmoor Point reflects the broader, rounded nature of the headland. The results of the cliff top and cliff base recession rates in the sections defined above are shown in Figure 7.21 to Figure 7.24. The cliff top recession rates have been included in this section as the headlands are an important part of the study and as such must be considered in detail.

Around Hanover Point the cliffs are low and steep; the pattern of recession is broadly similar for the cliff top and base with recession rates at and 0-300m updrift of the headlands greater than the average for the whole coast, with the rates at Hanover Point being slightly greater. The stretch of the coast northwest of Hanover Point is at right angles to the prevailing direction of wave approach, the shore platform to the west of Hanover Point is narrower in the cross-shore direction and does not extend as far alongshore on the west as it does on the east (Figure 5.2), leaving this section more exposed to wave attack. The lower recession rates east of Hanover Point, in Brook Bay, coincides with low incidence of wave energy

concentration (Chapter 5). The variations in cliff top recession rates around Hanover Point are all statistically significant to the 95% confidence level. The same is true for the variations in cliff base recession rates except when comparing the area 600-300m updrift and the area 0-300m down drift of the headland apex (Appendix 7).
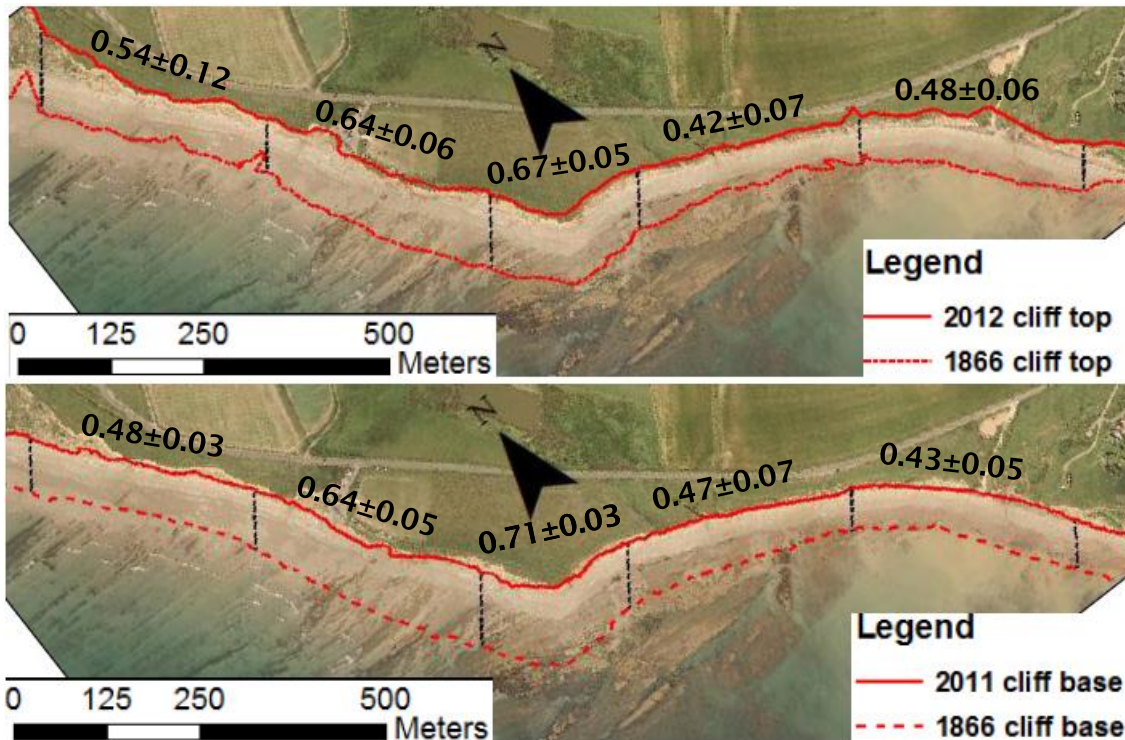
Figure 7.21: Patterns of cliff top and cliff base recession around Hanover Point, values are average recession rates for each section in m/a ± the standard deviation also in m/a

Sudmoor Point is a wide rounded headland, and the "point" or apex of the headland is not as clearly defined as that of Hanover Point. The whole of Sudmoor Point is eroding at a rate below average for the coastline (Figure 7.22). The higher rates of cliff top recession seen between 0 and 300 m updrift are related to the Roughlands compound landslide complex. Large block failures occur at the centre of Roughlands where the basal shear surface descends from near the cliff top to beach level (Stuiver, 2010). Despite focussing of wave energy occurring across Sudmoor Point (Figure 5.3), it appears that the protection from the extensive shore platforms and support provided by the Sudmoor Point Sandstone (Figure 4.3) has caused Sudmoor Point to grow over the study period. Comparing the recession rates for each of the sections using a series of z tests showed that the variations in

both the cliff top and cliff base are all statistically significant to the 95% confidence level (Appendix 8).
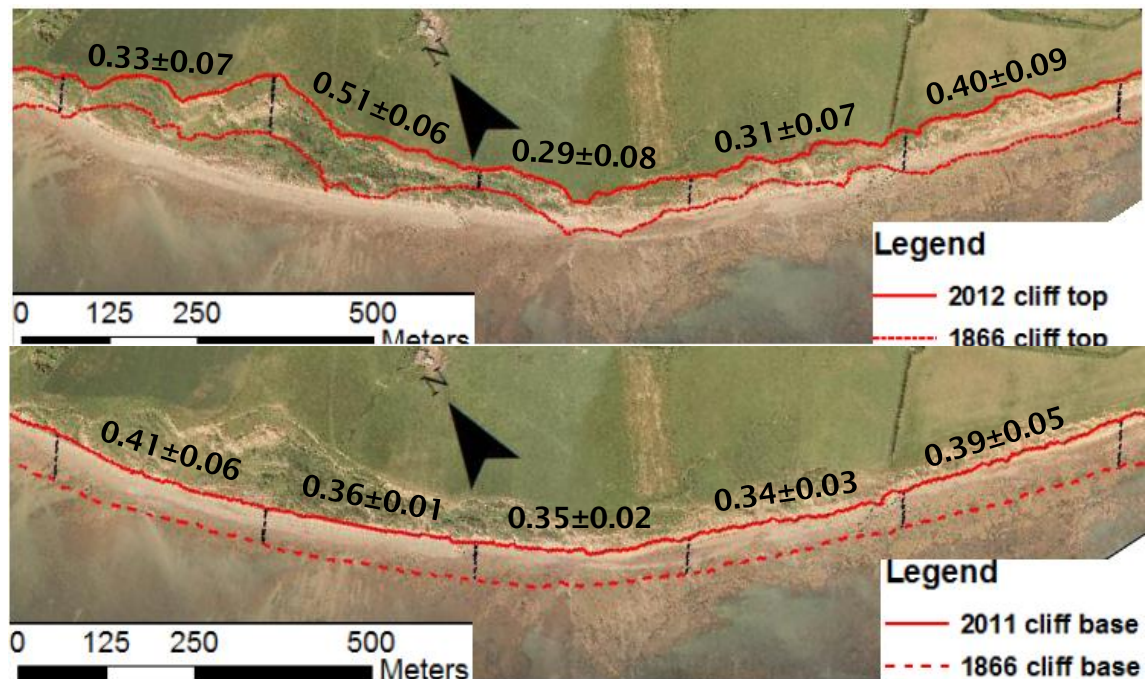
Figure 7.22: Patterns of cliff top and cliff base recession around Sudmoor Point, values are average recession rates for each section in m/a ± the standard deviation also in m/a

The mudstone cliffs around Ship Ledge are approximately 20 m high and relatively steep. The platform of Ship Ledge is also mudstone; it is a locally elevated section of the platform extending from Hanover Point to just east of the ledge itself. The termination of the shore platform to the east comes as the Wessex Mudstone gives way to the Vectis Shales, bringing with it a decrease in beach width (but an increase in BWA) and an inland shift in the offshore depth contours (Figure 5.2). The pattern of cliff top recession (Figure 7.23) broadly replicates the pattern predicted by the conceptual model described in Figure 2.7, with the highest rates of recession seen down drift of the platform, and a lower rate at the headland. All variations, aside from the comparison between the two down drift sections have been shown to be statistically significant to the 95% confidence level (Appendix 9). The pattern of cliff base recession around the platform echoes that of the cliff top with a less defined increase in the down drift rates. This led to the finding that the difference between recession rates at Ship Ledge and the section 0 – 300m down drift are statistically insignificant. All other combinations were found to be significant at the 95% confidence level (Appendix 9). The high rates of recession are unlikely to be caused by the variations in beach width, since none exist, and as

stated in Chapter 6 the beaches provide little or no protection to the cliff base from the erosive power of the waves. It is the total loss of intertidal shore platform as the geology changes from mudstone to shale which allows more wave energy to reach the cliff base increasing the recession rates.
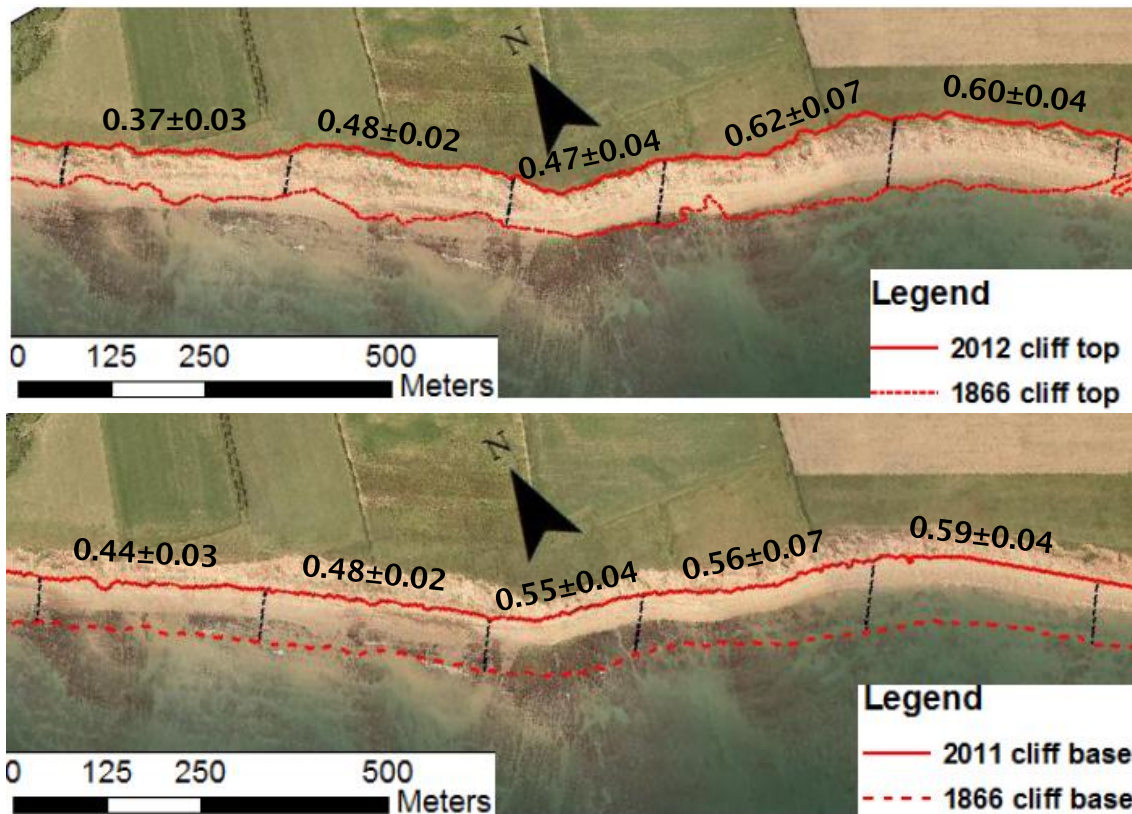
Figure 7.23: Patterns of cliff top and cliff base recession around Ship Ledge, values are average recession rates for each section in m/a ± the standard deviation also in m/a

The results shown in Figure 7.23 suggest that a subtle headland is forming behind Ship Ledge, particularly when considering the cliff top recession rates. The cliff base recession rates indicate a steady increase from west to east. At the ledge itself the recession rates begin to exceed the average for the whole coast. If these patterns of recession continue a headland may start to exhibit the form outlined by the conceptual model of headland formation described in Figure 2.7.

Atherfield Point, as indicated by the long-term recession rates shown in Figure 7.5, appears to be a headland in decline. The average cliff top and cliff base recession rates are greatest at the headland. The variations in recession rate shown in Figure 7.24 have been found to be statistically significant to the 95% confidence level (Appendix 10). The beach between Marsh Chine and Atherfield Point,

although composed of coarse gravels is unlikely to protect the cliffs up drift of the headland. In fact the long-term recession rates for both the cliff top and base are greater than the whole coast average. Results of the wave refraction modelling indicate that Atherfield Point is subject to wave energy concentration under common wave conditions. It appears that the platform has failed to attenuate enough wave energy to protect the cliff thus causing the headland to decline. How this decline and the variations in the recession of the other headlands has affected the coastal evolution will be looked at the next section by considering the changing indentation of its bays.
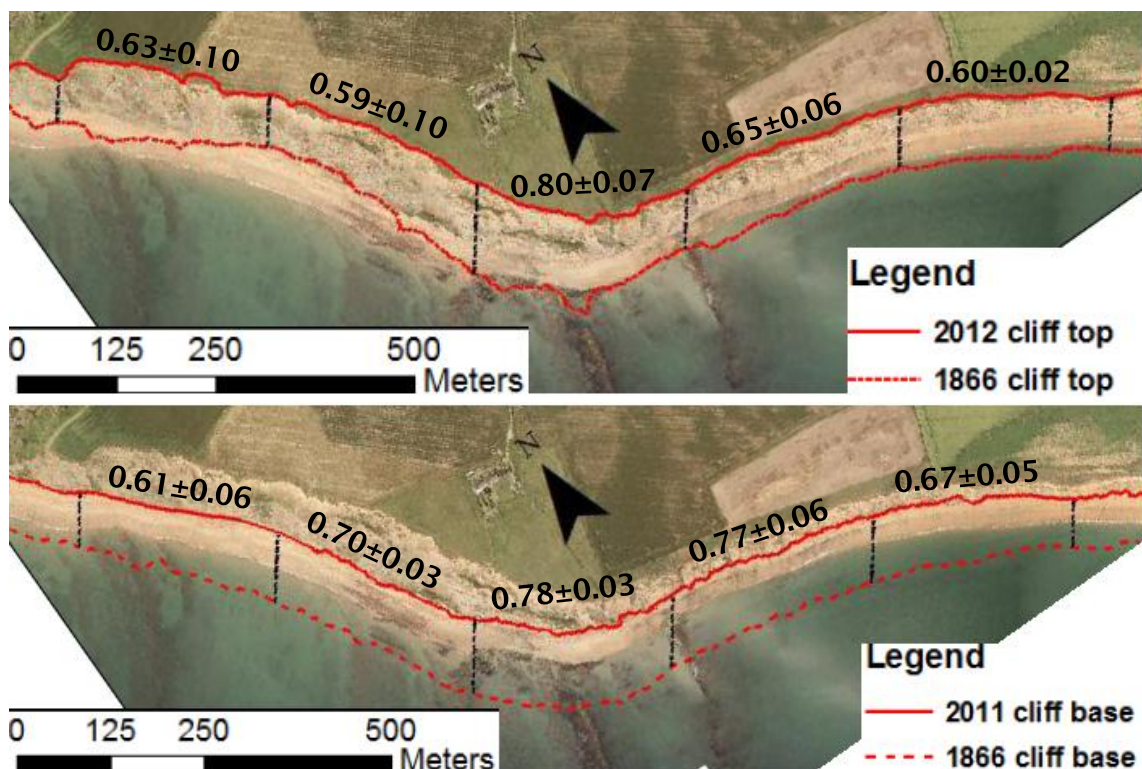
Figure 7.24: Patterns of cliff top and cliff base recession around Atherfield Point, values are average recession rates for each section in m/a ± the standard deviation also in m/a

7.5   Headland Bay Indentation Factor

Changes in the indentation index of the bays can provide an insight into the evolution of these headland and bay systems. The Indentation Factor (IF) was devised by Spagnolo et al. (2008) as a method of quantifying the indentation of a bay. It is calculated using Equation 7.1:

$$IF = \frac{L_a}{L_c} \qquad\qquad 7.1$$

Where, *IF* = Indentation Factor, L_a = Actual length of the bay following the coastline and L_c = Chord length of the bay, i.e. the straight line distance between the two headlands. The Indentation Factor (IF) gives a measure of how deep or shallow a bay is, the larger the value the deeper the bay. Looking at how the indentation changes over time will provide information on how the bay is evolving. In this case the length of the bay was measured for both the cliff base and the cliff top. Table 7.3 shows the variations in IF from 1866 to 2011 and from 1866 to 2012 for the cliff base and cliff top respectively, calculated using the 1866 OS map and results of the dGPS surveys.

Table 7.3: Changes in Indentation Factor (IF) of the bays separated by the three established headlands and Ship Ledge which splits Brighstone Bay into East and West. The IF was calculated for the cliff top and cliff base lines.

	TOP			BASE		
	1866	2012	Change	1866	2011	Change
Compton Bay	1.25	1.19	-0.01	1.12	1.11	-0.01
Brook Bay	1.20	1.12	-0.08	1.06	1.09	+0.03
Brighstone Bay West	1.12	1.08	-0.04	1.03	1.10	+0.07
Brighstone Bay East	1.20	1.12	-0.08	1.05	1.09	+0.04
Chale Bay	1.10	1.15	+0.05	1.06	1.08	+0.02

The indentation measured at the cliff base of all the bays, except Compton, has increased over the study period (1866 to 2011, Table 7.3). While the indentation measured at the cliff top, with the exception of Chale Bay has decreased over the study period (1866 to 2012, Table 7.3). The only consistent changes occur at the either end of the study site in Compton Bay and Chale Bay, where the stable headlands of Freshwater Bay and Rocken End hold their position over time. In Compton Bay a small decrease in IF of 0.01 is seen in the cliff top and base, reflecting the decline of Hanover Point to the south. To the southern end of the study frontage Chale Bay shows and increase in indentation for the cliff top and cliff base line (Table 7.3). This is despite the decline of Atherfield Point and can be attributed to large scale landsliding around Blackgang Chine over the study period.

It is worth noting the Indentation Factors are small, reflecting the subtle nature of the headlands and bays seen on this coastline. To provide a comparison for context the IF for a number of bays in the area were calculated. These were Poole,

Studland, Christchurch, Freshwater and Whitecliff Bays, and their IF values ranged from 1.16 to 1.55, with an average value of 1.38 (Table 7.4).

Table 7.4: The Indentation Factors of a number of Bays around the south coast of Hampshire, Dorset and the Isle of Wight.

	Cliff Base Indentation Factor
Christchurch Bay	1.17
Poole Bay	1.48
Swanage Bay	1.55
Freshwater Bay	1.33
Whitecliff Bay	1.37
Southwest Coast Average	1.09

The variations in IF on the southwest coast over the study period do not exceed 0.08. This combined with the conflicting results for cliff top and cliff base indicate that the variations recorded are not significant. No systematic changes in the indentation of the bays can be drawn out from the data.

7.6 Headland Development and Migration

As outlined in Section 2.4 the potential for headland migration exists where the strike of the shore platform forming beds is not perpendicular to the overall orientation of the coastline. This is based on the assumption that the general orientation of the coastline is controlled by prevailing wave conditions and therefore coastline retreat will occur broadly parallel to it. The predicted rates of headland migration per meter recession were calculated using the following equation:

$$M = R/\tan(\alpha) \hspace{3cm} (7.2)$$

Where, M is Migration, R is Recession (m), which in this case is 1m and α is the deviation of the strike from the orientation of coastline in degrees. The potential for headland migration is zero when α is 90°, the rate gradually increases in both direction from that angle. Less than 90° the direction of migration is updrift and more than 90° migration is down drift (Figure 7.23).
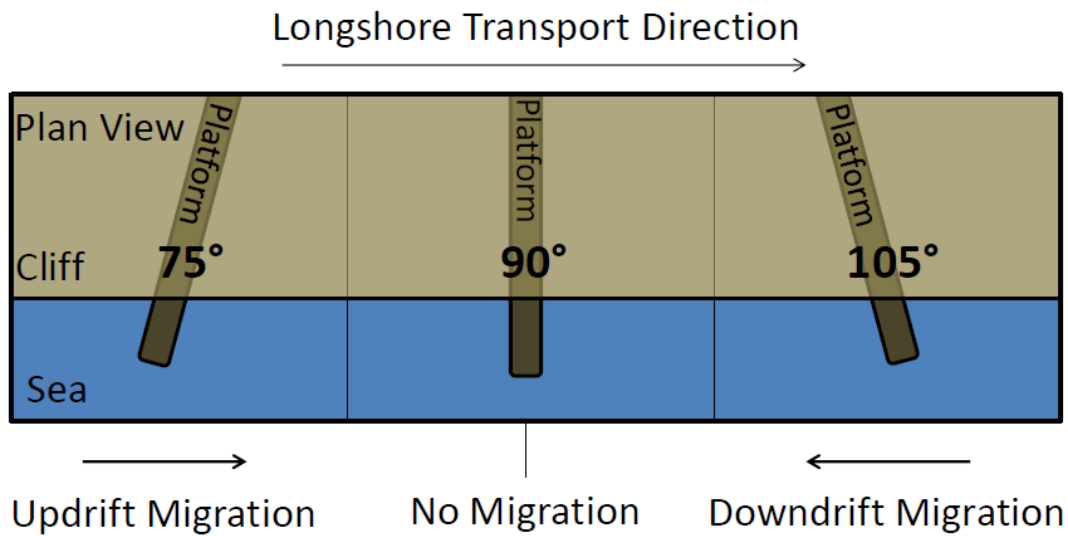
Figure 7.25: Schematic showing the potential migration of headlands with variations in platform strike relative to the coastline

Before this prediction method can be tested, a number of parameters must be defined, including the coastline orientation and apex of the headland itself. The coastline orientation was determined by running a line of best fit through the cliff base line from Compton Chine to Rocken End. The line was then displaced landward of the coastline as shown in Figure 7.26.
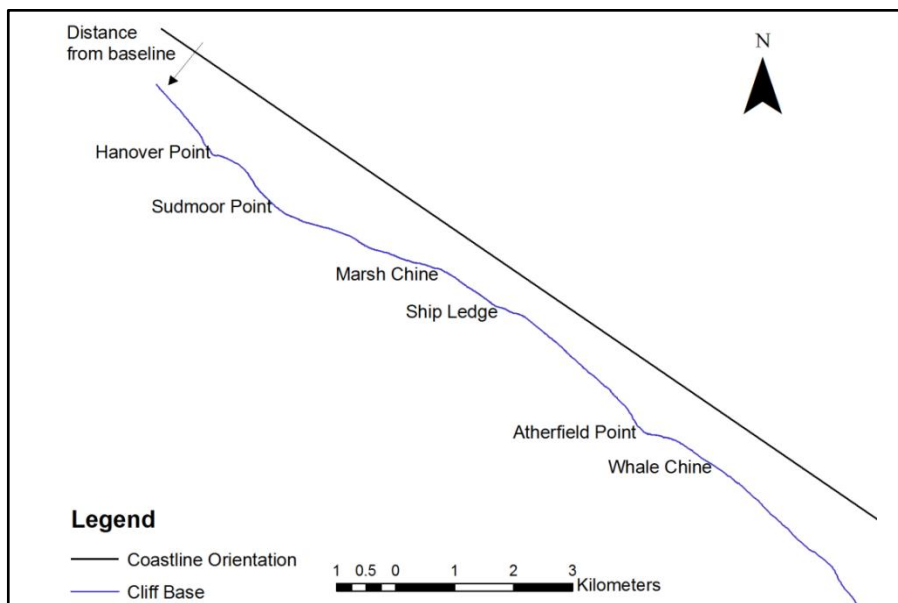
Figure 7.26: Schematic showing the baseline representing the overall coastline orientation.

The location of the headlands apex was defined as the greatest deviations from that orientation measured perpendicular to it for each of the surveys available. To compare the headlands over the study period the effects of retreat were removed (e.g. the average retreat between 1866 and 1909 was removed from the 1909 dataset and so on) results are presented in Figure 7.27 to Figure 7.30.

The east-west strike of the platform around Hanover Point gives an α value of 143°. Using Equation 7.2 it was calculated that the migration of Hanover Point would be downdrift at a rate of 1.3m per meter retreat, or approximately 193m over the study period. However, comparison of the cliff base lines from old OS maps and the recent dGPS survey reveal updrift migration of 5 m (Figure 7.27). This is insufficient to demonstrate a significant headland migration over the study period.
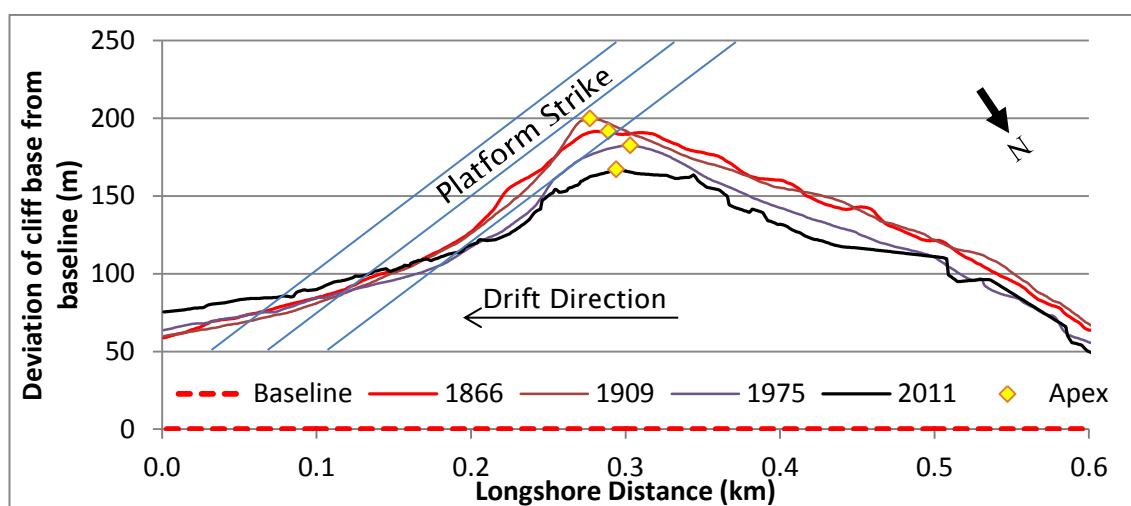
Figure 7.27: Migration of Hanover Point and development of coastal planform between 1866 and 2011 using the cliff base as the measure of cliff position. The strike of the platform forming beds is represented by the blue lines. Corrections for retreat have been made to allow comparison between years.

The high α value of the strike of the platforms around Hanover Point are demonstrated by the strike lines drawn onto Figure 7.27. When considering the protection from cliff recession provided by a shore platform the location of the elevated beds relative to the coastline may be more important than the strike of the bed. In these situations the widest point of the platform, relative to the coastline orientation will not be where the platform bed meets the cliff base, but some distance updrift of it. This can be seen in the platform at Hanover Point, where the seaward most bed of the intertidal platform, that offers the greatest protection from wave erosion, crosses the coastline in Brook Bay. The wide multi bed nature

of Hanover Point enhances that affect (Figure 4.14). Therefore the migration of the headland is likely to be controlled by the maximum width of the shore platform relative to the coastal orientation, explaining why the migration of Hanover Point is insignificant over the study period. Removing the effect of retreat and stacking the results as they appear in Figure 7.27 does reveal a change in the shape of Hanover Point over the study period. A blunting of the headlands can be observed in line with the decline of Hanover Point over the study period.

The wide rounded nature of Sudmoor point makes defining the apex of the headland more ambiguous. Over the study period and down drift migration of 77m was recorded, although the location of the defined apex switched back and forth between surveys indicating the apex cannot be defined as a single point and must be considered as a zone approximately 75m wide. The close grouping of the cliff base lines in Figure 7.28 where retreat has been corrected for indicates the stability of the headland form over time. This is reflected in the low, uniform recession rates measured around Sudmoor Point (Figure 7.21).
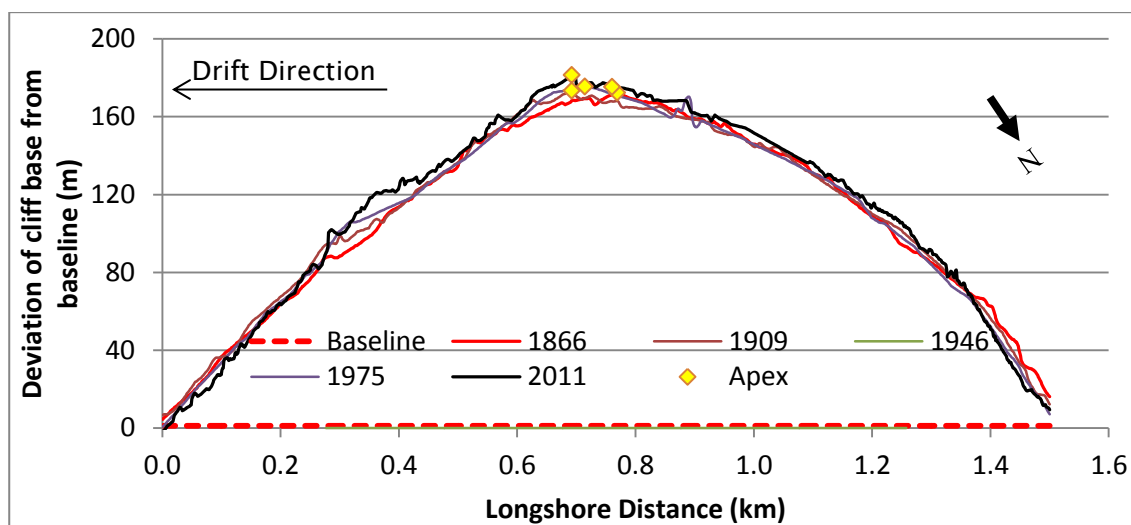
Figure 7.28: Migration of Sudmoor Point and development of coastal planform between 1866 and 2011 using the cliff base as the measure of cliff position. Corrections for retreat have been made to allow comparison between years.
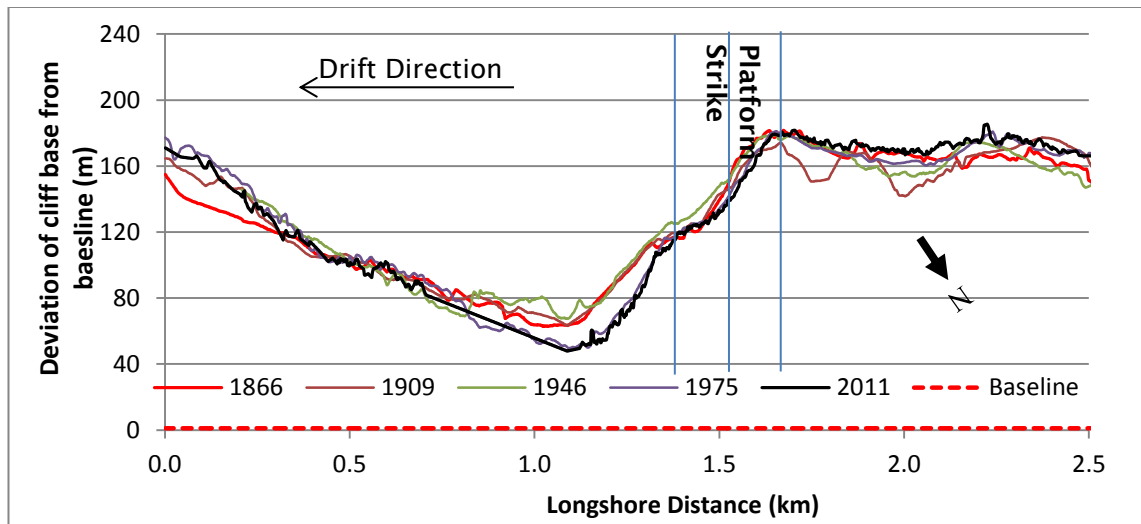
Figure 7.29: Development of the coastal planform around Ship Ledge between 1866 and 2011 using the cliff base as the measure of cliff position. The strike of the platform forming beds is represented by the blue lines. Corrections for retreat have been made to allow comparison between years.

The cliff base planform around Ship Ledge does not have a defined apex and since this is a potentially forming headland no migration is expected and has not been measured. There is however a visible deepening of the indentation down drift of the ledge (Figure 7.29). This is in line with the larger recession rates observed down drift of the intertidal platform.

At Atherfield Point a small amount (17m) of updrift migration was recorded (Figure 7.30). In this case the strike of the platform forming beds is approximately 90° to the orientation of the coastline, so no migration was predicted. In terms of the scale of the headland a change in the apex location of 17m is insignificant. The high recession rates observed around Atherfield Point over the study period are reflected in the changing form of the headland. The correction for retreat in Figure 7.30 has allowed comparison of the headlands planform over time. Comparing the bold red and black lines representing the 1866 and 2011 planform respectively, reveals the smoothing or decline of the headland.
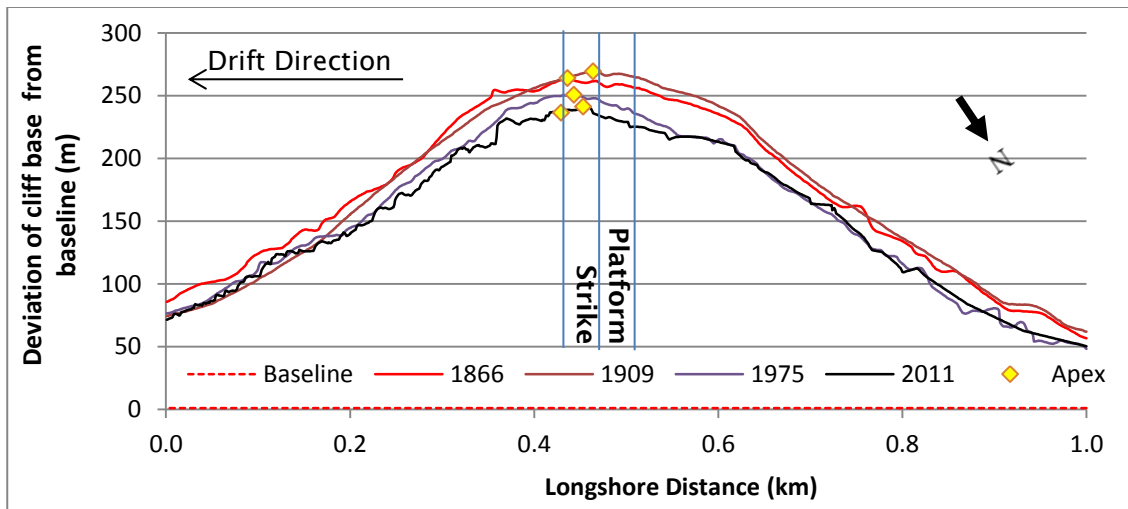
Figure 7.30: Migration of Atherfield Point and development of coastal planform between 1866 and 2011 using the cliff base as the measure of cliff position. The strike of the platform forming beds is represented by the blue lines. Corrections for retreat have been made to allow comparison between years.

The lack of migration measured over the study period at Atherfield Point supports the suggestion that when α is equal to 90° that headland migration will not occur. The insignificant migration seen at Hanover Point required reassessment of the hypothesis for platforms whose value of α strays too far from 90°. The rapid rates of headland migration predicted seem unlikely due to the time required for headland formation and evolution, as evidenced by the evolution of the cliffs behind Ship Ledge recorded over the 145 year study period, and the lack of migration measured at Hanover Point. In these circumstances it may be the width of the platform relative to the coastal orientation that controls headland migration.

7.7 Summary

Having considered all the parameters that control recession rates individually it would appear that no one factor is responsible for longshore variations in recession rate along the coastline. The Principal Component Analysis showed that the Vectis Formation, Mudslides (CBUe) and intermediate coherence were related to increased recession rates while steep cliffs with high level sliding were associated with reduced recession rates. However these results only accounted for 30% of the variance seen in the data indicating that it is the interaction of all the above within the current shoreline morphology that controls the variations in recession rates.

Analysis of recession rates have revealed that of the three established headlands along the southwest coast of the Isle of Wight, two (Hanover and Atherfield Point) are in decline and one (Sudmoor Point) is growing. The changes in bay indentation, with the exception of Chale Bay which is affected by the hold of the position of the Rocken End headland to the south and landsliding at Blackgang Chine, support the results of the cliff recession analysis. Ship Ledge, or more precisely the edge of the mudstone platform that extends from Hanover Point to Ship Ledge and raises the sea bed bathymetry where it outcrops, seems to be developing into another subtle headland.

There is no single clear control on cliff recession rates. The geology shows the greatest influence with the Vectis and Atherfield Clay Formations retreating faster, on average, than the Wessex and Ferruginous Sand Formations. These variations cannot be wholly attributed to the geology. Variations in recession rates are a result of the interaction between many factors, as mentioned previously the coastline represents a coupled system and it is difficult to identify the influence of individual features as feedbacks between different elements will occur.

Despite predictions of headland migration there is no evidence of significant migration of any of the established headlands along the south west coast. The lack of migration observed during the study period of 145 years, indicates this timescale is not long enough to observe changes in headland location, therefore headland migration is not likely to be of concern to coastal managers. The comparison of successive surveys does reveal a blunting of the headland form at Hanover and Atherfield Points. This blunting, caused by the maximum rates of erosion being centred at the headlands, is in line with the model of headland erosion outlined by Komar (1985) and described in Section 2.2.1.

8. Discussion

Before embarking on a discussion of the results of this study, it is worthwhile revisiting its aim (Section 1.3.1) and objectives (Section 1.3.2). The aim of this project is to evaluate the controls on headland formation and evolution using the southwest coast of the Isle of Wight as a study site. There were at least three possible controls: 1) geological and geotechnical properties of the cliff and platform, 2) wave energy concentration, and 3) sediment volume and supply. Therefore the first three objectives were to investigate the factors defined above, and in particular any longshore variations that could lead to variations in recession rates (Section 1.3.2). These objectives formed the basis of the first three results Chapters (Chapters 4 to 6) and will be summarised and discussed in Sections 8.1 to 8.3.

Chapter 7 examined the correlation between the possible controls outlined above and recession rates along the coastline between 1866 and 2011/12, and a more detailed analysis of the recession rates around the four headlands. The results of Chapter 7 will be combined with the findings of Chapters 4 to 6 in Section 8.4 to address objective 4, i.e. investigate how the above factors influence headland formation and evolution through the refinement and testing of a conceptual process-based model. In Section 8.4, the conceptual models of cross-shore interaction (Section 2.1.4; Figure 2.4), Headland Formation (Section 2.3; Figure 2.7) and Headland Evolution (Section 2.4; Figure 2.8 and Figure 2.9) will also be revisited and assessed in light of the results. Section 8.5 summarises the findings relating to headland formation and evolution including the lessons for the Isle of Wight and its future management (Section 8.5.1), and the lessons for other sediment-starved coastlines; where the geological properties of the intertidal and sub-aerial cliff influence coastal planform evolution (Section 8.5.2). The final Section of this Chapter (Section 8.6) will look at the potential areas of further work that could fill the gaps in knowledge identified during this project.

8.1   Geology and Geotechnical Assessment

Objective 1 of this project was to determine the importance of longshore variations in shore platform and cliff geology, in particular the influence of their geotechnical properties on shoreline morphology and local recession rates. This Section aims to summarise and interpret the results of Chapter 4 and Section 7.2.1, taking one

geological formation at a time, and incorporating information on the geology, morphology and geotechnical aspects of each. The influence of the structural geology will also be explored in terms of intertidal platform formation and headland location.

Along the entire length of the study site the cliff face geology is comprised of soft rocks, i.e. the inter-bedded mudstones, shales and sandstones of the Wessex and Vectis Formations and the clay and sandstones of the Atherfield Clay and Ferruginous Sand Formations. The cliffs range in height from 10 to 60m and display a number of cliff morphologies.

8.1.1 Wessex Formation

The Wessex Formation, comprised of mudstones inter-bedded with irregular sandstones, is both the oldest and most prevalent geological formation present within the study area. Taking up 57 % of the cliff face area and forming 91% of the intertidal platform by area. It dominates the central portion of the coastline, outcropping between Barnes High and the Compton Farm Landslide, with a break between Small Chine and Shippard's Chine (Figure 4.1 and Figure 4.2). Extensive intertidal platforms exist along the entire length of its exposure (Figure 6.8b). The average cliff base recession rates for the Wessex Formation is very slightly lower than that of the coastline as a whole (Figure 7.9), i.e. $0.46ma^{-1}$ compared to $0.49ma^{-1}$ and displays the lowest recession rate of all the formations. The variations have been shown to be statistically significant to the 95% confidence level.

The dominant cliff morphology is CBUa (steep cliffs with talus at the base), followed by CBUb (compound landslides) and CBUc (steep cliffs with high level landsliding). The average cliff base recession rate for these morphologies is close to that of the entire coastline, being 0.51, 0.49 and $0.45ma^{-1}$ respectively (Figure 7.12). The variations between CBUc and CBUa/CBUb are statistically significant, but the variations in recession rate between CBUa and CBUb are not.

The apparent resistance to erosion displayed by the Wessex Formation is not necessarily related to its coherence. The coherence of the Wessex Formation, as with much of the Vectis and Atherfield Clay Formations is predominantly intermediate, with some variations related to the appearance of sandstones. However, neither the Vectis Formation nor the majority of the Atherfield Clay

Formation forms intertidal platforms and both show higher than average rates of recession ($0.6ma^{-1}$ each). The variations in behaviour, morphology and recession rates imply that coherence, as measured by simple field index tests, is not a sufficient measure of rock strength. It can describe the material strength at a cm scale, but does not describe the strength of the cliff or platform as a whole, or its resistance to erosion. No significant statistical relationships were found between coherence and recession rates. The mass properties and weathering behaviour of the lithologies must also be considered.

The mass properties of a sedimentary rock are strongly influenced by their depositional environment and subsequent natural compaction by deep burial. It appears that the mudstones owe their relative resistance to erosion and platform forming potential to their depositional environment. Laid down in a fluvial environment the mudstones represent over bank deposits, rapid deposition during flood events led to the formation of their massive structure (Section 4.3.3) allied to their burial under an estimated 1000 m of overlying sediment. This massive structure means there are no regular bedding planes or planes of weakness that can be utilised by the waves. The mudstones behave in a non-plastic way even when saturated (Rust and Gardener, 2002). The typical mode of aerial weathering displayed by mudstones, including those of the Wessex Formation, involves the continual wetting and drying of the surface layers forcing them to crack as they dry allowing moisture to penetrate deeper and deeper into the rock, increasing the thickness of the weathered layer (Kollios, 1993). The short period of exposure of the shore platform to the air prevents the mudstones from drying out, much of the sand free platform is only exposed at a mid-tide water level or lower. A study by Kanyaya and Trenhaile (2005) subjected a number of lithologies to continued wetting and drying cycles to simulate their exposure at different tidal levels. Their results suggested that down wearing rates decreased with elevation within the intertidal zone. This was thought to be because it takes longer for rocks to desorb water that to absorb water. This indicates that due to their regular inundation platforms are unlikely to dry out sufficiently to crack the surface and therefore weathering of the platform will proceed slower than that of the cliffs. This may go some way to explain the extensive platform formation within the Wessex Formation, which is not seen in the other formations.

8.1.2   Vectis Formation

The Vectis Formation can be split into three members, two predominantly Shale members named after the chines that cut through them (Cowleaze and Shepherds) and a sandstone member called the Barnes High Member. The Vectis overlies the Wessex and flanks it either side of the coast, outcropping in Compton Bay and between Barnes High and Atherfield Point (Figure 4.3). Although displaying the same coherence as the Wessex Mudstones, i.e. intermediate coherence (Figure 4.20), the Vectis Shales display a higher than average cliff base recession rate (Figure 7.9): $0.6ma^{-1}$ compared to the whole coast average of $0.49ma^{-1}$ or the Wessex average of $0.46ma^{-1}$. The Vectis Shales also fail to produce intertidal platforms. In the absence of the supportive Barnes High Sandstone the dominant mode of failure is through mudsliding (Section 4.1.2). Mudsliding shows the higher rate of recession than all other CBUs (0.68 m a^{-1}). The cliff base recession rates of the Vectis Shales are significantly lower in Compton Bay compared to their exposure in Brighstone Bay. These variations are statistically significant to the 95% confidence level. This discrepancy has been attributed to a combination of the increased dip and reduced thickness of the beds in Compton Bay, providing more support to the those beds and where weaknesses had led to landsliding, the talus produced reduced the cliff base recession rates.

Results of particle size distribution indicate higher clay content than the Wessex Mudstones (Figure 4.22) which may contribute to its greater erodibility. Conflicting results on the proportion of swelling clays present within the Vectis Shales makes interpretation more difficult. Analysis of samples collected for this project (Section 4.4.2) show a relatively low level of Smectite (16%), but analysis of sample collected by Rust and Gardener (2002) showed 57% Smectite and Vermiculite. Both sets of samples were tested using XRD methods. This discrepancy in the results may simply be related to the natural variability within the shales. The small sample size used to calculate clay content and mineralogy is a major limitation of this study. Analysis of many more samples is required to fully understand the influence these factors have on the erodibility of these formations and to ensure any variations observed are not simply due to the natural variability within each formation.

As with the Wessex Formation the dominant control on the behaviour of the shales lies with their depositional environment and mass properties. Laid down in a brackish lagoonal environment the high clay content and slow rate of deposition allowed the alignment of clay minerals, creating a fissile structure. Field observations showed the Vectis Formation to be thickly laminated (6 to 20 cm) to thinly bedded (20-60 mm). These laminations become even finer as weathering proceeds, forming what is sometimes referred to as paper shales. This laminated bedding is the major control on the behaviour and increased erodibility of the Vectis Shales. When saturated, as they are in the intertidal zone, the fissile shales are easily disaggregated, preventing the formation of intertidal shore platforms. In the cliffs the laminations allow water into the shales leading to failure by mudsliding.

8.1.3   Atherfield Clay Formation

The Atherfield Clay Formation is exposed in two areas. The narrow exposure in Compton Bay lies wholly within the large scale landslide (Figure 4.3), while the type section forms the cliffs around Atherfield Point. As with the Vectis Formation the average cliff base recession of the Atherfield Clay is greater than the whole coast average at 0.60 m a^{-1}. The rate of recession is also significantly lower in Compton Bay than to the southeast around Atherfield Point. These variations are statistically significant to the 95% confidence level. The explanation for this variation in recession rates north and southeast of Hanover Point is the same as that given for the Vectis Shales.

The Atherfield Clay Formation is fairly consistently of intermediate coherence. Although as stated previously coherence has no statistically significant relationship with recession rates and does not show any correlation with cliff behaviour. The coherence deviated from intermediate in the Perna Beds. These two thin beds of sandy clay and calcareous sandstone, 0.85 and 0.54 m thick respectively form the shore platform known as Atherfield Ledge, behind which Atherfield Point has formed. The lower bed of sandy clays have a coherence borderline C1/C2 (coherent/ intermediate coherence), while the calcareous sandstone is coherent.

The inability of the other members of the Atherfield Clay Formation to produce intertidal shore platforms is related to their composition and mass properties. The

Upper Lobster Beds and Crackers have a high sand and low cement content, when saturated they lose their tensile strength and rapidly disaggregate. The mass properties of the Chale Clay and the Lower Lobster beds are similar to that of the sandy clay of the Perna beds, despite this they fail to produce an intertidal platform. This is thought to be related to the increased joint density of these beds compared to the Perna Clays.

The results of particle size distribution are ambiguous, the clay content of the Chale Clay and Lower Lobster Beds (45%) is close to that measured for the Perna Clay sample taken from the cliff (42%), but higher than that recorded for the Perna Clay sample taken from the platform (21%). The higher clay content may have reduced their platform forming potential. Another explanation for this discrepancy may be related to the protection and support afforded to the Perna Clay by the calcareous sandstone of the Perna Beds but not to the Chale Clay or the Lower Lobster Beds.

8.1.4 Ferruginous Sand Formation

The silty clays and muddy sands of the Ferruginous Sand Formation are exposed at the far ends of the study area. Their low coherence and lack of tensile strength when saturated prevents them from forming intertidal platforms. Their average cliff base recession rate is close to the average for the whole coastline, which is $0.12ma^{-1}$ slower than both the Vectis and Atherfield Clay Formations. This is due to the high frequency, low magnitude of failure events of the Ferruginous Sands. As with the Atherfield Clay and Vectis Formations the cliff base recession rate of the Ferruginous Sands is greater south of Hanover Point, in Chale Bay, than to the north, in Compton Bay. The lower rates in Compton Bay appear to be related to the wide shallow sloping beach present in that area and the large scale landslide providing talus protecting the cliff base. The steeper shoreface and increased wave energy under storm conditions seen in Chale Bay may be responsible for the increase in that area.

8.1.5 Summary

The results of the PCA showed that there is a correlation between increase recession rates and the Vectis Shales and mudslide (CBUe) and between reduced recession rates and increased platform width and steep cliffs with talus at the base

CBUa). The key factor in terms of the geology and how it influences recession rates is the resistance of the beds in the intertidal zone. The more resistant beds forming intertidal shore platforms which provide a degree of protection to the cliff base and lead to the formation of the subtle headlands seen. It seems that the major controls on resistance in the intertidal zone are the mass properties of the lithology. The uncemented, poorly consolidated sandstone beds of the Ferruginous Sand and Atherfield Clay Formations disaggregate rapidly when saturated, failing to form intertidal platforms and producing a steeper shoreface in Chale Bay. The fissile nature of the Vectis Shales allows water to penetrate into the beds leading to weathering and erosion in the intertidal zone, lowering the shoreface and again failing to form intertidal shore platform. The mudstones and sandstones of the Wessex Formation and Perna Beds of the Atherfield Clay Formation form extensive intertidal platforms due to the massive nature of the mudstones and clays and the well cemented nature of the sandstone. The massive structure of the mudstones and clays does not provide many planes of weakness, unlike the shales which can be utilised by the erosive potential of the waves.

8.2   Longshore Variations in Wave Conditions

The second objective of this study was to examine the longshore variations in nearshore bathymetry and consider how those variations influence wave energy reaching the shoreline. Wave refraction modelling was carried out to identify areas of wave energy concentration or dissipation under a number of wave conditions, including common waves and less common storm waves (as described below). This section summarises the results of the modelling and considers the influence wave energy has on longshore variations in recession rates.

The nearshore bathymetry appears to be strongly influenced by the seabed lithology (Figure 5.2). Seaward extensions of the 20 and 30 m contours coincide with the presence of the Wessex Mudstones and the Perna Beds of the Atherfield Clay (the two intertidal platform forming beds). While landward migration of the 2 and 5 m contours can be correlated with the presence of the Vectis Shales and Ferruginous Sands. In general the shoreface slope increases from the northwest to the southeast.

Common waves were defined as the wave conditions likely to occur on average 35 times in 1 year (Hs-1m, Tp-5.5s). Two types of storm waves were defined, 5:1 year waves (Hs-3.5m, Tp-6.5s) and 1:50 year waves (Hs-6.02m, Tp-8.1s Table 3.11). The patterns of wave energy concentration from the common and storm waves differed considerably. Common waves showed wave energy concentration predominantly at the established headlands (i.e. Hanover, Sudmoor and Atherfield Points) and near Hardman Rock (Figure 5.3b). While the storm waves resulted in the greatest wave concentration in Chale Bay, south of Atherfield Point (Figure 5.4b and Figure 5.5b).

This variation is thought to be related to the relative depths at which these waves "feel bottom". The common waves are first influenced by the bathymetry at 23.6m water depth; therefore they are more sensitive to variations in the near shore bathymetry at depths of less than 20 m. The 5:1 year and 1:50 year storm waves are affected further offshore at 33.0 m and 51.2 m respectively, where the variations in the 30 m plus contours are less complex. The main feature is the landward shift of the 30 m contour in the presence of the Vectis Shales and Ferruginous Sands (Figure 5.2).

Overall the amount of energy reaching the shoreline was greater for the storm waves, as would be expected since the waves had more energy to start with. Interestingly the levels of wave energy at the shoreline are broadly similar for the 5:1 year and 1:50 year storm waves despite a 2.51m difference in initial wave heights (Figure 5.4b and Figure 5.5b) This can be explained by considering, once again the depth at which these wave "feel bottom". The 1:50 year storm waves are affected by the sea bed at a depth of 51.2m, i.e. 18.2 m deeper than that of the 5:1 year storm waves, giving a greater distance for wave energy dissipation to occur. This is supported by the work of Dickson et al. (2007) who found that increasing wave height had very little impact of sediment transport rates. However the surges associated with the storms will increase the water level allowing larger waves to reach the shoreline increasing the erosion potential (Haigh et al., 2011).

Simple linear regression analysis found no correlation between wave energy concentration and long-term recession rates (Table 7.2), despite the peaks in wave energy coinciding with Hanover and Atherfield Points under common waves, both headlands are in decline. This is due to the other peaks in wave energy around

Sudmoor Point and Hardman Rock, neither of which display higher than average recession rates. The results of the PCA failed to demonstrate a significant correlation between common wave and recession rates, there was however a weak correlation with storm waves and recession rates. This indicates that wave power alone cannot explain the observed variations in recession rate. The refraction modelling also confirmed that the location of the headlands is not controlled by variations in wave energy reaching the cliff base. The wave refraction analysis uses only three wave conditions and a simple monochromatic wave model. However, for the purposes of this project it was sufficient to determine the most common areas of wave energy concentration and understand the longshore variations in wave energy distribution.

8.3   Beach Volumes and Sediment budget

The third objective of the project was to study the interaction between beach volumes, and sediment budget, in the presence of intertidal shore platforms and the influence these features have on local recession rates. This was achieved through sampling and analysis of a number of beach sediment and cliff samples and the calculation of a sediment budget. The one off nature of sediment sampling provides only a snap shot in time of the beaches sediment distribution. The long timescale, over which the process of headland formation and evolution occurs, means that further sampling within the time frame of the research would not offer any insight into the long-term behaviour of the beach. The methods used are shown in Section 3.4 and 3.5 respectively, while the results are presented in Chapter 6 and are summarised here.

8.3.1   Beach Characteristics

The study area was divided into three distinct subsections based on changes in beach character and median grain size (Figure 6.4, Figure 6.8- 6.8 and Figure 6.1). These sections are 1) Compton Chine to Marsh Chine; 2) Marsh Chine to Atherfield Point and 3) Atherfield Point to Whale Chine. In Section 1 the beach consists of medium to fine sand with a median grain size of 1.9φ or 0.27mm (Figure 6.1), this is reflected in its dissipative form (i.e. shallow beach slope where wave energy is dissipated over a large distance).

The width of the beach in Section 1 is strongly related to the dimensions of the intertidal shore platform (Figure 6.8). In the northern end of Compton Bay where there is no intertidal platform present the beach width is around 80 m, dropping dramatically as the intertidal platform width increases towards Hanover Point (Figure 6.8a). A small peak in beach width is seen in Brook Bay, corresponding with a drop in platform width near the outflow of Brook Chine. Between Sudmoor Point and Marsh Chine there is a steady increase in beach width with the decrease in platform width and elevation (Figure 6.8 and 6.6a). This is likely to be related to the tendency of shore platforms to mimic the profile of an equilibrium beach. Therefore the sediment storage capacity of the platform is reduced (Trenhaile, 2004), i.e. the accommodative space in which the sediment would be deposited is taken up by shore platform.

Changes in BWA (Beach Wedge Area) within Section 1 appear to be controlled by the location of partial sediment transport boundaries (Figure 6.9b). There are two peaks in BWA in Section 1. The first is up drift of the Compton Farm Landslide; the potential causes for this peak are two-fold. 1) The talus from the landslide falling on the beach appears to block sediment transport, building up the beach volume. 2) The Ferruginous Sand cliffs in the area up drift of the landslide are the largest source of beach grade sediment on the coastline (Figure 6.11). The second peak in BWA is updrift of Hanover Point where the headland itself and intertidal platforms potentially act as a partial barrier to longshore transport.

The transition between Section 1 and Section 2 comes with the loss of intertidal platform and steepening of the shoreface (Figure 5.2, Figure 6.7). This allows more wave energy to reach the beach and cliff base leading to an increase in the LCD and median grain size. This in turn causes a small drop in beach width and an increase in BWA around Marsh Chine (Figure 6.1, 6.5 and 6.6). Both the drop in beach width and increase in BWA are directly related to the increase in median grain size leading to an increase in the angle of friction and therefore beach slope and the amount of sediment present above MHWS. The drop in grain size and BWA at Atherfield Point indicate that the headland and its associated intertidal platform act as a transport barrier to gravel while allowing finer sediment to pass around it. Within Section 3 (Atherfield Point to Whale Chine) a steady increase in median grain size in mirrored in the steady increase in BWA.

It is important to remember that the values of BWA were calculated from data between 2004 and 2009 and as such only represent a snapshot view in terms of both the study period and the timescale of coastal evolution. As with the sediment distribution of the beach, the BWA has been assumed to be stable over time.

The relationships between the various beach and platform dimensions and recession rates were investigated using simple linear regression analysis. There was no relationship between platform width and recession rates with the analysis returning R^2 values of 0.0004 (Figure 7.16). Similarly, initial analysis of the beach width vs. recession rates showed no relationship ($R^2 – 0.012$). However when considering the beach width above 40 m a negative relationship emerged with and R^2 value of 0.23 (Figure 7.14). A large part of this correlation is a consequence of the low recession rates in the north end of Compton Bay where the beach width is around 80 m. The presence of a large scale landslide in this area providing talus to the cliff base, combined with the large source of beach grade sediment from the Ferruginous Sands, may be partially responsible for the reduction in cliff base recession rates in this area. The cliff top recession in the same area exceeds 1 m a^{-1} (Figure 7.5).

A study into the relationship between BWA and recession rates on the Norfolk and Suffolk coasts by Lee (2008) defined the threshold value of BWA, below which no influence on recession rates is observed, as 20m^2. The BWA on the southwest coast only exceeds this value in three locations, for a total distance of approximately 1 km. this implies that the beach volumes are insufficient to protect the cliff from erosion. An argument supported by the unexpected *positive* relationship observed between BWA and recession rates (Figure 7.15), an increase in recession rate with BWA being recorded, but the R^2 value was only 0.056 indicating that there is no significant relationship between the two. The Principal Component Analysis shows a correlation between increased BWA and increased cliff base recession rates. The use of BWA as an indicator of the protection provided by the beach on this study site may not be appropriate. The differing locations and timescales of the studies make direct comparison potentially misleading. The previous applications of BWA have been on the Norfolk and Suffolk coasts by Lee (2008) and on the Holderness Coast by Quinn et al. (2010). The maximum BWA recorded by Quinn et al. (2010) was only 8 m^2, but a relationship between BWA and recession rates was still observed. This demonstrates that the limit below which BWA has an influence on

recession rates varies from place to place. Another consideration is the relative exposure of the coastlines studied to wave energy. The southwest coast is directly exposed to North Atlantic swell and storm wave, while the other study sites located on the east coast experience a lower energy wave climate. This could be cause to raise the threshold value for the southwest Isle of Wight. Both Lee (2008) and Quinn et al. (2010) considered the variations in BWA and recession rates over a decadal time scale while this study looks at BWA on a decadal timescale and recession rates over a century timescale. The final difference between this and previous studies is the complexity of the geology and morphology of the coastline. The coastlines of Norfolk, Suffolk and Holderness are predominantly glacial tills with uniform geotechnical properties. There is not the variation in platform elevation and cliff lithology that is seen on the southwest coast of the Isle of Wight. For these reasons, combined with the low beach volumes on the southwest coast indicate that measurement of BWA does not provide an insight in to the controls of recession rates for this coastline. Although the PCA did highlight the relationships between many of the beach parameters and cliff base recession rates the low percentage of variable given by the two principle components (30%) does not constitute a dominant control on recession rates. It would appear that neither the volumes of beach material nor the widths of shore platform present on the southwest coast are sufficient to significantly influence cliff base recession rates over the study period.

8.3.2   Sediment Budget

A sediment budget was constructed to consider the long-term inputs and outputs of sediment to the coastal system. The main sources of sediment considered were cliff erosion and sea bed sediments. The fine grained nature of much of the coastline means that 87% of the material eroded from the cliff will be lost offshore in suspension. The increase in LCD (Littoral Cut-off Diameter) between beach sections also reduces the amount of viable beach material produced by the cliffs. For example in Compton Bay where the LCD is at its lowest, 69% of the Ferruginous Sands eroded from the cliff will remain on the beach, that figure reduces to 8% in Chale bay where the LCD is greatest (Table 6.1). This drop in the beach grade sediment produced by the cliff is related to an increase in LCD not a decrease in grain size. It follows that the largest average annual input of beach grade material from cliff erosion is found in the north end of Compton Bay. Sand

input to the beach is associated with the supply of sand from the cliffs controlled by the location of the sand rich beds such as the large channel sandstone at Sudmoor Point and the Tidal Bar sandstone bed known as the Barnes High Sandstone (Figure 6.11).

An interesting feature of the sediment budget on this coastline is related to the distribution of gravels in the cliffs and on the beach. The dominant source of gravels to the coastline is the Pleistocene Valley Gravels which outcrop in the cliff top between Small Chine (800m north of Hanover Point) to Marsh Chine (Figure 4.3 and Figure 6.12). This is in contrast with the occurrence of gravels on the beach, which appear in significant volumes from Marsh Chine southwards to Atherfield Point. The lack of gravel on the backshore within Section 1 could be explained by the preferential and rapid longshore transport of larger sediment. Larger particles are "shaken" to the surface in a process known as kinetic sieving leading to vertical sorting (Dasgupta and Manna, 2011, Gleason and Hardcastle, 1973), leaving them exposed to transport by waves. Large waves have been found to transport larger particles at a faster rate than finer sediment (Jolliffe, 1964).

Given the volume of gravel available in the cliffs, the large beach volumes found between Marsh Chine and Atherfield Point imply that Atherfield Point acts as a partial sediment transport barrier. Barrett (1985) also proposed that Atherfield Point confines the littoral transport of gravel, a position Bray et al. (2004) found debatable, though the evidence from the sediment distribution seen in this report appears to support the theory. The angular nature of the gravel observed in the cliff compared to the more rounded beach gravel seen also calls into question the source of the beach gravel. However work by Bray (1997) and Dornbusch et al. (2002) suggests that angular flints lose several per cent of their weight over a short period of time becoming sub angular, this can be up to 10% in the first year. Dornbusch et al. (2002) considered it possible that the annual weight loss of shingle could be as high as ~1.9%.

In the 19th Century, when the average recession rates for the whole coast were lower, the source of gravel from the cliffs would have been at least double what it is today. At present the cliff top gravel deposits extend only as far south as Marsh Chine, but a report by Codrington (1870) indicates that the gravel deposits in the cliff top extended south to Blackgang Chine, the source being the south eastern

extension of the Western Yar Valley Gravels. Even with this increase in sediment source it would take between 30 and 45 years to build up the volume of sediment currently seen on the beach between Marsh Chine and Atherfield Point. This estimate does not take into account the loss of volume through abrasion or longshore transport around Atherfield Point. It is not possible to draw a direct link between the increase in recession rate and the drop in gravel input from the cliffs. As the increase in gravel would have only influenced the beach volumes southeast of Marsh Chine, due to the dominant direction of littoral drift, while the increase in recession rates was seen across the whole coastline. The well rounded nature of the gravel also implies that the majority of the gravels originate from sea bed deposits (Brampton et al., 1998). However, there is little hard evidence in the literature for onshore sediment pathways of gravel, there is some anecdotal evidence of rapid temporary changes in gravel volumes and character on the southwest coast. It is more likely that the gravels have persisted on the beach for some time becoming well-rounded though wave action and abrasion.

Analysis of potential sediment transport revealed a general northwest to southeast trend in sediment transport. The low potential transport rates along the coastline indicate that the coastline is broadly drift aligned. It is around the headlands that the orientation of the coastline deviates from this alignment and the potential for sediment transport increases. The reversal of transport direction between Sudmoor Point and Marsh Chine coincides with an area of low beach widths and volumes where extensive shore platforms occupy much of the shoreface (Figure 6.8). There is evidence that Hanover and Atherfield Points act as partial sediment transport barriers, so although the potential for transport increases in those areas the actual rate may not increase.

These results indicate that the beach levels seen on the southwest coast are insufficient to significantly influence recession rates. And that this is a situation unlikely to change over time since the coastline as a whole is starved of beach grade sediment. Measurements made from maps and aerial photographs from 1866, 1909, 1975 and 2008 indicate that beach width has been stable over the study period. However there may have been larger beach volumes in the past due to the greater cliff top extent of gravel deposits contributing to the sediment budget increasing the beach slope and volume but not beach width.

8.4   Summary

The key findings of Chapters 4 to 7 are summarised here. The controlling factor on the planform evolution and recession rates is the lithology and in particular the mass properties and clay content of these beds outcropping in the intertidal zone, which determines if intertidal platforms will form. Figure 8.1 shows the lithology of both the land and the seabed. The location of the intertidal platforms is also marked on highlighting the relationship between lithology and intertidal platform formation, with platforms only forming in the Wessex and Atherfield Clay Formations.
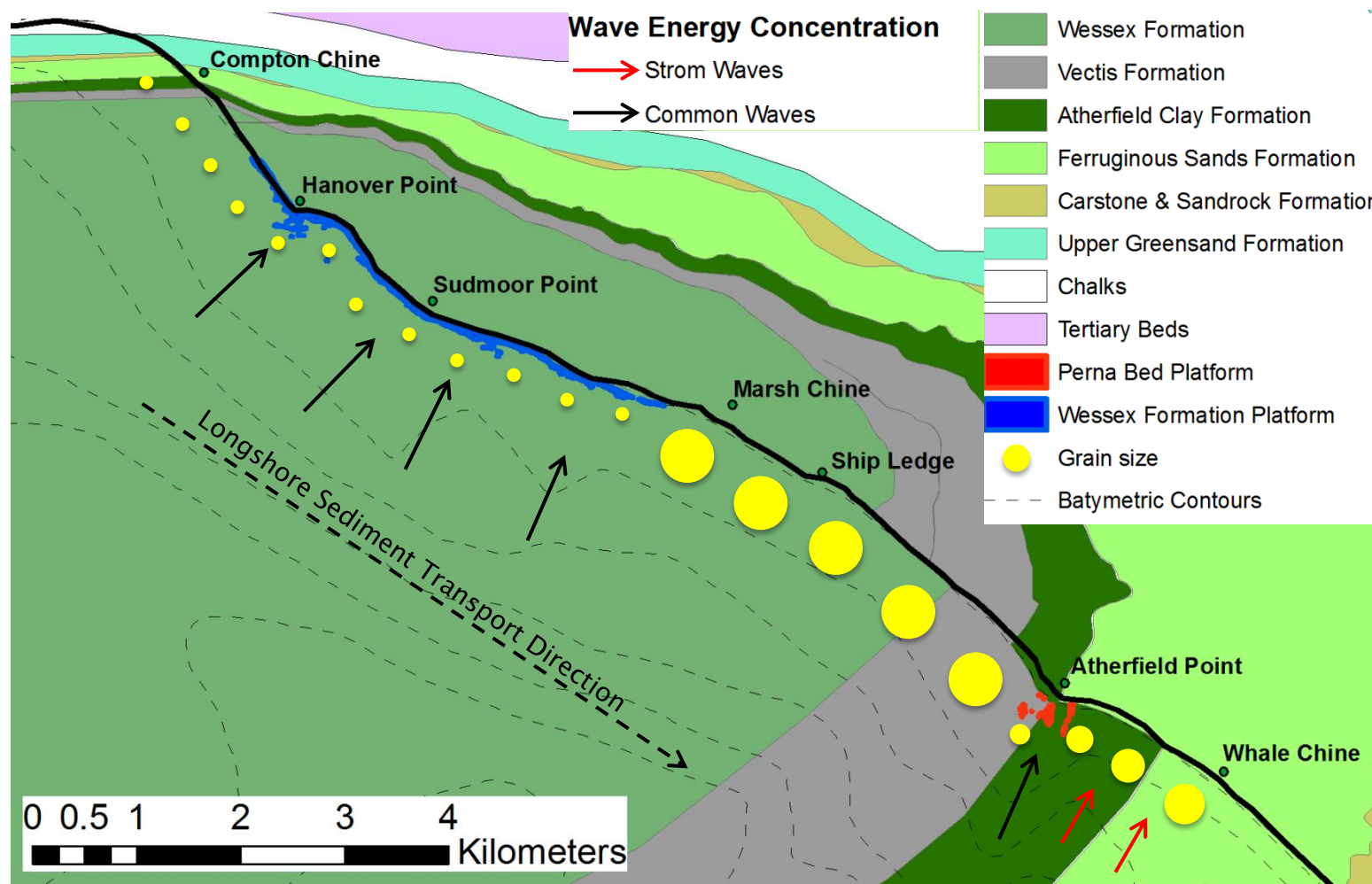
Figure 8.1: Summary of the key factors along the southwest coast of the island, including the lithology, beach, platform and wave energy concentration

The secondary control on recession rates and planform evolution is the longshore variations in wave energy reaching the cliff base, the locations of wave energy concentration are marked on Figure 8.1 as black and red arrows for common and storm waves respectively. The common waves concentrate their energy at the headlands causing Hanover and Atherfield Point to decline. The storm waves produce the greatest wave energy in Chale Bay. These longshore variations in wave energy are controlled by the seabed bathymetry which is in turn controlled by the seabed geology. The variations in beach character are shown in Figure 8.1, indicated by the change in median grain size along the shoreline which is represented by yellow circles. The relative size of the circles is proportional to the relative grain size in the phi scale. The increase in grain size corresponds to an increase in beach slope and beach volume. The direction of longshore sediment transport from the northwest to southeast is also shown. However, overall the beach volumes were found to be insufficient to significantly influence recession rates.

8.5 Headland Formation and Evolution

8.5.1 Intertidal Platform Formation

The hypothesis outlined in Section 2.3 proposes that localised elevations in intertidal shore platforms are responsible for the formation of the subtle headlands seen on the southwest coast. Therefore it is critical to first identify the controls on these variations in platform elevation. The results of the geological and geotechnical assessments indicate that the mass properties of the rock are a significant factor (Section 4.3.3). The loss of tensile strength during saturation of the poorly cemented sandstones of the Ferruginous Sand and the Atherfield Clay Formations has led to their rapid disaggregation in the intertidal zone. The fissile nature of the Vectis Shales promoted their erosion when submerged. In contrast, the massive properties of the Wessex Mudstones and Perna Clays allow the formation of extensive shore platforms.

Another influence on the platform-forming potential of the material is the clay content and mineralogy of the beds. It is presumed that the potential of a rock to form a shore platform is reduced with an increase in clay content and the

proportion of swelling clays therein. Results from this study have shown that the Wessex Mudstones and Perna Clays have lower clay content than the Atherfield Clays and the Vectis Shales (Figure 4.22). The results for the Wessex and Vectis Formations are supported by the work of Rust and Gardener (2002) who recorded higher clay content in the shales than the mudstones. They also analysed the clay mineralogy and found a higher proportion of swelling clays in the shales, a result not supported by the results of this study (Section 4.4.2). The small sample size of both studies and the natural variability within the beds means it is not possible to make any firm conclusions without further sample analyses.

The geometry of the beds is also important. The angle at which these beds dip is critical to the increased elevation in the shore platform and cliff/platform junction. Wright (1970), in a study of the shore platforms of southern England found that the influence of structural control on the elevation of the junction was only observed in areas where the dip of the beds did not exceed 8°. Above this angle, undercutting of the platform occurs and the jointing of the bed is the significant control on wave erosion. In addition to the dip, the orientation, or strike, of the bed in relation to the coastline and its prevailing wave conditions will also be important. These factors, combined with the resistance to erosion of the underlying beds, will control the undercutting of the platform (Figure 8.2). Greater undercutting of the platform will reduce its elevation.

For example, a platform where the underlying geology is weak and exposed to the full force of the waves will be undercut faster, reducing its stability as shown in Figure 8.2 b and c. This is observed with the Barnes High Sandstone, a coherent bed that fails to form a substantial intertidal platform due to the weakness of the surrounding shales despite its low angle of dip (2-3°) and strike at close to 90° from the coastal orientation and prevailing wave direction. While a platform where the underlying geology is reasonably resistant and due to its orientation to incoming waves, is sheltered, the platform will have greater stability (Figure 8.2 a and d). This is seen in the relationship between the Perna Sandstone and underlying Perna Clays. The Perna Clays provide support to the overlying sandstone beds due to their massive structure that would not be provided by the Vectis Shales below.
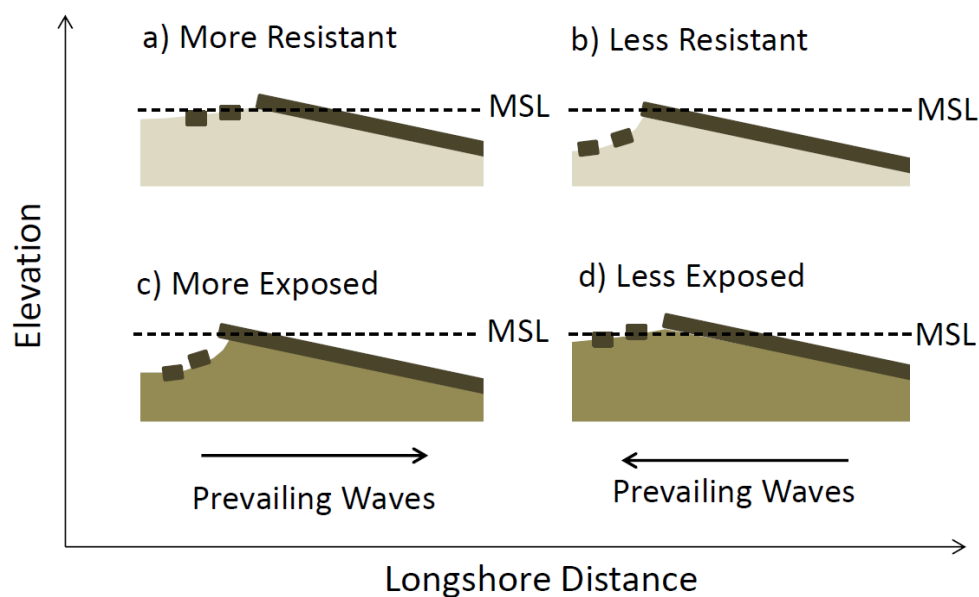
Figure 8.2: Controls of platform elevation related to the resistance of underlying beds (a and b) and the exposure to wave energy (c and d).

The thickness of the beds and their joint spacing is another factor. The closer the joint spacing the more susceptible a platform bed is to erosion, with the joints representing points of weakness that can be utilised by waves. Kennedy and Dickson (2006) found that the elevation of the jointed platforms were lower than those composed of broadly similar, but unjointed geology. This is supported by the findings of this study with the massively bedded marls forming intertidal platforms, but the fissile shales fail to do so. Joint spacing is also important when considering the fate of the resistant, platform forming unit, once it has detached from the main bed. If the joint spacing is such that the blocks produced by erosion are too large to be washed away under the prevailing wave condition they will remain in place protecting the underlying beds from erosion. This can be observed with the calcareous sandstone of the Perna Beds at Atherfield Ledge. The next section considers how, once formed, these intertidal platforms can lead to the formation of a subtle headland.

8.5.2   Headland Formation

The hypothesised mode of headland formation proposed in Figure 2.7 was based on the conceptual model of cross-shore interactions described in Figure 2.4. This model of interactions was designed as a generic overview of coastal processes, including the influence of beaches, surficial sediment, shore platforms and recent

recession rates. The results of this study indicate that for the southwest Isle of Wight the beaches are of insufficient volume to significantly influence recession rates on the coastline (Section 6.1 and 7.2.3). The area of cliff behind Ship Ledge has been identified as a potentially forming headland. Although a poorly defined feature on a map, in the field this potential headland is readily identified. It represents an opportunity to test the hypothesis of headland formation outlined in Figure 2.7. The hypothesis states that the potential influences of a localised intertidal platform will be three fold:

- Firstly by reducing the amount of wave energy reaching the cliff base, thus reducing local cliff recession rates (Stephenson and Kirk, 2000) (Figure 2.7.a).

- The second may counteract the first by increasing the wave energy directed at the cliff base due to refraction, the balance between these two effects will determine if a headland will grow, be maintained or decline (Figure 2.8).

- Thirdly by blocking longshore transport of beach sediment, building a protective beach up-drift, while starving the downdrift coast of sediment, potentially accelerating erosion in the manner of terminal groyne syndrome (Brown, 2008, Brown and Barton, 2007) (Figure 2.7.b).

The hypothesis described above dictates that the lowest rates of recession will be seen directly behind the intertidal platform, the highest rates will be down drift where the beach is starved of sediment and the rates updrift will be intermediate. The results of Chapter 6 indicate that beach volumes have been insufficient to influence recession rates over the last 145 years. This does not rule out the possibility that variations in beach volumes had an influence on the formation of the established headlands. It does however imply that any signs of headland formation recorded within the study period should not be influenced by beach volumes.

Ship Ledge and the surrounding cliffs are part of the Wessex Formation. Around the ledge no variation in the cliff geology or coherence is seen, but a clear increase in platform coherence and elevation is observed (Figure 4.20). The increase in coherence and platform elevation is thought to be related to an increase in silt content and cementation of the mudstones. The dip of the beds at Ship Ledge is 2

to 3° towards the south east and is more likely to represent the plunge of the anticline than the dip of the limb itself (Figure 4.11). There is some evidence of an increase in wave energy density to the south of Ship Ledge under common wave conditions (Figure 5.3). The beach width remains constant across the front of Ship Ledge (Figure 6.8a), and while the BWA drops at Ship Ledge itself the levels increase to the north and south at a similar rate (Figure 6.9b).

The results of cliff top recession rates between 1866 and 2012, averaged for the area behind the platform and the 300m stretch of coast up and down drift of it replicate the pattern predicted by the conceptual model (Figure 7.21a: Figure 2.7). The cliff base recession rates between 1866 and 2011 averaged for the same areas as for the cliff top do not show the same pattern, but a steady increase in recession rate from downdrift to up drift (Figure 7.21b). Although the pattern of cliff top recession is consistent with the hypothesised model of headlands formation on a soft cliff coast, the configuration of the beach is not. The increased exposure to wave energy down drift seen in the results of the wave refraction modelling (Figure 5.2), caused in the conceptual model by variation in beach level is achieved though the loss of the intertidal shore platform down drift of the ledge and the inland shift of the 2m depth contour. So although the variations in exposure are the same, the mechanism for those variations is different. This supports the argument that beach volumes are insufficient to influence recession rates.

The future of the headland that appears to be forming behind Ship Ledge is unclear. The extent of the intertidal platform and its persistence as the cliff erodes are unknown. If recession rates continue in the same configuration the set back of the coast down drift of Ship Ledge will continue to grow. The higher rates of recession seen behind the platform compared to updrift will reduce the prominence of the headland viewed from updrift. However due to the high rates of recession down drift of the headland the overall effect will be a sharp change in the orientation of the coastline at Ship Ledge, which, like at Hanover Point can be interpreted as a headland. For the three established headlands on the southwest coast direct evidence of their mode of formation does not exist although there is cartographic evidence that they have persisted for 400 years (Section 7.1). Indirect evidence from the current coastal planform, beach and platform configuration can be interpreted to make an educated guess as to their mode of formation. As with Ship Ledge the change in the orientation of the coastline at Hanover Point is most

prominent in the down drift section indicating that the rates of erosion downdrift were higher during the formation of the headland. Hanover Point displays the beach configuration predicted in Figure 2.7, with a wide beach (Figure 6.8a) and large BWA (Figure 6.9b) updrift of the platform compared to the area down drift. In this sense Hanover Point can be considered to act as a partial transport barrier. The location of Brook Chine at the head of Brook Bay may have enhanced the down drift erosion around Hanover Point. The drop in platform width and elevation in that area (Figure 6.8b and Figure 6.9a) appears to be related to down cutting by the outflow from Brook Chine, which in the past was significantly larger than it is today (Flint, 1982). The bending of the anticline axis around Hanover Point changes the exposure of the sandstone beds in the platform and cliffs (Figure 4.10 and Figure 4.3a). The loss of supportive sandstones beds down drift of Hanover Point with the change in coastline orientation relative the fold axis may have also enhanced the down drift recession.

The broad rounded nature of Sudmoor Point means it is not possible for this headland to have formed in the way described in Figure 2.7. The wide horizontally bedded platform and smooth change in coastal orientation does not have the capacity to block sediment transport. The low inputs of beach grade sediment, the partial barrier to sediment transport updrift in the form of Hanover Point and the low sediment storage capacity of the platform in this area means it is unlikely that beach sediment has played any part in the formation of this headland. The extent and elevation of the intertidal platform and the stabilisation of the cliff though the support of the Sudmoor Point Sandstone are the most important factors in the formation and continued growth of this headland.

Atherfield Point is unique on this coastline in that the lithology of the cliff is different updrift and down drift of the headland. All other headlands and platforms fall entirely within the Wessex Formation; Atherfield Point involves the Vectis, Atherfield Clay and Ferruginous Sand Formations. In terms of the narrow cross-shore extent of the shore platform, Atherfield Point most strongly resembles the conditions described in the model (Figure 2.7). There is evidence that Atherfield Point act as a partial barrier to sediment transport, specifically for gravels, although there is a slight increase in beach width from north to south of Atherfield Ledge (Figure 6.8a). The BWA drops to almost nothing at the headland itself,

increasing abruptly either side, with the largest values seen updrift of the headland (Figure 6.9b).

The steep shoreface observed in Chale Bay due the disaggregation of the Ferruginous Sands when saturated causes the increase in wave energy reaching the shoreline down drift required for headland formation. Unlike Hanover Point and the headland forming behind Ship Ledge the change in orientation is equally apparent on the updrift and down drift side of Atherfield Point. This is likely to be related to the inability of the Vectis Shales to create intertidal platforms creating a relatively steep shoreface up drift of the headland as well as down drift and the uniform beach levels on both sides of the headland.

8.5.3   Headland Evolution

There are several aspects of headland evolution to be considered. These are the mode of headland erosion, the controls on the growth and decline of headlands once formed, and the migration of the headlands with continued erosion or sea-level rise. Each will be addressed in turn, referring back to the original hypothesis related to them.

8.5.3.1   Headland Erosion

As outlined in Section 2.2.1, two contrasting models have been developed in the wider literature to describe the way headlands erode. Both are based on the theoretical distribution of wave energy. The first by May and Tanner (1973) is based on the sediment transport potential as driven by longshore variations in wave energy distribution. Sediment will be transported from an area of high wave energy, to an area of low wave energy, i.e. from the headland to the bay head. This model assumes that where the change in the rate of sediment transport is greatest the erosion potential will be at its maximum level. That maximum potential is on the flanks of the headland leading to the formation of a needle like promontory. The headland is thought to act as a divide to sediment transport and as such has the lowest transport and erosion potential (Figure 2.5).

The second model developed by Komar (1985) hypothesised that the maximum erosion would occur where the maximum wave energy was found, which due to wave refraction, is at the headland itself. The headland was not necessarily viewed as a transport divide so eroded material would be carried away leading to the

formation of a subdued headland. The changes in the form of the declining headlands of Hanover and Atherfield Points shown Figure 7.27 and 7.18 respectively indicate that on the southwest coast the mode of erosion most closely resembles that described by the Komar (1985) model. Between 1866 and 2011 the apex of both headlands became less pronounced. This indicates that although the headlands act as a partial divide to sediment transport the divide is not absolute and the May and Tanner (1973) model is not appropriate.

8.5.3.2 Headland Growth and Decline

The hypothesis presented in Section 2.4 states that the fate of a headland once formed is controlled by the balance between wave refraction and wave attenuation over its intertidal shore platform (Figure 2.8). The results of the wave refraction modelling show that under common wave conditions (i.e. wave that occur 35 times in 1 year or once every 10.4 days) wave energy density at the coastline peaks at Hanover and Atherfield Point and either side of the apex of the wide round headland at Sudmoor Point. These peaks indicate areas where refraction will outweigh attenuation on a regular basis leading to increased exposure of the cliff toe. The long-term recession rates indicate that those headlands exposed to increased wave energy density, i.e. Hanover and Atherfield Points, are the headlands in decline. However Sudmoor Point which does receive increased wave energy densities is growing. In fact the peaks in wave energy at Sudmoor Point exceed those seen at Hanover Point so it is not solely waves influencing recession rates. Further consideration of the geology of the cliffs and platforms, in terms of platform resistance and hence elevation and cliff strength and hence resistance to erosion is required to understand these inconsistent results.

The extensive platform around Hanover Point is ridged with frequent channel sandstones, there is a clear east west strike and the dip is approximately 20° to the north. The extensive deposits of fossilised trees, known as the 'Pine Raft', that once dominated the shore platform have all but disappeared; potentially removing some protection once afforded to the headland. This removal of the Pine Raft over time may have contributed to the decline of this headland. The localised nature of the platform sandstones are related to the fluvial depositional environment, the sandstones are channel fills and as such are laterally discontinuous. The future of Hanover Point is dependent on the persistence of these beds. Once the current

platform beds are eroded away by marine processes the headland will decline rapidly unless further platform forming beds are revealed as cliff recession continues.

Sudmoor Point is a broad rounded headland fronted by a predominantly mudstone platform of fairly consistent intermediate coherence. The dip of the beds is close to horizontal and they form a wide flat shore platform along the length of the headland. The cliffs at Sudmoor Point are dominated by the sandstone of the same name, which provides stability in contrast to the compound landsliding at Roughlands and near Chilton Chine on either side of its exposure. The Sudmoor Point Sandstone also provides protection to the cliff base as large blocks of sandstone cover the beach across much of its exposure. The protection and stability provided by the Sudmoor Point Sandstone may explain the continued growth of the headland over the past 145 years despite the concentration of wave energy seen under common wave conditions.

Finally, the decline of Atherfield Point correlates with the increase in wave energy reaching the coastline in that area. Consideration of changes in lithology at Atherfield Ledge does however reveal a reduction in the thickness of the Perna beds which form the intertidal platform over the study period due to the natural lateral variability in bed thickness. This decrease may be contributing to the decline of the headland.

8.5.3.3   Headland Migration

The hypothesis outlined in Figure 2.9 describes the longshore migration of headlands over time as recession of the cliff proceeds. The theory assumes that lithology controls the platform geomorphology and is based on the angle between the strike of the platform forming bed and the orientation of the coastline. The further from 90° this angle is, the faster the migration of the headland will be. If the angle is less than 90° then migration is expected to be updrift, while over 90° the expected direction of migration is down drift. On this basis Hanover Point was expected to migrate downdrift at a rate of 1.3 m per meter retreat, totalling 193 m over the 145 year study period. In reality the migration recorded was 5m updrift.

This lack of migration may be related to the extensive nature of the shore platform, and the angle of the strike to coastal orientation being less than 45°. The conceptual model needs revising for these situations, where the width of the shore

platform relative to the coastal orientation, is greatest up drift of the location where the platform bed cuts across the cliff base. Since the orientation of the coastline is broadly speaking at right angles to the direction of wave approach the width of the platform relative to that line gives a good indication of the protection afforded by the platform.

The strike of Atherfield Ledge relative to the coastal orientation is 90°, therefore no migration was expected and only a small distance of 17m was measured. In terms of the scale of the headland 17m can be considered an insignificant distance. This result supports the hypothesis that no headland migration will occur when the strike of the platform is perpendicular to the orientation of the coastline. The results around Hanover Point however suggest that there is an angle beyond which the strike of the platform does not directly control the migration of the headland due to the greatest seaward extent of the bed being up or down drift of the location that it crosses the cliff base. It can be argued that this is true at all angles of strike as when the strike is at 90° to the coastline, the maximum width of the platform relative to the coastline is at the apex of the headland.

Over the study period no significant migration of the headlands was measured. This implies that at an engineering timescale and under current rates of sea level rise headland migration is of no concern to coastal managers. Rises in sea level, shifting the location of intertidal platforms, or changes in the exposed geology through continued recession may influence headland migration. Migration of headlands is likely to occur over a geological time scale as it is controlled by variations in geological outcrops, however due to the complex nature of the structural geology and laterally inconsistent nature of the sandstone beds it will be difficult to predict how the headlands will migrate in the future without detailed geological investigation including landward of the cliff face and numerical modelling.

8.6   Lessons Learned

The dominant control on the formation of subtle headlands as seen on the southwest coast of the Isle of Wight is the geological and geotechnical properties of the shore platform. The location of Brook Chine seaward of its current position may have enhanced the erosion of Brook Bay. The current volumes of beach sediment

are insufficient to influence recession rates; the results of the sediment budget suggest that this situation is not likely to have been different in the past. However, a decrease in the input of gravel from the cliff over the past 150 years was indicated by the diminishing thickness of valley gravel deposits topping the cliff. Hence, beach volumes may have declined with time.

The evolution of the headlands is controlled by the persistence of the shore platforms, the stability of the headland cliffs and the concentration of wave energy directed towards them. Again the beach volumes do not appear to have any influence on headland evolution. The mode of headland erosion observed on the southwest coast matches the model devised by Komar (1985), with the headlands of Hanover and Atherfield Point becoming increasingly blunted over the study period. Migration of the headlands does not appear to be controlled directly by the strike of the platform in relation to the coastal orientation but by the width of the platform relative to the coastline orientation.

8.6.1   Lessons for the Isle of Wight

This project has provided a number of insights into the controls of cliff recession and coastal planform evolution on the southwest coast of the Isle of Wight. For instance the beach volumes were shown to be insufficient to significantly influence recession rates, despite Hanover and Atherfield Points acting as partial transport barriers. The dominant controls on recession rates and the formation of subtle headlands are the geological and geotechnical properties of the shore platform and cliff base. The evolution of the headlands is controlled by the balance of wave refraction and attenuation, and the persistence of the platform forming beds. The results of the study also show that over a century timescale (i.e. a coastal management/SMP timescale) at least, headland migration does not occur.

In terms of the SMP management strategy of the southwest Isle of Wight these findings have minimal implications. The current strategy of no active intervention will remain appropriate due to the low value of the cliff top in general and it's designation as an Area of Outstanding Natural Beauty (AONB) and a Special Area of Conservation (SAC). However there are locations along the cliff top where property or infrastructure is at risk (Figure 8.3). The A3055 (Military Road) near Hanover Point is the major current example.

Figure 8.3: Location of Infrastructure, amenities and properties along the south west coast of the Isle of Wight (Image taken from Google Earth)

Although the official line is for no active intervention for the coastline, the Military Road represents an important tourist route around the coast with significant economic benefits. Therefore, where a recent landslide threatened the road in Brook Bay, drainage works have been put in place to slow the cliff top recession and extend the life of the road on its current route.

Other areas of economic value are the Brighstone Holiday Centre, Isle of Wight Pearl, Grange Farm and Chine Farm Campsites and the Coastguard Cottages at Atherfield Point (Figure 8.3). A better understanding of the controls on the coastal system and drivers of future change will improve predictions of recession rates. This will allow the local council, business owners and homeowners and insurance companies to make well informed decisions on the future of infrastructure and business plans.

For this coastline, the drivers of future change are strongly related to changes in the lithology outcropping at the cliff face and in the intertidal zone. For example, the reduction in the platform elevation around Hanover Point due to the erosion of the 'Pine Raft' may lead to continuing increases in recession rate at the headland in the future. Equally, the persistence of Ship Ledge as an intertidal platform will control the development of the headland behind it. As recession continues across the study frontage more resistant beds may be revealed leading to localised reduction in recession rates in different areas.

As well as changes in the exposed lithology through recession processes, predicted increases in sea level will have an influence. Rising sea levels will shift the intertidal zone upwards changing the intertidal geological exposure. This will have an influence on recession rates around all the headlands. For Hanover Point where the loss of the 'Pine Raft' may have already reduced the platform elevation relative to sea level, this increase will be of particular significance. For all headlands there is likely to be a rapid increase in recession rates with sea level rise through a reduction in attenuation allowing a greater proportion of wave energy to reach the cliff base. That is until a new equilibrium is reached. The influence of changing sea levels and geological exposure are explored in generic terms in Section 9.2.

8.6.2   Lessons for other sediment-starved coastlines

The final objective of this project was to consider the generic applications of this information for other coastlines (Section 1.3.2). The wider implications for the findings of this thesis are considered here. The main contribution is related to the improved understanding of longshore interactions between waves, beaches and platforms on coastlines with variable cliff base and platform strength. The results can be used to improve prediction of future patterns and rates of recession on the southwest coast of the Isle of Wight and other coastlines with variations in geological strength. Understanding the influence of shore platforms, how and why they form and evolve is of great importance. It highlights the need for detailed geological investigation on coastlines with variations in geological strength. Complex cliff face geology leads to variations in recession rate as cliffs retreat, so even with constant sea levels, erosion rates may vary with time. Therefore, a simple projection of historical recession rates will not adequately describe this process.

These results also provide an insight into the long-term evolution of a coastline and in particular the influence of underlying geology on a sediment-starved system. A sediment-starved coastline can be defined as a coastline where the sediment supply is insufficient to build up protective beaches capable of regulating recession rates. There may be a threshold value of BWA which defines a sediment-starved coastline, but this is likely to vary from coastline to coastline depending on wave conditions and beach grain size. For example in the results of Lee (2008) this value is thought to be around 20 m^2. However the results of (Quinn et al., 2010) see an influence on recession rate with BWA as small as 3$m^3\,m^{-1}$. The BWA of the southwest coast shows no relationship with recession rates and varies between 1 and 33 $m^3\,m^{-1}$.

Unlike the model described by Valvo et al. (2006) and Limber and Murray (2011), where the longshore distribution of sediment regulates recession rates and an equilibrium coastal configuration will develop, here locally elevated intertidal shore platforms control the position and evolution of subtle headlands and coastal indentations. These variations in platform elevation are controlled by the structural geology and erosional resistance of the platform forming beds. Due to the complex laterally variable nature of the geological exposure the coastal configuration of these coastlines exists in a state of dynamic equilibrium.
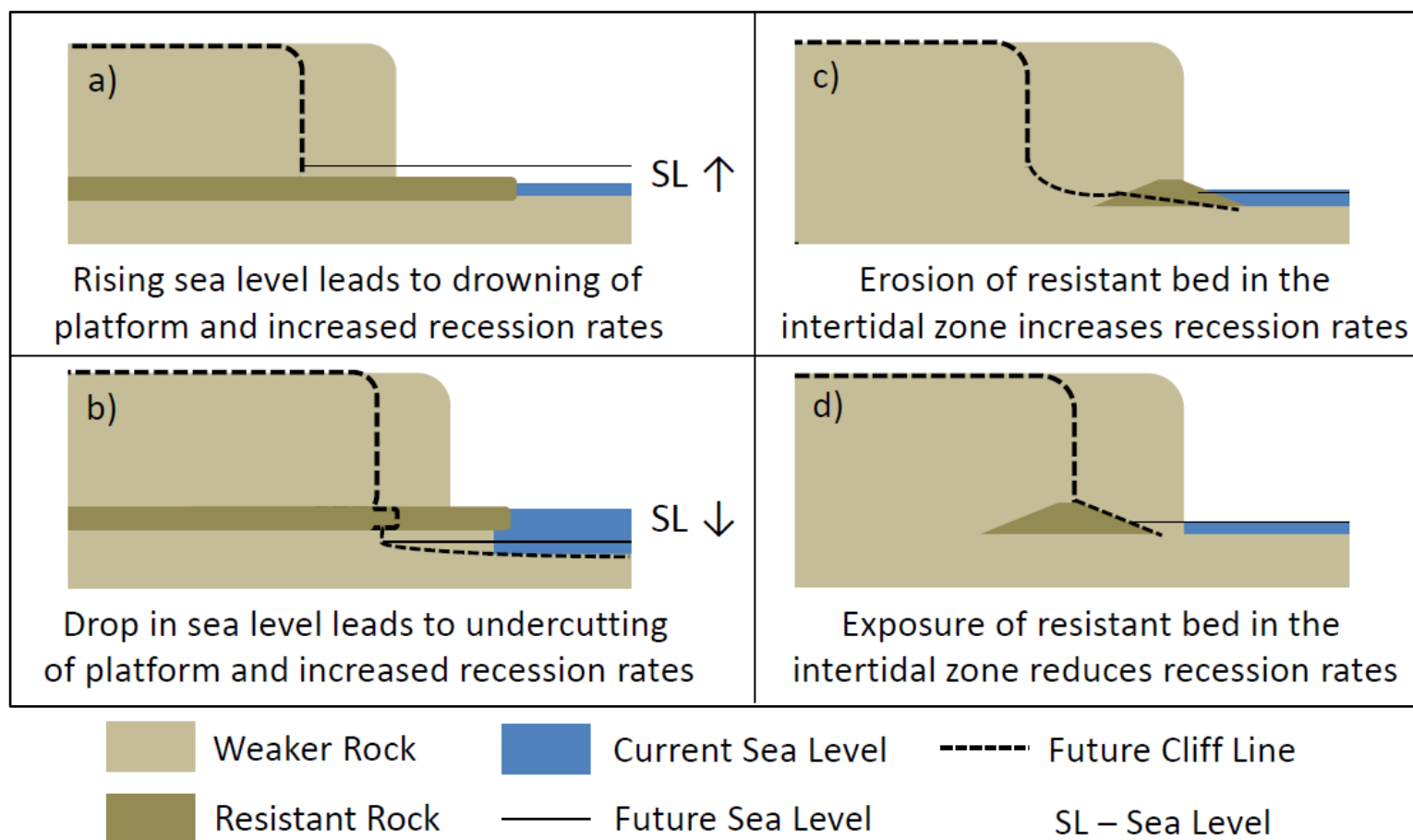
Figure 8.4: Schematic showing illustrative examples of the potential impact of a number of scenarios on recession rate. The influence of changing sea levels on a coastline protected by a horizontal shore platform is shown in panel a and b. While the impact of laterally discontinuous but relatively resistant beds on recession rates are shown in panel c and d.

Any changes in the system, such as a change in sea level or exposed cliff face lithology will disrupt that dynamic equilibrium potentially leading to rapid changes in recession rates. Idealised examples of these changes informed by the southwest coast of the Isle of Wight are displayed in Figure 8.4. Panels a and b within Figure 8.4 show two of the potential influences that changes in sea level could have on recession rates on a coastline where a thin, but resistant horizontally bedded platform exists in the intertidal zone.

An increase in sea level will drown the platform reducing the protection provided to the cliff behind, resulting in an increase in recession rates (Figure 8.4a). Alternatively a drop in sea level would remove the platform bed from the intertidal zone; the weaker material below will be eroded leading to undercutting of the platform. This may be initially marked by a decrease in cliff top recession rates as the former cliff base is no longer being eroded, but would be followed by a subsequent increase in recession rates when the undercutting of the platform catches up with the cliff line. Equally if a change in sea level brings a resistant bed into the intertidal zone which forms a protective platform the recession rates are likely to fall.
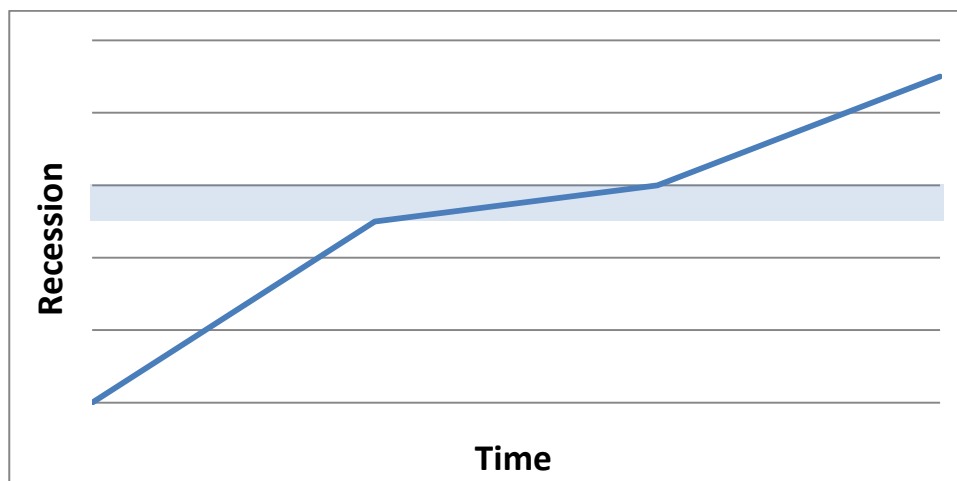
Figure 8.5: Expected changes in recession rate as a resistant bed passes through the intertidal zone due to a constant sea level rise (Figure 8.4 a and b), or exposure of a laterally discontinuous bed as erosion continues (Figure 8.4 c and d). The shaded blue area marks the period when the resistant bed crosses the intertidal zone.

The hypothetical changes in retreat rates as sea level rises from below to above a more resistant bed are shown in Figure 8.5. The rate of retreat at each stage is influenced by the location of the resistant platform forming bed. The lowest rates of retreat occur when the resistant bed inhabits the intertidal zone, as indicated by

the shaded area in Figure 8.5. When the water level is below the resistant bed, undercutting occurs and the bed offers little protection, therefore recession rates will be at their highest. However when the water level is above the resistant bed, although the bed is no longer in the intertidal zone the shoreface slope is likely to be shallower, so some attenuation of wave energy will occur producing an intermediate retreat rate.

An example of an area where these changes may occur can be seen at Forelands on the eastern end of the Isle of Wight, where the Bembridge Limestone occupy the intertidal zone (Figure 8.6).

Figure 8.6: Aerial photograph of the Bembridge headland (Source: Google Earth) and inset showing the Bembridge Limestone platform (Source: www.ukfossils.co.uk)

The influence of the emergence or erosion of a laterally discontinuous bed of more resistant platform forming material on recession rates is explored in Figure 8.4 c and d. Localised beds can form a platform and successfully reduced recession rates to form a headland, but once the recession has proceeded past them and the platform elevation is continually lowered over time their influence fades and recession rates will increase until a new dynamic equilibrium is reached (Figure 8.4 c).

This situation is a possibility for Hanover Point on the Isle of Wight and Ringstead Ledge in Dorset (Figure 8.7). Conversely the emergence of a resistant bed in the

intertidal zone as a cliff retreats will reduce recession rates (Figure 8.4d). The changes in retreat rates described in Figure 8.5 would also occur as cliff retreat reveals and subsequently erodes a laterally discontinuous, but more resistant bed, in the intertidal zone. The intermediate recession rate, in this case would be due to wave attenuation over the remaining portion of the resistant bed reducing the shoreface slope.

Figure 8.7: Aerial Photograph of Ringstead Ledge submerged by the tide (Source: Google Earth) and inset showing Ringstead Ledge exposed at low tide (Source: Alex McGregor, www.geograph.org.uk).

For coastlines with complex cliff lithology of variable strength and structure and with sea levels predicted to rise by up to 1 m by 2100 (IPCC, 2013) the potential for these rapid changes in recession rate must be considered. In reality coastlines are not either sediment-starved or sediment rich but a continuum exists between the two. At one end the dominant control on recession rates and planform evolution is the beach morphology and at the other the dominant control is the variations in cliff face and platform lithology.

8.7   Further Work

Following on from this project, four main areas have been identified requiring further research. These include: 1) a detailed field based study of the platform,

beach and wave interaction (Section 8.6.1); 2) further consideration of the geotechnical properties of the shore platform (Section 8.6.2); 3) the application of this knowledge to other sites around the Isle of Wight and the south coast of the UK (Section 8.6.3); and 4) the potential for artificial platforms to be used as a novel mode of coastal protection (Section 8.6.4). Each of these research areas are explored in more detail below.

8.7.1   Platform-Beach-Wave Interactions

The interactions between the platform, beach sediment and waves are fundamental to the understanding of this system. To further the understanding of the influence of shore platforms along this coastline a detailed field study would be required. Detailed mapping of the platform and beach elevation could be carried out using terrestrial laser scanners, to gain an understanding of how the beach elevations interact with the platform elevations. This will determine if the low beach volumes are solely due to the low input of sediment and the shore platforms acting as natural barriers to sediment transport or in some way related to the elevation of the platform occupying the equilibrium beach profile. Field measurements of wave energy variations across the platform and beaches will give a clearer indication of the impact of the platforms on wave refraction and attenuation. It will also help to develop a better understanding of longshore sediment transport rates and direction, particularly the reversals seen around the headlands by Rix (2000). Measurements of longshore variations in wave energy will also give an insight in to the mechanisms of headland erosion in terms of the May and Tanner (1973) and Komar (1985) models. The timescale of these measurements would vary from hours for the wave attenuation study, to months or years for repeated surveys of platform and beach elevations. Data from CCO could be incorporated for the upper beach and potentially for the platform itself if LiDAR surveys were carried out at low tide.

8.7.2   Geotechnical Properties of the Shore Platforms

One of the findings of this thesis concerns the formation of intertidal platforms, and what controls the variations in their elevation. The conclusion was that it is related to their lithology, mass properties and geometry. These controls need to be considered in greater detail. The variation in elevation of a platform of similar

lithology would also be addressed. This would require sampling and analysis of the platform at numerous locations. Analysis of the grain size distribution, clay content and mineralogy and geotechnical properties (such as joint spacing and cementation) for all samples could be correlated to variations in platform elevation. The influence of sea water saturation on the chemistry and weathering processes of the lithology could be ascertained through comparison of cliff and platform samples of the same lithology.

8.7.3   Application of Knowledge to Other Sediment-Starved Cliffed Coasts

The knowledge and understanding of how intertidal shore platforms can influence recession rates could be applied to other coastlines that are more sensitive to changes in sea level rise. One potential area for study is Bembridge on the eastern end of the Isle of Wight (Figure 8.6). Currently Bembridge is protected by an extensive near horizontal intertidal shore platform, and represents the most eastern point of the Isle of Wight despite the cliffs behind the platform consisting of relatively weak Bembridge Marl. Due to the horizontal nature of the platform, the weakness of the overlying cliffs and the housing on the cliff top, this coastline is highly susceptible to increase in sea level as outlined in Figure 8.4a. Therefore further study on the impact of sea level rise in this area would be of interest to the Isle of Wight Council in terms of future shoreline management planning. Other areas of interest include Ringstead Bay (Figure 8.7) and Kimmeridge Bay in Dorset.

8.7.4   Engineering Potential of Artificial Platforms

An understanding of how these platforms influence recession rates could be used to develop a novel coastal defence strategy, where by artificial platforms are used to manipulate recession rates at specific locations. Their use would be ideal along coastlines with a high aesthetic and conservation value. Erosion would not be stopped, only slowed, allowing time for mitigations measures, such as relocation of cliff top infrastructure, to be executed. With further study the optimum intertidal elevation and cross-shore/longshore extent of a platform can be calculated for a required purpose; i.e. to reduce erosion without causing a major barrier to longshore sediment transport or to modify the shape of a coastline.

As yet no work has been carried out on the feasibility of installing artificial platforms as a mode of coastal protection, and that is beyond the scope of this project. Further research in the form of hydrodynamic and sediment dynamic modelling of shore platforms to understand how they reduce recession rates without influencing longshore transport would be required before this concept could be taken forward to the next stage. In terms of the design of such structures, issues of cost and practicality would need consideration. Especially in respect of the foundations since the link between the artificial structure and the underlying rock could prove a potential source of weakness. It is also possible to use a modified version of the SCAPE model to add artificial platforms to a coastline and investigate their potential influence (Carpenter et al., In Review-a, Carpenter et al., In Review-b).

9.   Conclusions

The aim of this research was to evaluate controls on headland formation and evolution on soft rock, cliffed coasts. A number of potential controls were identified including the geological /geotechnical properties of the cliff and platform, longshore variations in wave energy distribution and sediment volume and supply. The conclusions of this study will be outlined here in terms of the aim and objectives set.

The first objective was to determine the importance of longshore variations in shore platform and cliff lithology, in particular the influence of their geotechnical properties on local recession rates. It was found that the location of the headlands appears to be controlled by localised intertidal platform elevations; the increased elevation of these platforms is controlled by their lithology, mass properties and geometry. The geology was found to be the dominant control on cliff recession rates.

The second objective was to examine the longshore variations in near shore bathymetry and consider how those variations influence the distribution of wave energy along the shoreline. The near shore bathymetry was found to be strongly related to the sea bed geology, with localised increases in sea bed elevation coinciding with the location of more resistant geology. The distribution of wave energy is strongly influenced by these variations. Under common wave conditions refraction causes concentration of energy at and around the headlands. No correlation was found between wave energy and recession rates. The results indicate that the headland bay system is not a result of increased levels of wave energy producing the bays, but that the headlands persist despite concentration of wave energy towards them.

The third objective was to investigate the interactions between beach volumes, sediment budget and cliff recession rates, in the presence of intertidal shore platforms and the influence these features have on local recession rates. Currently, on the southwest coast of the Isle of Wight the beach volumes are insufficient to have a significant influence on recession rates. The results of the sediment budget suggest that this situation has persisted since the late 19th Century and will continue into the future. That said there is some evidence of changes in the gravel input to the coastline since then, with the extent of the valley gravels topping the cliffs decreasing by 65%, although the difference in sediment input is small in

absolute terms. It is not clear if the small beach volumes are solely due to the low sediment supply or the platforms taking up the shoreface mimicking the equilibrium profile form. However no statistically significant relationships were found between beach volumes, beach width or platform width and recession rates.

The fourth objective was to investigate how the factors outlined above influence headland formation and evolution through the refinement and testing of a number of conceptual process-based models. These included models of headland formation (Section 2.3 and 8.4.2), headland erosion (Section 2.2.1 and 8.4.3) and headland migration (Section 2.4 and 8.4.3). The hypothesised mode of headland formation is an idealised model, the nature and dimensions of the intertidal platform vary in reality and other factors including the presence of chines and changes in coastal orientation will influence recession rates. However the premise that the local elevations in shore platform elevations are responsible for the location and formation of the headlands has been supported by the findings of this project.

The declining headlands of the southwest coast are eroding in the way described by Komar (1985), with maximum erosion at the headland and the dulling of the point as erosion progresses. It appears that the migration of the headlands is controlled by the maximum width of the platform relative to the coastal orientation to the strike of the beds as hypothesised. Over a century timescale (coastal management/SMP timescale) migration of the headlands is not seen and therefore is of little concern to coastal managers. Over a millennia timescale (geological timescale) however, the migration of headlands will likely occur, along with the emergence and disappearance of headlands due to changes in the geological structure and lithology as the coast retreats and relative sea level changes.

The final objective was to consider the generic applications of this information for the management of the southwest coast and other coastlines. In terms of the management of the southwest coast the understanding of the coastal system developed in this thesis will improve predictions of future rates and patterns of retreat. For the management of other sediment-starved coastlines where the lithology of the intertidal zone is the dominant control on planform evolution, two areas of management application have been identified. Changes in sea level or the resistance of lithology exposed in the intertidal zone as recession continues has the potential to cause rapid changes in recession rate. This is of concern to coastal managers and requires detailed study of the geology of complex soft cliff coasts

with valuable cliff top infrastructure. There also exists the potential to develop a novel coastal defence strategy where artificial resistant platforms are used to manipulate recession rates.

The processes described here are probably quite common around the world's coast, but a lack of research in the published literature prevents us being more quantitative. Further study and synthesis would be useful.

Appendices

Appendix 1: XRD Methodology

XRD Methods Summary (Provided by R.Pearce of the NOC, Southampton)

The <2µm clay mineral fraction was separated according to Stokes Law, and the samples analysed using standard clay techniques after saturation with Mg^{2+} ions. Samples were run as air-dried (A/D), ethylene glycolated, and heated preparations (at 375ºC and 550ºC. Saturation with ethylene glycol (EG) confirms the presence/ absence of expandable clay phases, and heating to 550ºC assists with identification of chlorite and/ or kaolinite. The semi-quantitative analysis method for the clays was based on that detailed by Biscaye (1965), results are presented as closed sum calculations.

Precision values and detection limits for total clay of ±10-20% (of the amount present) are likely. Minerals quoted as present, but which are close to the detection limit should not be relied upon as an accurate record. The <2µm clay mineral data should indicate relative changes in clay contents (precision ±5-10%), but should not be relied upon as absolute clay concentrations without independent verification.

Samples were run on a PANalytical X'Pert pro diffractometer machine fitted with a Cu X-ray tube. The machine operating conditions were set at 35kV, 40mA utilising automatic slits and a step size of 0.02º 2θ at 1 second/ step.

Appendix 2: Cliff Talus Coherence
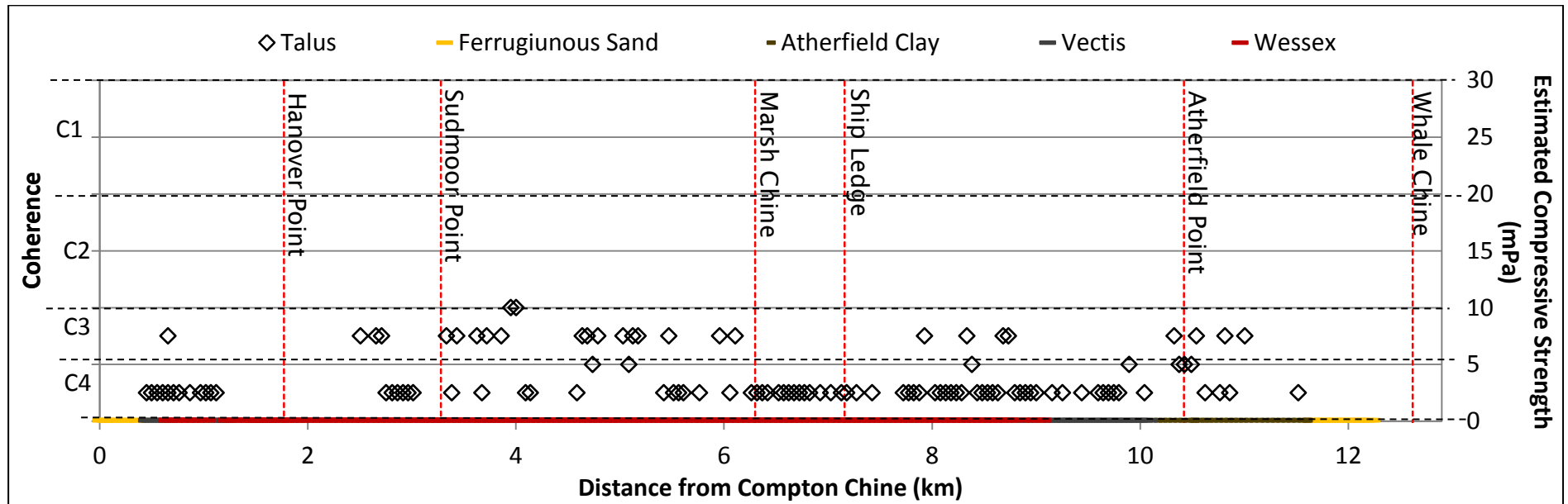
Figure A2.1: Coherence of talus at cliff base across the study frontage.
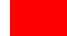
Appendix 3: Lithology Recession Statistics

Table A3.1: Summary Statistics of recession rates for each geological formation

Formation	Count	Sum	Average	Variance
Ferruginous Sands	85	41.01	0.48	0.01
Atherfield Clay	125	74.78	0.60	0.02
Vectis	154	93.15	0.60	0.02
Wessex	855	396.39	0.46	0.01

Table A3.2: Statistical significant of the variation between the means of the geological formations. The critical t value was 1.66

	Vectis	Atherfield Clay	Ferruginous Sands
Wessex	t stat: 12.73	t stat: 9.47	t stat: 2.15
Vectis		t stat: 0.38	t stat: 9.22
Atherfield Clay			t stat: 7.25

🟨 Means Statistically Different at the 95% Confinence Level
🟥 Means Not Statistically Different at the 95% Confinence Level

Appendix 4: Lithology either side of Hanover Point

Table A4.1: Statistical significance of the variations between the means of the geological formations north and southeast of Hanover Point.

t-Test: Two-Sample Assuming Unequal Variances	Ferruginous Sand Formation	
SIGNIFICANT	*Southeast*	*North*
Mean	0.52	0.36
Variance	0.00	0.00
Observations	64	21
Hypothesized Mean Difference	0	
Df	78	
t Stat	30.57	
P(T<=t) one-tail	1.79E-45	
t Critical one-tail	1.66	
	Atherfield Clay Formation	
SIGNIFICANT	*Southeast*	*North*
Mean	0.63	0.36
Variance	0.02	0.00
Observations	111	14
Hypothesized Mean Difference	0	
Df	119	
t Stat	19.83	
P(T<=t) one-tail	8.04E-40	
t Critical one-tail	1.66	
	Vectis Formation	
SIGNIFICANT	*Southeast*	*North*
Mean	0.63	0.28
Variance	0.01	0.00
Observations	144	10
Hypothesized Mean Difference	0	
Df	28	
t Stat	28.07	
P(T<=t) one-tail	2.38E-22	
t Critical one-tail	1.70	
	Wessex Formation	
INSIGNIFICANT	*Southeast*	*North*
Mean	0.47	0.46
Variance	0.02	0.01
Observations	132	723
Hypothesized Mean Difference	0	
Df	147	
t Stat	0.34	
P(T<=t) one-tail	3.67E-01	
t Critical one-tail	1.66	

Appendix 5: Cliff Behavioural Unit Recession Statistics

Table 5.1: Summary statistics of recession rates for each cliff behavioural unit

CBU	Count	Sum	Average	Variance
a) Steep Cliff with Talus at base	719	366.26	0.51	0.01
b) Compound Landslide	107	52.32	0.49	0.02
c) Steep cliff with high level sliding	215	96.47	0.45	0.01
d) Undercliff from Sepage Erosion	58	30.65	0.53	0.00
e) Mudslides	57	38.98	0.68	0.01
f) Large Scale Landslide with unknown structure	52	14.66	0.28	0.00

Table A5.2: Statistical significant of the variation between the means of the Cliff

Behaviour Units (CBU). The critical z value was 1.64

	CBUb	CBUc	CBUd	CBUe	CBUf
CBUa	z value: 1.47	z value: 7.63	z value: 3.28	z value: 11.15	z value: 26.37
CBUb	N/A	z value: 2.69	z value: 2.83	z value: 9.68	z value: 13.50
CBUc		N/A	z value: 10.00	z value: 14.19	z value: 16.34
CBUd			N/A	z value: 9.92	z value: 28.48
CBUe				N/A	z value: 10.00
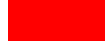
Means Statistically Different at the 95% Confinence Level
Means Not Statistically Different at the 95% Confinence Level

Appendix 6: Coherence Recession Statistics

Table A6.1: Summary statistics of recession rates for cliff coherence levels

Coherence	Count	Sum	Average	Variance
C4	5	1.89	0.38	0.00
C3	7	4.32	0.62	0.02
C3/C2	10	4.77	0.48	0.01
C2	108	55.66	0.52	0.01
C2/C1	7	3.65	0.52	0.01
C1	5	2.68	0.54	0.05

Table A6.2: Statistical significant of the variation between the means of the cliff coherence levels. The critical t value varied between 1.77 and 2.13.

	C3	C3/C2	C2	C2/C1	C1
C4	t stat: 3.82	t stat: 2.46	t stat: 5.66	t stat: 3.72	t stat: 1.51
C3		t stat: 2.06	t stat: 1.71	t stat: 1.43	t stat: 0.70
C3/C2			t stat: 1.06	t stat: 0.94	t stat: 0.54
C2				t stat: 0.18	t stat: 0.19
C2/C1					t stat: 0.13

Means Statistically Different at the 95% Confinence Level

Means Not Statistically Different at the 95% Confinence Level

Appendix 7: Hanover Point Recession Statistics

Table A7.1: Summary stats of cliff top recession rates around Hanover Point

Cliff Top	Count	Sum	Average	Variance
Updrift (600-300m)	300	160.99	0.54	0.014
Updrift (300-0m)	300	192.10	0.64	0.003
Hanover Point	200	134.57	0.67	0.003
Updrift (0-300m)	300	127.28	0.42	0.005
Updrift (300-600m)	300	144.60	0.48	0.004

Table A7.2: Statistical significant of the variation between the means of the cliff top recession rates around Hanover Point. The critical z value was 1.64.

Cliff Top	Updrift (300-0m)	Hanover Point	Downdrift (0-300m)	Downdrift (300-600m)
Updrift (600-300m)	z value: 4.73	z value: 25.01	z value: 4.30	z value: 3.54
Updrift (300-0m)		z value: 29.73	z value: 9.96	z value: 3.00
Hanover Point			z value: 28.83	z value: 46.28
Updrift (0-300m)				z value: 14.47

Table A7.3: Summary stats of cliff base recession rates around Hanover Point

Cliff Base	Count	Sum	Average	Variance
Updrift (600-300m)	300	143.01	0.48	0.001
Updrift (300-0m)	300	192.18	0.64	0.003
Hanover Point	200	141.34	0.71	0.001
Updrift (0-300m)	300	141.10	0.47	0.005
Updrift (300-600m)	300	127.51	0.43	0.003

Table A7.4: Statistical significant of the variation between the means of the cliff base recession rates around Hanover Point. The critical z value was 1.64.

Cliff Base	Updrift (300-0m)	Hanover Point	Downdrift (0-300m)	Downdrift (300-600m)
Updrift (600-300m)	z value: 44.89	z value: 79.67	z value: 1.42	z value: 14.15
Updrift (300-0m)		z value: 17.06	z value: 32.97	z value: 48.21
Hanover Point			z value: 50.77	z value: 72.72
Updrift (0-300m)				z value: 8.77

Appendix 8: Sudmoor Point Recession Statistics

Table A8.1: Summary stats of cliff top recession rates around Sudmoor Point

Cliff Top	Count	Sum	Average	Variance
Updrift (600-300m)	300	100.42	0.33	0.004
Updrift (300-0m)	300	152.80	0.51	0.004
Sudmoor Point	300	87.38	0.29	0.006
Updrift (0-300m)	300	93.12	0.31	0.004
Updrift (300-600m)	300	120.88	0.40	0.008

Table A8.2: Statistical significant of the variation between the means of the cliff top recession rates around Sudmoor Point. The critical z value was 1.64.

Cliff Top	Updrift (300-0m)	Sudmoor Point	Downdrift (0-300m)	Downdrift (300-600m)
Updrift (600-300m)	z value: 33.81	z value: 7.53	z value: 4.72	z value: 10.78
Updrift (300-0m)		z value: 37.77	z value: 38.52	z value: 16.82
Sudmoor Point			z value: 3.31	z value: 16.35
Updrift (0-300m)				z value: 14.63

Table A8.3: Summary stats of cliff base recession rates around Sudmoor Point

Cliff Base	Count	Sum	Average	Variance
Updrift (600-300m)	300	123.28	0.41	0.003
Updrift (300-0m)	300	108.71	0.36	0.000
Sudmoor Point	300	105.53	0.35	0.001
Updrift (0-300m)	300	103.22	0.34	0.001
Updrift (300-600m)	300	117.24	0.39	0.002

Table A8.4: Statistical significant of the variation between the means of the cliff base recession rates around Sudmoor Point. The critical z value was 1.64.

Cliff Base	Updrift (300-0m)	Sudmoor Point	Downdrift (0-300m)	Downdrift (300-600m)
Updrift (600-300m)	z value: 15.11	z value: 16.20	z value: 18.31	z value: 4.93
Updrift (300-0m)		z value: 5.53	z value: 9.56	z value: 10.75
Sudmoor Point			z value: 2.99	z value: 12.34
Updrift (0-300m)				z value: 14.78

Appendix 9: Ship Ledge Recession Statistics

Table A9.1: Summary stats of cliff top recession rates around Ship Ledge

Cliff Top	Count	Sum	Average	Variance
Updrift (600-300m)	300	67.65	0.23	0.01
Updrift (300-0m)	300	75.68	0.25	0.01
Ship Ledge	200	69.68	0.35	0.005
Updrift (0-300m)	300	117.75	0.39	0.03
Updrift (300-600m)	300	120.02	0.40	0.02

Table A9.2: Statistical significant of the variation between the means of the cliff top recession rates around Ship Ledge. The critical z value was 1.64.

Cliff Top	Updrift (300-0m)	Ship Ledge	Downdrift (0-300m)	Downdrift (300-600m)
Updrift (600-300m)	z value: 2.87	z value: 14.19	z value: 13.95	z value: 15.94
Updrift (300-0m)		z value: 12.24	z value: 12.30	z value: 14.31
Ship Ledge			z value: 4.05	z value: 5.30
Updrift (0-300m)				z value: 0.59

Table A9.3: Summary stats of cliff base recession rates around Ship Ledge

Cliff Base	Count	Sum	Average	Variance
Updrift (600-300m)	300	130.54	0.44	0.001
Updrift (300-0m)	300	143.79	0.48	0.0004
Ship Ledge	200	109.51	0.55	0.002
Updrift (0-300m)	300	166.82	0.56	0.005
Updrift (300-600m)	300	178.37	0.59	0.002

Table A9.4: Statistical significant of the variation between the means of the cliff base recession rates around Ship Ledge. The critical z value was 1.64.

Cliff Base	Updrift (300-0m)	Ship Ledge	Downdrift (0-300m)	Downdrift (300-600m)
Updrift (600-300m)	z value: 20.44	z value: 30.78	z value: 27.04	z value: 50.42
Updrift (300-0m)		z value: 20.27	z value: 15.89	z value: 40.76
Ship Ledge			z value: 1.65	z value: 11.52
Updrift (0-300m)				z value: 7.97

Appendix 10: Atherfield Point Recession Statistics

Table A10.1: Summary stats of cliff top recession rates around Atherfield Point

Cliff Top	Count	Sum	Average	Variance
Updrift (600-300m)	298	186.36	0.63	0.010
Updrift (300-0m)	301	176.31	0.59	0.011
Atherfield Point	299	240.02	0.80	0.005
Updrift (0-300m)	300	196.12	0.65	0.003
Updrift (300-600m)	301	181.90	0.60	0.000

Table A10.2: Statistical significant of the variation between the means of the cliff top recession rates around Atherfield Point. The critical z value was 1.64.

Cliff Top	Updrift (300-0m)	Atherfield Point	Downdrift (0-300m)	Downdrift (300-600m)
Updrift (600-300m)	z value: 4.73	z value: 25.01	z value: 4.30	z value: 3.54
Updrift (300-0m)		z value: 29.73	z value: 9.96	z value: 3.00
Atherfield Point			z value: 28.83	z value: 46.28
Updrift (0-300m)				z value: 14.47

Table A10.3: Summary stats of cliff base recession rates around Atherfield Point

Cliff Base	Count	Sum	Average	Variance
Updrift (600-300m)	298	180.31	0.61	0.004
Updrift (300-0m)	301	210.53	0.70	0.001
Atherfield Point	299	234.18	0.78	0.001
Updrift (0-300m)	300	231.35	0.77	0.003
Updrift (300-600m)	301	202.40	0.67	0.002

Table A10.4: Statistical significant of the variation between the means of the cliff base recession rates around Atherfield Point. The critical z value was 1.64.

Cliff Base	Updrift (300-0m)	Atherfield Point	Downdrift (0-300m)	Downdrift (300-600m)
Updrift (600-300m)	z value: 23.06	z value: 43.51	z value: 34.32	z value: 15.04
Updrift (300-0m)		z value: 32.45	z value: 19.66	z value: 8.55
Atherfield Point			z value: 3.29	z value: 35.05
Updrift (0-300m)				z value: 24.20

List of References

AAGAARD, T., NIELSEN, J., JENSEN, S. G. & FRIDERICHSEN, J. 2004. Longshore sediment transport and coastal erosion at Skallingen, Denmark. *Danish Journal of Geography,* 104**,** 5-14.

AMIN, S. M. N. & DAVIDSON-ARNOTT, R. G. D. 1997. A statistical anaylsis of the controls on shoreline erosion rates, Lake Ontario. *Journal of Coastal Research,* 13**,** 1093-1101.

ANDERS, F. J. & BYRNES, M. R. 1991. Accuracy of shoreline change rates as determined from maps and aerial photographs. *Shore and Beach,* 59**,** 17-260.

ANDREWS 1990. Monk's Bay, Shingle beach replenishment, Technical Report, HR Wallingford.

ANFUSO, G. 2005. Sediment-activation depth values for gentle and steep beaches. *Marine Geology,* 220**,** 101-112.

BARRETT, M. G. 1985. Isle of Wight - Shoreline erosion and protection. *Paper to SCOPAC, Newport (Isle of Wight).*

BARTON, M. E. & COLES, B. J. 1984. The characteristics and rates of the various slope degradation processes in the Barton Clay cliffs of Hampshire. *Quaterly Journal of Engineering Geology and Hydrology,* 17**,** 117-136.

BENUMOF, B. T. & GRIGGS, G. B. 1999. The dependence of seacliff erosion rates, cliff material properties and physical processes, San DIego, California. *Shore and Beach,* 67**,** 29-41.

BIRD, E. 1997. *The shaping of the Isle of Wight,* Bradford on Avon, UK, Ex Libris.

BIRD, E. 2008. *Coastal Geomorphology: An Introduction* Chichester, UK, John Wiley and Sons, Ltd.

BRAMPTON, A. H., EVANS, C. D. R. & VELEGRAKIS, A. F. 1998. Seabed sediment mobility west of the Isle of Wight. London: CIRIA.

BRAY, M. J. 1997. Eposidic shingle supply and the modified development of Chesil Beach, England. . *Journal of Coastal Research,* 13**,** 1035-10349.

BRAY, M. J., CARTER, D. J. & HOOKE, J. M. 2004. Isle of Wight. *SCOPAC Coastal Sediment Transport Study.* University of Portsmouth.

BRISTOW, H. W. 1862. *The Geology of the Isle of Wight,* London, Longman, Green, Longman and Roberts.

BROWN, S. 2008. *Soft cliff retreat adjacent to coastal defences, with particular reference to Holderness and Christchurch Bay, UK.* PhD, University of Southampton.

BROWN, S. & BARTON, M. E. 2007. Downdrift erosion and frequency of coastal landsliding. *In:* MCINNES, R., JAKEWAYS, J., FAIRBANK, H. & MATHIE, E. (eds.) *Landslides and Climate Change - Challenges and Solutions.* Taylor and Francis.

CARPENTER, N. E., DICKSON, M., NICHOLLS, R. J. & POWRIE, W. In Review-a. Investigating the effects of varied lithology on soft cliff geomorphology and recession rates. *Marine Geology.*

CARPENTER, N. E., NICHOLLS, R. J., POWRIE, W. & DICKSON, M. In Review-b. Development of a process-based model to understand the effects of variable lithology: An Isle of Wight case Study. *Coasts, Marine Structures and Breakwaters.* Edinburgh, UK: ICE.

CARR, A. P. 1962. Cartographic record and historical accuracy. *Geography,* 47**,** 135-144.

CARTER, R. W. G., JENNINGS, S. C. & ORFORD, J. D. 1990. Headland erosion by waves. *Journal of Coastal Research,* 6**,** 517-529.

CELIKOGLU, Y., YUKSEL, Y. & KABDASLI, M. S. 2004. Longshore sorting on a beach under wave action. *Ocean Engineering,* 21**,** 1351-1375.

CHAPMAN, D. M. 1981. Coastal erosion and the sediment budget, with special reference to the gold coast, Australia. *Coastal Engineering,* 4**,** 207-227.

CIAVOLA, P., TABORDA, R., FERREIRA, Ó. & DIAS, J. A. 1997. Field observations of sand-mixing depths on steep beaches. *Marine Geology,* 141**,** 147-156.

CLAYTON, C. R. I. & SERRATICE, J. F. 1993. The mechanical properties and behavior of hard soils and soft rocks. *In:* ANAGNOSTOPOULOS, A. (ed.) *Geotechnical Engineering of Hard Soils- Soft Rocks.* Rotterdam: Balkema.

CODRINGTON, T. 1870. On the superficial deposits of the south of Hampshire and the Isle of Wight. *Quaterly Journal of the Geoloical Society of London,* 26**,** 528-551.

COLENUTT, G. W. 1938. Fifty years of Island coastal erosion. *Proceedings Isle of Wight Natural History & Archaeological Society,* 3**,** 50-57.

COLENUTT, G. W., HOOLEY, R. W. & HERRIES, R. S. 1906. Excursion to the Isle of Wight, Whitsuntide, 1906. *Proceedings of the Geologists' Association,* 19**,** 357-366.

COLLINS, M. B. & SITAR, N. 2008. Processes of coastal bluff erosion in weakly lithified sands, Pacifica, Californis, USA. *Geomorphology,* 97**,** 483 - 501.

COLMAN, S. M. & FOSTER, S. F. 1994. A sediment budget for Southern Lake Michigan: Source and sink models for different time intervals. *Journal of Great Lakes Research,* 20**,** 215-228.

CROWELL, M., LEATHERMAN, S. P. & BUCKLEY, M. K. 1991. Historical shoreline change:Error analysis and mapping accuracy. . *Journal of Coastal Research,* 7**,** 839-852.

DALEY, B. & STEWART, D. J. 1979. Week-end field meeting The Wealden Group in the Isle of Wight. *Proceedings of the Geologists' Association,* 90**,** 51-54.

DASGUPTA, P. & MANNA, P. 2011. Geometrical mechanism of inverse grading in grain-flow deposits: An experimental revelation. *Earth-Science Reviews,* 104**,** 186-198.

DAVIDSON-ARNOTT, R. G. D. & LANGHAM, D. R. J. 2000. The effects of softening on nearshore erosion of a cohesive shoreline. *Marine Geology,* 166**,** 145-162.

DAVIDSON-ARNOTT, R. G. D. & OLLERHEAD, J. 1995. Nearshore erosion on a cohesive shoreline. *Marine Geology,* 122**,** 349-365.

DAVIES, J. C. 1986. *Statistics and Data Analysis in Geology*, John Wiley & Sons.

DEAN, R. G. 1991. Equilibrium Beach Profiles: Characteristics and Applications. *Journal of Coastal Research,* 7**,** 53-84.

DEFRA 2002. The Futrue Coast Project. Project code FD2002.CD-ROM. More information at: http://www.defra.gov.uk/environ/fcd/futurecoast.htm.

DEL RIO, L. & GRACIA, F. J. 2009. Erosion risk assessmentof active coastal cliffs in temperate environments. *Geomorphology,* 112**,** 82-95.

DICKSON, M., WALKDEN, M. J. A. & HALL, J. W. 2007. Systematic impacts of climate change on an eroding coastal region over the twenty-first century. *Climate Change,* 84**,** 141-166.

DORNBUSCH, U., ROBINSON, D. A., MOSES, C. A. & WILLIAMS, R. B. G. 2008. Temporal and spatial variations of chalk cliff retreat in East Sussex, 1873 to 2001 *Marine Geology,* 249**,** 271-282.

DORNBUSCH, U., WILLIAMS, R. B. G., MOSES, C. & ROBINSON, D. A. 2002. Life expectancy of shinge beaches: measuring in situ abrasion. *Journal of Coastal Research***,** 249-255.

EBERSOLE, B. A., CIALONE, M. A. & PARATER, M. D. 1986. RCPWAVE- A linear Wave Propogation Model of Engineering Use. *Technical Report CERC-86-4.* U.S. Army Engineer Waterways Experiment Station, Vicksburg, MS.

ESTEVES, L. S., WILLIAMS, J. J., NOCK, A. & LYMBERY, G. 2009. Quantifying shoreline changes along the Sefton coast (UK) and the implications for research-informed coastal management. *Journal of Coastal Research.*

EUROSION 2004. Living with coastal erosion in Europe: Sediment and space to sustainability: Major findings and plocy recomendations of the EUROSION project. European Commision, Directorate General Environment.

EVANS, D. J., KIRBY, G. A. & HULBERT, A. G. 2011. New insight into the structure and evolution of the Isle of Wight Monocline. *Proceedings of the Geologists' Association,* 122**,** 764-780.

FINKELSTEIN, K. 1982. Morphological variations and sediment transport in crenulate-bay, Kodiak Island, Alaska. *Marine Geology,* 47**,** 261-281.

FITTON, W. H. 1847. A stratigraphic account from Atherfield to Rocken End, on the southwest coast of the Isle of Wight. *Quaterly Journal of the Geoloical Society of London,* 3**,** 289-327.

FLINT, K. E. 1982. Chines on the Isle of Wight: Channel adjustment and basin morphology in relation to cliff retreat. *The Geographical Journal,* 148**,** 225-236.

GELINAS, P. J. & QUIGLEY, R. M. 1973. The influence of geology on the erosion rates along the north shore of Lake Erie. *International Assosiation of Great Lakes Research. Proceedings of the 16th Confernce of Great Lakes Research.***,** 421-430.

GLEASON, R. & HARDCASTLE, P. J. 1973. The significance of wave parameters in the sorting of beach pebbles. *Estuarine and Coastal Marine Science,* 1**,** 11-18.

GULYAEV, S. A. & BUCKERIDGE, J. S. 2004. Terrestrial methods for monitoring cliff erosion in an urban environment. *Journal of Coastal Research,* 30**,** 871-878.

HACKNEY, C., DERBY, S. E. & LEYLAND, J. 2013. Modelling the response of soft cliffs to climate change: A statistical, process-responsemodel using accumulated excess energy. *Geomorphology,* 187**,** 108-121.

HAIGH, I., NICHOLLS, R. J. & WELLS, N. Rising sea levels in the English Channel 1900 to 2100 ICE- Maritime Engineering, 2011. 81-92.

HAJDARWISH, A., SHAKOOR, A. & WELLS, N. A. 2013. Investigating statistical relationships among clay mineralogy, index engineering properties, and shear strength parameters of mudrocks. *Engineering Geology,* 159**,** 45-58.

HALL, J. W., MEADOWCROFT, I. C., LEE, E. M. & VAN GELDER, P. H. A. J. M. 2002. Stochastic simulation of episodic soft coastal cliff recession. *Coastal Engineering,* 46**,** 159-174.

HALLERMEIER, R. J. 1981. A Profile Zonation for Seasonal Sand Beaches from Wave Climate. *Coastal Engineering,* 4**,** 253-277.

HAPKE, C. J., REID, D. & RICHMOND, B. 2009. Rates and trends of coastal change in California and the regional behaviour of the beach and cliff system. *Journal of Coastal Research,* 25**,** 603-615.

HICKS, D. M. 1985. *Sand dispersion from an ephemeral delta on a wave dominated coast, Santa Cruz, California.* Ph.D., University of California.

HR Wallingford, 2002. Risk, Performance and Uncertainty in Flood and Coastal Defence - A Review. *Flood and Coastal Defence R&D Programme.* DEFRA/Envirnoment Agency.

HUTCHINSON, J. N. 1965. A reconnaissance of coastal landslides in the Isle of Wight Building Research Station: Department of Scientific and Industrial Research.

INKPEN, R. J., TWIGG, L. & STEPHENSON, W. J. 2004. The use of multilevel modeling in evaluating controls on erosion rates on inter-tidal shore platforms, Kaikoura Peninsula, South Island, New Zealand. *Geomorphology,* 57**,** 29-39.

INSOLE, A., DALEY, B. & GALE, A. 1998. *The Isle of Wight. Geologists' Association Guide No.60,* London, UK, Geologists' Association.

IPCC 2013. Summary for Policymakers. *In:* STOCKER, T. F., QIN, D., PLATTNER, G.-K., TIGNOR, M., ALLEN, S. K., BOSCHUNG, J., NAUELS, A., XIA, Y., BEX, V. & MIDGLEY, P. M. (eds.) *Climate Change 2013: The Physical Science Basis. Contribution of Working Group I to the Fifth Assessment Report of the Intergovernmental Panel on Climate Change.* Cambridge, United Kingdom and New York, NY, USA: Cambridge University Press.

JACKSON, M. D., YOSHIDA, S., MUGGERIDGE, A. H. & JOHNSON, H. D. 2005. Three-dimensional reservoir characterization and flow simulation of heterolithic tidal sandstones *The American Assosication of Petroleum Geologists Bulletin,* 89**,** 507-528.

JENKINSON, H. I. 1879. *Jenkinson's Smaller Practical Guide to the Isle of Wight*, E. Stanford.

JOLLIFFE, I. P. 1964. An experiment designed to compare the relative rates of movement of beach pebbles. *Proceedings of the Geologists' Association,* 75**,** 67-86.

JONES, D. G. & WILLIAMS, A. T. 1991. Statistical analysis of factors influencing cliff erosion along a section of the West Wales Coast, U.K. *Earth Surface Processes and Landforms,* 16**,** 95-111.

KANA, T. W. 1995. A mesoscale sediment budget for Long Island, New York. *Marine Geology,* 126**,** 87-110.

KANYAYA, J. I. & TRENHAILE, A. S. 2005. Tidal wetting and drying on shore platforms An experimental assessment. *Geomorphology,* 70**,** 129-146.

KAY, E. 1969. A consideration and report of factors in the present retreat of the coast, and cliff falls in South Wight. Report to Ventnor U.D.C.

KENNEDY, D. M. & DICKSON, M. E. 2006. Lithological control on the elevation of shore platforms in a microtidal setting. *Earth Surface Processes and Landforms,* 31**,** 1575-1584.

KOLLIOS, A. 1993. Geosynthetics design for erosion control of hard marls. *In:* ANAGNOSTOPOULOS, A. (ed.) *Geotechnical Engineering of Hard Soils - Soft Rocks.* Rotterdam: Balkema.

KOMAR, P. D. 1985. Computer models of shoreline configuration: Headland erosion and the graded beach revisited. *In:* WOLDENBURG, M. J. (ed.) *Models in Geomorphology.* London: Allen & Unwin.

KOMAR, P. D. & INMAN, D. L. 1970. Longshore Sand Transport on Beaches. *Journal of Geophysical Research,* 75**,** 5914-5927.

KRUMBEIN, W. C. 1934. Size Frequency distribution of sediments. *Journal of Sedimentary Petrology,* 4**,** 65-77.

LACEY, S. 1985. Coastal sediment processes in Poole and Christchurch Bays and the effects of coast protection works. University of Southampton

LEE, E. M. 2002. Soft cliffs:Prediction of recession rates and erosion control techniques (R&D Project FD2403/1302). London: DEFRA/Environment Agency.

LEE, E. M. 2008. Coastal cliff behaviour: Observations on the relationship between beach levels and recession rates. *Geomorphology,* 101**,** 558-571.

LEE, E. M. & CLARK, A. R. 2002. *Investigation and Management of Soft Rock Cliffs,* London, UK, Thomas Telford.

LEIGHTON, T. 1891. Excursion to the Isle of Wight. *Proceedings of the Geologists' Association,* 12**,** 145-171.

LIMBER, P. W. & MURRAY, A. B. 2011. Beach and sea-cliff dynamics as a driver of long-term rocky coastline evolution and stability. *Geology.*

LIMBER, P. W., PATSCH, K. B. & GRIGGS, G. B. 2008. Coastal sediment budgets and the littoral cutoff diameter: A grain size threshold for quantifying active sediment inputs. *Journal of Coastal Research,* 24**,** 122-133.

MASON, S. J. 1985. *Beach Development, Sediment Budget and Coastal Erosion at Holderness.* PhD, University of Sheffield.

MAY, J. P. & TANNER, W. F. 1973. The littoral power gradient and shoreline changes. *In:* COATES, D. R. (ed.) *Coastal Geomorphology.* Binghampton, N.Y: S.U.N.Y.

MAY, V. J. 2007. Southwest Isle of Wight. *Geological Conservation Review.*

MOORE, L. J. 2000. Shoreline mapping techniques. *Journal of Coastal Research,* 16**,** 111-124.

MOORE, L. J. & GRIGGS, G. B. 2002. Long-term cliff retreat and erosion hotspots along the central shores of the Monterey Bay National Marine Sanctuary. *Marine Geology,* 181**,** 265-283.

MOORE, R., BARTER, P., MCCONNELL, K., RIBY, J. & MATTHEWS, C. 2002. Cliff behavior assessment and management strategy, Filey Bay, Yorkshire, UK. *In:* MCINNES, R. & JAKEWAYS, J. (eds.) *Instability - Planning and Management.* London: Thomas Telford.

NEWSHAM, R., BALSON, P. S., TRAGHEIM, D. G. & DENNISS, A. M. 2002. Determination and predistion of sediment yields from the recession of the Holderness Coast, NE England. *Journal of Coastal Conservation,* 8**,** 49-54.

NICHOLLS, R. J., DREDGE, A. & WILSON, T. 2000. Shoreline change and fine grained sediment input: Isle of Sheppey Coast, Thames Estuary, UK. *In:* PYE, K. & ALLEN, J. R. L. (eds.) *Coastal and Estuarine Environments: Sedimentology, geomorphology and geoarchaeology.* London: Geological Society.

NORMAN, M. W. 1887. *A popular guide to the geology of the Isle of Wight, with a note on its relation to that of the Isle of Purbeck*, Cambridge University Press.

OGAWA, H., KENCH, P. & DICKSON, M. 2012. Field measurements of wave characterisitics on a near-horizontal shore platform, Mahia Peninsula, North Island, New Zealand. *Geographical Research,* 50**,** 179-192.

OLIVER, R. 1996. Taking to the water: some examples of Ordnance Survey mapping of the coast. *Sheetlines, newsletter of the Chales Close Society,* 45**,** 9-27.

PALMER, M. J. (ed.) 1991. *Ground Movements of the Encombe Landslide at Sandgate, Kent,* London, UK: Thomas Telford.

PETHICK, J. 1984. *An Introduction to Coastal Geomorphology,* London, Arnold.

POSFORD, DUVIVIER & BGS 1999. SCOPAC Research Project. Sediment Inputs to the Coastal System. Phase 3. Inputs from the Erosion of Coastal Platforms and Long Term Sedimentary Deposits, Report to SCOPAC.

POULTON, C. V. L., LEE, J. R., HOBBS, P. R. N., JONES, L. & HALL, M. 2006. Preliminary Investigation into Monitoring Coastal Erosion using

Terrestrial Laser Scanning: Case Study at Happisburgh, Norfolk. *Bullentin of the Geological Society of Norfolk,* 56**,** 45-64.

QUINN, J. D., ROSSER, N. J., MURPHY, W. & LAWRENCE, J. A. 2010. Identifying the behavioural characteristics of clay cliffs using intensive monitoring and geotechnical numerical modelling. *Geomorphology,* 120**,** 107-122.

RADLEY, J. D. & ALLEN, P. 2012. The Wealden (non-marine Lower Cretaceous) of the Wessex Sub-basin, southern England. *Proceedings of the Geologists' Association,* 123**,** 319-373.

REDSHAW, P. G. 2013. Investigation of the Roughlands Landslide Complex, Southwest Isle of Wight, UK. PhD. Transfer Report, University of Southampton.

REDSHAW, P. G., BARTON, M. E. & STUIVER, C. Landslides on a Cretaceous Fluvial Sediment. World Landslide Forum 3, 2-6 June 2014. In Review Beijing.

RIX, K. 2000. The trends and controls of the coastal bedload sediment transport paths ('The Needle' to 'St.Catherine's Point', Isle of Wight); a medium to large scale numerical computer model. King's College London.

ROSATI, J. & KRAUS, N. C. 1999. Sediment budget analysis system (SBAS). *Coastal and Hydraulics Engineering Technical Note.* Vicksburg, MS: U.S. Army Engineer Research and Development Center.

RUDD, J. 1570. *Vecta Myght Map* [Online]. Available: http://www.islandeye.co.uk/history/maps_of_the_Isle_of_wight/vecta-wyght-map.html [Accessed [23/09/2013].

RUGGIERO, P., KOMAR, P. D., MCDOUGAL, W. G., MARRA, J. J. & BEACH, R. A. 2001. Wave runup, extreme water levels and the erosion of properties backing beaches. *Journal of Coastal Research,* 17**,** 407-419.

RUST, D. & GARDENER, J. 2002. Lithological and structural controls on style and rate of coastal slope failure: Implications for future planning and remedial engineering measures, SW coast, Isle of Wight *In:* MCINNES, R. & JAKEWAYS, J. (eds.) *Instabiltiy: Planning and Management.* London: Thomas Telford.

RYAN, P. D., HARPER, D. A. T. & WHALLEY, J. S. 1995. *PALSTAT, Statistics for palaeontologists*, Chapman & Hall (now Kluwer Academic Publishers).

SCHWARTZ, M. L. (ed.) 2005. *Encyclopedia of Coastal Science,* Dordrecht: Springer.

SILVESTER, R. 1985. Natural headland control of beaches. *Continental Shelf Research,* 4**,** 581-596.

SIMPSON, M. I. 1985. The stratigraphy of the Atherfield Clay Formation (Lower Aptian, Lower Cretaceous) at the type and other localities in Southern England. *Proceedings of the Geologists' Association,* 96**,** 23-45.

SKAFEL, M. G. & BISHOP, C. T. 1994. Flume experiments on the erosion of till shores by waves. *Coastal Engineering,* 23**,** 329-348.

SOARES, L. 1993. Determination of the coherence grade of the soft rocks. *In:* ANAGNOSTOPOULOS, A. (ed.) *Geotechnical Engineering of Hard Soils - Soft Rocks.* Rotterdam: Balkema.

SPAGNOLO, M., LLOPIS, I. A., PAPPALARDO, M. & FREDERICI, P. R. 2008. A new approach for the study of coastal indentation index *Journal of Coastal Research,* 24**,** 1459-1468.

SPEED, J. 1611. *Wight Island Map* [Online]. Available: http://www.islandeye.co.uk/history/maps_of_the_Isle_of_wight/1611-map-isle-of-wight-speed.html [Accessed [23/09/2013].

STEPHENSON, W. J. & KIRK, R. M. 2000. Development of shore platforms on Kaikoura Peninsula, South Island, New Zealand. Part One: The role of waves. *Geomorphology,* 32, 21-41.

STEWART, D. J., RUFFELL, A., WACH, G. & GOLDRING, R. 1991. Lagoonal sedimentation and fluctuating salinities in the Vectis Formation (Wealdeb Group, Lower Cretaceous) of the Isle of Wight, Southern England. *Sedimentary Geology,* 72, 117-134.

STUIVER, C. S. 2010. The factors influencing recession rates on soft cliff coasts: Southwest Isle of Wight. *School of Civil Engineering and the Environment.* Unpublished MSc Thesis: University of Southampton.

SUNAMURA, T. 1992. *Geomorphology of rocky coasts,* Chichester, John Wiley and Sons.

SUNAMURA, T. & KRAUS, N. C. 1984. Prediction of average mixing depth of sediment in the surf zone. *Marine Geology,* 62, 1-12.

SUTHERLAND, J. 2012. Error analysis of Ordnance Survey map tidelines, UK *Proceedings of the ICE- Maritime Engineering,* 165, 189-197.

TAYLOR, J. A., MURDOCK, A. P. & PONTEE, N. I. 2004. A macroscale analysis of coastal steepening around the coast of England and Whales. *The Geographical Journal,* 170, 179-188.

THIELER, E. R., HIMMELSTOSS, E. A., ZICHICHI, J. L. & ERGUL, A. 2009. Digital Shoreline Analysis System (DSAS) version 4.0 - An ArcGIS extension for calculating shoreling change. U.S. Geological Survey.

THOMPSON, C. E. L. & AMOS, C. L. 2004. Effect of sand movement on a cohesive substrate. *Journal of Hydraulic Engineering* 130, 1123-1125.

THORNTON, L. E. & STEPHENSON, W. J. 2006. Rock Strength: A control of shore platform elevation. *Journal of Coastal Research,* 22, 224-231.

TRENHAILE, A. S. 2004. Modeling the accumulation and dynamics of beaches on shore platforms. *Marine Geology,* 206, 55-72.

TRENHAILE, A. S. 2009. Modeling the erosion of cohesive clay coasts. *Coastal Engineering,* 56, 59-72.

TWIDALE, C. R., BOURNE, J. A. & VIDAL ROMANI, J. R. 2005. Beach etching and shore platforms. *Geomorphology,* 67, 47-61.

UNDERHILL, J. R. & PATERSON, S. 1998. Genesis of tectonic inversion structures: seismic evidence for the development of key structures along the Purbeck-Isle of Wight Disturbance. *Journal of the Geological Society,* 155, 975-922.

VALENTIN, H. 1954. Land loss at Holderness. *In:* STEERS, J. A. (ed.) *Applied Coastal Geomorphology.* London: Macmillan.

VALVO, L. M., MURRAY, A. B. & ASHTON, A. 2006. How does underlying geology affect coastline change? An initial modeling investigation. *Journal of Geophysical Research,* 111, 1-18.

VAN RIJN, L. C. 1993. *Principles of Sediment Transport in Rivers, Estuaries and Coastal Seas,* The Netherlands, Aqua Publications.

VINCENT, L., DEMIRBILEK, Z. & WEGGEL, J. R. 2002. Estimation of Nearshore Waves. *Coastal Engineering Manual* U.S. Army Engineer Waterways Experiment Station, Vickisburg, MS.

WALKDEN, M. J. A. & DICKSON, M. 2006. The response of soft rock shore profiles to increased sea level rise. Tyndall Centre for Climate Change Research.

WALKDEN, M. J. A. & DICKSON, M. 2008. Equilibrium erosion of soft rock shores with a shallow or absent beach under increased sea level rise. *Marine Geology,* 251, 75-84.

WALKDEN, M. J. A. & HALL, J. W. 2005. A predictive mesoscale model of the erosion and profile development of soft rock shores. *Coastal Engineering,* 52**,** 535-563.

WALKER, J. 1815. *Isle of Wight Map* [Online]. Available: http://freepages.genealogy.rootsweb.ancestry.com/~genmaps/genfiles/ COU_files/ENG/HAM/walker_iow_1815.htm [Accessed [23/09/2013].

WHITE, H. J. O. 1921. *Short account of the geology of the Isle of Wight,* London, HMSO.

WOLTERS, G. & MULLER, G. 2008. Effect of cliff shape on internal stresses and rock slope stability. *Journal of Coastal Research,* 24**,** 43-50.

WRIGHT, L. W. 1970. Variation in the level of cliff/shore platform junction along the south coast of Great Britain. *Marine Geology,* 9**,** 347-353.

WRIGHT, P. 1981. Aspects of the coastal dynamics of Poole and Christchirch Bays. University of Southampton.

YOSHIDA, S., JACKSON, M. D., JOHNSON, H. D., MUGGERIDGE, A. H. & MARTINIUS, A. W. 2001. Outcrop studies of tidal sandstones for reservoir characterisation (Lower Cretaeaous Vectis Formation, Isle of Wight, southern England). *In:* MATINSEN, O. J. & DREYER, T. (eds.) *Sedimentary Environments Offshore Norway - Palaeozoic to Recent.* Amsterdam: Elsevier Scince B.V.

YOUNG, A. P. & ASHFORD, S. A. 2006. Applications of Airbourne LIDAR for Seacliff Volumetric Change and Beach-Sediment Budget contributions. *Journal of Coastal Research,* 22**,** 307-318.